

Resection-dependent canonical non-homologous end-joining induces genomic rearrangements



TECHNISCHE
UNIVERSITÄT
DARMSTADT

Vom Fachbereich Biologie der Technischen Universität Darmstadt
zur
Erlangung des akademischen Grades
eines Doctor rerum naturalium
genehmigte Dissertation von

M.Sc. Ronja Anugwom, geb. Biehs
aus Idar-Oberstein

1. Referent: Prof. Dr. Markus Löbrich
2. Referent: Prof. Dr. Kay Hamacher

Tag der Einreichung: 01.11.2017
Tag der mündlichen Prüfung: 13.12.2017
Darmstadt 2017
D 17

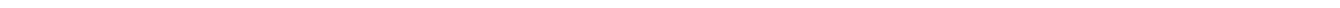
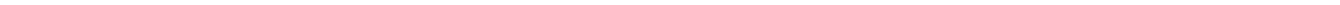


Table of contents

TABLE OF CONTENTS	I
PREFACE	III
1. SUMMARY	1
1.1. ZUSAMMENFASSUNG.....	3
2. INTRODUCTION	5
2.1. DNA DAMAGE RESPONSE	5
2.1.1. <i>Post-translational modifications</i>	5
2.1.2. <i>Cell cycle control</i>	6
2.1.3. <i>DNA repair</i>	7
2.2. DOUBLE-STRAND BREAK REPAIR	7
2.2.1. <i>DSB Recognition</i>	7
2.2.2. <i>Homologous recombination (HR)</i>	9
2.2.3. <i>Canonical non-homologous end-joining (c-NHEJ)</i>	14
2.2.4. <i>Error-prone end-joining</i>	19
2.2.5. <i>End-joining in genetic recombination</i>	23
2.3. AIM OF THIS STUDY	26
3. RESULTS	27
3.1. THE END-JOINING REPORTER SYSTEM IN GC92 CELLS AND ASSOCIATED ASSAYS	27
3.1.1. <i>Analysis of misrepair events in GC92 cells</i>	28
3.1.2. <i>Overall repair of distant endonuclease-induced DSBs in GC92 cells</i>	32
3.1.3. <i>Sequence analysis of the misrejoined break sites in GC92 cells</i>	33
3.1.4. <i>Comparing the misrepair of distant and close endonuclease-induced DSBs</i>	34
3.2. END-JOINING-ASSOCIATED PROTEINS AND THEIR ROLE IN THE REPAIR OF DISTANT DSBs	36
3.2.1. <i>Misrepair is dependent on c-NHEJ factors</i>	36
3.2.2. <i>Varying roles for PARP1 in different end-joining mechanisms</i>	40
3.2.3. <i>The misrejoining of distant DSB ends relies on various polymerases</i>	43
3.2.4. <i>ARTEMIS is essential for the misrepair of DSBs</i>	44
3.2.5. <i>Misrepair in 53BP1-depleted cells is conducted by alt-EJ</i>	47
3.3. RESECTION IN END-JOINING: HOW RESECTION BARRIERS CAN BE OVERCOME	51
3.3.1. <i>Misrepair relies on the pro-resection factor BRCA1</i>	51
3.3.2. <i>The resection initiating factor CtIP is required for the misrejoining of distant DSB ends</i>	53
3.3.3. <i>The kinase PLK3 activates CtIP for the misrejoining of distant DSBs</i>	62
3.3.4. <i>Nucleases conducting resection in this novel repair pathway</i>	69
4. DISCUSSION	75
4.1. THE REPAIR OF ENDONUCLEASE-INDUCED DSBs	76
4.1.1. <i>Enhancing the accuracy of reporter assay analysis</i>	76
4.1.2. <i>Beyond the reporter assay: the γH2AX foci assay in GC92 cells</i>	77
4.1.3. <i>Radiation-induced DSBs in comparison to endonuclease-induced DSBs</i>	78
4.2. RESECTION-DEPENDENT C-NHEJ (RES-CNHEJ)	79
4.2.1. <i>Barriers to resection during res-cNHEJ</i>	79
4.2.2. <i>Initiation of resection during res-cNHEJ</i>	83
4.2.3. <i>Nucleases conducting resection during res-cNHEJ</i>	85
4.2.4. <i>Processing of resection intermediates during res-cNHEJ</i>	89
4.2.5. <i>Completion of repair during res-cNHEJ</i>	91
4.2.6. <i>Additional factors involved in res-cNHEJ</i>	93

4.3.	REPAIR PATHWAY CHOICE FOR THE MISREJOINING OF DISTANT NUCLEASE-INDUCED DSBS	96
4.3.1.	<i>Cell cycle-specific misrepair of distant DSB ends</i>	96
4.3.2.	<i>Contribution of res-cNHEJ to the misrepair of distant endonuclease-induced DSBs</i>	99
4.3.3.	<i>Alternative end-joining of nuclease-induced DSBs</i>	101
4.4.	RATIONALE FOR RES-CNHEJ	105
4.4.1.	<i>Relevance of the location, structure, and complexity of the DSB ends</i>	105
4.4.2.	<i>How error-prone is res-cNHEJ?</i>	106
4.4.3.	<i>Genetic recombination as the physiological origin of res-cNHEJ?</i>	108
4.4.4.	<i>A role for res-cNHEJ in checkpoint control?</i>	109
4.5.	FINAL STATEMENT	111
5.	MATERIALS & METHODS	112
5.1.	MATERIALS	112
5.1.1.	<i>Consumable materials and appliances</i>	112
5.1.2.	<i>Software and external facilities</i>	113
5.1.3.	<i>Chemicals</i>	113
5.1.4.	<i>Solutions, buffers, and media</i>	114
5.1.5.	<i>Reagents, kits, ladders, and enzymes</i>	116
5.1.6.	<i>Primers, siRNAs, and gRNAs</i>	117
5.1.7.	<i>Inhibitors, nucleotides, and nucleotide analogues</i>	118
5.1.8.	<i>Antibodies and beads</i>	119
5.1.9.	<i>Plasmids</i>	121
5.1.10.	<i>Cell lines and bacteria</i>	122
5.2.	CELLULAR BIOLOGICAL METHODS	123
5.2.1.	<i>Cell culture, transfections, and treatments</i>	123
5.2.2.	<i>Flow cytometry and magnetic-activated cell sorting (MACS)</i>	127
5.2.3.	<i>Immunofluorescence</i>	128
5.3.	BIOCHEMICAL METHODS	129
5.3.1.	<i>Protein extracts, immunoprecipitation, and immunoblotting</i>	129
5.3.2.	<i>Tandem affinity purification mass spectrometry (TAP-MS)</i>	131
5.4.	MOLECULAR BIOLOGICAL METHODS	132
5.4.1.	<i>DNA purification, amplification, digestion, and ligation</i>	132
5.4.2.	<i>Bacteria preparation, transformation, plasmid isolation, and sequence analysis</i>	133
5.5.	ANALYSIS	134
5.5.1.	<i>Quantification and descriptive statistics</i>	134
5.5.2.	<i>Inferential statistics</i>	135
6.	REFERENCES	137
7.	DIRECTORIES	IV
7.1.	ABBREVIATIONS	IV
7.2.	LIST OF FIGURES	VII
7.3.	LIST OF TABLES	VIII
8.	APPENDIX	IX
8.1.	SUPPLEMENTAL FIGURES AND RAW DATA	IX
8.2.	CURRICULUM VITAE	XXIV
8.3.	PUBLICATIONS, AWARDS, AND CONFERENCE CONTRIBUTIONS	XXIV
8.4.	ACKNOWLEDGEMENTS	XXVI
EHRENWÖRTLICHE ERKLÄRUNG	XXVII	

Preface

In this dissertation, I am pleased to present to you my work “Resection-dependent canonical non-homologous end-joining induces genomic rearrangements” wherein I will introduce you to a novel DNA repair pathway, which endangers the genomic integrity.

This dissertation was generated under the supervision of Prof. Dr. M. Löbrich at the *Technische Universität Darmstadt* (Technical University Darmstadt), Germany in his Radiation Research and DNA repair working group. The laboratory work of this dissertation was performed from July 2013 until October 2016 at *Technische Universität Darmstadt* and from October 2015 to March 2016 at MD Anderson Cancer Center, Houston, Texas, USA in the Department of Experimental Radiation Oncology under the supervision of J. Chen, PhD.

The declaration of authorship can be found at the very end of this thesis (*Ehrenwörtliche Erklärung*). Any data obtained in collaboration or by undergraduate students under my supervision are explicitly declared as such in the according figure legends. This thesis generally uses an impersonal style of writing.

Parts of this dissertation were published in the peer-reviewed journal articles Barton et al. (2014) “Polo-like kinase 3 regulates CtIP during DNA double-strand break repair in G_1 ” in *The Journal of Cell Biology* and Biehs et al. (2017) “DNA double-strand break resection occurs during non-homologous end-joining in G_1 but is distinct to resection during homologous recombination in G_2 ” in *Molecular Cell*. Figures involving data included in one of these publications are named in the according figure legends.

The structure of this dissertation mostly adheres to the classical structure of a thesis from the biological sciences. However, some results are discussed within the results section of this thesis instead of the discussion section to make it easier for the reader to follow the reasoning behind the experimental design. In addition, the materials and methods section can be found after the discussion section to not disrupt the flow. Furthermore, the lists of abbreviations, figures, and tables are located after the references to enable all materials supporting the comprehension of the content to be combined in one place.

I hope you enjoy reading this dissertation as much as I enjoyed researching this topic.

1. Summary

DNA double-strand breaks (DSBs) are the main threat to genomic integrity. The majority of DSBs are repaired by canonical non-homologous end-joining (c-NHEJ), where the two DSB ends are rejoined with minimal processing. Some studies suggest that the rejoining of DSBs by c-NHEJ can be error-prone by causing sequence alterations and/or the misrejoining of two separate DSBs. Such genomic rearrangements are a driving force in carcinogenesis. However, it remains an ongoing discussion as to how such rearrangements arise, as other studies associate genomic rearrangements with alternative end-joining (alt-EJ) and factors favoring resection. During alt-EJ the involvement of resection results in the loss of genetic information. However, there is evidence that alt-EJ mechanisms only play a role in human cells, which are deficient for certain repair proteins. This is the case in combination with genetic defects or in tumor cells. Thus, it remains unclear how mutagenic end-joining, which results in genomic rearrangements, operates and is regulated in wild-type human cells.

To answer this question, mutagenic end-joining repair was investigated in this study by combining a reporter assay with other molecular biological assays. This reporter assay monitors the misrejoining of two 3.2 kilobase distant DSB ends under the loss of the intervening fragment. In addition, the sequence alterations at the misrejoined break sites were analyzed and overall repair was investigated. Furthermore, two approaches were taken to understand the circumstances under which error-prone end-joining is employed in wild-type human cells: the misrejoining of DSBs was compared between different reporter assays and the interactions of proteins involved in this pathway were analyzed.

The results of this study show that distant DSB ends are misrejoined by a hitherto undescribed slow repair mechanism, which is specific for the G₁ phase of the cell cycle. These misrejoined break sites are frequently associated with sequence alterations, especially small deletions (less than 50 nucleotides). These deletions are the result of limited resection. Surprisingly, the DSB ends remain protected by the key c-NHEJ factor KU during this undescribed repair mechanism. This feature distinguishes this end-joining process from all previously described pathways involving resection. Indeed, the absence of factors such as KU or the anti-resection factor 53BP1 results in increased genomic rearrangements by alt-EJ. Hence, in this novel repair pathway, c-NHEJ factors are pivotal in ensuring resection remains limited.

Resection-dependent c-NHEJ is initiated by the activation of the resection factor CtIP. This is achieved through damage-inducible phosphorylation by the kinase PLK3 at Ser327, Thr847, and probably additional sites. Subsequently, the phosphorylation of CtIP at Ser327 results in its interaction with the pro-resection factor BRCA1. Similar to its role in S/G₂ phase, the BRCA1-

CtIP interaction seems to be important to overcome the resection barrier posed by 53BP1. Resection is executed by the exonuclease EXO1. Although EXO2 and MRE11 are also involved, the endonuclease function of MRE11 is dispensable for this repair pathway, indicating that resection is conducted from the DSB end. This is a key step limiting resection since the endonucleolytic cut by MRE11 overcomes the protected or blocked DSB ends during other resection processes to generate large single-stranded DNA overhangs. Thus, the initiation and execution of resection in this novel pathway is finely tuned to ensure that resection remains limited.

Strikingly, the impairment of factors involved in the initiation or execution of resection does not result in unrepaired DSBs. This indicates that a repair pathway switch occurs in their absence. Although the absence of this novel error-prone repair pathway results in less genomic rearrangements, the remaining rearrangements are associated with worse sequence alterations, including longer deletions. Importantly, the limited resection process during resection-dependent c-NHEJ produces short single-stranded DNA regions, which form intermediate structures. These structures need to be resolved by the endonuclease activity of ARTEMIS, which is dependent on its interaction with the key c-NHEJ component DNA-PKcs. Thus, once resection has taken place, both ARTEMIS and DNA-PKcs are indispensable for repair completion.

The break sites are mostly misrejoined using microhomologies, and thus require the single-stranded DNA gaps to be filled-in by polymerases. POL θ , which is typically associated with microhomologies, acts in this novel repair pathway, but the c-NHEJ-associated polymerases POL λ/μ are also involved. The ligation step is conducted by the c-NHEJ ligase LIG4 and not by LIG1/3, which ligate DSB ends during alt-EJ. To summarize, despite its error-prone characteristics, this novel repair pathway restricts the loss of genetic information to a minimum. This is accomplished by rejoining the break sites using microhomologies, by keeping resection limited with the help of c-NHEJ factors, and by preventing an endonucleolytic cut by MRE11.

In conclusion, this study characterizes a novel G₁-specific mutagenic resection-dependent c-NHEJ pathway in human cells. In addition, this study shows how protein-protein interactions influence the choice to utilize this DSB repair pathway. The occurrence of resection in combination with c-NHEJ factors is a unique feature of this repair pathway and was hitherto thought to be mutually exclusive. Furthermore, the discovery of this pathway clarifies the role of alt-EJ as a type of backup mechanisms to compensate for missing repair proteins. Hence, in the ongoing discussion of how genomic rearrangements arise, this novel repair pathway unifies the contradicting observations of other studies.

1.1. Zusammenfassung

DNA Doppelstrangbrüche (DSBs) sind die größte Gefahr für die genomische Integrität. Die Mehrheit aller DSBs wird durch die kanonische nicht-homologe Endverknüpfung (c-NHEJ) repariert, bei der die beiden Bruchenden nach minimaler Prozessierung miteinander verknüpft werden. Manche Studien suggerieren, dass c-NHEJ durch Sequenzmodifikationen und/oder die Fehlverknüpfung zweier separater DSBs fehlerbehaftet sein kann. Solche genomische Umlagerungen sind eine treibende Kraft der Karzinogenese. Allerdings bleibt die Entstehung dieser Umlagerungen ungewiss, denn andere Studien assoziieren genomische Umlagerungen mit alternativer Endverknüpfung (alt-EJ) und resektionsfördernden Faktoren. Die Beteiligung von Resektion führt während des alt-EJ zu dem Verlust genetischer Informationen. Jedoch gibt es Hinweise, dass alt-EJ in humanen Zellen nur eine Rolle spielt, wenn diese nicht über bestimmte Reparaturproteine verfügen. Dies ist bei Gendefekten und in Tumorzellen der Fall. Daher bleibt unklar, wie in humanen Wildtyp-Zellen mutagene Endverknüpfung, welche zu genomischen Umlagerungen führt, stattfindet und reguliert wird.

Um diese Frage zu beantworten, wurde die mutagene Endverknüpfungsreparatur in dieser Studie mittels eines Reporter-Assays in Kombination mit anderen molekularbiologischen Analysemethoden untersucht. Dieser Reporter-Assay misst die Fehlverknüpfung zweier 3,2 Kilobasen entfernter DSB-Enden, die durch den Verlust des dazwischenliegenden Fragmentes entsteht. Zusätzlich wurden die Sequenzveränderungen an den fehlverknüpften Bruchstellen analysiert und die Gesamtreparatur untersucht. Außerdem wurden zwei Ansätze gewählt, um zu verstehen unter welchen Bedingungen fehlerbehaftete Endverknüpfung in humanen Wildtyp-Zellen stattfindet: die Fehlverknüpfung von DSBs wurde zwischen verschiedenen Reporter-Assays verglichen und Interaktionen von Proteinen, die in diesem Reparaturweg beteiligt sind, wurden analysiert.

Die Ergebnisse dieser Studie zeigen, dass voneinander entfernt liegende DSB-Enden durch einen bisher unbeschriebenen langsamen Reparaturmechanismus fehlverknüpft werden, der spezifisch für die G₁ Phase des Zellzyklus ist. Die fehlverknüpften Bruchstellen sind häufig mit Sequenzveränderungen assoziiert, vor allem mit kurzen Deletionen (unter 50 Nukleotide). Diese Deletionen resultieren aus limitierter Resektion. Überraschenderweise werden die DSB-Enden in diesem unbeschriebenen Reparaturweg durch KU geschützt, einem Kernfaktor des c-NHEJ. Dieses Merkmal unterscheidet diesen Endverknüpfungsprozess von allen zuvor beschriebenen Reparaturwegen, bei denen Resektion involviert ist. Tatsächlich führt die Abwesenheit von KU oder des Antiresektionsfaktors 53BP1 zu vermehrten genomischen Umlagerungen durch alt-EJ. Daher sind c-NHEJ-Faktoren ausschlaggebend in diesem neuen Reparaturweg, um zu gewährleisten, dass die Resektion limitiert bleibt.

Resektionsabhängiges c-NHEJ wird durch die Aktivierung des Resektionsfaktors CtIP initiiert. Dies wird mittels Phosphorylierung durch die Kinase PLK3 an Ser327, Thr849 und vermutlich weiteren Stellen erreicht. Darauf folgend interagiert das an Ser327-phosphorylierte CtIP mit dem Pro-Resektionsfaktor BRCA1. Vergleichbar zu seiner Rolle in der S/G₂ Phase, scheint die BRCA1-CtIP Interaktion wichtig zu sein, um die 53BP1-Resektionsbarriere zu überwinden. Die

Resektion wird von der Exonuklease EXO1 durchgeführt. Obwohl EXD2 und MRE11 auch involviert sind, ist die Endonukleasefunktion von MRE11 entbehrlich für diesen Reparaturweg, was daraufhin deutet, dass die Resektion vom DSB-Ende durchgeführt wird. Dies ist ein entscheidender Schritt um die Resektion zu limitieren, denn der endonukleolytische Schnitt durch MRE11 überwindet in anderen Resektionsprozessen geschützte oder blockierte DSB-Enden und generiert so große einzelsträngige DNA-Überhänge. Folglich ist die Initiierung und Durchführung der Resektion in diesem neuen Reparaturweg fein abgestimmt um sicherzustellen, dass die Resektion limitiert bleibt.

Bemerkenswerterweise führt die Beeinträchtigung von Faktoren, die an der Initiierung oder Durchführung der Resektion beteiligt sind, nicht zu unreparierten DSBs. Dies deutet darauf hin, dass ohne diese Faktoren ein Wechsel des Reparaturweges stattfindet. Obwohl die Abwesenheit dieses neuen fehlerbehafteten Reparaturwegs in weniger genomischen Umlagerungen resultiert, sind die verbleibenden Umlagerungen mit schlimmeren Sequenzmodifikationen verbunden, inklusive längeren Deletionen. Der limitierte Resektionsprozess in diesem neuen Reparaturweg führt zu kurzen einzelsträngigen Bereichen, die intermediäre Strukturen ausbilden. Diese Strukturen müssen durch die Endonukleaseaktivität von ARTEMIS aufgelöst werden, was von ihrer Interaktion mit DNA-PKcs abhängig ist, einer Kernkomponente des c-NHEJ. Folglich sind ARTEMIS und DNA-PKcs unentbehrlich sobald Resektion stattgefunden hat.

Die Bruchstellen werden zumeist unter der Verwendung von Mikrohomologien verknüpft und erfordern daher das Auffüllen der einzelsträngigen DNA-Bereiche durch Polymerasen. POL θ , welche mit Mikrohomologien in Verbindung gebracht wird, agiert in diesem Reparaturweg aber auch die c-NHEJ-assoziierten Polymerasen POL λ/μ sind involviert. Der Ligationsschritt wird von der c-NHEJ Ligase LIG4 durchgeführt und nicht von LIG1/3, welche DSB-Enden während alt-EJ ligieren. Zusammengefasst beschränkt dieser neue Reparaturweg trotz seiner fehlerbehafteten Charakteristiken den Verlust von genetischen Informationen an fehlverknüpften Bruchenden auf ein Minimum. Dies wird erreicht durch die Verknüpfung der Bruchstellen unter der Verwendung von Mikrohomologien, durch die Limitierung der Resektion mithilfe von c-NHEJ Faktoren, sowie mittels der Verhinderung eines endonukleolytischen Schnitts durch MRE11.

Zusammengefasst charakterisiert diese Studie einen neuen, G₁-spezifischen, mutagenen, resektionsabhängigen c-NHEJ Weg in humanen Zellen. Zusätzlich zeigt die Studie, wie Protein-Protein Interaktionen die Entscheidung beeinflussen, diesen DSB-Reparaturweg zu benutzen. Die Kombination von Resektion und c-NHEJ-Faktoren ist ein einzigartiges Merkmal dieses Reparaturwegs, da bisher angenommen wurde, dass sich diese Prozesse gegenseitig ausschließen. Darüber hinaus verdeutlicht die Entdeckung dieses Reparaturweges, dass alt-EJ eine Ansammlung von Backup-Mechanismen ist, um für fehlende Reparaturproteine zu kompensieren. Folglich vereint dieser neue Reparaturweg in der fortlaufenden Diskussion wie genomischen Umlagerungen entstehen, die widersprüchlichen Beobachtungen anderer Studien.

2. Introduction

Deoxyribonucleic acid (DNA) is the carrier of genetic information in all living organisms. Endogenous cellular processes and exogenous sources damage the DNA on a daily basis. Thus, it is of utmost importance for any organism to protect and maintain its genetic information. Failure to do so endangers genomic integrity, which may result in carcinogenesis¹⁴³. Therefore, it is a never-ending quest in biological research to understand the cellular mechanisms that preserve the genome. In addition to the basic research argument to investigate and understand these mechanisms, the knowledge gained in this field has clinical relevance to understand tumor development and to improve cancer treatment possibilities.

2.1. DNA damage response

DNA is a polymer, which consists of a sugar-phosphate backbone and the four bases adenine, thymidine, guanine, and cytosine. It is built from units called nucleotides (nt) and its double helix structure is organized around histone octamers (consisting of two copies each of the histones H2A, H2B, H3, and H4)³⁶³. The arrangement of 147 nt around a histone octamer is called a nucleosome. Nucleosomes form the chromatin, which can be packed in an extended (euchromatin) or condensed (heterochromatin) form¹⁹⁰. DNA can be damaged by a multitude of endogenous and exogenous factors. Intracellular processes, which can result in DNA damage include free radicals in the cell, meiosis, V(D)J recombination, class switch recombination (CSR), and the collapse of replication forks, while external influences include chemotherapeutics, ionizing radiation, and carcinogenic substances^{143,146}. DNA can be damaged in a variety of ways, including base mismatches, bulky adducts, abasic sites, single-strand breaks (SSBs), double-strand breaks (DSBs), and inter- and intrastrand crosslinks^{39,146,248}.

2.1.1. Post-translational modifications

In response to DNA damage, cells react with a variety of measures, which are largely regulated by post-translational modifications of proteins. These modifications include phosphorylation, ubiquitination, SUMOylation, neddylation, methylation, acetylation, and PARylation of specific amino acids in a certain protein to induce the recruitment, activation, inhibition, degradation, and/or interaction of factors^{50,55,307,345}. PARylation, which is also called poly ADP-ribosylation, is catalyzed by PARPs (poly (ADP-ribose) polymerases) to rapidly attach ADP-ribose to the carboxyl group of acidic amino acids following DNA damage induction⁴⁰⁴. In contrast, phosphorylation is executed by kinases and involves the addition of a phosphate group to the amino acids serine (Ser, S), threonine (Thr, T), or tyrosine (Tyr, Y). Kinases associated with the DNA damage response typically target Ser or Thr followed by a glutamine (Gln, Q) after DNA

damage induction ²⁶¹. Several proteins involved in the DNA damage response have a BRCT (BRCA1 C-terminal) domain, which enables the proteins to specifically bind to phosphorylated amino acids. Ubiquitination involves the linkage of the small protein ubiquitin to lysine (Lys, K) residues in a three-step process involving E1, E2, and E3 ubiquitin ligases, while SUMOylation uses SUMO (small ubiquitin-like modifier) and neddylation uses NEDD8 (ubiquitin-like protein NEDD8) ^{50,56,307}. Both methylation and acetylation typically occur at Lys residues and involve the addition of a methyl or acetyl group, respectively ³¹⁶. In concert, these modifications induce a highly-controlled interplay of proteins to initiate and regulate DNA repair, cell cycle control, senescence, and apoptosis ^{39,44,50,55,60,217,307,345}.

2.1.2. Cell cycle control

The reaction to certain types of DNA damage is dependent on the cell cycle phase, and thus it is important to understand the regulation of the cell cycle by cyclin complexes, consisting of regulatory cyclins and CDKs (cyclin-dependent kinases, Figure 2.1) ³¹⁴. The cell cycle consists of gap phase 1 (G₁), synthesis (S), gap phase 2 (G₂), and mitosis. In G₁, complexes of CyclinD with either CDK4 or 6 phosphorylate Rb (retinoblastoma protein) resulting in the release of E2F (E2F transcription factor 1) ⁸⁷. This initiates a positive feedback loop in which CyclinE is upregulated ^{101,225,406}. Subsequently, CyclinE/CDK2 complexes begin to form leading to the transition to S phase by the recruitment of replication factors. This complex is dependent on active CDC25A, which activates it by dephosphorylation ^{101,221,246}. CyclinA/CDK2 takes over during S phase and is replaced by the CyclinB/CDK1 complex in G₂ phase ^{118,221}. This complex is also called mitosis promoting factor since dephosphorylation removes its inhibitory function and results in the initiation of cell division ¹¹⁸. Importantly, due to a high degree of similarity between their active sites, CDK1 can take over for CDK2 ³⁴⁰.

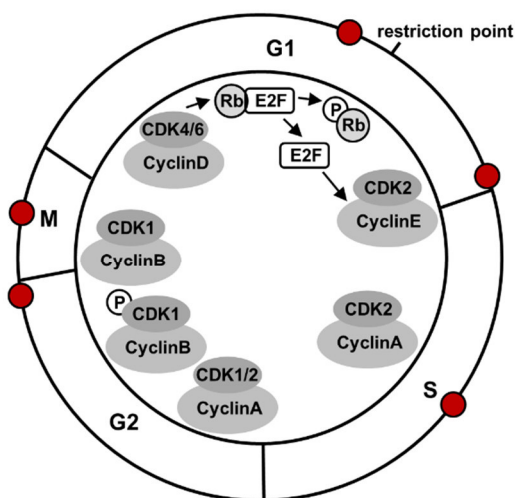


Figure 2.1 Cell cycle regulation

Simplified model of the cell cycle regulation by cyclins and CDKs. The cell cycle consists of 4 phases. In G₁, CyclinD/CDK4/6 dominate and phosphorylate Rb, resulting in the release of E2F and the crossing of the restriction

point. CyclinE/CDK2 is upregulated and the cells can enter S phase where CyclinA/CDK2 prevails. The CyclinB/CDK1 complex must be dephosphorylated for the cells to be able to enter mitosis. The cell cycle is controlled and can be arrested at several points (red circles). Based on Satyanarayana and Kaldis (2009); Bretones et al. (2015).

Checkpoints are able to block the progression of the cell cycle to ensure the integrity of the genome, full DNA replication, and accurate chromosome segregation. The cell cycle can be disrupted in early G₁ phase, during G₁/S transition, intra-S, during G₂/M transition, and in mitosis (Figure 2.1) ^{349,433}.

2.1.3. DNA repair

DNA repair is executed by a multitude of repair mechanisms, which specifically address certain types of DNA damage. Error-free or high-fidelity repair mechanisms include base excision repair, nucleotide excision repair, and mismatch repair, which repair base mismatches, abasic sites, bulky adducts, SSBs, and other varieties of minor DNA damage ^{39,403}. Compared to these high-fidelity mechanisms, other DNA repair pathways deal with DNA damage that is more difficult to repair, namely DSBs and inter- and intrastrand crosslinks. However, the cell has developed specific mechanisms to recognize and deal with even the most dangerous DNA damage, namely the DSB (chapter 2.2). In addition to highly effective DNA repair pathways that maintain genetic information, cells also employ error-prone mechanisms, which are associated with loss of genetic information and thus play a key role in the initiation of carcinogenesis ^{51,161,413}. The impairment of genes encoding proteins involved in DNA repair pathways can favor mutagenic events and enhance the possibility of carcinogenesis and tumor progression ¹⁴³. In fact, the combination of defective genes and the use of error-prone repair mechanisms allows cancer cells to accumulate DNA damage and enhance their genomic instability to develop further mutations ^{134,193}. Indeed, targeting these molecular mechanisms is a growing and promising field in cancer treatment ²⁴⁸.

2.2. Double-strand break repair

The most severe type of DNA damage is the DSB because it endangers genome stability by impairing the genetic information on both DNA strands ²⁹⁷. On average, 10 DSBs arise endogenously each day in a human body ²⁴². There are several mechanisms to repair DSBs and the pathway choice is dependent on the cell cycle phase, the chromatin status, and the complexity of the DSB. The different DSB repair pathways vary in their speed and accuracy. How these DSB repair mechanisms are orchestrated is of specific interest.

2.2.1. DSB Recognition

First, DSBs need to be recognized (Figure 2.2). Central to the recognition of DNA DSBs are the MRN (MRE11 (meiotic recombination 11), RAD50 (radiation repair protein 50), and NBS 1 (Nijmegen breakage syndrome 1)) complex and the KU (KU70 (XRCC6, X-ray repair cross-

complementing protein 6) and KU80 (XRCC5, X-ray repair cross-complementing protein 5)) heterodimer^{95,303,342,431}. The rapid recruitment of MRE11 and NBS1 to the DSB ends is dependent on PARP1¹⁵⁸. MRN and KU hold the DSBs together^{95,188} and recruit the PIKKs (phosphatidylinositol 3-kinase-related kinases) ATM (ataxia telangiectasia mutated) and DNA-PKcs (DNA-dependent protein kinase catalytic subunit), respectively^{65,119,311}. Together KU70/80 and DNA-PKcs form the DNA-PK (DNA-dependent protein kinase) holoenzyme¹⁸⁸. Contrary to former assumptions^{79,125}, it has only recently been shown that MRE11 and KU do not affect the recruitment of each other to DSBs with KU binding directly to the DSB end and MRN associating with the side^{11,64,74,184,435}. A model was proposed suggesting that large complexes of DNA-PK and MRN/ATM assemble at the DSBs right after damage induction wherein DNA-PKcs regulates ATM activity through phosphorylation⁴³⁵. ATM is activated via an interaction with NBS1 but implemented by autophosphorylation^{21,119,342}. The active PIKKs are able to phosphorylate the histone variant H2AX at Ser139 to form γ H2AX (Figure 2.2)^{58,368,398}. Mechanistically, this is caused by a positive feedback loop, allowing the γ H2AX signal to spread 1 to 2 megabase pairs (Mbp)^{17,329,386}. In the presence of single-stranded DNA (ssDNA), the PIKK ATR (ATM- and Rad3-related) can also conduct this phosphorylation. Next, ATM and MRN recruit MDC1 (mediator of DNA damage checkpoint protein 1) to bind to γ H2AX^{211,367} and together they recruit RNF8 (E3 ubiquitin protein ligase RING finger protein 8). In concert with UBC13 (ubiquitin conjugating enzyme E2 N) and HERC2 (HECT and RLD domain-containing E3 ubiquitin protein ligase 2) RNF8 ubiquitinates histone H2A and its variants^{8,31,174}. This allows the binding of another ubiquitin protein ligase, RNF168, to ubiquitinated H2A type histones, which then interacts with UBC13 and amplifies the RNF8-dependent ubiquitination^{8,14,110}. This chain of interactions builds the binding platform for several proteins involved in DNA repair, including BRCA1 (breast cancer susceptibility protein 1)^{55,393}. Importantly, BRCA1 also forms a complex involving MRN, which is exclusive to S/G₂ phase⁷⁸.

Just like BRCA1, 53BP1 (tumor suppressor p53-binding protein 1) is recruited to the DSB by several mechanisms. First, its BRCT2 domain binds directly to γ H2AX²³. Second, ubiquitination of H2A at Lys15 allows 53BP1-binding via its ubiquitin-dependent recruitment (UDR) motif^{3,301}. In addition, 53BP1 binds to Lys20 dimethylated histone H4 (H4 Lys20me2) via its Tudor domain, which is facilitated through several mechanisms: one such mechanism is the ubiquitin-dependent removal of L3MBTL1 (lethal (3) malignant brain tumor-like protein) from H4 Lys20me2 by VCP (valosin-containing protein)^{3,301}. VCP is a factor that targets ubiquitinated proteins to segregate them from binding partners or cellular structures⁴⁵. In fact, H4 Lys20me2 guides 53BP1 to pre-replicative chromatin³⁰⁸. Moreover, the methyl-histone-binding Tudor domain enables 53BP1 to interact constitutively with chromatin in the absence of DNA damage,

which is a weak interaction compared to the damage-inducible localization of 53BP1 at the DSB ^{30,49,179,430}. Recently, TIRR (Tudor interacting DNA repair regulator) was discovered to interact with the Tudor domain of 53BP1 restricting the access of 53BP1 to chromatin prior to DNA damage ¹¹². RNF168 ubiquitinates and ATM phosphorylates 53BP1 to control its downstream response to DSBs ^{43,127}. The phosphorylation is required for 53BP1 to interact with RIF1 (RAP1-interacting factor homolog) and PTIP (PAXIP1, PAX interacting protein 1) ^{96,127,186,353,369}. The interaction with RIF1 disrupts the TIRR-53BP1 complex and allows for proper 53BP1 localization to the chromatin ¹¹². In S/G₂ phase of the cell cycle, 53BP1 is dephosphorylated by PP4C (Ser/Thr-protein phosphatase 4 catalytic subunit) if timely DSB repair does not occur ^{186,353}. This is promoted by BRCA1 in concert with BARD1 (BRCA1-associated RING domain protein 1) to disrupt the phosphorylation-dependent 53BP1 interaction with RIF1 and PTIP (Figure 2.2) ^{96,127,186,353}. Another important factor to abort RIF1-binding to 53BP1 is SCAI (suppressor of cancer cell invasion) ¹⁸⁵. Therefore, the late downstream signaling of the DSB recognition differs in G₁ phase compared to S/G₂, which has an impact on the DSB repair pathway choice ^{178,353}.

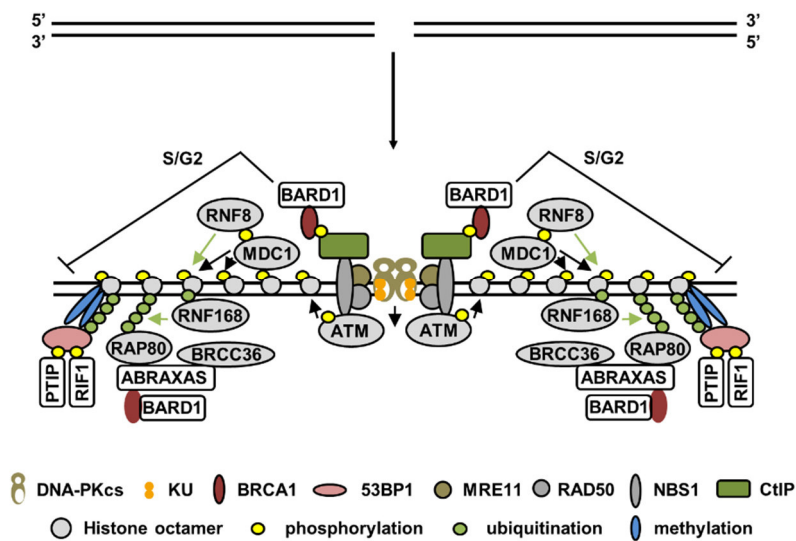


Figure 2.2 DSB recognition

Simplified model for the DSB recognition. The DSB is recognized by the KU heterodimer and the MRN complex. KU recruits DNA-PKcs and MRN recruits ATM. DNA-PKcs regulates the ATM activity. The two kinases phosphorylate the histone variant H2AX, which expands via a positive feedback loop. MRN and ATM recruit MDC1 to bind to γ H2AX, which then recruits RNF8. RNF168 binds to RNF8-dependent ubiquitin chains and subsequently builds the platform for many downstream factors. 53BP1 binds to methylated and ubiquitinated histones as well as γ H2AX. In S/G₂ phase, BRCA1-BARD1 promotes 53BP1 dephosphorylation. Based on van Attikum and Gasser (2009); Panier and Boulton (2014); Brown and Jackson (2015); Feng et al. (2015); Shibata (2017).

2.2.2. Homologous recombination (HR)

Homologous recombination (HR) is a high-fidelity DSB repair pathway because it utilizes homologous sequences as a template for repair. In human cells, HR is limited to S/G₂ phase of the cell cycle since it requires the presence of the sister chromatid to use as a matrix for DNA

synthesis^{138,200}. DSB repair by HR is conducted in a slow process and is associated with the remodeling of the chromatin^{34,147,204,288}. HR repair is the preferred repair pathway for DSBs resulting from replication errors such as stalled replication forks, complex DSBs from high-LET (linear energy transfer) irradiation, DSBs in H3 Lys36me3-decorated transcriptionally active regions, and DSBs in heterochromatic regions identified by H3 Lys9me3 and H4 Lys20me^{13,17,74,75,140,147,202,288,312}. HR can be divided into three sections: the degradation of one DNA strand to generate large regions of ssDNA, the strand invasion of the sister chromatid by the generated 3' ssDNA tail, and the template DNA synthesis and subsequent dissolution/resolution of HR intermediates^{262,337}. The degradation of one DNA strand is executed by a process called resection in which the hydrolysis of the phosphodiester bond (the linkage between two nucleotides) is catalyzed by nucleases²⁴⁹. Overcoming the barriers opposing resection in a regulated manner is crucial for efficient HR.

Central to the initiation of HR is the binding of the MRN complex to the DSB and subsequent recruitment of ATM (Figure 2.3)^{95,189}. Due to its limitation to S/G₂ phase, HR is initiated in a cell cycle-dependent manner. As mentioned in chapter 2.2.1, BRCA1 promotes the dephosphorylation of ATM-phosphorylated 53BP1 if timely DSB repair does not occur, and thus disrupts 53BP1's interaction with RIF1 and PTIP^{96,127,178,186,353}. This is possible due to the cell cycle-dependent formation of the BRCA1-C complex, which consists of the MRN complex, CtIP (CtBP-interacting protein), BRCA1, and BARD1^{78,183,295}. The formation of this complex is dependent on the interaction of BRCA1 with CtIP, which requires the constitutive activation of CtIP by phosphorylation at Ser327 through the S/G₂-specific CDK2/CyclinA complex (Figures 2.1, 2.3)⁴²⁸. Furthermore, CtIP is activated upon damage induction by SIRT6 (sirtuin-6)-dependent deacetylation^{75,201} and the SUMOylation of CtIP by CBX4 (E3 SUMO-protein ligase chromobox 4) is required for the recruitment of CtIP to damaged DNA³⁶⁰. The speed of resection is impaired in the absence of BRCA1 or if the BRCA1-CtIP interaction is blocked⁹³. Terminating RIF1-binding to 53BP1 allows BRCA1 to antagonize the anti-resection function of 53BP1, a process that is not yet fully understood. However, it has been shown that BRCA1-BARD1 ubiquitinates H2A Lys217 to allow SMARCAD1 (SWI/SNF-related matrix-associated actin-dependent regulator of chromatin subfamily A containing DEAD/H box 1)-binding, which results in the repositioning of nucleosomes including the bound 53BP1 (Figure 2.3)^{89,105}. The repositioning of 53BP1 is further promoted by SETDB1 (SET domain bifurcated 1), HP1 (CBX5, chromobox protein homolog 5), and SUV39 (suppressor of variegation 3-9 homolog 1)⁹. Nevertheless, 53BP1 also contributes to the remodeling of the chromatin during HR by tethering ATM at DSBs, which is known to phosphorylate and thus inactivate the heterochromatin building factor KAP1 (KRAB domain associated protein 1)^{141,204}. An additional barrier to

prevent resection is posed by RAP80 (BRCA1-A complex subunit RAP80). To overcome this barrier, BRCA1 primes 53BP1 to allow POH1 (26S proteasome non-ATPase regulatory subunit 14) access to remove RAP80^{203,283}. Moreover, the autophosphorylation of DNA-PKcs, a key step during DSB repair by end-joining (see next chapter 2.2.3), is attenuated by BRCA1 in a cell cycle-dependent manner and thus promotes repair by HR¹⁰⁰.

End resection during HR is conducted bi-directionally in two steps, short-range and long-range resection (Figure 2.3)^{135,354}. The key factor for short-range resection is MRE11 with its single-stranded endonuclease activity and its double-stranded 3' to 5' exonuclease activity^{304,383}. Resection is initiated by the MRN complex in concert with CtIP phosphorylated at Thr847 via the endonuclease function of MRE11, which induces a nick internal to the DSB^{75,177,339}. Subsequently, short-range resection takes place in a 3' to 5' direction towards the DSB through the exonuclease function of MRE11, which was assumed to create 50 to 300 base pair (bp) regions of ssDNA due to studies in the *Saccharomyces cerevisiae* system^{61,93,233,274}. However, Anand et al. (2016) revealed that the endonucleolytic cut is preferentially initiated roughly 20 nt away from the 5' terminus in the human system. Moreover, they showed that Thr847-phosphorylated CtIP and NBS1 have structural roles to promote DNA cleavage by the nuclease activity of MRE11 and the ATPase activity of RAD50, while the endonuclease activity of CtIP is dispensable. Furthermore, they observed that a second MRN-phosphorylated CtIP (pCtIP) complex can subsequently bind to induce an additional cut, which would allow 3' to 5' resection in a stepwise manner even beyond 20 nt. 3' to 5' resection is accelerated through the 3' to 5' exonuclease activity of EXD2 (exonuclease 3'-5' domain-containing protein 2), a CtIP-interacting protein⁵³.

The resulting ssDNA is coated with RPA (replication protein A) for stability and to prevent the formation of secondary structures³⁷. RPA is a heterotrimeric protein complex which binds the ssDNA in multiple steps⁴¹: the initial binding requires a ssDNA region of 8 to 10 nt while the stable binding of an RPA molecule is only possible at roughly 30 nt of ssDNA⁴². Another important step to ensure accurate resection is the removal of the KU heterodimer. It is not entirely clear when exactly KU is removed; however, multiple studies indicate that KU removal requires short-range resection and needs to be executed before long-range resection can take place^{74,75,128,184}. The removal of KU is not completely understood either, but it seems to entail a combination of KU phosphorylation, KU ubiquitination, and subsequent removal of KU from the DSB. Indeed, it was proposed that multiple mechanisms act simultaneously⁷⁴. KU70 is phosphorylated by S/G₂-specific CyclinA/CDK1/2 at Thr455 (Figure 2.1)^{81,128}. A connection between KU70 phosphorylation and DNA end resection was only recently found. In a structural-based approach, Lee et al. (2016) showed that phosphorylation of KU70 at the adjacent pillar

and bridge region (which is vital for the ring-like structure of the KU heterodimer around the DNA) induces a conformational change to allow KU dissociation by a lowered binding affinity, which they observed to be necessary for accurate DNA end resection. In addition, 3' to 5' resection has been shown to facilitate KU release where MRE11 exonuclease activity creates a DNA flap, which needs to be cleaved by the endonuclease activity of CtIP^{74,75,224}. Other studies focus on the importance of the ubiquitination of KU for its removal from DSB ends. Ismail et al. (2015) showed that RNF138, which binds to ssDNA or resected dsDNA (double-stranded DNA) overhangs, ubiquitinates KU80 to promote the removal of the KU heterodimer. Ubiquitinated KU is targeted and removed from the DNA by VCP⁴⁵.

To create large regions of 3' ssDNA tails, long-range resection is conducted from the MRE11-induced nick in a 5' to 3' direction by EXO1 (exonuclease 1)/BLM (Bloom syndrome protein) and/or BLM/DNA2 (DNA replication ATP-dependent helicase/nuclease DNA2)/WRN (Werner syndrome ATP-dependent helicase, Figure 2.3)^{67,287,382}. The MRN complex continues to play an important role by recruiting 5' to 3' resection factors³⁷¹. In addition, the recruitment of EXO1 and BLM is promoted by the ATM-mediated phosphorylation of CtIP, which is only possible after CtIP is already hyper-phosphorylated following DNA damage induction by CDK complexes³⁹⁷. EXO1 has 5' to 3' dsDNA exonuclease activity, endonuclease activity on 5' flaps^{227,230}, and is phosphorylated at Ser639, Thr732, and Ser815 by S/G₂-specific CDK complexes^{128,349}. Several studies indicate that full EXO1 activity requires stimulation by factors such as MRE11, CtIP, BRCA1 and/or additional unknown proteins^{62,121,169,170,373,381,382}. In fact, it has been shown that EXO1 is removed from ssDNA by RPA if it is not supported²⁸². The current working model suggests an initial stimulation of EXO1 activity by the MRN complex and/or its interaction partners, which is then assumed by BLM for the majority of the 5' to 3' resection process¹⁶. BLM and WRN are both RecQ helicases, which unwind dsDNA, including secondary structures, by translocating along ssDNA in a 3' to 5' direction^{92,352}. In addition to EXO1-dependent resection, 5' to 3' resection is also conducted with either BLM and/or WRN in concert with DNA2^{16,371}. RPA stimulates the unwinding of the DNA by the helicases and binds the unwound 3' strand to protect it from digestion¹⁶. DNA2 has endonuclease activity and thus RPA directs the DNA2 nuclease activity towards the degradation of the 5' strand in a stepwise endonucleolytic digestion^{16,240,282}.

The finely-tuned resection process generates 2 to 4 kilobases (kb) of ssDNA in each direction of the DSB with a reduced nucleosome occupancy within 1 kb of the DSB^{17,434}. Therefore, another important part of the resection process is the limitation of the resection length. Indeed, HR is impaired in 53BP1-depleted cells where hyper-resection takes place^{203,204,292}. Central to the suppression of excessive resection is the BRCA1-A complex with the core components BRCA1,

ABRAXAS (BRCA1-A complex subunit Abraxas 1), RAP80, BRCC36 (BRCA1/BRCA2-containing complex subunit 36), and BARD1 (Figure 2.3)^{66,162,283,395}. Importantly, while the assembly is hierarchical, the BRCA1-A complex is dynamic, as the components undergo changes in their internal protein-protein interactions¹⁶⁷. The BRCA1-A complex is formed downstream of the γ H2AX pathway (Figure 2.2) and is therefore assembled at a slower rate than the pro-resection BRCA1-C complex, which it competes with to limit resection^{83,283,295}. For the BRCA1-A complex to prevail, it seems to be essential that the BRCA1-C complex is disrupted. This might be achieved by the degradation and/or inactivation of CtIP through several mechanisms. CtIP inactivation is achieved through its constitutive acetylation by an unknown Lys acetyltransferase^{75,201} and may also be influenced by its neddylation¹⁹⁹. Despite the role of the ATM-dependent phosphorylation of CtIP in recruiting long-range resection factors, hyperphosphorylation of CtIP has also been associated with the dissociation of the BRCA1-CtIP interaction in response to damage induction^{238,281}. This includes CtIP phosphorylation at Ser276 and Thr315 by S/G₂-specific CDK complexes following the initiation of resection, resulting in PIN1 (Peptidyl-prolyl cis-trans isomerase NIMA-interacting 1)-binding to CtIP, which leads to the ubiquitination and subsequent degradation of CtIP³⁶⁶. In another mechanism, long-range resection is limited by HELB (DNA helicase B), which is recruited to ssDNA in an RPA-dependent manner³⁸⁰. Importantly, HELB is phosphorylated in S/G₂ by CDK2 complexes leading to its nuclear export and consequent low HELB concentrations in the nucleus. In contrast, nuclear HELB concentrations are high during G₁ phase, which counteracts long-range resection and thus also makes HELB an important factor in DSB repair pathway choice³⁸⁰.

The next step in HR requires a complex of BRCA1/BRCA2/PALB2 (partner and localizer of BRCA2), which is regulated by ATR-activated CHK1 (checkpoint kinase 1) and ATM-activated CHK2 (checkpoint kinase 2)¹⁹. Interestingly, the assembly of the complex is cell cycle-dependent and key in limiting HR to S/G₂ phase²⁹⁹. The BRCA1/BRCA2/PALB2 complex interacts with RAD51 (DNA repair protein RAD51 homolog 1) and is responsible for placing it on the ssDNA under RPA displacement^{77,306,374}. Importantly, if KU is not removed at this stage, RPA cannot exchange with RAD51⁷⁴. RAD51 forms a nucleoprotein filament, which is pivotal for the strand invasion of the sister chromatid and the subsequent homology search^{208,337,407}. Finally, the DNA strand is elongated by DNA polymerases, HR intermediates are dissolved or resolved by helicases and nucleases, and the DNA ends are ligated^{168,262}.

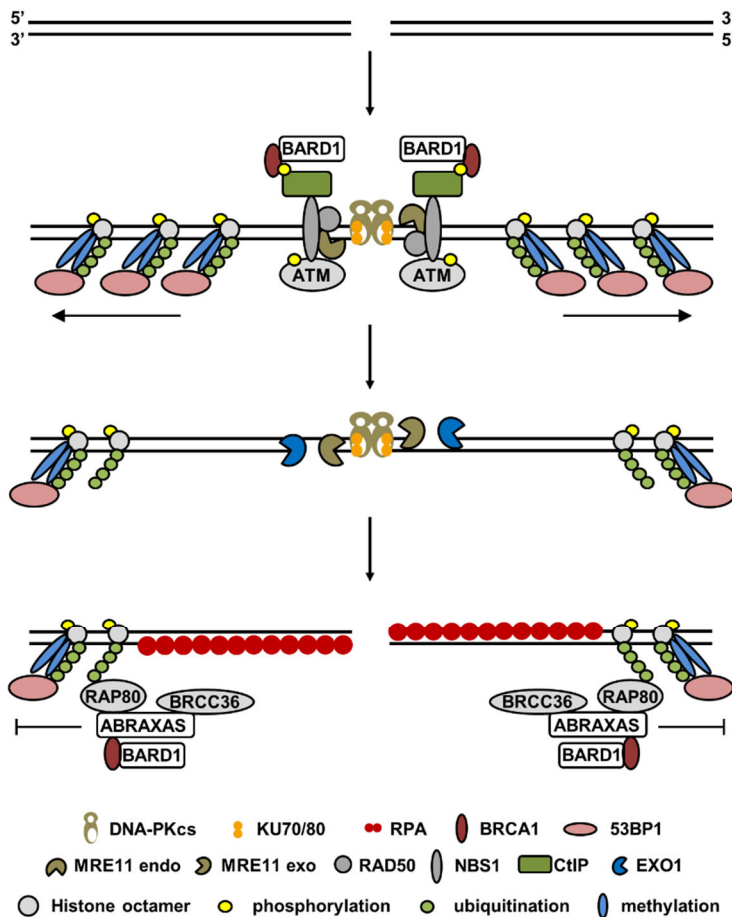


Figure 2.3 Homologous recombination (HR)

Simplified model for bidirectional resection during HR. Resection barriers are overcome in a cell cycle-dependent manner by BARD1/BRCA1/CtIP-pS327, which involves the displacement of 53BP1. Resection is initiated by an endonucleolytic cut internal to the DSB end by MRN/CtIP-pT847. From that nick, short-range resection is conducted by the 3' to 5' exonuclease activities of MRE11 and EXO2, while long-range resection is executed by the 5' to 3' exonuclease activity of EXO1 or the 3' to 5' helicase activity of BLM or WRN in concert with the endonuclease activity of DNA2. KU is removed from the DSB ends and RPA protects the generated ssDNA. Resection is limited by the BRCA1-A complex. Based on Coleman and Greenberg (2011); Ohta et al. (2011); Savage and Harkin (2015); Hustedt and Durocher (2017).

2.2.3. Canonical non-homologous end-joining (c-NHEJ)

DSB end-joining repair is the joining of the two DSB ends. In contrast to HR, end-joining is active in all cell cycle phases. However, different end-joining mechanisms exist and the deployment of each mechanism is dependent on the structure of the break ends, the chromatin status, and the availability of repair factors. Canonical non-homologous end-joining (c-NHEJ) is responsible for the repair of the majority of DSBs. It is a simple rejoining of the DNA ends, which is sufficient to repair regular DSBs quickly. In a simplified model, KU70 and KU80 protect the DSB ends and together with the catalytic subunit DNA-PKcs, form DNA-PK to hold the break ends together^{85,188}. The XRCC4 (X-ray repair cross-complementing protein 4)/XLF (XRCC4-like factor, also Cernunnos)/LIG4 (DNA ligase 4)/PAXX (paralog of XRCC4 and XLF) complex then

joins the ends ^{6,191,290,345}. However, there is much more detail worth mentioning in the c-NHEJ process.

The KU70/80 heterodimer is rapidly recruited to DSBs and binds the DNA ends under the formation of a ring-like structure (Figure 2.4) ³⁹⁴. KU prevents nucleolytic degradation of the DNA ends and recruits and interacts with an array of NHEJ proteins ^{151,239,362}. KU recruits and interacts with DNA-PKcs to form the DNA-PK holoenzyme ¹⁸⁸. For DNA-PKcs to bind, KU translocates from the DSB end inwards for a distance of roughly 10 bp, which equals one helical turn ^{271,321,424}. The two DNA-PK molecules at the DSB ends form a long-range complex and thus keep the break ends in proximity ^{103,149,231}. KU also interacts with PAXX, which promotes KU accumulation at DSB ends ^{244,290}. Additionally, KU80 rapidly recruits BRCA1 to the DSB in G₁ phase and this interaction is required for the stabilization of KU80 at the break end and precise joining of the ends ^{197,336,405}. Concurrently, BRCA1 interacts with the MRN complex to suppress the nuclease activity of MRE11 in G₁ phase through its interaction with NBS1 ^{336,412} and DNA-PKcs phosphorylates ATM to inhibit its activity ⁴³⁵. Both mechanisms channel repair towards c-NHEJ. Another factor rapidly recruited to DSBs is PARP1. Although KU and PARP1 compete to bind to the broken DNA ends and KU limits but does not prevent PARP1 recruitment to the DSBs, PARP1 regulates and promotes c-NHEJ by a number of mechanisms ^{79,275,401}. PARP1 acts at DSBs in the presence of KU and contributes to DSB repair via c-NHEJ by rapid chromatin expansion in concert with CHD2 (chromodomain-helicase-DNA-binding protein 2), which coincides with the efficient distribution of XRCC4 ²⁵⁰. PARP further regulates efficient NHEJ through the retention of KU at the DSBs, which is realized by the KU70 PAR-interacting motif ⁹⁰. Finally, PARP1 stimulates DNA-PKcs kinase activity and can form a complex with DNA-PK to influence the DNA-PK conformational change required for c-NHEJ ^{85,334,361,404}.

KU also recruits the XRCC4/LIG4 complex and XLF (Figure 2.4) ^{6,150,191,259,263,379,422}. DNA-PKcs enhances the recruitment of XRCC4 and XLF and in return, XRCC4/LIG4 potentiates the association of KU with DNA-PKcs ^{85,113}. Additionally, LIG4 recognizes the PAR chains by PARP1, which further mediates the rapid recruitment of the LIG4 complex ⁴⁰⁴. XRCC4 and XLF interact directly ⁶ and XLF/XRCC4/LIG4 form a filament along the DNA ³²³. The XRCC4/XLF/LIG4 filaments on both DSB ends align in a side-by-side position to then pair the DSB ends in an end-to-end configuration ^{54,187,323}. While KU and DNA-PKcs are both required for the connection of the DNA ends in the aforementioned long-range complex, the end-to-end alignment of the DSB ends marks the beginning of the second phase of c-NHEJ ¹⁴⁹. Within seconds of the formation of the long-range complex, the ends are brought together into a short-range complex. This transition is dependent on the catalytic activities of DNA-PK and XLF/XRCC4 ^{149,323}. The interaction of two DNA-PK molecules in combination with the stimulating contact of DNA-PKcs

with the DNA induces the autophosphorylation of DNA-PK, which disrupts the DNA-PK complex (Figure 2.4) ^{40,108,267,271}. It is not entirely clear how this disruption and subsequent release of the complex is orchestrated with the later steps of c-NHEJ ¹⁰⁹. However, it has been shown that autophosphorylation leads to an immediate conformational change and releases DNA-PKcs from the break ends ^{267,388}. Structural analyses have observed that DNA-PK also exists in a form where DNA-PKcs does not interact with the DNA but is loosely bound to the “arm” of KU80 ⁴⁰⁹. Therefore, despite its release, DNA-PKcs might remain at the DSB ends due to this interaction. Another model proposes that the autophosphorylation of DNA-PKcs at two described clusters is conducted in multiple steps ²⁸⁵. In such a model, the autophosphorylation of the cluster adjacent to the putative DNA-binding domain (PQR) is conducted first and promotes the NHEJ process, while the autophosphorylation of the clustered ABCDE site causes the release of DNA-PKcs ^{285,409}. In any case, the intermolecular autophosphorylation of DNA-PKcs is required to relieve the physical block at the end ligation step, which is imposed by DNA-PKcs localization to the DSB ends ¹⁹⁸.

Before ligation can occur, most DSB ends need to be modified (Figure 2.4) ⁷¹. A variety of factors is involved in the processing and gap filling prior to ligation ¹⁰⁹. The extent to which the DSB ends are processed prior to DNA-PKcs release is not completely understood. However, one nuclease involved in the alteration of the DSB ends is ARTEMIS, which is recruited and interacts with DNA-PKcs following the phosphorylation of DNA-PKcs by ATM ¹⁹⁸. The DNA-PKcs phosphorylation sites on which the recruitment of ARTEMIS is dependent, are distinct and phosphorylated prior to the aforementioned DNA-PKcs intermolecular autophosphorylation sites ¹⁹⁸. Of note, DNA-PKcs autophosphorylation can occur at these sites in the absence of ATM. ARTEMIS is known to process common DNA substrates such as blunt ends, 3' overhangs, 5' overhangs, and is the only vertebrate endonuclease capable of opening hairpins ^{70,114,251}. It has been suggested, that ARTEMIS uses three contact points on its DNA substrates under the formation of a hairpin-like structure ⁷⁰. The first contact point is located on the 5' to 3' strand at the ssDNA/dsDNA transition, the second is directly across from the first on the 3' to 5' strand, and the third contact point with the catalytic site is located an equivalent distance of 1 nt in the 5' direction from the second contact point ⁷⁰. Consequently, an endonucleolytic cut by ARTEMIS mostly creates a 3' overhang but can also create a blunt end. With the formation of the aforementioned short-range complex, the DSB ends are bridged by the XRCC4/XLF/LIG4 filament (Figure 2.4) ^{54,323}. The assembly, activity, and retention of the XRCC4/XLF/LIG4 complex is promoted by APLF (aprataxin and PNK-like factor) to accelerate the ligation process ^{151,333}. The processing of the DSB ends probably continues beyond the release of DNA-PKcs. ARTEMIS also interacts with LIG4, suggesting that ARTEMIS might further contribute to the

processing of the DNA ends with its 5' to 3' exonuclease activity, which is suppressed by its interaction with DNA-PKcs^{151,182,270}. Other nucleases proposed to be involved in the processing step are MRE11 and APLF, which both have a 3' to 5' exonuclease activity^{322,378,404}. Furthermore, WRN interacts directly with KU and promotes c-NHEJ via its helicase and 3' to 5' exonuclease activity (Figure 2.4)^{88,298,350}.

In addition, gap-filling is required at non-complementary termini during c-NHEJ¹⁵¹. Two polymerases are connected to c-NHEJ, namely POL λ (DNA polymerase lambda) and POL μ (DNA-directed DNA/RNA polymerase mu)^{63,124,253,293,388,420}. POL λ is associated with high-fidelity repair. This polymerase connects clean 3' to 5' gaps of a paired terminus and conducts error-free NHEJ by accurate gap-filling⁴²⁰. POL μ is involved in the end-bridging of non-complementary DNA ends as it occurs in V(D)J recombination (see chapter 2.2.5). Furthermore, POL μ has no proofreading activity, is known for its template-independent DNA synthesis and high frequency of 1 bp deletions resulting in a frameshift^{293,420}. The template-independent addition of nucleotides leans heavily towards the addition of thymidine^{152,153}. Finally, ligation of the “clean” DSB ends can take place via the LIG4 complex (Figure 2.4). Importantly, LIG4 is capable of ligating nicks and compatible 4 nt overhangs on its own but requires XRCC4 to ligate ssDNA or long 3' and/or 5' overhangs, which is only possible when the DNA end consists of more than one thymidine^{152,153}. LIG4/XRCC4 can also ligate DSB ends that share 2 bp of microhomology (MH; which are identical short sequences of base pairs terminal or internal to both sides of the DSB) and/or have 1 nt gaps, which is further stimulated by XLF²⁴². In the presence of KU, the XRCC4/XLF/LIG4 complex additionally ligates blunt ends and at low efficiencies, even incompatible DNA ends^{152,153,242}. The trapped KU is ubiquitinated for the disassembly of the NHEJ machinery after or near completion of the c-NHEJ repair process (Figure 2.4)²⁶⁸. Two E3 ubiquitin ligases have been proposed to conduct this ubiquitination during c-NHEJ, RNF8 and the SCF (Skp, Cullin, F-box containing) complex^{126,317,318}. The ubiquitination of KU is promoted by its neddylation⁵⁶. Finally, the ubiquitinated KU80 is recognized and removed by VCP⁴⁵.

The complexity, location, and structure of the break ends greatly dictates which factors are involved in the c-NHEJ process and the outcome of repair^{72,145,302,370}. When the two DSBs are “clean” without any modification, even DNA-PKcs is not required for c-NHEJ repair^{71,326}. Indeed, biochemical studies have shown that the KU-DNA-PKcs complex formation is highly dependent on the structure of the DNA ends and preferentially forms on dsDNA with a 3' or 5' poly-pyrimidine ssDNA extension³²⁰. Although it has been shown that translocations (which are interchromosomal genomic rearrangements) in human cells arise from c-NHEJ, it is an ongoing discussion as to how error-prone c-NHEJ truly is^{33,142,302}.

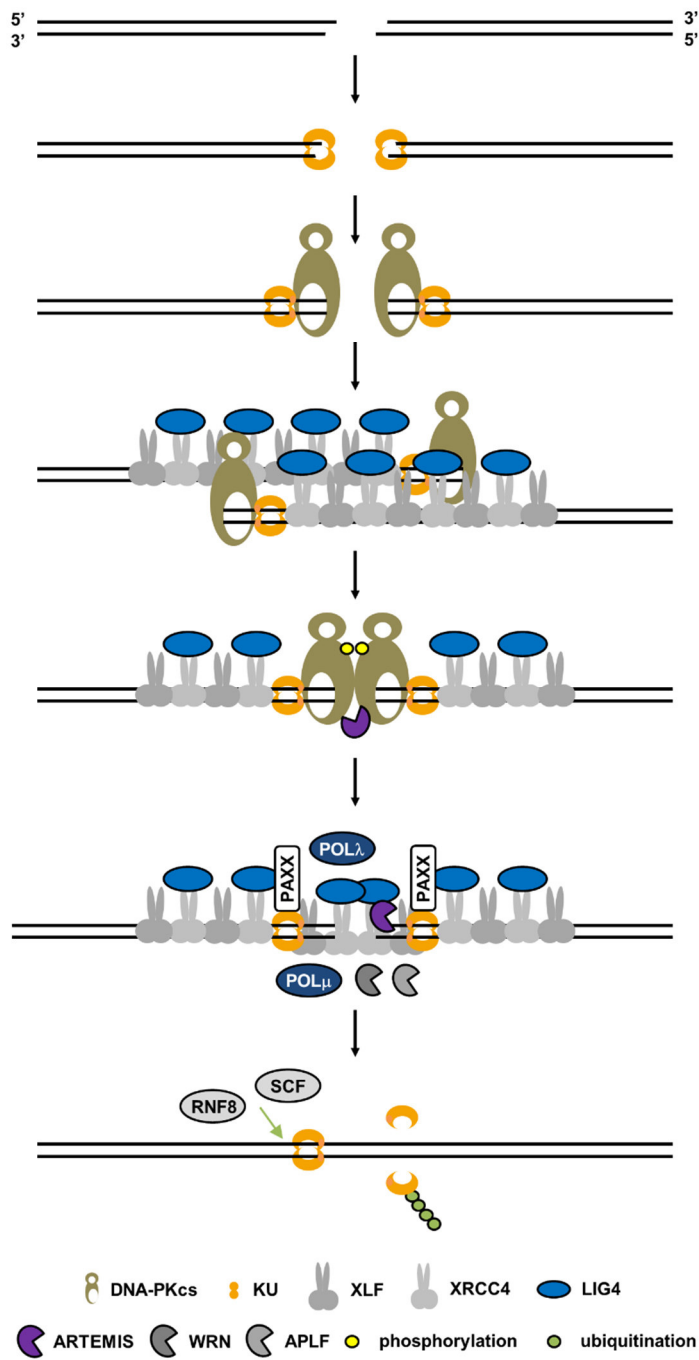


Figure 2.4 Canonical non-homologous end-joining (c-NHEJ)

Simplified model of c-NHEJ. The KU70/80 heterodimer rapidly binds to the DSB ends under formation of a ring-like structure and recruits DNA-PKcs, XRCC4/LIG4, and XLF. KU translocates inwards to allow DNA-PKcs-binding. XRCC4/LIG4/XLF builds a filament along the DNA. These filaments on both sides of the DSB interact with each other to initiate the alignment of the DSB ends in an end-to-end configuration. The catalytic activity of DNA-PKcs activates ARTEMIS and together with the catalytic activity of XRCC4/LIG4 brings the break ends together from a long-range to a short-range complex. The DNA-PK autophosphorylation disposes of DNA-PKcs and the XRCC4/LIG4/XLF filament bridges the two DSB ends. Of note, here this is displayed in two steps but is more likely a fluent process. PAXX is bound to KU and is required for the efficiency of the ligation complex. The DSB ends are processed by nucleases and gaps are filled by polymerases. After ligation, KU is disposed of by ubiquitination. Based on Grundy et al. (2014); Williams et al. (2014); Reid et al. (2015); Graham et al. (2016); Chang et al. (2017).

2.2.4. Error-prone end-joining

As mentioned in chapter 2.1.3, error-prone repair mechanisms are considered to be a driving force in carcinogenesis^{51,161,413}. Additionally, cancer cells are frequently mutated in genes encoding proteins involved in repair or cell cycle control and exploit error-prone repair mechanisms^{134,143,193}. Just like c-NHEJ, error-prone end-joining mechanisms consist of three steps: the recognition of the DSB, the processing of the break ends, and the ligation¹³¹. However, error-prone DSB repair utilizes other factors compared to c-NHEJ, which results in the frequent occurrence of deletions and/or insertions of base pairs^{106,260,265,322}. Deletions arise by resection and the subsequent misrejoining of DNA regions adjacent, near, or distant from the DSB ends. Error-prone end-joining mechanisms are associated with all sizes of deletions but many studies have observed a significant number of deletion sizes above 50 and up to several hundred nucleotides^{257,401,414}. As described in chapter 2.2.3, DSBs are also processed during c-NHEJ. However, this processing is believed to result in losses of only up to 4 nt^{226,265,322}.

Microhomology-mediated end-joining (MMEJ)

One error-prone end-joining mechanism is microhomology-mediated end-joining (MMEJ). This pathway rejoins DSBs using microhomologies (MHs), which are identical short sequences of base pairs terminal or internal to both sides of the DSB^{38,102,207}. As mentioned in chapter 2.2.3, small MHs (some studies have observed up to 5 nt MHs) at the rejoined break end are also observed in c-NHEJ^{226,265,302,322}. Therefore, the definition of MMEJ in regard to the size of a MH varies in different studies. Some working groups refer to MHs of up to 25 nt with a minimum of 5 nt^{106,226,265}. Recent investigations revealed that MMEJ-mediated rejoining in human cells can be conducted with as little as 1 nt of MH, but the preferred length used by the involved polymerase is at least 3 nt^{38,207,346,347}.

To initiate MMEJ, multiple domains of PARP1 bind to DNA, which results in interdomain contact that rapidly activates PARP1 via an intramolecular mechanism (Figure 2.5)²²³. The subsequent PARP1 automodification builds a scaffold to recruit further factors such as the MRN complex^{346,375,404}. MRN bridges the DSB ends to keep the breaks in proximity^{146,431}. Resection during MMEJ is predominantly thought to be conducted by MRN in complex with CtIP, which initiates a nick internal to the DSB end and then conducts resection in a 3' to 5' direction towards the break end, resulting in 3' overhangs^{38,346,410}. However, contradictory studies report that EXO1 and/or BLM/DNA2 execute resection in the 5' to 3' direction²⁶⁰. It is unclear if there is a decision between these two types of resection or if both exist simultaneously as is the case for *S. cerevisiae*³⁴⁷. In any case, resection is delayed in cells lacking MRE11 and CtIP, but can still occur via EXO1³⁴⁷. Resection creates ssDNA and thus unveils sequences of MHs, which are

annealed for rejoining^{38,102,207,347}. The repair is influenced by the location of the MHs (Figure 2.5, example with the MH located terminal to one DSB end and internal to the other). It has been proposed that resection is executed to the point that a suitable MH is uncovered, which could determine which proteins conduct resection and how limited resection is during MMEJ^{207,346}. Importantly, the binding of ssDNA by RPA prevents the annealing of MHs and therefore, RPA is considered to be a major factor antagonizing MMEJ²⁶⁴.

The annealing of the MH can create unpaired ssDNA and leaves DNA gaps, which need to be filled (Figure 2.5). During MMEJ, gaps are filled by POL θ (DNA polymerase theta). Importantly, distinctions have been made between MMEJ and a pathway specifically described as POL θ -mediated end-joining^{178,414}. POL θ is a low-fidelity polymerase, which can bypass abasic sites and other lesions¹⁷¹. Its polymerase activity is template-independent and extends single-stranded 3' ends of DNA¹⁷¹. In MMEJ, POL θ binds to the 5' terminus phosphate of the opposing DNA end to extend the annealed 3' overhang under the displacement of the 5' strand²⁰⁷. The central role of POL θ in MMEJ explains the preferred rejoining under the usage of at least 3 nt, as the stability of the annealed intermediate is enhanced with MHs starting at this size, and thus promotes the repair by POL θ ^{38,414}. Due to unique contact points in its active site, POL θ can tightly grasp the 3' terminus, which allows the extension of the DNA even with such short-paired primers⁴¹⁰. Wyatt et al. (2016) showed that MHs between 4 and 6 nt were most frequently observed in rejoined DNA sequences after POL θ -mediated repair. Additionally, POL θ is frequently observed to cause templated insertions^{171,410}. This is suggested to be caused by POL θ performing mismatch extension of the 3' overhangs from unpaired ssDNA regions²⁰⁷.

The heterodimer XPF (ERCC4, ERCC excision repair 4, endonuclease catalytic subunit)/ERCC1 (ERCC excision repair 1, endonuclease non-catalytic subunit) has been associated with the removal of the 5' flaps generated by POL θ (Figure 2.5)^{346,347}. Nevertheless, the involvement of additional nucleases remains uncertain (Figure 2.5)^{38,347}. In addition, certain 3' overhangs created by unpaired ssDNA might be processed by nucleases before the nucleotide extension by POL θ takes place³⁸. Finally, ligation is conducted by the LIG3 (DNA ligase 3)/XRCC1 (X-ray repair cross-complementing protein 1) complex^{102,116,346}. The recruitment of XRCC1 is dependent on binding to PARP1-generated PARs⁴⁰⁴ and it has been suggested that LIG1 (DNA ligase 1) can carry out ligation in the absence of LIG3^{38,346,347}.

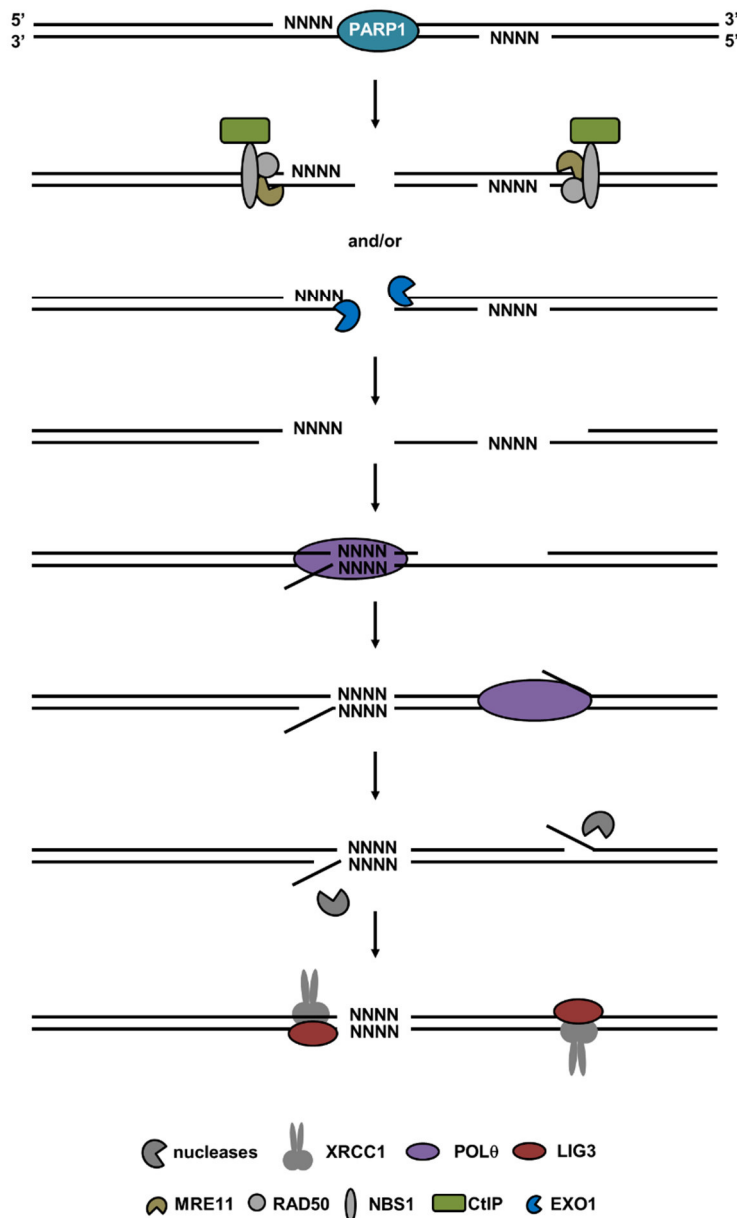


Figure 2.5 Microhomology-mediated end-joining (MMEJ)

Simplified model of MMEJ as an alt-EJ process with a terminal-internal MH. PARP1 binds the DSB ends and builds the scaffold for the recruitment of other proteins. Limited resection takes place by MRN together with CtIP, which first introduces a nick and then resects in the 3' to 5' direction. EXO1-mediated resection might also play a role, either at the DSB ends or at the location of the MRN-CtIP-induced nick to conduct resection in the 5' to 3' direction. Unveiled MHs are annealed and POLθ binds to the 5' terminus phosphate of the opposing DNA strand to extend the DNA from the 3' end under the displacement of the 5' strand. The flaps are removed by nucleases and ligation occurs via XRCC1/LIG3. Based on Decottignies (2013); Mashimo et al. (2013); Kent et al. (2015); Sfeir and Symington (2015); Wei and Yu (2016); Wyatt et al. (2016); Seol et al. (2017).

The question is under which conditions is MMEJ performed? It remains uncertain whether MMEJ-mediated DSB repair is a backup for abrogated repair pathways to ensure survival or if it has a role in wild-type (WT) human cells ³⁴⁷. Moreover, it is unclear whether every microhomology-mediated rejoining is executed as outlined in Figure 2.5. The best indication of a role for MMEJ in a WT situation is its participation in certain repair events during class switch

recombination (see chapter 2.2.5) ^{131,226,289,421}. Further, POL θ -mediated repair has been observed in WT cells with predominantly short deletions below 50 nt and in KU-deficient cells in combination with deletions up to several hundred nucleotides ⁴¹⁴. Another clue for MMEJ in WT cells has been provided by experiments conducted in *Caenorhabditis elegans* by Koole et al. (2014). Here, POL θ was shown to be essential for the repair of replication-induced DSBs at G-quadruplex structures caused by difficult to replicate regions of tandem guanines. Remarkably, the loss of small patches of DNA and the usage of MHs for rejoining in POL θ -mediated repair prevented a profound loss of sequences surrounding these G-quadruplex structures, and thus evaded genomic havoc. In addition, MMEJ has been associated with poor NHEJ substrates and with resection when it takes place during G₁ phase of the cell cycle ⁴¹⁴. Converse to a possible role for MMEJ in a WT situation, it has been shown that although MMEJ and HR share the initial end-resection step ³⁸⁴, a number of HR factors, including BRCA1, suppress MMEJ ^{7,399}. Furthermore, repair by MMEJ has been associated with abrogated c-NHEJ, aborted HR in tumors with mutated BRCA1/2, and with hyper-resection, as it takes place in cells deficient for KU or 53BP1 ^{178,181,414}. Surprisingly, Pfister et al. (2014) revealed that a reduction in CtIP protein does not prevent MMEJ, but increases it compared to HR in G₂ phase. An increase in MMEJ has also been observed following the impairment of HR-related long-range resection factors ³⁹⁹. In addition, POL θ overexpression has been associated with poor survival in breast and colon cancer patients due to an increased capability of the cancer cells to deal with high levels of DSBs by the usage of error-prone DSB repair ²³².

Alternative end-joining (alt-EJ)

A term generally associated with all types of error-prone end-joining is alternative end-joining (alt-EJ) ¹⁸¹. Although the involvement of MMEJ in a WT situation remains unclear, cells deficient for certain proteins can use MMEJ as a backup mechanism and therefore, MMEJ can be alt-EJ. However, not all alt-EJ is conducted using MHs. Furthermore, it has been proposed that alt-EJ is distinct from MMEJ and requires additional factors such as WRN, ligation by LIG1, and explicitly does not use XRCC1 ^{102,116,359}. Mansour et al. (2010) found a requirement for PARP1 in KU-deficient cells, but contradictory to other findings ⁴¹⁴, did not observe rejoining using MHs. In any case, alt-EJ, either with or without microhomology-mediated rejoining, has been frequently observed as a backup mechanism in non-WT situations. In addition, several HR factors and c-NHEJ factors have been shown to suppress alt-EJ ^{7,256}. Therefore, alt-EJ has also been called KU- and XRCC4/LIG4-independent end-joining ³⁵⁷. Despite this, overexpression of EXO1 reduces the frequency of repair by c-NHEJ and enhances mutagenic DSB repair resulting in increased deletions and insertions ²⁶⁰. Furthermore, while the increased resection in KU-deficient cells has been observed to be EXO1-dependent ³⁸², resection in 53BP1-deficient cells

is not ²². An additional factor that generally seems to be required in alt-EJ is the nuclease ARTEMIS ²⁷⁸. However, the function of ARTEMIS might differ compared to its role in c-NHEJ, as neither DNA-PKcs nor LIG4 would be available as interaction partners. In conclusion, the alt-EJ mechanisms seem to differ depending on which factors of regular DSB repair proteins are missing or are overexpressed. Therefore, alt-EJ might be a backup strategy and not a dedicated pathway ¹¹⁶. Other factors influencing the use of alt-EJ are the cell line and the species. It has been shown that alt-EJ plays a more important role in mice than humans ³¹³, which could be caused by the 50-fold higher amounts of DNA-PK in human cells ¹³⁰.

2.2.5. End-joining in genetic recombination

In addition to the importance of end-joining in repairing DSBs by c-NHEJ and error-prone end-joining mechanisms, end-joining has a special role in T and B lymphocytes, which belong to the adaptive immune system. The focus of the immune response is generating antibody diversity. Antibodies (also called immunoglobulin) in human cells consist of a heavy and light chain, each containing a variable and a constant region. The variable region provides the antibody its specificity for antigen-binding ²⁸. Two important pathways in genetic recombination are V(D)J (variable, diversity, joining) recombination and class switch recombination (CSR). Both pathways begin with the endogenous induction of DSBs at defined positions in a controlled and highly-regulated manner. The factors involved in the response and repair of these DSBs heavily overlap with the damage response and end-joining machineries. Therefore, patients with inherited mutations in genes encoding proteins involved in the repair machinery (e.g. ARTEMIS), have a defective immune system in addition to their radio-sensitivity ¹⁹⁴. As the aim of these genetic recombination pathways is antibody diversity, they employ repair factors to purposely misjoin DSB ends to create new sequences.

V(D)J recombination

The diverse assembly of the variable region of immunoglobulin and T cell receptor genes in developing B and T cells is conducted by V(D)J recombination ^{26,115}. It is also called antigen receptor gene rearrangement and is responsible for providing a highly-diverse set of antigen receptors ^{115,139}. In the heavy chain variable region, exons are assembled from V, D, and J segments, while light chain exons are assembled from V and J segments ²⁶. V(D)J recombination is initiated during G₁ phase by the binding of lymphoid-specific RAG1/2 (recombination activating gene) in concert with HMG1 (high mobility group 1) at highly-conserved recombination signal sequences ^{139,391}. RAG1/2 generates DSBs under the formation of hairpins at the coding ends, while blunt ends are formed at the intervening gene segment, which is then excised as a circular DNA fragment ³⁹¹. The DSB is recognized by the c-NHEJ heterodimer

KU70/80. KU recruits the catalytic subunit DNA-PKcs, which interacts with ARTEMIS to open the hairpin structures of the coding ends²⁵¹. TdT (terminal deoxynucleotidyl transferase), a lymphoid-specific protein, increases the diversity by incorporating non-templated nucleotides²⁵⁵. The ligation step is executed by the XLF/XRCC4/LIG4 complex^{180,391}. Additional proteins have been described as functioning in V(D)J recombination, namely γ H2AX, ATM, the MRN complex, and PARP1⁴²³. While γ H2AX, ATM, and the MRN complex contribute to the stabilization of the broken DNA ends, the interaction of PARP1 and DNA-PKcs facilitates the genomic integrity during V(D)J recombination^{165,277,404,423}. In addition to its stabilizing role, γ H2AX prevents the processing of hairpin-sealed coding ends by any nuclease other than ARTEMIS¹⁶⁴. Surprisingly, Helmink et al. (2011) observed that in the absence of H2AX, CtIP can efficiently promote the hairpin opening. In addition, TOPBP1 and 53BP1 are critical factors in V(D)J recombination^{157,212,416}. Indeed, Difilippantonio et al. (2008) show that the loss of 53BP1 impairs the joining of distant V-DJ segments, which exhibit extensive degraded coding ends, thus demonstrating the role of 53BP1 in maintaining genomic stability during the joining of long-range DSB ends.

Class switch recombination (CSR)

The immunoglobulin gene diversification of mature B cells is conducted by CSR and somatic hypermutation. CSR is an alteration, which allows expression of an antibody with the same antigen-binding specificity, but switches the antibody class by recombination of the heavy chain constant region^{4,115}. The efficient and specific activation of CSR in B cells is dependent on cytokines from T cells^{115,254}. AID (activation-induced cytidine deaminase) induces lesions at large guanine- and cytosine-rich switch regions of repetitive DNA sequences by deamination of cytosine^{4,115,365}. AID is a lymphoid-specific protein. In fibroblast cell lines, the expression of AID induces CSR, preferentially in actively-transcribed regions^{115,296,425}. The lesions induced by AID are converted into SSBs by the base excision repair pathway in which the backbone of the DNA is disrupted by the removal of the damaged base^{196,365}. The formation of DSBs results from either two close SSBs or requires the EXO1-dependent mismatch repair pathway^{24,364,365}. Thus, single-stranded overhangs are generated by EXO1 processing during the induction of the DSB, which either need to be excised or filled-in to generate ends suitable for the end-joining process^{137,309,364,365,419}. Several DNA polymerases have been implicated in the DNA synthesis process to fill those gaps, including POL θ ⁴¹⁹. The DSBs induced in two of the switch regions are distant and therefore, CSR is a complex form of DSB repair⁴. Similar to V(D)J recombination, the intervening fragment is excised as a circular fragment. ATM, γ H2AX, and the MRN complex contribute to the stabilization of the broken DNA ends but in contrast to V(D)J recombination, ATM and MRN are not sufficient to hold the DSB ends together, and thus γ H2AX is essential for

the stabilization process in CSR ⁴²³. Furthermore, together with MDC1 and ATR, these factors facilitate CSR and in their absence show varying levels of impact on the overall levels of CSR ²¹⁵.

Another essential part of CSR is the modification of histones to position the switch regions near each other prior to DSB induction, which places them within the same chromosomal loop ³⁶⁵. Several specific histone modifications have been identified as promoting CSR ²³⁵. Interestingly, PTIP plays a role in long-range chromatin interactions and promotes the chromatin changes that are critical for CSR ^{97,344}. 53BP1 (the interaction partner of PTIP) plays a central role in CSR by performing an anchoring role required for the long-range synapsis ^{4,157}. 53BP1 explicitly favors long-range CSR by protecting the DNA ends from excessive resection and preventing short-range rejoining, which would result in intra-switch region recombination ^{47,324}. The protection of DNA ends from resection by 53BP1 is independent of the distance of the DSBs. However, the distance between the DSBs is essential for 53BP1-dependent facilitation of the joining of distant intrachromosomal DSB ends and corresponds to the dissemination of the γ H2AX signal ⁴⁸. RIF1, another 53BP1-interacting protein, also promotes CSR ³⁹². Furthermore, DSB repair during CSR involves the c-NHEJ factors KU70/80, DNA-PKcs, and the XLF/XRCC4/LIG4 complex ^{4,46,254,391}. The absence of ARTEMIS reduces the overall amount of CSR ^{328,330,331}. Even cells lacking XRCC4/LIG4, XLF, or KU can still perform a fraction of CSR, but under the enhanced usage of MHs for rejoining ^{131,160,234}. This indicates a switch to alternative repair mechanisms in the absence of c-NHEJ factors during CSR. This repair pathway switch is dependent on CtIP ²²⁶. The absence of 53BP1 also promotes microhomology-mediated alternative rejoining processes in CSR ^{47,57,107}. However, even in a WT situation, some junctions use MHs for rejoining distant DSBs, which is also dependent on CtIP ^{226,289,421}. As the switch region is full of repetitive sequences, microhomology-mediated rejoining of the DSBs could be promoted. Therefore, CSR could be the physiological cause for repair pathways using MHs ¹³¹.

2.3. Aim of this study

DSB repair by end-joining has the potential to be error-prone due to sequence alterations and/or the misrejoining of two DSB ends, which causes genomic rearrangements. Thus, error-prone end-joining endangers genomic stability by promoting carcinogenesis and tumor progression^{51,99,134,161,193,413}. However, the use of error-prone end-joining is poorly understood in WT human cells. While some studies show that c-NHEJ causes interchromosomal genomic rearrangements in WT human cells^{142,302,357}, other studies link the formation of intrachromosomal genomic rearrangements to resection, which results in sequence alterations during alt-EJ^{148,322}. However, in human cells, alt-EJ mechanisms are suggested to be restricted to cells deficient for certain repair proteins, which is the case for genetic defects or as frequently observed in tumor cells^{22,143,181}. Thus, it remains unclear how error-prone end-joining, resulting in intrachromosomal genomic rearrangements, operates in WT human cells and how that pathway compares to alt-EJ.

To investigate mutagenic end-joining in this study, a reporter assay (in which two DSBs get induced in an intrachromosomal-integrated reporter construct) was utilized and combined with other molecular biological assays to investigate: (i) if DSBs are repaired in this assay, by analyzing the overall repair capability after DSB induction; (ii) if the two DSBs are misrejoined after the loss of the intervening fragment, by monitoring intrachromosomal genomic rearrangements; (iii) if the misrejoined break sites feature sequence alterations; and (iv) how the structure of other reporter constructs influences the misrejoining of DSBs. This was complemented by the investigation of protein-protein interactions to characterize: (1) the circumstances under which error-prone end-joining is utilized in WT human cells; (2) which factors are involved in this type of error-prone end-joining; (3) does error-prone end-joining in WT human cells involve resection (like alt-EJ)? (4) If so, how is it initiated and (5) how does it operate? Moreover, (6) how does this repair pathway compare to other DSB repair mechanisms; and (7) is there a benefit for the cell to use this pathway, taking into account its mutagenic character?

3. Results

The purpose of this study was the investigation of how distant endonuclease-induced DNA DSBs are misrepaired by an error-prone end-joining mechanism and to characterize the newly-discovered underlying repair pathway. The first chapter of the results section introduces the assays and analyses performed in this study, the second chapter focuses on end-joining factors involved in this error-prone repair mechanism, and the third chapter uncovers how this repair mechanism is initiated and executed.

3.1. The end-joining reporter system in GC92 cells and associated assays

The center of this study was the end-joining reporter system in GC92 cells^{155,322} (Figure 3.1 A). GC92 cells are SV40-transformed GM639 human fibroblasts, which contain an intrachromosomal-integrated reporter construct. This construct consists of a promoter region, several genes encoding surface reporter proteins, and two cohesive recognition sites for the endonuclease I-SceI, which are 3.2 kb apart. The endonucleolytic cleavage by I-SceI at its recognition site induces a DSB. The accurate repair of an I-SceI-induced DSB cannot be distinguished from the situation prior to the damage induction. However, the two I-SceI-induced DSBs can be misrejoined if they are present at the same time. Misrejoining occurs by the inversion or loss of the intervening fragment (of note, inversion events are rare and were not further investigated in this study). The misrejoining of the distant DSB ends results in the expression of the *CD4* reporter gene, and thus CD4-positive cells represent and enable the quantification of misrepair events in GC92 cells (Figures 3.1 A, B). Furthermore, sequence analysis of the misrejoined site provides information about repair-associated alterations of the DNA sequence adjacent to the break site. The reporter assay provides information about GC92 cells in which misrepair took place, but not about the overall repair of I-SceI-induced DSBs. To assess the overall repair of the I-SceI-induced DSBs, the GC92 reporter assay was combined with the γ H2AX foci assay, which uses the histone modification γ H2AX as a marker to visualize DSBs (Figures 3.1 A, C). The first part of this results section focuses on introducing the assays and their analyses in detail.

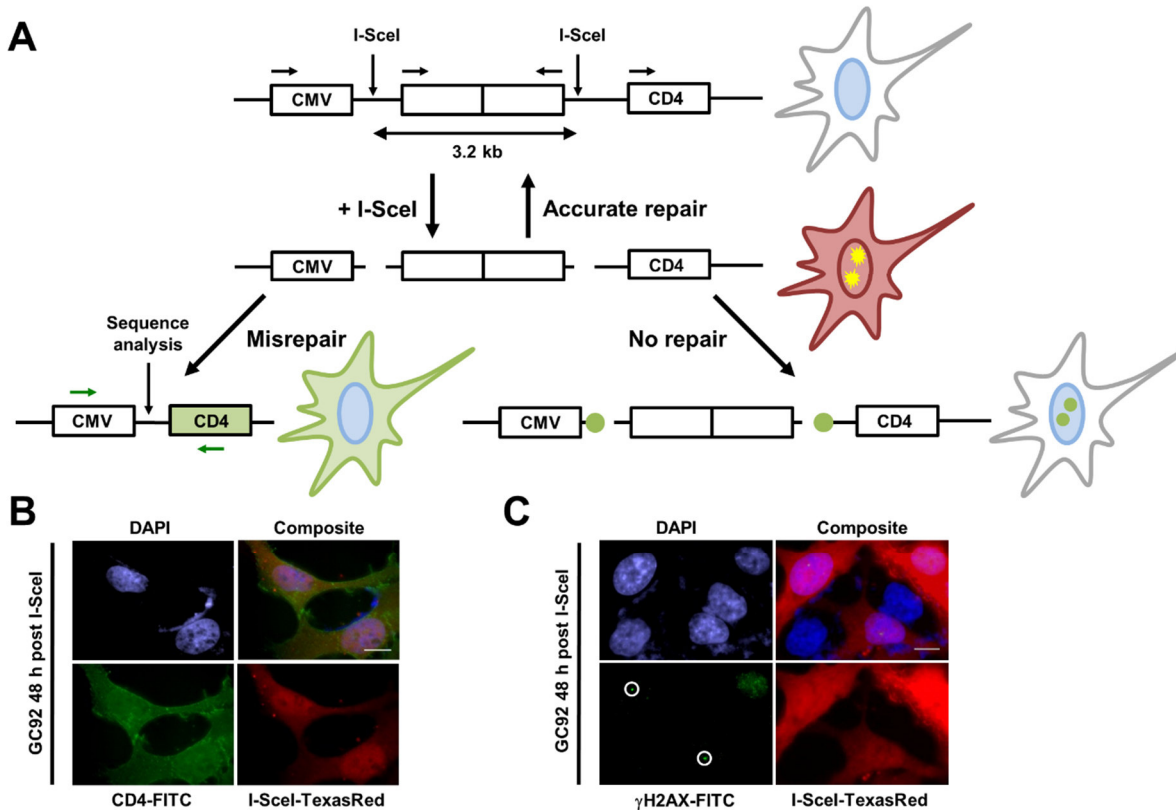


Figure 3.1 Misrepair and overall repair of distant I-SceI-induced DSBs can be assessed by the combination of the GC92 reporter assay with the γ H2AX foci assay

(A) The end-joining reporter system in GC92 cells and associated assays. The end-joining reporter assay in GC92 SV40-transformed human fibroblast cells contains two 3.2 kb distant I-SceI endonuclease recognition sites, where DSBs can be induced by I-SceI (red cell). Analysis of the CD4 reporter protein (green cell) reveals which cells have undergone misrepair by loss of the intervening fragment and analysis of γ H2AX foci (green dots) provides data about the overall repair. Sequence analysis was performed with the displayed primers (green arrows) to allow direct analysis of the misrejoined site. The diagram is based on Rass et al. (2009) and not drawn to scale. (B, C) Misrepair events as per CD4 expression (B) and overall repair analysis by the γ H2AX foci assay (C) in GC92 cells. GC92 cells were transfected with the I-SceI plasmid and treated with EdU and nocodazole 30 min prior to harvest. Harvest took place 48 h after I-SceI plasmid transfection. All cells were stained with anti-I-SceI and either anti-CD4 or anti- γ H2AX (white circles) antibody (AB) plus DAPI. Representative images were captured with a 63x objective using Metafer Isis software. The scale bar represents 10 μ m.

3.1.1. Analysis of misrepair events in GC92 cells

To analyze misrepair events by the frequency of CD4-positive GC92 cells, damage was induced by the transfection of a plasmid encoding I-SceI protein. As a first step, the fluctuation of I-SceI protein levels over time was analyzed (Figure 3.2 A). Therefore, GC92 cells were harvested at multiple timepoints post-I-SceI plasmid transfection and the frequency of I-SceI-positive cells was investigated by immunofluorescence microscopy. The first signs of I-SceI were observed 12 h after transfection of the I-SceI plasmid and I-SceI levels were highest after 48 h (also confirmed by immunoblotting Figure S8.1 a) with 34.2% of I-SceI-positive cells (Figure 3.2 A). At 72 h post-I-SceI plasmid transfection, I-SceI protein levels declined strongly and the remaining I-SceI-positive cells only showed weak I-SceI protein levels (Figures 3.2 A, S8.1 a). Therefore, harvesting of the GC92 cells for reporter assay experiments in this study was not

conducted earlier than 72 h post-I-SceI transfection, to avoid analyzing cells while damage induction was still fully active.

Next, how misrepair events arise over time was investigated as per the frequency of CD4-positive GC92 cells following I-SceI plasmid transfection. However, classical reporter assay analysis via flow cytometry showed huge fluctuations in the measured frequency of CD4-positive cells. Therefore, the origins of these fluctuations were first investigated. Two factors were uncovered as reasons for these fluctuations and the analysis was optimized accordingly. First, the preferred method for reporter assay analysis in this study was the detection of CD4-positive cells by immunofluorescence microscopy instead of the typically-used flow cytometry. The usage of flow cytometry for reporter assay experiments showed high background fluctuations (further described in chapter 5.5.1), which would require sample sizes at least 3 to 10-fold greater than the sample sizes used in other studies to obtain somewhat meaningful results^{35,155,322}. Additionally, microscopic analysis of reporter assay experiments lacked false positive events, which means in all experiments conducted during this study, CD4-positive cells were exclusively observed in cells positive for I-SceI. Consequently, the standard deviation (*SD*) was reduced in samples analyzed by microscopy, which increased the effect size, and thus decreased the required sample size to gain meaningful results. The second factor greatly influencing the frequency of CD4-positive GC92 cells is the transfection efficiency of the I-SceI plasmid, as it affects the frequency of I-SceI-positive cells, and thus the frequency of cells in which DSBs are induced. Indeed, plasmid transfection efficiencies in GC92 cells vary greatly from less than 1% to nearly 80% positive cells ($M = 28.1\%$, $SD = 17.4\%$) after transfection with a plasmid encoding the reporter protein RFP (Figure S8.1 b). The transfection efficiencies of the similar-sized I-SceI plasmid also varied greatly. Thus, when analyzed in all cells, the high fluctuations of CD4-positive cells could be attributed to fluctuating transfection efficiencies ($M = 2.7\%$, $SD = 1.7\%$, Figure S8.1 c). This problem was tackled in other studies by normalizing the treated sample to an untreated control, which fails to solve the problem, as differences in plasmid transfection efficiencies were still observed, even in simultaneously transfected samples. Therefore, the logical solution would be to limit the measurement of misrepair events to cells with damage induction by only analyzing CD4-positive cells in all I-SceI-positive cells. However, as described earlier, cells could not be harvested before I-SceI activity declined to avoid analysis during fully active damage induction. This problem was solved by co-transfection of the I-SceI plasmid with an RFP plasmid. In contrast to I-SceI protein levels, RFP protein was detectable in 25.0% of the cells 24 h after transfection (Figure 3.2 A). RFP expression peaked at 72 h with 32.4% positive cells. To further examine the expression of RFP co-transfected with the I-SceI plasmid, the frequency of cells positive for both proteins was

analyzed (Figure 3.2 B). The frequency of RFP-positive cells was slightly lower ($M = 27.3\%$) compared to I-SceI-positive cells ($M = 33.8\%$) 48 h after transfection with both plasmids. Strikingly, the frequency of cells positive for both proteins was similar to the frequency of RFP-positive cells at 26.4%, indicating that RFP-transfected cells typically also contained the I-SceI plasmid. Therefore, RFP could be used as a marker for cells transfected with the I-SceI plasmid and was thus representative of cells where damage induction occurred. After solving the high fluctuation problem during analysis, the kinetics with which misrepair events arose post-I-SceI plasmid transfection were analyzed by microscopy-based detection of CD4-positive cells among all RFP-positive GC92 cells (Figure 3.2 A, S9.2 a). The quantity of CD4-positive cells among RFP-positive cells grew exponentially from 24 h to 72 h post-I-SceI transfection to 9.8% and declined slightly thereafter. This observation was essential in establishing 72 h post-I-SceI transfection as the optimum timepoint to harvest the GC92 cells for analysis, as I-SceI was strongly reduced at this time and CD4-positive cells were maximal.

For some experiments during this study, it was necessary to transfect cells with plasmids encoding tagged proteins. In these experiments, the exogenous protein levels needed to be present prior to damage induction. Hence, the experimental conditions needed to be adjusted. As described earlier, simultaneous transfection of the RFP and I-SceI plasmids resulted in nearly every RFP-positive cell also being I-SceI-positive (Figure 3.2 B). Interestingly, this behavior was not only observed after simultaneous transfection but also if transfection of the RFP plasmid occurred 36 h before the I-SceI plasmid. To further investigate this curious behavior, other plasmids were co-transfected with either the RFP or the I-SceI plasmid. A plasmid encoding an RFP-tagged 102 kDa protein was co-transfected with or transfected 36 h prior to I-SceI plasmid transfection (Figures S8.2 b). While 17.2% or 18.2% of the cells were positive for the tagged protein, the frequency of cells positive for both proteins was nearly identical under both transfection procedures. This behavior was not observed when transfection of two plasmids took place at least 48 h apart (Figure S8.2 c). In conclusion, transfection of cells with an RFP or a tagged protein plasmid 36 h prior to I-SceI plasmid transfection ensured that over 95% of cells positive for RFP or the tagged protein were also positive for I-SceI (Figures 3.2 B, S8.2 b). This knowledge was used to adjust the experimental conditions and develop a standardized protocol (Figure 5.1) and standardized analysis for all misrepair measurements in GC92 cells, which could also be applied in experiments where exogenous protein was investigated. Ultimately, if the frequency of CD4-positive cells among all damage-induced cells (analyzed by RFP-positive cells) 72 h post-I-SceI and RFP co-transfection from all experiments during this study was combined, the mean value of misrepair events was at 9.6% (95% confidence interval (95% CI) [9.2%, 9.9%]) and the population was normally distributed (Figures S8.3 a, b).

In the GC92 reporter assay, DSBs are induced when I-SceI is present in the cells, which is a duration of roughly 60 h. Therefore, it is not possible to state in which cell cycle phase the DSBs were induced or in which cell cycle phase misrepair took place. To analyze in which cell cycle phase misrepair events arise, GC92 cells were synchronized with a double thymidine block. Subsequently, the cells were held in G₁ 16 h after thymidine release by serum starvation or in G₂ 8 h after thymidine release by treatment with the CDK1 inhibitor RO-3306 over the entire duration of the DSB induction and repair time (Figure S8.3 c). EdU treatment was used to mark cells progressing in the cell cycle, and thus exclude them from analysis. The frequency of misrepair events in G₁ phase cells was 8.7%, which was similar to asynchronously grown cells. In contrast, the frequency of misrepair events in G₂ phase cells was 2.7%, which was significantly lower ($p < 0.001$) than asynchronously grown cells. The effect size ($d = 6.14$) exceeded Cohen's convention for a large effect ($d = 0.80$)⁸². Hence, the majority of misrepair events are generated during G₁ phase. Importantly, the application of the cell cycle-specific analysis of misrepair events was very harmful to the cells, and thus the results have to be carefully considered. However, the G₁ specificity of the misrejoining of the two distant I-SceI-induced DSBs in GC92 cells was confirmed during this work by additional experiments (chapter 3.3.3).

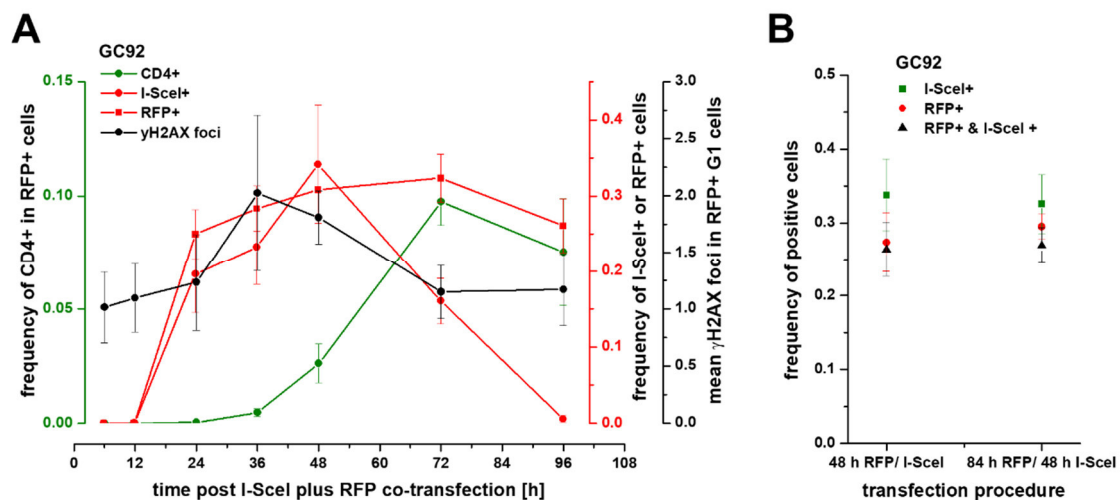


Figure 3.2 Misrejoining of distant DSB ends and overall repair in GC92 cells in relation to I-SceI levels
 (A) Rise of DSBs and misrepair events over time post-I-SceI transfection in GC92 cells. (B) Effect of co-transfection or transfection of the I-SceI and RFP plasmids 36 h apart. (A) GC92 cells were co-transfected with the RFP and I-SceI plasmids and treated with EdU and nocodazole 30 min prior to harvest. Harvest took place at multiple timepoints post-I-SceI transfection. Cells were stained with anti-I-SceI, anti-CD4, or anti- γ H2AX plus anti-RFP AB and DAPI. (B) GC92 cells were either co-transfected with the RFP and I-SceI plasmids or RFP was transfected 36 h prior to I-SceI and harvesting occurred 48 h post-I-SceI transfection. Cells were stained with anti-I-SceI or anti-CD4 plus anti-RFP AB and DAPI. (A, B) Samples were scanned using Metafer software and plasmid-transfected cells were analyzed. RFP was used as a marker for cells with damage induction (see chapter 3.1.1). Data represent the mean of 4 independent experiments performed in duplicate ($n = 4$). Error bars show the SD

3.1.2. Overall repair of distant endonuclease-induced DSBs in GC92 cells

To assess overall repair of the I-SceI-induced DSBs, the γ H2AX foci assay was applied in GC92 cells co-transfected with the I-SceI and RFP plasmids. When a DSB is induced, the histone variant H2AX is phosphorylated several Mbp from the DSB end³²⁹, which can be detected by immunostaining as a γ H2AX focus. As the two DSBs induced by I-SceI are only 3.2 kb apart in the GC92 reporter system, the expected increase of γ H2AX foci in an unrepaired situation would be 1 focus (Figures 3.1 A, C). However, γ H2AX foci could also increase by 2 if the two distant DSB ends are not held in proximity after damage induction or if the reporter construct is integrated more than once.

In the γ H2AX foci assay, it is possible to analyze DSB repair in a cell cycle-dependent manner. Therefore, GC92 cells were co-transfected with the RFP and I-SceI plasmids and treated with EdU and nocodazole 30 min before harvest. The EdU and DAPI intensities were scanned under the microscope to identify the cell cycle phase of each RFP-positive cell (figures S8.4 a, b). However, this only enables the allocation of a cell cycle phase to a cell at the moment of harvest, but fails to provide information about when DSBs were induced or repaired over the 72 h post-I-SceI transfection. In addition, the cell cycle distribution in CD4-positive and CD4-negative cells was similar at the time of harvest, which clearly shows that misrepaired cells still progressed in the cell cycle. Despite this, it was necessary to analyze γ H2AX foci in a cell cycle-dependent manner since S and G₂ phase cells had at least 10x higher background levels of γ H2AX foci than the expected theoretical effect of an unrepaired situation. Therefore, only cells in G₁ phase at the time of harvest were analyzed. First, γ H2AX foci were analyzed in GC92 cells co-transfected with the I-SceI and RFP plasmids at multiple timepoints post-plasmid transfection. The background mean γ H2AX foci in G₁ RFP-positive cells fluctuated between 1.0 and 1.2 foci before I-SceI protein levels increased (24 h post-I-SceI transfection) and returned to background levels with the decrease of the I-SceI signal at 72 h post-I-SceI transfection (Figure 3.2 A). At 36 h post-I-SceI transfection, a maximum mean value of 2.0 γ H2AX foci was observed in G₁. This observation was important for the validation of the established experimental procedure (Figure 5.1) with the cell harvest at 72 h post-I-SceI transfection. At this timepoint γ H2AX foci had returned to background levels, showing that repair was mostly complete. This was not surprising, as the I-SceI levels were strongly reduced and the maximum number of CD4-positive cells also occurred at 72 h post-I-SceI plasmid transfection. However, since damage induction and repair is fluent over the entire time I-SceI is present in the cells, the maximum mean γ H2AX foci value is not expected to occur at a specific timepoint. Thus, the observed maximum mean value of 2.0 γ H2AX foci (meaning an increase

of approximately 1 focus) might not represent an unrepaired situation but could be attributed to a mixture of cells with repaired and unrepaired DSBs.

In conclusion, the overall repair was analyzed using the mean value of γ H2AX foci in G₁ phase cells with damage induction by I-SceI (analyzed in RFP-positive cells). This resulted in a mean value of 1.1 foci (95% CI [1.1, 1.2]) per cell when all experiments from this study were combined (Figure S8.5 a). The mean value for γ H2AX foci in cells without I-SceI DSB induction (RFP-negative cells) was 1.2 foci, which was very similar compared to the mean value for γ H2AX foci in cells with I-SceI-induced DSBs (RFP-positive cells, Figure S8.5 b). Therefore, the mean γ H2AX foci in RFP-negative cells qualified as a control to compare conditions with and without DSB induction to ensure that effects observed during this study truly originated from two unrepaired distant I-SceI-induced DSBs. Such controls were performed for every γ H2AX foci experiment in this study and the mean values ranged from 0.8 to 1.3 foci. Surprisingly, the mean value for γ H2AX foci in misrepaired CD4-positive cells was 0.4 foci, which was significantly lower ($p = 0.001$, $d = 3.49$) compared to the mean value of γ H2AX foci in RFP-positive cells, and thus also lower than the background level. A more detailed analysis revealed that the median number of γ H2AX foci in RFP-positive cells within one experiment was either 0 or 1 (Figure S8.5 c).

3.1.3. Sequence analysis of the misrejoined break sites in GC92 cells

In addition to the reporter assay and the γ H2AX foci assay, the DNA sequences adjacent to the misrejoined break sites were analyzed in GC92 cells to monitor repair-associated alterations. GC92 cells were transfected with the I-SceI plasmid and the CD4-positive cells were enriched by magnetic-activated cell sorting (MACS) 72 h post-transfection. The DNA was amplified and in contrast to other studies^{154,155,322}, the primers used for the DNA amplification were placed further apart to maximize the information about the sequences. The sequences were analyzed with regard to alterations such as deletions or insertions of nucleotides at the misrejoined break sites. The I-SceI recognition site consists of 18 bp and nucleolytic cleavage by I-SceI produces a 4 nt 3' overhang (see Table 8.2). Misrejoining of the distant DSB ends with loss of the intervening fragment and no additional base deletions was called high-fidelity misrepair event and produced a new I-SceI recognition site. Analysis of all sequences (Table 8.1, 8.2) showed that 90% of all misrejoined sites ranged from no additional deletions to deletions of less than 50 nt, with the majority of deletions being fewer than 10 nt (Figures 3.3 A). The mean value of additional deletions at the misrejoined sites was 34 nt (Figure 3.3 B). Closer inspection of the misrejoined break sites revealed that misrejoining of distant DSB ends occasionally included insertions, which ranged from 2 to 31 nt in size (Figure 3.3 C). Furthermore, the insertions were

found in combination with all sizes of deletions, and the inserted sequences were often templated (Figure 3.3 C, Table 8.2). In addition, most DSB ends were misrejoined with the use of MHs. MHs were observed in combination with all deletion sizes (Figure 3.3 C) and maximally 4 nt long, which was concurrently the most common MH size (Figure 3.3 D).

In conclusion, upon I-SceI damage induction, misrepair events arose primarily in G₁ phase in approximately 10% of I-SceI-positive GC92 cells by loss of the intervening fragment. All of the induced DSBs were repaired, as the number of γ H2AX foci after damage induction was approximately equal to 1 γ H2AX focus in cells without damage induction. The majority of the misrepaired events were connected with the additional loss of nucleotides at the misrejoined sites. These deletions suggest that the process involved in the generation of these misrepair events includes the digestion of bases from the DSB end. Hence, resection could be involved in the misrepair of distant DSBs, which is a frequently-observed feature in error-prone repair mechanisms^{207,257,401}.

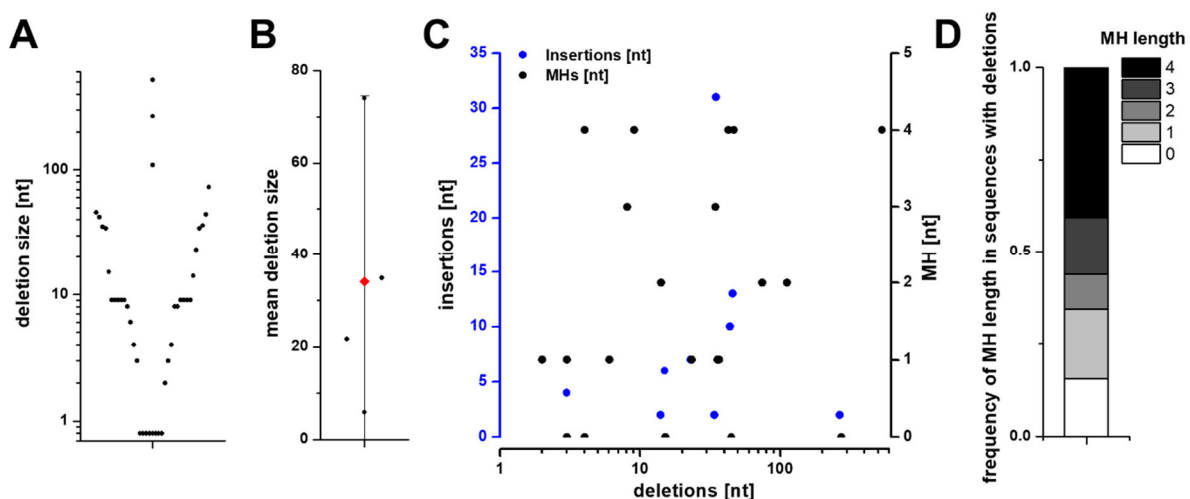


Figure 3.3 Sequence analysis of misrejoined break sites

GC92 cells were harvested 72 h post-I-SceI transfection and incubated with anti-CD4 AB and magnetic MicroBeads for MACS enrichment. After cell lysis, DNA purification, and amplification, the DNA was sequenced. (A, B) Distribution of deletion sizes of all 40 analyzed sequences from the 4 independent experiments (A) or of the mean values from the 4 independent experiments (B) ($n = 4$). (A) Events with no additional deletions were given a value < 1 nt to include them in the logarithmic scale. (B) Error bar shows the (95% CI). (C) Insertion size (blue) of each sequence in relation to its deletion size of the 9 observed insertions and MH size (black) of each sequence in relation to its deletion size for all 32 sequences with additional deletions from the 4 independent experiments ($n = 4$). (D) Frequency of MH length used for rejoining in all 32 sequences with additional deletions from the 4 independent experiments ($n = 4$). (A, B, C, D) For further details see Tables 8.1, 8.2. Most sequences were part of the analysis in Biehs et al. (2017).

3.1.4. Comparing the misrepair of distant and close endonuclease-induced DSBs

Additional reporter systems were used and compared to the end-joining reporter construct in GC92 cells throughout this study to establish how the choice of proteins for misrepair in the GC92 end-joining reporter system is influenced by its structure. These additional reporter systems were end-joining reporter constructs in GCS5 and GCSH14 fibroblast cell lines¹⁵⁴

(Figures 3.4 A). Both cell lines showed similar I-SceI protein level kinetics as GC92 cells. In addition, HeLa pGC cells were used as controls to validate the efficiency of inhibitors for proteins that are known to be involved in error-free gene conversion. The end-joining construct in GCSH14 cells is similar to the GC92 reporter construct but with GFP as a reporter protein instead of CD4 and with an approximately 200 bp shorter distance between the reporter gene and the second I-SceI recognition site (Figure 3.4 A). GCSH14 cells were harvested 72 h post-I-SceI and RFP co-transfection for analysis of the frequency of GFP-positive cells. Surprisingly, the mean value of misrepair events in GCSH14 cells was 7.7%, which was significantly lower ($p = 0.005$, $d = 1.66$) in comparison to the mean value of 10.1% misrepair events in the GC92 cells (Figure 3.4 B). Taking the sequence analysis of the misrejoined break sites in GC92 cells into account (Figures 3.3 A, Tables 8.1, 8.2), an explanation could be that larger deletions might harm the *GFP* gene because it is closer to the second I-SceI recognition site than the *CD4* gene in GC92 cells (Figure 3.4 A).

In contrast to the end-joining reporter systems in GC92 and GCSH14 cells with two distant I-SceI recognition sites, the GCS5 cell line contains an end-joining reporter construct with two I-SceI recognition sites in close proximity (Figures 3.4 A). The end-joining reporter construct in GCS5 cells contains GFP as a reporter just like the end-joining construct in GCSH14 cells does. However, the intervening fragment between the two I-SceI recognition sites is only 34 bp long, much shorter than the 3.2 kb of the end-joining constructs in GC92 or GCSH14 cells. The expression of the *GFP* gene in GCS5 cells is prevented by a Koz-ATG insert in the intervening fragment. At 72 h post-I-SceI and RFP co-transfection misrepair events in GCS5 cells occurred in 29.7% GFP-positive cells, which was more frequent compared to CD4-positive GC92 cells (Figures 3.4 B, C). The increased frequency of misrepair events in GCS5 compared to GC92 cells might be due to the proximity of the two DSBs. Thus, GCS5 cells were used to compare misrepair of distant DSB ends in GC92 cells to the misrepair of close DSBs.

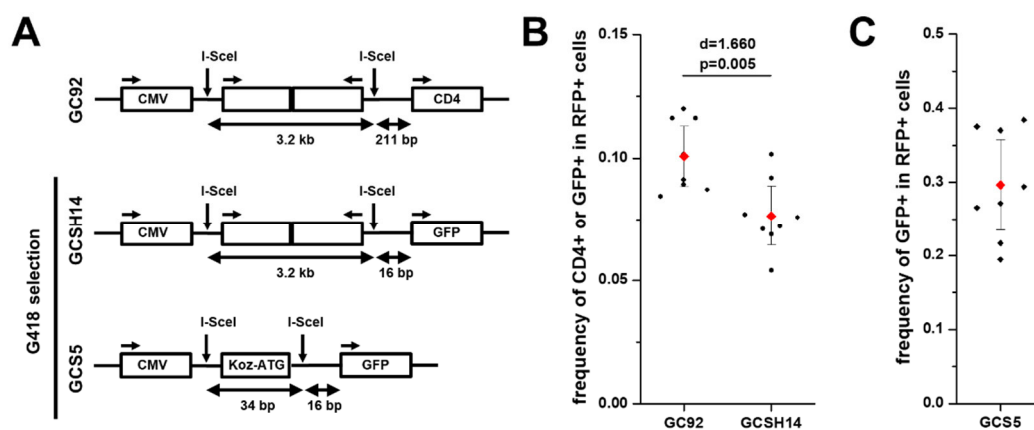


Figure 3.4 Misrepair of two relatively-close and two relatively-distant I-SceI-induced DSBs

(A) End-joining reporter constructs in GC92, GCS5, and GCSH14 cells. GCS5 and GCSH14 human fibroblast cells containing end-joining reporter constructs can be selected using G418. Both constructs have *GFP* as a reporter gene. While the two I-SceI recognition sites in GCSH14 cells are 3.2 kb apart from each other, the intervening fragment in GCS5 cells is only 34 bp long with *GFP* expression being prevented by a Koz-ATG insert. The diagrams are based on Rass et al. (2009) Guirouilh-Barbat et al. (2016) and not drawn to scale. (B, C) Misrepair events in GC92, GCSH14, GCS5, and HeLa pEJ cells. GC92, GCSH14, GCS5, and HeLa pEJ cells were harvested 72 h post-co-transfection with the RFP and I-SceI plasmids. Cells were stained with anti-CD4 or anti-GFP plus anti-RFP AB and DAPI. Samples were scanned using Metafer software and only plasmid-transfected cells were analyzed. RFP was used as a marker for cells with damage induction (see chapter 3.1.1). Data represent the mean of 8 independent experiments performed in duplicate ($n = 8$). Error bars show the 95% CI. Effect size was calculated by Cohen's d and p -value was obtained by two-sample Student's t -test.

3.2. End-joining-associated proteins and their role in the repair of distant DSBs

The second part of this study focused on proteins associated with end-joining and what influence the impairment of these proteins has on the misrepair and overall repair of distant and close endonuclease-induced DSBs. Therefore, the main experimental procedure involved the depletion, inhibition, or knock-out (KO) of proteins in the end-joining reporter cell systems and utilization of the assays described in part one.

3.2.1. Misrepair is dependent on c-NHEJ factors

First, which end-joining factors are involved in the misrejoining of DSB ends was investigated. In human cells, the majority of DSBs are repaired by c-NHEJ in all cell cycle phases (Figure 2.4). During c-NHEJ, the DSB ends are protected by the KU70/80 heterodimer and held together by DNA-PKcs^{188,362}. Together, this complex is called DNA-PK. LIG4 is necessary for the ligation of the DSB ends¹⁹¹. Inhibition of the c-NHEJ core component DNA-PK by Nu7441 prevents DNA-PKcs autophosphorylation. Thus, the DNA-PK complex gets stuck on the break ends, which prevents the completion of repair^{99,117}. Accordingly, inhibition of DNA-PK in GC92 cells resulted in a decrease of misrepair events by 90% (Figure 3.5 A). Close inspection of the single DNA-PK components revealed that the depletion of KU70/80 increased misrepair events to 17.3%, while depletion of DNA-PKcs decreased misrepair events to 1.5% (Figure 3.5 B). A decrease of misrepair events to 5.0% was also observed after depletion of LIG4. In GCS5 cells, where the two DSBs are close to each other, DNA-PK inhibition, LIG4, or KU70/80 depletion resulted in a decrease of misrepair events from nearly 30% to levels between 1.2% and 1.5% (Figures 3.5 A, S8.6 a). DNA-PKcs depletion alone led to a two-thirds decrease in misrepair events (Figures S8.6 a).

To examine the cause of the decreased misrepair in GC92 cells after impairment of c-NHEJ factors, the γ H2AX foci assay was used. Both, DNA-PK inhibition and DNA-PKcs depletion resulted in γ H2AX foci increasing to 3.1 or 2.6, respectively (Figures S8.6 b, c). Both increases were significant ($p \leq 0.001$) compared to the control. Therefore, it can be concluded that the decrease of misrepair events in GC92 cells after DNA-PK inhibition or DNA-PKcs depletion is

caused by unrepaired DSBs. In contrast, KU70/80 depletion did not have an effect on the γ H2AX foci assay compared to the control (Figure S8.6 c), which corresponds to the increased quantity of misrepair events in the reporter assay. Finally, LIG4 depletion caused an increase to 1.7 γ H2AX foci. Although this increase was not significant ($p = 0.182$), the effect size ($d = 2.12$) exceeded Cohen's convention for a large effect⁸². Combined with the finding that misrepair events dropped by half compared to the control after LIG4 depletion (Figure 3.5 B), the missing 50% of misrepair events might be caused by unrepaired DSBs in a fraction of the cells. In conclusion, misrepair events of distant DSBs in GC92 cells is dependent on c-NHEJ factors. However, this dependency dwindles if the DSB ends are not protected by KU70/80.

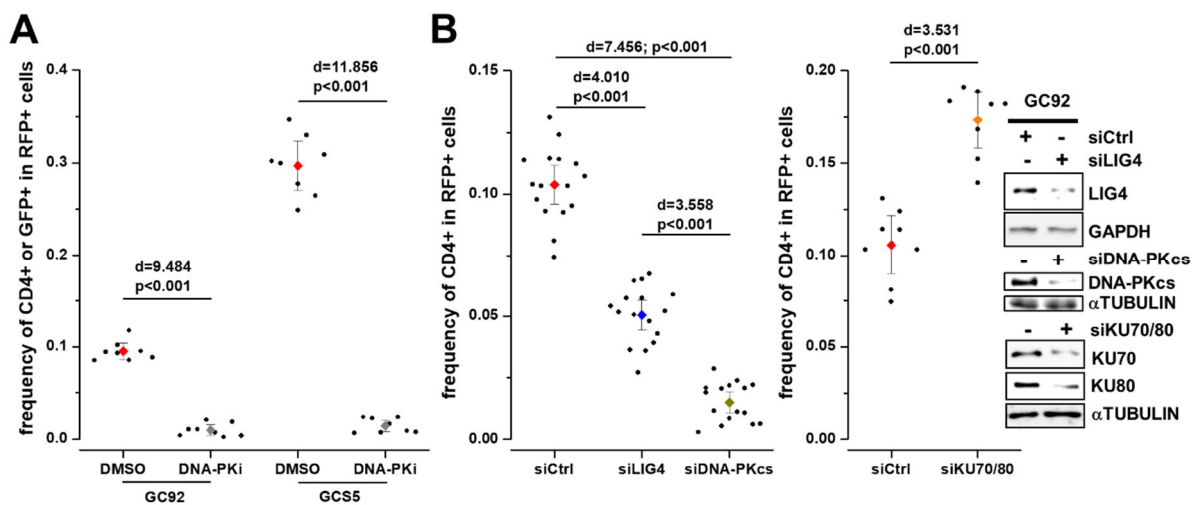


Figure 3.5 c-NHEJ factors are required in end-joining reporter systems

(A, B) Impact of DNA-PK inhibition (A) or depletion of core c-NHEJ factors (B) on misrepair in GC92 (A, B) and/or GCS5 (A) cells. GCS5 and/or GC92 cells were treated with inhibitors and/or siRNAs against DNA-PK (Nu7441), DNA-PKcs, KU70/80, or LIG4. As a control, cells were treated with DMSO or control siRNA. Harvesting occurred 72 h post-co-transfection with I-SceI and RFP plasmids. Downregulation by siRNA was confirmed by immunoblotting. Cells were stained with anti-CD4 or anti-GFP plus anti-RFP AB and DAPI. Samples were scanned using Metafer software and only plasmid-transfected cells were analyzed. Data represent the mean of 8 or 16 independent experiments performed in duplicate ($n = 8$ for A, B right; $n = 16$ for B left). RFP was used as a marker for cells with damage induction (see chapter 3.1.1). Error bars show the 95% CI. Effect size was calculated by Cohen's d and p -value was obtained by one-way ANOVA with Bonferroni correction (A, B left) or by two-sample Student's t -test (B right). (D) Several data points were part of the analysis in Biels et al. (2017).

At this point of the study, a predicament arose: on one hand, the generation of misrepair events is dependent on c-NHEJ factors, which includes the protection of the DSB ends by the KU70/80 heterodimer; on the other hand, the generation of misrepair events might involve resection (chapter 3.1.3). Simultaneously, it has been established in the literature^{239,273,362} that KU generally prevents resection. However, the additional deletions observed in the sequence analysis of the misrejoined sites (Figure 3.3 A, Table 8.1), indicate a resection size far smaller than observed in publications addressing this subject. The GC92 reporter assay is limited in providing information regarding the possibility of limited resection taking place while KU protects the DSB ends. Hence, the system was switched to address this question after X-ray

irradiation (X-IR). Experiments from members of the working group led to the speculation that slowly repairing DSBs during G₁ phase after X-IR might depend on the same repair pathway as misrejoining of distant DSBs. Therefore, experimental procedures, which are usually used to investigate resection in G₂ were modified and applied to examine the roles of core c-NHEJ factors and resection in the slow DSB repair in G₁ phase. Late DSB repair in G₂ phase is conducted by HR. In this process, resection takes place to generate large regions of ssDNA, which are protected by pRPA³⁷. Therefore, pRPA is considered an indirect marker for the presence of ssDNA. During HR, pRPA is exchanged with RAD51 to allow invasion of the sister chromatid and use it as a template for high-fidelity repair^{77,280}. This exchange is only possible if KU is no longer binding to the DSB ends⁷⁴.

First, the γ H2AX foci assay was performed in 82-6 hTERT cells after 7 Gy X-IR in samples treated with the DNA-PK inhibitor at various timepoints (Figures S8.7 a, b). NU7441 is a selective small molecule inhibitor for DNA-PK (IC₅₀ of 14 nM)^{99,172} that competes with ATP for the ATP-binding domain of DNA-PK³⁰⁵. It causes IR-induced DNA DSBs to persist due to trapping of DNA-PK at the DSB ends, preventing further repair³⁷⁷. As DNA-PK is required for the fast repair process, the inhibitor was added 6 h, 8 h, 10 h, or 12 h post-irradiation to ensure that the fast repair component was concluded. Analysis of γ H2AX foci 14 h post-irradiation revealed that the cells were unable to repair DSBs from the moment the DNA-PK inhibitor was added. Thus, the repair of DSBs is dependent on DNA-PK throughout the slow repair process in G₁ phase. After establishing that the slow repair requires the core c-NHEJ component DNA-PK, the question of whether resection can occur in the presence of KU was directly addressed by KU foci analysis. Due to their size and the fact that only two KU molecules bind to a DSB, KU foci analysis required confocal laser scanning microscopy (CLSM). In HeLa cells, KU80 foci largely co-localized with γ H2AX foci in G₁ as well as in G₂ (Figure 3.6 A). At 8 h post-4 Gy X-IR, co-localization of KU80 with γ H2AX foci was often observed along with a drop in the DAPI intensity (Figures 3.6 A, C). However, co-localization studies with KU80 and γ H2AX foci were problematic since γ H2AX forms large blotches, especially at late timepoints. To ensure that the KU80 foci were specific and did not result from non-specific background signals (as observed in unirradiated samples, Figure 3.6 B), co-localization of KU80 with RAD51 foci was investigated in G₂. KU80 foci did not co-localize with RAD51 foci (Figures 3.6 D, E). Finally, it was investigated if KU80 foci co-localize with pRPA foci. This experiment required high doses of irradiation since pRPA foci are only observed in G₁ phase after high doses of X-IR or after high-LET irradiation³⁶. KU80 was observed to co-localize almost completely with pRPA 4 h post-10 or 20 Gy X-IR (Figures 3.6 F, G). Thus, resection occurs at the break site despite the presence of KU. In conclusion, the involvement of c-NHEJ factors was shown in the slow repair

process in G₁ and KU could be linked to resected DSB ends. However, this combination was surprising because although resection is frequently associated with error-prone end-joining mechanisms^{102,116}, it is generally accepted that c-NHEJ factors prevent resection^{239,273,362}.

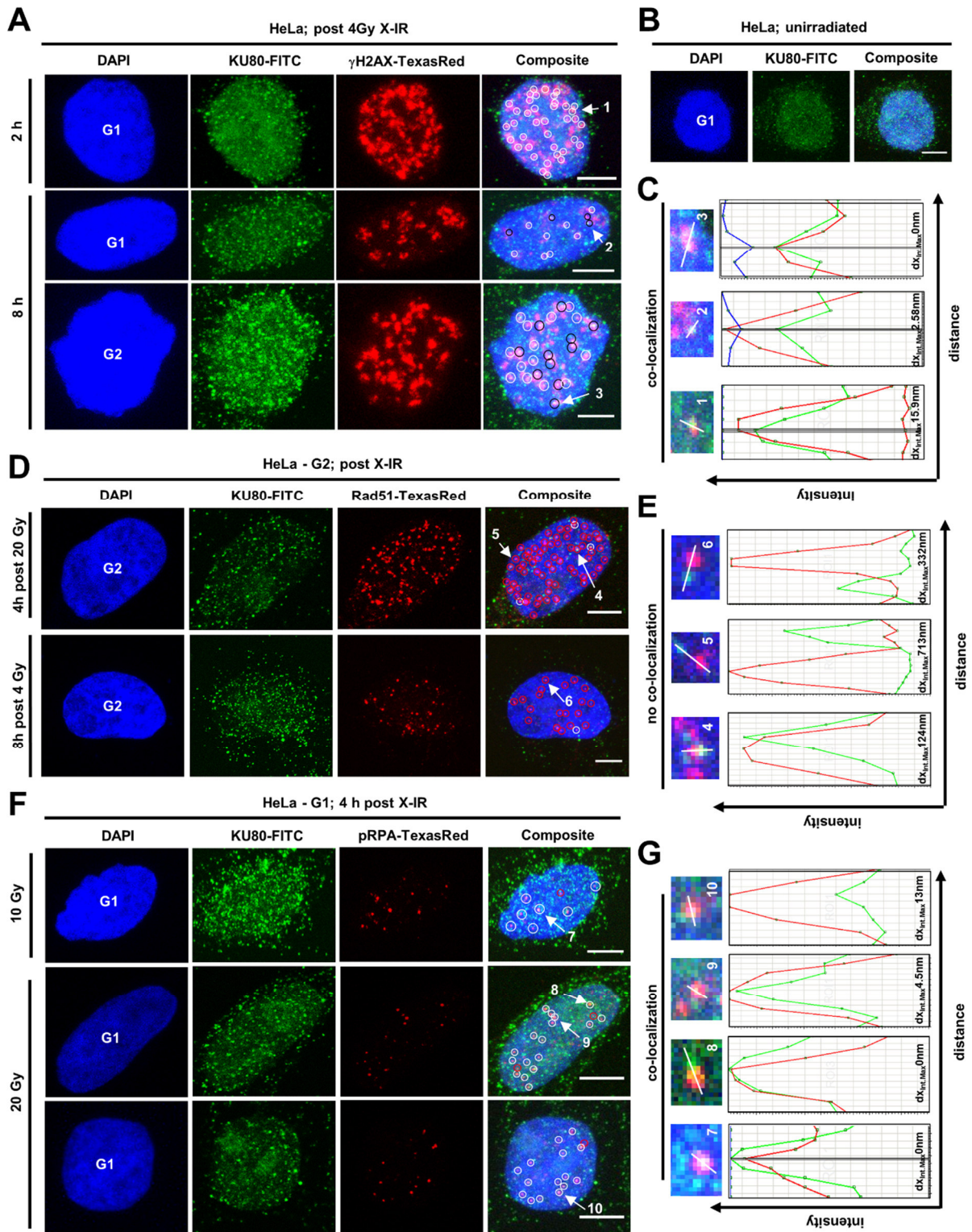


Figure 3.6 KU80 foci co-localize with pRPA foci after high doses of X-IR in G₁ phase
 HeLa cells were treated with EdU and nocodazole 30 min prior to X-IR and harvested at the indicated timepoints. (A, D, F) KU80 foci co-localize with γ H2AX (A) and pRPA (F) but not with RAD51 (D) foci. (B) KU80 foci in unirradiated samples. (A, B, D, F) Cells were stained with anti- γ H2AX, anti-RAD51, or anti-pRPA plus anti-KU80 AB and DAPI. Images were obtained with a 100x objective using CLSM. Scale bar is 5 μ m. Images were analyzed with

LAS AF Lite software. No co-localization (red circles), co-localization (white circles), and co-localization in concert with a DAPI signal drop (local DAPI minimum, black circle) was analyzed. All pRPA or RAD51 foci were analyzed for co-localization with KU80. γ H2AX foci co-localization with KU80 foci are merely examples. Of note, the experimental procedure was conducted together with M. Steinlage and CLSM images were taken together with J. Mirsch. (C, E, G) Exemplary line blots of co-localization analysis. Each co-localization was confirmed by line blot with maximum intensity $I_{\max} > 100$ (arb. units) and distance (max. intensity) $dx < 20$ nm (with the majority being smaller than 5 nm). (B, D, E, F, G) Some co-localization analyses were included in Biehs et al. (2017).

3.2.2. Varying roles for PARP1 in different end-joining mechanisms

In addition to the c-NHEJ repair pathway, a backup end-joining pathway called alt-EJ has been described. This type of DSB repair is known to include deletions due to resection. Alt-EJ usually takes over in the absence of KU and the described deletions are often several hundred nucleotides long^{207,257,401}. The mechanism involves factors such as PARP1 and ligation is conducted by LIG1/3³⁵⁹. Although the misrejoining of distant DSB ends in GC92 cells has been established as occurring in a manner dependent on c-NHEJ factors, whether the impairment of alt-EJ factors also impacts misrepair events was investigated. First, PARP1 was examined. PARP inhibitors often have an effect on the cell cycle^{20,195,252}, which makes them tricky to work with in experiments such as the reporter system because inhibitor treatment was required over the duration of several days. The PARP inhibitor PJ34 proved to be unsuitable because the impact on the cells was severe, resulting in 20x fewer cells than the minimum required for analysis. However, treatment with the PARP inhibitor Olaparib over several days did allow analysis although Olaparib also has a strong effect on the cell cycle, which impacts the measurements of DNA repair activity¹⁹⁵. Nevertheless, Olaparib (IC50 of PARP1 = 5 nM and PARP2 = 1 nM) is known to have fewer side effects²⁶⁹. Recently, the van Houten working group at the University of Pittsburgh used atomic force microscopy²⁹ to find that Olaparib does not trap PARP1 on DNA as so many other PARP inhibitors do, but affects the PARylation dynamics by enhanced PARP1 mobility (conference contribution²⁴³).

In GC92 cells, Olaparib treatment resulted in a significant decrease ($p = 0.003$) in misrepair events from 10.3% in the untreated sample to 4.4% with an effect size of 3.56 (Figure 3.7 A). Since PARP inhibitors are not specific, the experiment was also confirmed by PARP1 depletion (Figure 3.7 B). In contrast, in GCS5 cells, where the two DSBs are induced only 34 bp apart from each other, no effect was observed after PARP inhibition by Olaparib (Figure 3.7 A) or after PARP1 depletion (Figure S8.8 a). As established in chapter 3.2.1, misrepair in GC92 cells increases after KU70/80 depletion (Figure 3.5 B) even though c-NHEJ factors are otherwise required for the misrejoining of distant DSB ends. As PARP1 is involved in alt-EJ, a pathway that takes over, especially in KU70/80-deficient cells^{257,401}, the combined effect of KU70/80 depletion and Olaparib inhibitor treatment was analyzed. The increased misrepair levels after KU70/80 depletion were reduced by treatment with Olaparib to 1.2%, which is significantly

lower ($p < 0.001$, $d = 9.22$) than inhibition or depletion of PARP1 alone (Figure 3.7 B). To further analyze the misrepair events in GC92 cells, the γ H2AX foci assay was used. Olaparib treatment or PARP1 depletion did not impair overall repair in GC92 cells after I-SceI damage induction (Figures 3.7 C, S8.8 b). However, Olaparib treatment in combination with KU70/80 depletion resulted in a significant increase ($p < 0.001$) of γ H2AX foci from 0.9 to 3.0 with an effect size of 7.40 (Figures 3.7 C). In conclusion, PARP1 is required for 50% of the misrejoining of distant DSBs in GC92 cells but is not necessary for repair of the DSBs. Conversely, KU70/80 depletion makes DSB repair entirely dependent on PARP1.

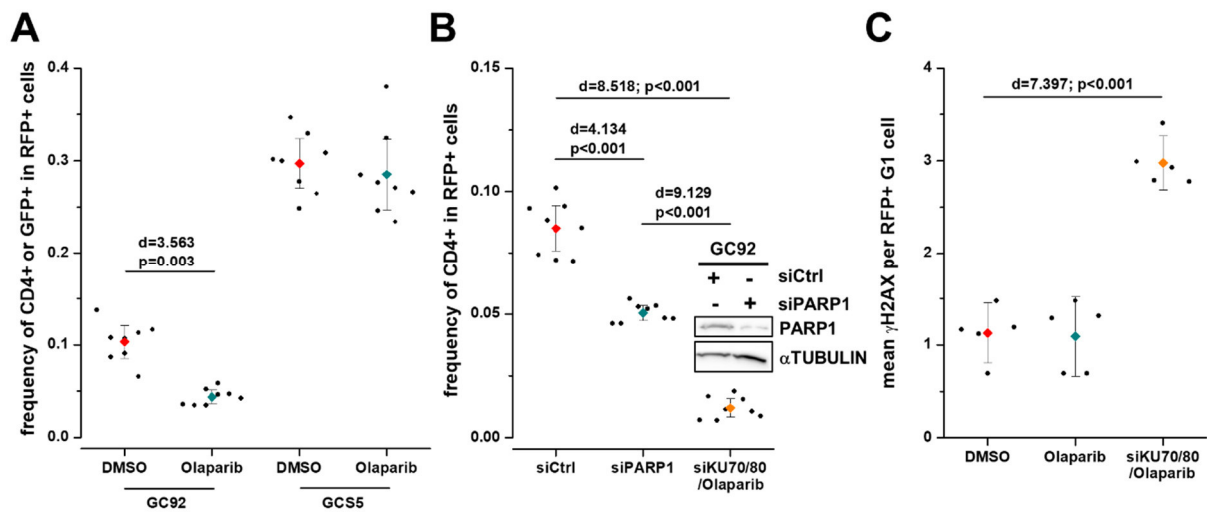


Figure 3.7 PARP1 has multiple roles in different end-joining mechanisms

(A, B, C) Impact of PARP inhibition (A, C), PARP1 depletion (B), or PARP inhibition in combination with KU70/80 depletion (B, C) on misrepair (A, B) and overall repair (C) in GC92 (A, B, C) and/or GCS5 (A) cells. GCS5 and/or GC92 cells were treated with inhibitors and/or siRNAs against PARP (Olaparib), PARP1, and/or KU70/80. As a control, cells were treated with DMSO or control siRNA. (A, B) Harvest occurred 72 h post-co-transfection with I-SceI and RFP plasmids. Downregulation by siRNA was confirmed by immunoblotting. Cells were stained with anti-CD4 or anti-GFP plus anti-RFP AB and DAPI. Samples were scanned using Metafer software and only plasmid-transfected cells were analyzed. Data represent the mean of 8 independent experiments performed in duplicates ($n = 8$). (C) Cells were co-transfected with RFP and I-SceI plasmids and treated with EdU and nocodazole 30 min prior to harvest. Harvest took place 72 h post-plasmid transfection. Cells were stained with anti- γ H2AX, anti-RFP AB, and DAPI. Samples were scanned using Metafer software and only plasmid-transfected G₁ cells were analyzed. Data represent the mean of 5 independent experiments ($n = 5$). (A, B, C) RFP was used as a marker for cells with damage induction (see chapter 3.1.1). Error bars show the 95% CI. Effect size was calculated by Cohen's d and p -value was obtained by one-way ANOVA with Bonferroni correction.

Next, the influence of alt-EJ ligases LIG1/3 on the misrejoining of distant DSBs in GC92 cells was investigated. Depletion of LIG1/3 did not alter the percentage of misrejoining events in GC92 cells (Figure 3.8 A). However, a comparison was difficult, as the data significantly deviated from a normal distribution at the 0.05 level. With a reduction to only 9.8% misrepair events from 10.4% in control cells, the effect size was 0.32, which is a small effect under Cohen⁸² and negligible in comparison to other effects observed in this study. Although confirmation of LIG1/3 downregulation by immunoblotting gave consistent results when no additional proteins were depleted, the data looked like a bimodal distribution, which could result from

variations in siRNA efficiency. As observed in chapter 3.2.1, depletion of the c-NHEJ ligase LIG4 reduced misrepair in GC92 cells by half. Additional depletion of the alt-EJ ligases LIG1/3 caused a reduction in misrepair events to 1.1% with an effect size of 4.18 (Figure 3.8 A). As before, the data significantly deviated from a normal distribution at the 0.05 level. Additional PARP inhibition in combination with LIG4 depletion resulted in a significant reduction ($p < 0.001$) in misrepair events to 1.0% (Figure 3.8 B). In contrast, PARP inhibition in combination with LIG1/3 depletion did not show any additional effect compared to PARP inhibition alone. According to the highly-reduced misrepair in GC92 cells, depletion of all three ligases or LIG4 in combination with the PARP inhibitor caused a repair defect with 2.8 or 3.0 γ H2AX foci, respectively (Figure S8.8 c).

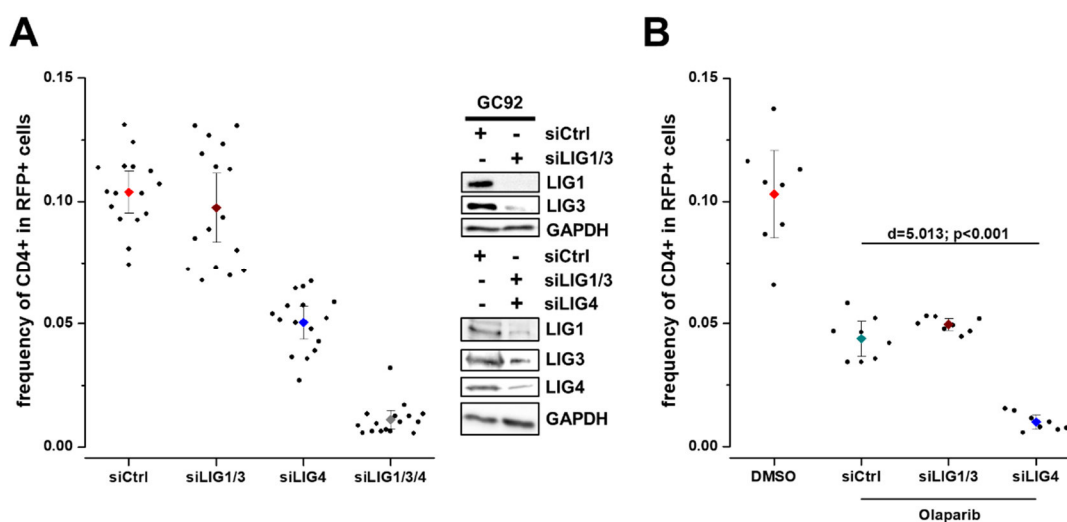


Figure 3.8 The role of LIG1/3 is limited to alt-EJ

(A, B) Impact of depletion of several ligases with (B) or without (A) PARP inhibitor treatment on misrepair in GC92 cells. GC92 cells were treated with inhibitors and/or siRNAs against PARP (Olaparib), LIG4, and/or LIG1/3. As a control, cells were treated with DMSO or control siRNA. Harvest took place 72 h post-co-transfection with the I-SceI and RFP plasmids. Downregulation by siRNA was confirmed by immunoblotting. Cells were stained with anti-CD4, anti-RFP AB, and DAPI. Samples were scanned using Metafer software and only plasmid-transfected cells were analyzed. Data represent the mean of 8 or 16 independent experiments performed in duplicate ($n = 8$ for B; $n = 16$ for A). RFP was used as a marker for cells with damage induction (see chapter 3.1.1). Error bars show the 95% CI. Effect size was calculated by Cohen's d and p -value was obtained by one-way ANOVA with Bonferroni correction. (A) Several data points were part of the analysis in Biels et al. (2017).

As the depletion of LIG1/3 did not show an effect on the measurement of misrepair events in GC92 cells and the data distribution had a bimodal behavior, the misrejoined sites were investigated by sequence analysis. The distribution of additional deletions after depletion of LIG1/3 was almost identical compared to the control (Figure 3.9 A Tables 8.1, 8.3), as was the mean deletion size of the 4 independent experiments (Figure 3.9 B). The insertion size at sites with additional deletions was also similar, though LIG1/3-depleted samples featured far fewer misrejoined sites with insertions (Figures 3.9 C). Upon closer inspection, no insertions were observed at misrejoined sites where additional deletions were bigger than the mean value of 36.92 nt. After LIG1/3 depletion, the use of MHs at misrejoined break sites with additional

deletions showed similar behavior compared to the control (Figure 3.9 D). Nevertheless, the largest class of MHs in control cells (4 nt) was reduced in favor of 2 nt MHs and, for the first time, even the use of 6 nt MHs was observed. Finally, LIG1/3 does not seem to play a role in the misrejoining of distant DSB ends, but if present, may influence the insertions at the misrejoined sites with long deletions and even the size of the MHs used for rejoining. However, if the c-NHEJ ligase LIG4 is depleted, LIG1/3 can take over to generate half of the misrepair events in a PARP1-dependent manner.

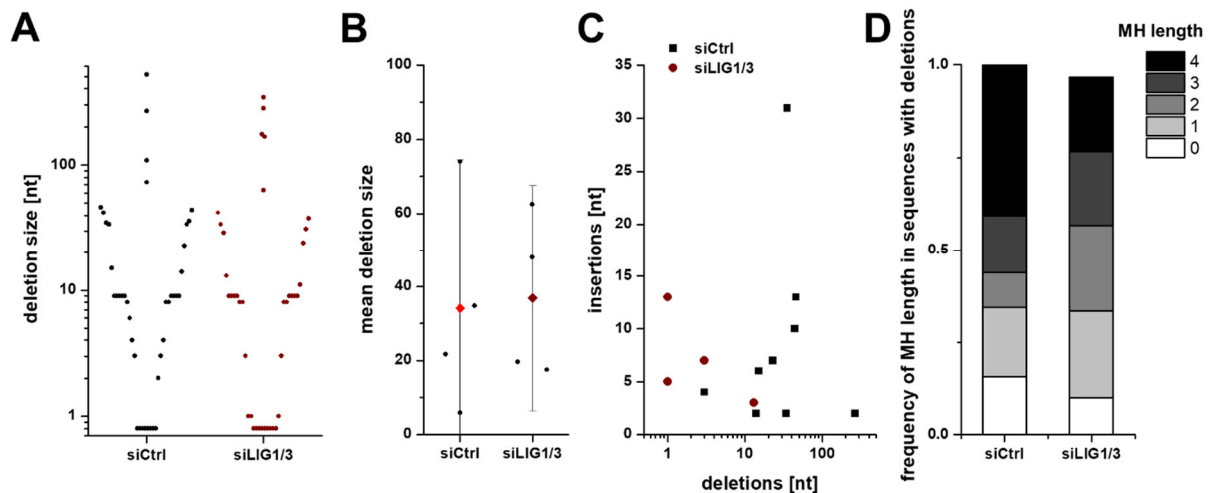


Figure 3.9 LIG1/3 depletion barely influences misrejoined sites in GC92 cells

GC92 cells were treated with siRNA against LIG1/3 (and control siRNA) and harvested 72 h post-I-SceI transfection. Cells were incubated with anti-CD4 AB and magnetic MicroBeads to be enriched by MACS. After cell lysis, DNA purification, and amplification, the DNA was sequenced. (A, B) Distribution of deletion sizes for all 40 (siCtrl) or 39 (siLIG1/3) analyzed sequences from the 4 independent experiments (A) or of the mean values from the 4 independent experiments (B) ($n = 4$). (A) Events with no additional deletions were given a value < 1 nt to include them in the logarithmic scale. (B) Error bars show the 95% CI. (C) Insertion size of each sequence in relation to its deletion size of the 9 (siCtrl) or 4 (siLIG1/3) observed insertions ($n = 4$). (D) Frequency of MH length used for rejoining in all 32 (siCtrl) or 30 (siLIG1/3) sequences with additional deletions from the 4 experiments ($n = 4$). (A, B, C, D) For further details see Tables 8.1, 8.3. Most sequences were part of the analysis in Biehs et al. (2017).

3.2.3. The misrejoining of distant DSB ends relies on various polymerases

Polymerases play an important role in DNA repair. Two polymerases are connected to c-NHEJ, namely POL λ and POL μ ⁴²⁰. In contrast, POL θ is involved in MMEJ, a pathway associated with the use of MHs³⁸. POL θ is observed to create templated insertions and preferentially use 4 nt MHs for rejoining^{171,410}. Co-depletion of both c-NHEJ-associated polymerases POL λ and POL μ significantly reduced the mean misrepair events from 8.4% to 5.1% with an effect size of 3.80 ($p < 0.001$, Figure 3.10 A). In contrast, single depletion failed to generate this impact, indicating that when only POL λ or POL μ is impaired, the other polymerase can mostly take over. Depletion of POL θ resulted in a reduction to 5.6% misrepair events. Combined depletion of all three polymerases reduced misrejoining of distant DSBs even further to only 1.2%. Indeed, γ H2AX foci analysis showed an increase from 1.1 to 2.6 foci after depletion of all three polymerases, validating the hypothesis that the reduction in misrepair was due to a lack of

repair (Figure 3.10 B). Depletion of either $POL\lambda/\mu$ or $POL\theta$ increased γ H2AX foci to 1.6. Although the difference of the means compared to the control was not significant at the 0.05 level, the effect sizes ($d_{siPOL\lambda/\mu} = 1.66$; $d_{siPOL\theta} = 1.55$) exceeded Cohen's convention for a large effect⁸². These data suggest that depletion of either $POL\lambda/\mu$ or $POL\theta$ results in a partial repair defect. Furthermore, $POL\lambda/\mu$ and $POL\theta$ all play a role in the misrejoining of distant DSBs after I-SceI damage induction in the GC92 reporter system, but independently of one another.

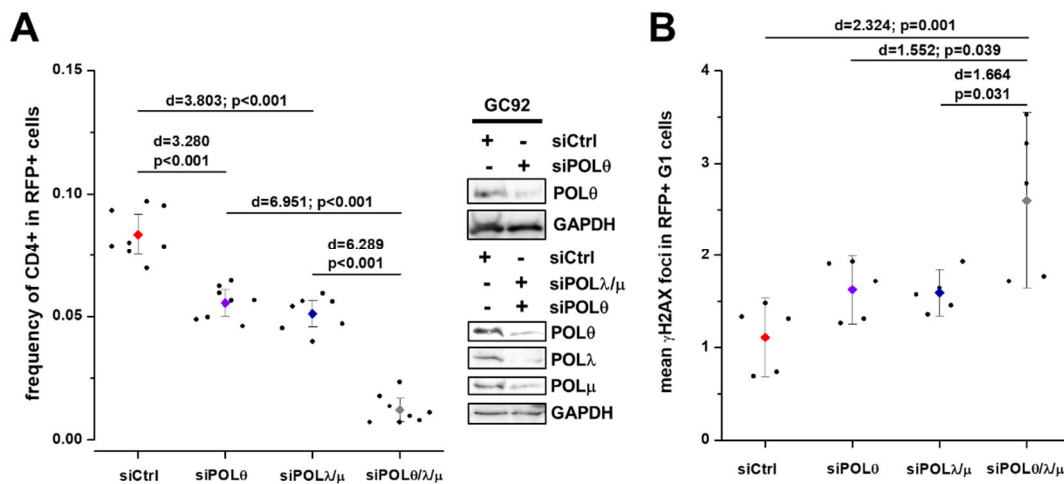


Figure 3.10 Misrepair in GC92 cells requires $POL\lambda/\mu$ and $POL\theta$

(A, B) Impact of depletion of several polymerases on misrepair (A) or overall repair (B) in GC92 cells. GC92 cells were treated with siRNAs against $POL\lambda/\mu$ and/or $POL\theta$. As a control, cells were treated with control siRNA. (A) GC92 cells were harvested 72 h post-co-transfection with the I-SceI and RFP plasmids. Downregulation by siRNA was confirmed by immunoblotting. Cells were stained with anti-CD4, anti-RFP AB, and DAPI. Samples were scanned using Metafer software and only plasmid-transfected cells were analyzed. Data represent the mean of 8 independent experiments performed in duplicate ($n = 8$). (B) Cells were co-transfected with RFP and I-SceI plasmids and treated with EdU and nocodazole 30 min prior to harvest. Harvest took place 72 h post-plasmid transfection. Cells were stained with anti- γ H2AX, anti-RFP AB, and DAPI. Samples were scanned using Metafer software and only plasmid-transfected G₁ cells were analyzed. Data represent the mean of 5 independent experiments ($n = 5$). (A, B) RFP was used as a marker for cells with damage induction (see chapter 3.1.1). Error bars show the 95% CI. Effect size was calculated by Cohen's d and p -value was obtained by one-way ANOVA with Bonferroni correction.

3.2.4. ARTEMIS is essential for the misrepair of DSBs

At this point of the study, it has been established that misrepair events in GC92 cells arise in a c-NHEJ-dependent manner. However, certain factors associated with alt-EJ contribute to the generation of misrepair events. The nuclease ARTEMIS is closely associated with DNA-PKcs in c-NHEJ^{144,251}. There, ARTEMIS processes DSB ends before ligation, when necessary. Additionally, ARTEMIS plays a role in alt-EJ²⁷⁸ and is essential in V(D)J recombination¹⁰⁴, which makes it an interesting candidate to investigate in this study.

First, ARTEMIS was depleted by siRNA in GC92 cells and misrepair was measured (Figure 3.11 A). The mean percentage of misrejoining events dropped significantly from 10.4% to 1.8% with an effect size of 6.85 ($p < 0.001$). Surprisingly, the results in ARTEMIS-depleted GC92 cells differed from those in the master's thesis³⁵ where misrepair events were only reduced by

half (Figure S8.9 a). During the master's thesis, the frequency of CD4-positive cells among all cells was analyzed with 24 h less time for the downregulation by siRNA. This difference in the results underscores the importance of the analysis development in this study (e.g. to only analyze cells in which damage induction took place as described in chapter 3.1.1). Compared to GC92 cells, a smaller effect was observed in GCS5 cells, where misrepair dropped from 28.0% to 12.5% following ARTEMIS depletion (Figure 3.11 A). The generation of misrepair events in GCSH14 cells was also dependent on ARTEMIS (Figure S8.9 b).

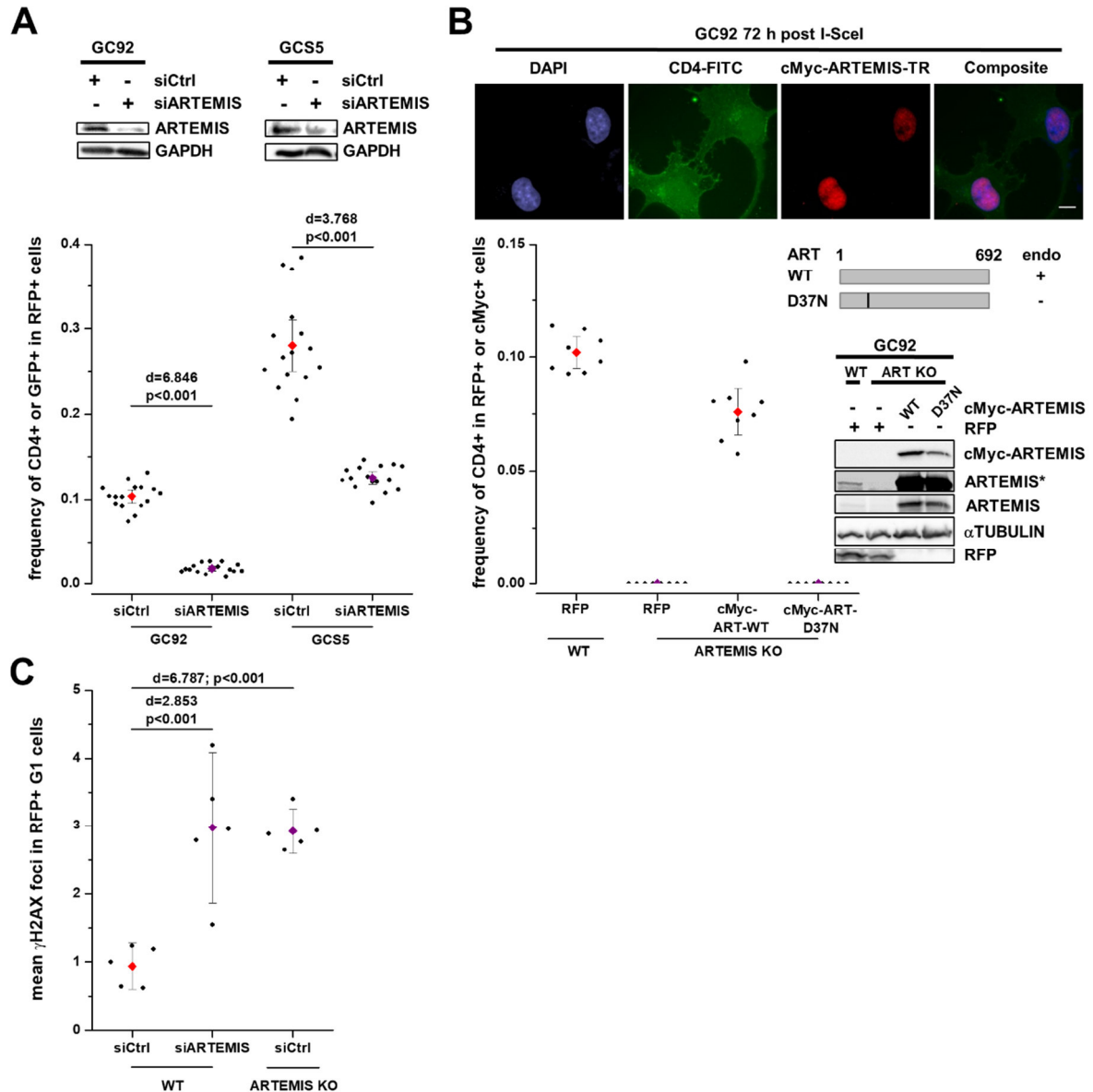


Figure 3.11 ARTEMIS is required for misrejoining of DSB ends

(A, B, C) Impact of the absence (A, B, C) and complementation (B) of ARTEMIS on misrepair (A, B) or overall repair (C) by depletion in GC92 (A, C) or GCS5 (A) cells or in GC92 ARTEMIS KO cells (B). GC92, GCS5, or GC92 ARTEMIS KO cells were treated with siRNA against ARTEMIS. As a control, cells were treated with DMSO or control siRNA. (A) Cells were harvested 72 h post-co-transfection with the I-SceI and RFP plasmids. (B) GC92 WT or ARTEMIS KO cells were transfected with the RFP, cMyc-ART-WT, or cMyc-ART-D37N plasmid. After 36 h, cells were transfected with I-SceI and harvested after an additional 72 h. Representative images were captured with a 63x objective using Metafer Isis software. Scale bar represents 10 μ m. Diagram of the WT exogenous ARTEMIS and the endonuclease

mutant D37N are not drawn to scale. (A, B) Downregulation, KO, and expression of exogenous plasmids were confirmed by immunoblotting. Cells were stained with anti-CD4 or anti-GFP plus anti-RFP or anti-cMyc AB plus DAPI. Samples were scanned using Metafer software and only plasmid-transfected cells were analyzed. Data represent the mean of 8 or 16 independent experiments performed in duplicates ($n = 16$ for A; $n = 8$ for B). (C) Cells were co-transfected with the RFP and I-SceI plasmids and treated with EdU and nocodazole 30 min prior to harvest. Harvest took place 72 h post-plasmid transfection. Cells were stained with anti- γ H2AX, anti-RFP AB, and DAPI. Samples were scanned using Metafer software and only plasmid-transfected G₁ cells were analyzed. Data represent the mean of 5 independent experiments ($n = 5$). (A, B, C) RFP and cMyc were used as markers for cells with damage induction and exogenous protein (see chapter 3.1.1). Error bars show the 95% CI. Effect size was calculated by Cohen's d and p -value was obtained by one-way ANOVA with Bonferroni correction. (B, C) Several data points were part of the analysis in Biels et al. (2017).

Next, two GC92 KO cell lines were generated using CRISPR/Cas9 with different gRNAs (Figure S8.9 d). In both GC92 ARTEMIS KO cell lines, misrepair events were never observed (Figures 3.11 B, S8.9 c). All further experiments were conducted with the ARTEMIS KO cell line generated with gRNA #3. To exclude a loss of the end-joining substrate during the generation of the KO cell line causing the absence of misrepair events in GC92 ARTEMIS KO cells, exogenous epitope-tagged ARTEMIS protein was introduced into the cells by transfection with the WT ARTEMIS plasmid (Figure 3.11 B). The quantity of misrepair events in GC92 ARTEMIS KO cells positive for the cMyc-ARTEMIS protein rose to 7.6%. GC92 cells transfected with an ARTEMIS mutant plasmid encoding an ARTEMIS protein with Asp37 mutated to Asn (which results in the disruption of the endonuclease function) failed to generate any misrepair events. To elaborate on the findings in GC92 cells after ARTEMIS depletion or in GC92 ARTEMIS KO cells, the γ H2AX foci assay was conducted. The mean number of γ H2AX foci rose to 3.0 and 2.9, respectively. This was a significant difference ($p < .001$) compared to the control with effect sizes of 2.85 and 6.79 (Figure 3.11 C). These results demonstrate the absolute necessity of the endonuclease function of ARTEMIS in the misrejoining of distant DSBs after I-SceI damage induction.

Next, SFB-tagged ARTEMIS WT protein was precipitated and purified from stably-transfected HEK293 cells after no irradiation, 30 min, or 2 h post-X-IR with 5 Gy. Proteins that were co-precipitated with ARTEMIS were analyzed by mass spectrometry (MS) to further establish factors that might be of interest in this kind of end-joining repair. Of note, the protein name used in MS analysis is indicated in parenthesis whenever it differs from the protein name used in this thesis. Generally, interacting proteins either showed an increase (ratios > 2), decrease (ratios < 0.5), or maintained a more-or-less steady interaction (ratios between 0.5 and 2) with ARTEMIS (DCLRE1C) after damage induction and the indicated repair time (Table 8.4). Several established direct or indirect ARTEMIS interaction partners and novel potential interacting proteins were observed. The strongest interaction (indicated by the most interacting peptides) was with DNA-PKcs (PRKDC)^{144,251}. Several factors of the c-NHEJ machinery were co-precipitated with ARTEMIS (KU80 (XRCC5), KU70 (XRCC6), XRCC4, and LIG4). LIG4 showed

an interaction increase 2 h post-irradiation. Another established ARTEMIS interaction partner is the DNA damage checkpoint control protein TOPBP1, which showed a damage-inducible increase in interacting peptides with ARTEMIS 30 min and 2 h post-irradiation. TOPBP1 provides the binding platform for resection and anti-resection factors³⁵⁵, including anti-resection factor 53BP1. One of 53BP1s downstream factors is PTIP (PAXIP1), which was observed in this experiment and is an established ARTEMIS-interacting factor in a damage-inducible manner⁴⁰⁰. Furthermore, POH1 (PSMD14) was also observed to increasingly interact with ARTEMIS 2 h post-irradiation. POH1 has two roles in DSB repair: as a regulator of c-NHEJ it restricts 53BP1 accumulation and in G₂ it promotes HR by functioning in the process of relieving the anti-resection barrier posed by 53BP1^{59,203}. Another steady interaction was observed with all members of the MRN complex: MRE11, RAD50, and NBS1 (NBN)^{228,303,383}. Interestingly, a novel damage-inducible interaction increase was observed with NONO and SFPQ, which together form a complex, stabilize KU, and are involved in identifying and aligning the accurate DSB ends during c-NHEJ^{187,213,387}. Additionally, some chromatin remodeling factors were also observed to interact with ARTEMIS (e.g. MCRS1^{86,98}, KAP1 (TRIM28)). Interestingly, a damage-inducible increase in the interaction of DDX1 with ARTEMIS was observed. DDX1 plays a role in RNA clearance at DSBs and is thereby associated with facilitating template-guided repair of transcriptionally-active regions in the genome²³⁶.

In summary, ARTEMIS is an essential factor in the misrepair of DSBs and also in the resection process during repair in G₁ phase after X-IR. Furthermore, ARTEMIS is associated with an array of proteins involved in the DNA damage response, and thus provides the foundation for the analysis of which additional factors might be involved in this repair pathway.

3.2.5. Misrepair in 53BP1-depleted cells is conducted by alt-EJ

A factor mentioned in the ARTEMIS interaction studies (chapter 3.2.4) is 53BP1. 53BP1 builds the binding platform for many downstream factors in the DNA damage response and is essential in counteracting resection^{14,438}. The finding that the repair pathway, which is responsible for the misrejoining of distant DSBs, might involve resection but at the same time limits it by protecting the DSB ends through KU-binding, makes the anti-resection factor 53BP1 a strong candidate to be involved in this pathway. Depletion of 53BP1 by transfection with siRNA (Figures 3.12 A, B) or by CRISPR/Cas9 viral transduction with a gRNA (Figure S8.10 a), led to elevated frequencies of misrepair events in GC92 cells between 16.2% and 20.4% with the means differing significantly ($p < 0.001$) from the controls. These elevated levels were reduced to 10.1% in 53BP1-depleted cells upon transfection with a WT HA-53BP1 plasmid (Figure 3.12 B). Consistent with the elevated levels of misrepair events in GC92 cells after 53BP1 depletion, the mean γ H2AX foci level was not altered (Figure 3.13 B).

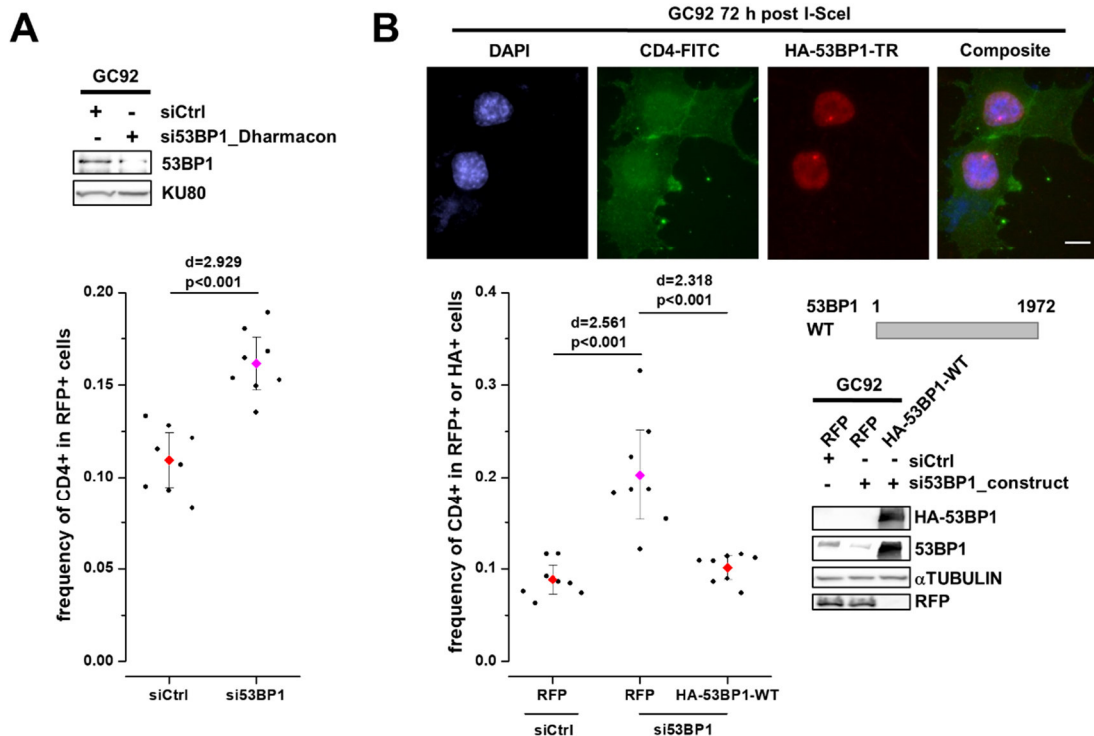


Figure 3.12 53BP1 depletion increases misrepair in GC92 cells

(A) Impact of 53BP1 depletion (A, B) and 53BP1 complementation (B) on misrepair in GC92 cells. GC92 cells were treated with siRNA against 53BP1. As a control, cells were treated with control siRNA. (A) Cells were harvested 72 h post-co-transfection with I-SceI and RFP plasmids. (B) Cells were transfected with the RFP or siRNA-resistant HA-53BP1-WT plasmid. 36 h after plasmid transfection, cells were transfected with I-SceI and harvested after an additional 72 h. Representative images were captured with a 63x objective using Metafer Isis software. Scale bar represents 10 μ m. Diagram of the exogenous WT 53BP1 is not drawn to scale. (A, B) Downregulation by siRNA and expression of exogenous plasmids were confirmed by immunoblotting. Cells were stained with anti-RFP or anti-HA plus anti-CD4 AB and DAPI. Samples were scanned using Metafer software and only plasmid-transfected cells were analyzed. Data represent the mean of 8 independent experiments performed in duplicate ($n = 8$). RFP and HA were used as markers for cells with damage induction and exogenous protein (see chapter 3.1.1). Error bars show the 95% CI. Effect size was calculated by Cohen's d and p -value was obtained by one-way ANOVA with Bonferroni correction (for B) or by two-sample Student's t -test (for A). Several data points were part of the analysis in Biehs et al. (2017).

To investigate how this increase in misrepair of distant DSBs emerges in 53BP1-depleted GC92 cells, additional factors were depleted and misrepair events and overall repair observed. Additional depletion of DNA-PKcs or LIG4, as well as additional inhibition of DNA-PK did not alter the increased frequency of misrepair events in 53BP1-depleted cells (Figure 3.13 A) and also did not impact the overall repair (Figure 3.13 B). Therefore, the block at the DNA ends by the DNA-PK inhibitor can be overcome in 53BP1-depleted GC92 cells, which was not possible in the WT situation (compare to Figure 3.5 A). This suggests the usage of another end-joining mechanism to generate misrepair events in 53BP1-depleted cells. As KU70/80 and 53BP1-depleted cells both showed an increase in misrepair events, the dependence of 53BP1-depleted cells on alt-EJ factors (similar to KU70/80-depleted GC92 cells) was tested (compare to Figure 3.7 B). PARP inhibition by Olaparib or depletion of PARP1 or LIG1/3 in 53BP1-depleted GC92 cells resulted in significant reduction ($p < 0.001$) in misrepair events to levels between 1.3%

and 2.3% with effect sizes between 10.30 and 9.01 (Figure 3.13 C). Moreover, for all conditions including depletion or inhibition of alt-EJ factors in addition to 53BP1 depletion, a significant rise of γ H2AX foci from 1.1 to levels between 2.5 and 2.8 (p -values between 0.011 and 0.023) was observed (Figure 3.13 D). Next, the previously-investigated polymerases (chapter 3.2.3) were depleted in GC92 cells in addition to 53BP1. Polymerases POL λ/μ neither impacted the increased frequency of misrepair events (Figure S8.10 b) nor the overall repair compared to the single 53BP1 depletion (Figure S8.10 c). However, co-depletion of POL θ with 53BP1 strongly reduced misrepair events in GC92 cells to 1.1% (Figure S8.10 b) and increased the mean γ H2AX foci to 3.0 (Figure S8.10 c).

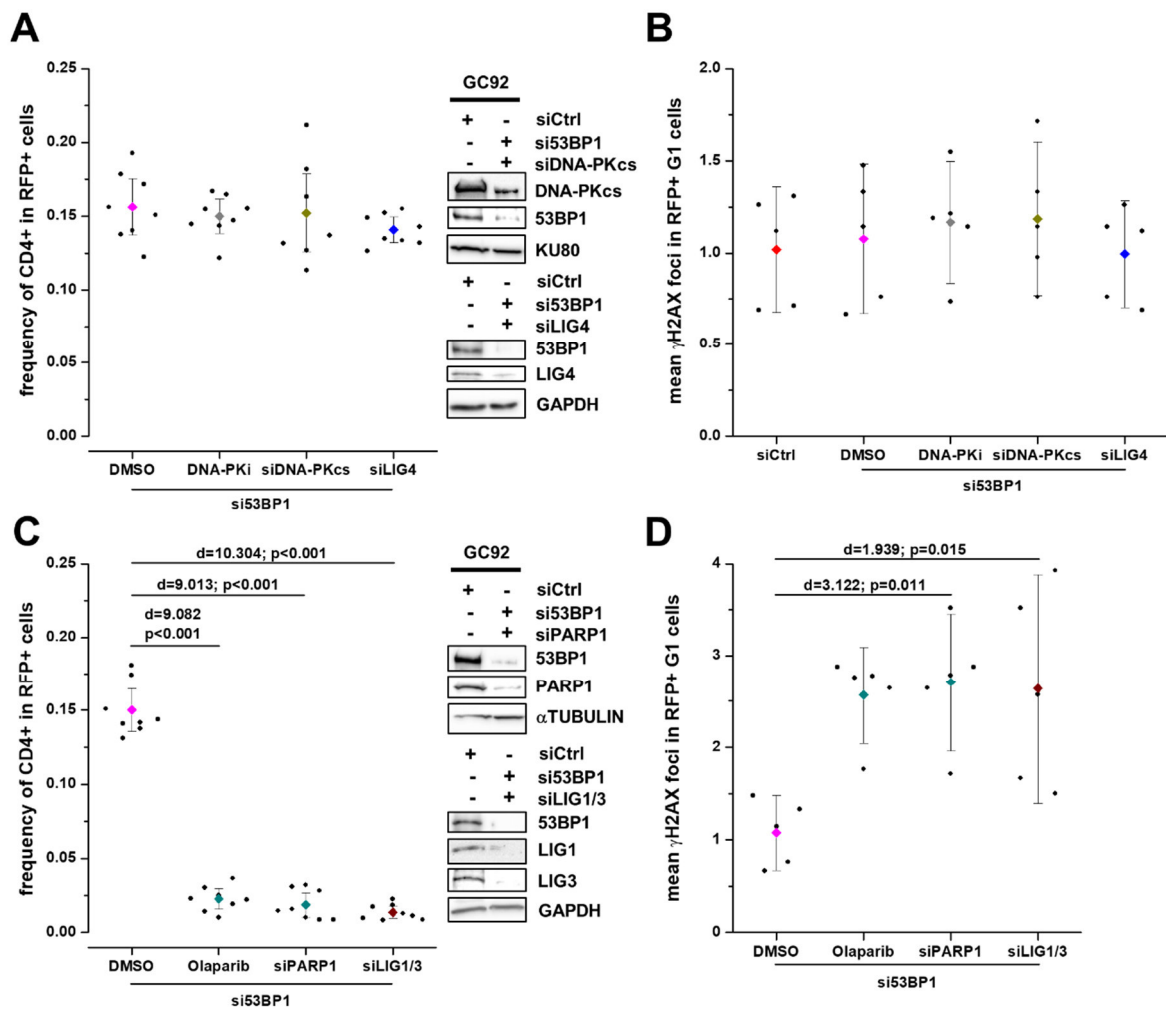


Figure 3.13 Misrepair in 53BP1-depleted GC92 cells requires alt-EJ factors

(A, B, C, D) Impact of inhibition or depletion of c-NHEJ factors (A, B) or alt-EJ factors (C, D) on misrepair (A, C) or repair (B, D) in 53BP1-depleted GC92 cells. GC92 cells were treated with inhibitors and/or siRNAs against DNA-PK (Nu7441), DNA-PKcs, LIG4, PARP (Olaparib), PARP1, LIG1/3, and/or 53BP1. As a control, cells were treated with DMSO or control siRNA. (A, C) Harvest took place 72 h post-co-transfection with I-SceI and RFP plasmids. Downregulation by siRNA was confirmed by immunoblotting. Cells were stained with anti-CD4, anti-RFP AB, and DAPI. Samples were scanned using Metafer software and only plasmid-transfected cells were analyzed. Data represent the mean of 8 independent experiments performed in duplicate ($n = 8$). (B, D) GC92 cells were co-transfected with RFP and I-SceI plasmids and treated with EdU and nocodazole 30 min prior to harvest. Harvest took place 72 h post-plasmid transfection. Cells were stained with anti- γ H2AX, anti-RFP AB, and DAPI. Samples were scanned using Metafer software and only plasmid-transfected G₁ cells were analyzed. Data represent the mean of

5 independent experiments ($n = 5$). (A, B, C, D) RFP was used as a marker for cells with damage induction (see chapter 3.1.1). Error bars show the 95% CI. Effect size was calculated by Cohen's d and p -value was obtained by one-way ANOVA with Bonferroni correction. (B, C, D) Several data points were part of the analysis in Biehs et al. (2017).

53BP1 is associated with several other factors. This includes PTIP and ARTEMIS⁴⁰⁰ in one downstream cascade and RIF1 and REV7¹²⁷ in another downstream cascade. Additionally, RAP80 is also described to pose a resection barrier in S/G₂ phase²⁰³. Therefore, the impact of impairment of these factors in the GC92 reporter assay was investigated next. 53BP1 depletion in GC92 ARTEMIS KO cells neither affected the abolished misrepair events in the ARTEMIS KO cell line (Figure 3.14 A) nor the repair defect in the γ H2AX foci assay (Figure S8.10 d). Impairment of RIF1 or REV7 by CRISPR/Cas9 viral transduction of gRNAs led to elevated frequencies of misrepair events in GC92 cells, comparable to 53BP1-depleted cells (Figure 3.14 B). In contrast, PTIP impairment by CRISPR/Cas9 viral transduction of a gRNA significantly reduced the misrepair events compared to the control to 4.2% ($p < 0.001$). Depletion of RAP80 increased misrepair events to 21.2%, which differed significantly ($p = 0.018$) from the control with an effect size of 1.34 (Figure 3.14 C).

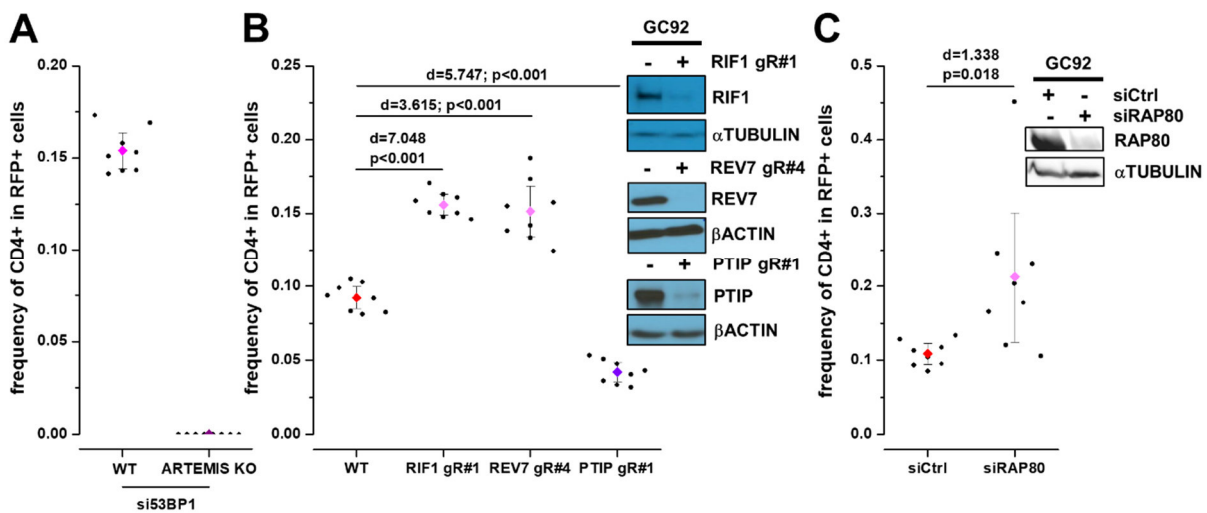


Figure 3.14 The absence of the known resection barrier proteins RIF1, REV7, and RAP80 increased, while the absence of the 53BP1-associated factor PTIP reduced the misrepair of distant DSB ends (A) Impact of 53BP1 depletion (A), 53BP1-associated factors impaired by CRISPR/Cas9 viral transduction (B), or RAP80 depletion (C) on misrepair in GC92 WT (A, B, C) or ARTEMIS KO (A) cells. (A, C) GC92 WT or ARTEMIS KO cells were treated with siRNAs against 53BP1 or RAP80. As a control, cells were treated with control siRNA. (B) GC92 cells were transduced with CRISPR/Cas9 and RIF1 #1, REV7 #4, or PTIP #1 gRNA plasmids and selected. (B, C) Downregulation by CRISPR/Cas9 or siRNA was confirmed by immunoblotting. (A, B, C) Cells were harvested 72 h post-co-transfection with the I-SceI and RFP plasmids and stained with anti-CD4, anti-RFP AB, and DAPI. Samples were scanned using Metafer software and only plasmid-transfected cells were analyzed. Data represent the mean of 8 independent experiments performed in duplicates ($n = 8$). RFP was used as a marker for cells with damage induction (see chapter 3.1.1). Error bars show the 95% CI. Effect size was calculated by Cohen's d and p -value was obtained by one-way ANOVA with Bonferroni correction (for B) or by two-sample Student's t -test (for C).

In summary, 53BP1 depletion proved to be an effective way to clarify that misrepair of distant DSBs in GC92 cells only occurs in an alt-EJ-dependent manner if resection barriers such as

53BP1 are absent. This is similar to the situation when DSB ends are not protected by KU70/80 (chapter 3.2.1) and is different to the WT situation where resection takes place using a repair mechanism dependent on c-NHEJ factors. Therefore, 53BP1 depletion can be used as a tool to investigate how the WT resection-dependent pathway differs from the backup pathway alt-EJ.

3.3. Resection in end-joining: how resection barriers can be overcome

As established in the first and second part of this results section, misrejoining of distant DSB ends might involve short resection and relies on various factors that are known resection barriers. The leading question of part three is how resection can occur in a pathway dependent on c-NHEJ factors and which mechanisms overcome the previously-described resection barriers.

3.3.1. Misrepair relies on the pro-resection factor BRCA1

BRCA1 plays a central role in counteracting the anti-resection factor 53BP1 in S/G₂ phase by promoting its dephosphorylation¹⁸⁶. BRCA1 is the pivotal component in a number of protein complexes involved in DNA repair. One complex, for instance, is the BRCA1-C complex, which initiates resection in S/G₂ and includes proteins such as MRE11 and CtIP^{78,412}. However, BRCA1 also forms the BRCA1-A complex, which is essential in regulating the extent of resection during HR by stabilizing 53BP1 in S/G₂ phase¹⁶². It involves factors such as ABRAXAS and RAP80. In G₁ phase, BRCA1 is rapidly recruited to the DSBs by KU80^{197,336}. To investigate BRCA1's role in the misrepair of distant DSBs, BRCA1 was depleted in GC92 cells. The mean frequency of misrepair in BRCA1-depleted cells was significantly reduced by half compared to the control ($p < 0.001$, Figure 3.15 A). Next, CRISPR/Cas9 technology was used to generate a GC92 BRCA1 KO cell line (Figure S8.11 a). The frequency of misrepair events was also reduced by half in this BRCA1 KO cell line compared to the WT, as were the misrepair events in GC92 cells in which BRCA1 was impaired by CRISPR/Cas9 viral transduction of another gRNA (Figure S8.11 b). BRCA1 depletion in GCS5 cells, which contain the reporter construct with two close DSBs, showed a decrease in misrepair events to one-third compared to the control (Figure S8.11 c).

Since BRCA1's role in S/G₂ is to antagonize 53BP1, BRCA1 was next co-depleted with 53BP1 in GC92 cells. In BRCA1-53BP1 co-depleted cells, misrepair events increased to 15.5%, which resembled the situation with single 53BP1 depletion (Figure 3.15 B, compare to 3.12 A). Thus, BRCA1 is specifically required to counteract 53BP1 in the misrejoining of distant DSB ends. However, BRCA1 is dispensable in the absence of 53BP1 and misrepair events are generated by alt-EJ (as established in chapter 3.2.5). Depletion of BRCA1 did not affect the abolished misrepair events in GC92 ARTEMIS KO cells (Figure 3.15 B). The γ H2AX foci assay was used to investigate overall repair. Although BRCA1 depletion reduced misrepair events by 50%, no impact was observed in the γ H2AX foci assay (Figure S8.11 d). While GC92 ARTEMIS KO cells

showed a full repair defect with an increase to 3 γ H2AX foci, BRCA1 depletion in GC92 ARTEMIS KO cells reduced this repair defect to 1.8 γ H2AX foci with an effect size of 1.83 compared to the control.

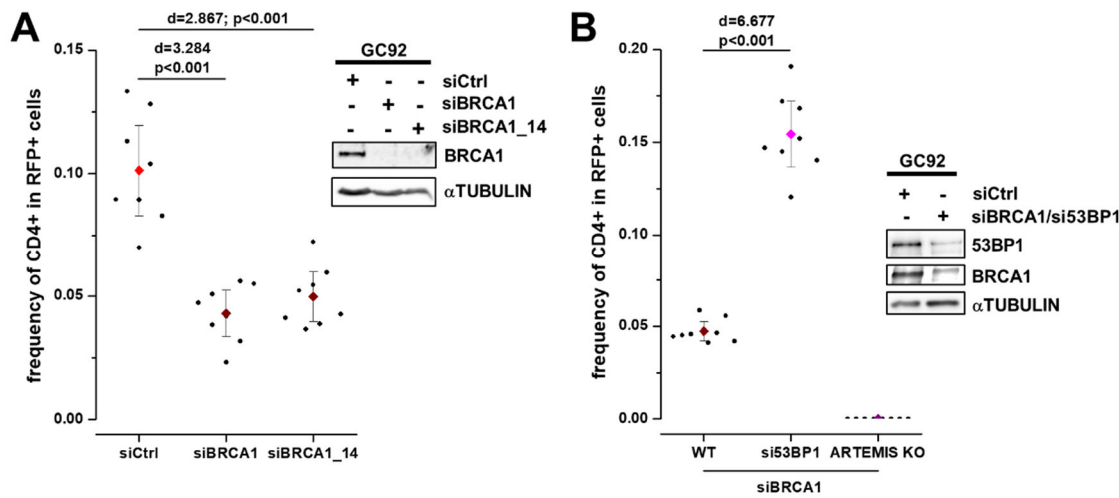


Figure 3.15 BRCA1 depletion decreases misrepair in GC92 cells

(A, B) Impact of BRCA1 depletion (A, B) or BRCA1-53BP1 co-depletion (B) on misrepair (A, B) in GC92 WT (A, B) or ARTEMIS KO (B) cells. GC92 WT or ARTEMIS KO cells were treated with siRNAs against BRCA1 and/or 53BP1. As a control, cells were treated with control siRNA. Cells were harvested 72 h post-co-transfection with I-SceI and RFP plasmids. Downregulation by siRNA was confirmed by immunoblotting. Cells were stained with anti-CD4, anti-RFP AB, and DAPI. Samples were scanned using Metafer software and only plasmid-transfected cells were analyzed. Data represent the mean of 8 independent experiments performed in duplicate ($n = 8$). RFP was used as a marker for cells with damage induction (see chapter 3.1.1). Error bars show the 95% CI. Effect size was calculated by Cohen's d and p -value was obtained by one-way ANOVA with Bonferroni correction. Several data points were part of the analysis in Biehs et al. (2017).

Due to the location of the gRNA, the generated GC92 BRCA1 KO cell line contains a BRCA1 protein with a deleted BRCT domain while the RING domain is still present (Figure S8.11 a). The BRCT domain is important for BRCA1s interaction with other proteins and the RING domain is the location of its E3 ubiquitin ligase activity¹²⁷. Therefore, which BRCA1 domains are required for the misrepair of distant DSBs was investigated next. Exogenous FLAG-BRCA1 protein was introduced into the cells by transfection (Figures 3.16 A). The frequency of misrepair events in BRCA1-depleted GC92 cells positive for the exogenous WT BRCA1 protein rose significantly to 10.1% compared to the BRCA1-depleted condition ($p < 0.001$, $d = 4.10$). Transfection with a BRCA1 mutant plasmid encoding a BRCA1 protein with Ile26 mutated to Ala, which partially impairs the BRCA1 RING domain, also resulted in frequencies of misrepair events similar to the control. However, Feng et al. (2015) proposed that this mutant has residual activity. Therefore, exogenous BRCA1 with a Cys61 mutated to Gly RING domain mutation was used. Here, the frequency of misrepair events remained at 50% compared to the control, which resembled the situation after BRCA1 depletion. Finally, GC92 cells were transfected with a BRCA1 plasmid with a BRCT domain mutant encoding a BRCA1 protein with Ser1655 mutated to Ala. The complementation with the BRCA1 BRCT mutant also failed to restore the full

frequency of misrepair events. The exogenous BRCA1 protein levels of the complementation experiments presented in Figure 3.16 A were low. In contrast, all other plasmids used in this study resulted in overexpression and high protein levels. Therefore, the effect of BRCA1 overexpression was examined next. The SFB-BRCA1 plasmid was used, which resulted in high quantities of exogenous BRCA1 in GC92 cells (Figure S8.11 e). The frequency of misrepair was not altered by BRCA1 overexpression.

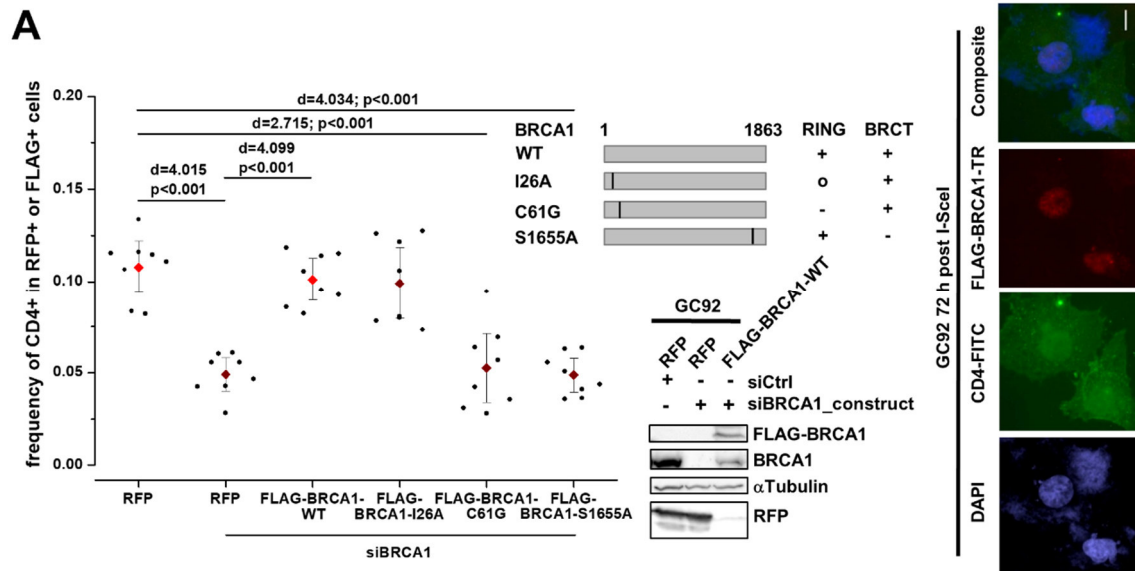


Figure 3.16 The RING and BRCT domains of BRCA1 are required for the misrepair of distant DSBs (A) BRCA1 complementation in BRCA1-depleted GC92 cells. GC92 cells were treated with siRNA against BRCA1. As a control, cells were treated with control siRNA. GC92 cells were transfected with the RFP or siRNA-resistant FLAG-BRCA1-WT, FLAG-BRCA1-I26A, FLAG-BRCA1-C61G, or FLAG-BRCA1-S1655A plasmid. 36 h after plasmid transfection, cells were transfected with I-SceI and harvest took place after an additional 72 h. Downregulation by siRNA and expression of exogenous plasmids were confirmed by immunoblotting. Cells were stained with anti-RFP or anti-FLAG plus anti-CD4 AB and DAPI. Samples were scanned using Metafer software and only plasmid-transfected cells were analyzed. Data represent the mean of 8 independent experiments performed in duplicate ($n = 8$). RFP and FLAG were used as a marker for cells with damage induction and exogenous protein (see chapter 3.1.1). Error bars show the 95% CI. Effect size was calculated by Cohen's d and p -value was obtained by one-way ANOVA with Bonferroni correction. Representative images were obtained with a 63x objective using Metafer Isis software. Scale bar represents 10 μm . Diagrams of the exogenous BRCA1 WT, the I26A partial RING domain mutant, the C61G RING domain mutant, and the S1655A BRCT domain mutant are not drawn to scale. Several data points were part of the analysis in Biehs et al. (2017).

To summarize, BRCA1 is an important factor in the misrejoining of distant and close DSB ends after I-SceI damage induction. For the misrejoining of distant DSBs, both the RING and the BRCT domain are required. In a 53BP1 impaired background, BRCA1 is dispensable for the misrepair of distant DSB ends.

3.3.2. The resection initiating factor CtIP is required for the misrejoining of distant DSB ends

As mentioned in the previous chapter (3.3.1), BRCA1 interacts with the endonuclease CtIP to initiate resection during HR ^{78,412}. In unirradiated samples, this interaction is exclusively

observed in S/G₂ phase and dependent on a CDK complex-mediated phosphorylation of CtIP at Ser327⁴²⁸. Hence, it was first tested if a BRCA1-CtIP interaction is possible in G₁. Exogenous GFP-CtIP was immunoprecipitated from G₁-synchronized HEK293 cells. The cells showed a synchronization in G₁ phase 24 h post-plasmid transfection (Figure S8.12 a). Thus, only transfected cells were immunoprecipitated using a GFP antibody. Upon damage induction, phosphorylation of CtIP at Ser327 was observed 30 min post-5 Gy X-IR (Figure S8.12 b). Simultaneously, CtIP was observed interacting with BRCA1 in irradiated cells, but not in the unirradiated sample. The damage-inducible BRCA1-CtIP interaction was confirmed by immunoprecipitation of endogenous BRCA1 from HEK293 cells, which pulled down exogenous GFP-CtIP 30 min post-irradiation. Additionally, exogenous GFP-CtIP phospho-mutant with Ser327 mutated to Ala was immunoprecipitated from G₁-synchronized HEK293 cells. As expected, no phosphorylation was observed at site 327. Moreover, BRCA1 did not interact with the exogenous CtIP phospho-mutant. The lack of interaction was confirmed by immunoprecipitation of endogenous BRCA1, which failed to co-immunoprecipitate the exogenous CtIP phospho-mutant. Therefore, in contrast to S/G₂ phase, the BRCA1-CtIP interaction exists in G₁ only in a damage-inducible manner. Similar to S/G₂ phase, it is also dependent on the phosphorylation of CtIP at Ser327.

The damage-inducible interaction of CtIP with BRCA1 in G₁ phase makes CtIP a promising candidate that might be involved in the misrepair of distant DSBs after I-SceI-induced damage. Indeed, CtIP depletion in GC92 cells resulted in a significant reduction of the mean misrepair events from 9.8% to 5.0% ($p < 0.001$, $d = 2.39$, Figure 3.17 A). This observation was confirmed after CtIP impairment by viral transduction of CRISPR/Cas9 in GC92 cells (Figure S8.13 a). However, the reduction in misrepair events did not impact overall repair in CtIP-depleted GC92 cells as per the mean value of γ H2AX foci (Figure 3.17 B). An even bigger effect ($d = 5.37$) was observed in the reduction of misrepair events in the GCSH14 reporter system, which also monitors distant DSBs (Figure 3.17 A). In contrast, CtIP depletion in the GCS5 reporter system with two relatively-close DSBs had no impact on its misrepair events. Next, CtIP was overexpressed in GC92 cells by transient transfection of a WT CtIP plasmid encoding exogenous RFP-CtIP (Figure 3.17 C). Surprisingly, misrepair events increased significantly to a mean value of 18.5% ($p < 0.001$) with an effect size of 3.82. To test if this effect was caused by the overexpression of the exogenous CtIP, a stable SFB-CtIP GC92 cell line was generated, which did not overexpress CtIP. Misrepair events in this cell line were not altered compared to the control. Thus, CtIP and BRCA1 interact in G₁ phase after damage-induction and depletion of each protein resulted in a 50% decrease in misrepair events in GC92 cells, but did not alter the overall repair efficiency. However, their roles in misrepair seem to differ since only

overexpression of CtIP resulted in increased misrepair of distant DSB ends and only BRCA1 depletion showed a decrease in misrepair of close DSB ends.

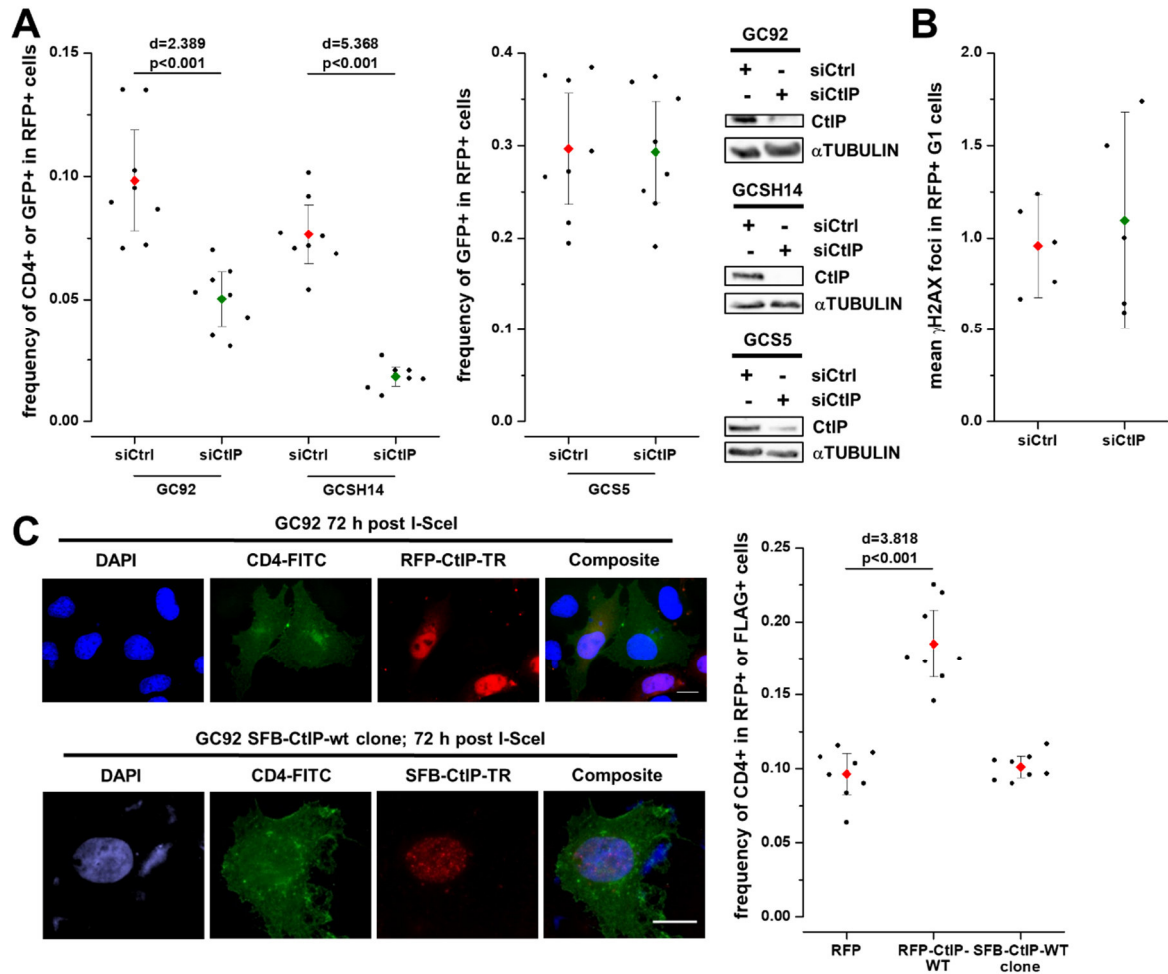


Figure 3.17 CtIP is required for misrejoining of distant DSB ends

(A, B, C) Impact of CtIP depletion (A, B) or exogenous CtIP (C) on misrepair (A, C) or overall repair (B) in GC92 (A, B, C), GCSH14, or GCS5 (A) cells. GC92, GCSH14, or GCS5 cells were treated with siRNA against CtIP. As a control, cells were treated with control siRNA. (A) Cells were harvested 72 h post-co-transfection with I-SceI and RFP plasmids. Downregulation by siRNA was confirmed by immunoblotting. (B) Cells were co-transfected with RFP and I-SceI plasmids and treated with EdU and nocodazole 30 min prior to harvest. Harvest took place 72 h post-plasmid transfection. Cells were stained with anti- γ H2AX, anti-RFP AB, and DAPI. Samples were scanned using Metafer software and only plasmid-transfected G_1 cells were analyzed. Data represent the mean of 5 independent experiments ($n = 5$). (C) GC92 cells were transfected with the RFP or RFP-CtIP-WT plasmid or a stable GC92 cell line was used, which does not overexpress SFB-CtIP-WT. 36 h after plasmid transfection, cells were transfected with I-SceI and harvest took place after an additional 72 h. Representative images were obtained with a 63x objective using Metafer Isis software. Scale bar represents 10 μ m. (A, C) Cells were stained with anti-RFP or anti-FLAG plus anti-CD4 or anti-GFP AB plus DAPI. Samples were scanned using Metafer software and only plasmid-transfected cells were analyzed. Data represent the mean of 8 independent experiments performed in duplicate ($n = 8$). (A, B, C) RFP and FLAG were used as a marker for cells with damage induction and exogenous protein (see chapter 3.1.1). Error bars show the 95% CI. Effect size was calculated by Cohen's d and p -value was obtained by one-way ANOVA with Bonferroni correction. Several data points were part of the analysis in Barton et al. (2014).

As CtIP seems to play an exclusive role in the misrejoining of distant DSBs, the misrejoined sites were investigated in CtIP-depleted GC92 cells by sequence analysis. The distribution of deletions after depletion of CtIP differed in many aspects from the distribution in control

sequences (Figure 3.18 A, Tables 8.1, 8.5). First, while the frequency of sequences with no additional deletions remained similar, the frequency of deletions below 10 nt was greatly reduced after CtIP depletion. Second, the categories with deletions between 10 nt and 50 nt were also reduced with the exception of additional deletions between 20 nt and 30 nt, which increased. Finally, all categories of additional deletions above 50 nt also increased after CtIP depletion with accumulations between 50 nt and 200 nt, as well as above 300 nt. Accordingly, the mean deletion size increased significantly from 34 nt to 120 nt after CtIP depletion ($p = 0.003$) with an effect size of 2.97 (Figure 3.18 B). The distribution of insertions in relation to the deletion size expectedly showed more insertions at bigger deletions due to the greater percentage of bigger deletions in total (Tables 8.1). Moreover, more insertions were observed after CtIP depletion compared to control cells and the mean insertion size increased (Figure 3.18 C). Surprisingly, the misjoining of distant DSBs without the use of MHs at sites with deletions more than tripled in CtIP-depleted cells compared to the control (Figure 3.18 D). Furthermore, the most frequent category in control cells of 4 nt MH length was completely abolished after CtIP depletion. These findings suggest that CtIP is involved in a pathway, which preferentially generates small deletions of fewer than 50 nt at the DSB and then misjoins distant DSBs using MHs, preferentially 4 nt long. In the absence of CtIP, the size of the deletions in the remaining 50% of misrepair events increases, bigger insertions are used, and distant DSBs are preferentially rejoined without the use of MHs. Due to the growth in deletion size some sequence alterations might harm the reporter gene and go unnoticed in the reporter assay. Therefore, the analyzed sequences were limited in their maximum size by selection of CD4-positive cells and the primers used for amplification.

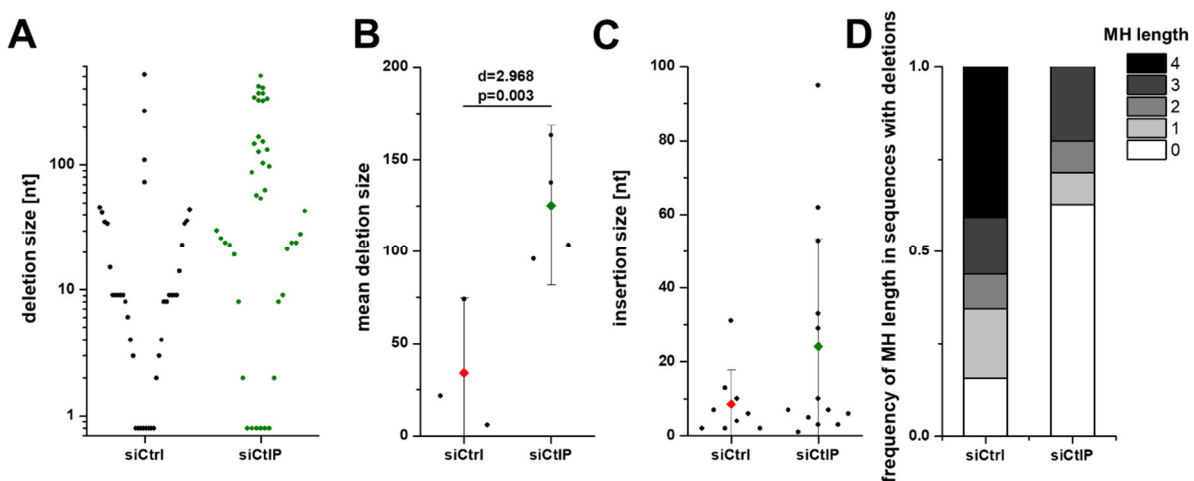


Figure 3.18 CtIP depletion results in an increase in the deletion size at the misrejoined sites of the remaining misrepair events and rejoining is primarily conducted without MHs

GC92 cells were treated with siRNA against CtIP (and control siRNA) and harvested 72 h post-I-SceI transfection. Cells were incubated with anti-CD4 AB and magnetic MicroBeads to be enriched by MACS. After cell lysis, DNA purification, and amplification, the DNA was sequenced. (A, B) Distribution of deletion sizes of all analyzed 40 (siCtrl) or 41 (siCtIP) sequences from 4 or 5 independent experiments (A) or of the mean value from the 4 or

5 independent experiments (B) ($n = 4$ for siCtrl; $n = 5$ for siCtIP). (A) Events with no additional deletions were given a value < 1 nt to include them in the logarithmic scale. (B) Error bars show the 95% CI. (C) Mean insertion size of the 9 (siCtrl) or 13 (siCtIP) observed insertions ($n = 4$ for siCtrl; $n = 5$ for siCtIP). Error bars show the *SD*. (D) Frequency of MH length used for rejoining in all 32 (siCtrl) or 35 (siCtIP) sequences with additional deletions from the 4 or 5 experiments ($n = 4$ for siCtrl; $n = 5$ for siCtIP). (A, B, C, D) For further details see Tables 8.1, 8.5.

To investigate how this decrease in misrejoining of distant DSBs arises in CtIP-depleted GC92 cells, additional proteins were impaired by depletion or inhibition. First, the impact of impaired c-NHEJ and alt-EJ factors in addition to CtIP depletion was examined. Inhibition of DNA-PK or depletion of DNA-PKcs further decreased the frequency of misrepair in CtIP-depleted GC92 cells (Figure 3.19 A). In contrast, PARP inhibition by Olaparib or additional depletion of LIG1/3 resulted in similar frequencies of misrepair events compared to CtIP depletion alone (Figures 3.19 A, S8.13 b). Next, CtIP was co-depleted in combination with polymerases investigated in previous chapters (3.2.3, 3.2.5). Additional depletion of POL θ did not impact the frequency of misrepair events in CtIP-depleted GC92 cells (Figure 3.19 B). Conversely, additional depletion of POL λ/μ further reduced the misrepair events to a mean value of 0.9%, which was a significant difference ($p < 0.001$) compared to the 4.6% in cells with only CtIP depletion. Accordingly, co-depletion of POL λ/μ with CtIP increased the mean value of γ H2AX foci to 2.7, while additional depletion of POL θ did not show a repair defect (Figure S8.13 c). Therefore, POL θ acts in one pathway together with CtIP to generate misrepair events in GC92 cells. This fits with POL θ s described preferential use of 4 nt MHs for rejoining⁴¹⁴, which were abolished in the sequence analysis of the misrejoined sites after CtIP depletion (Figure 3.18 D). Additionally, misrepair events that arise in the absence of CtIP rely on c-NHEJ-associated polymerases.

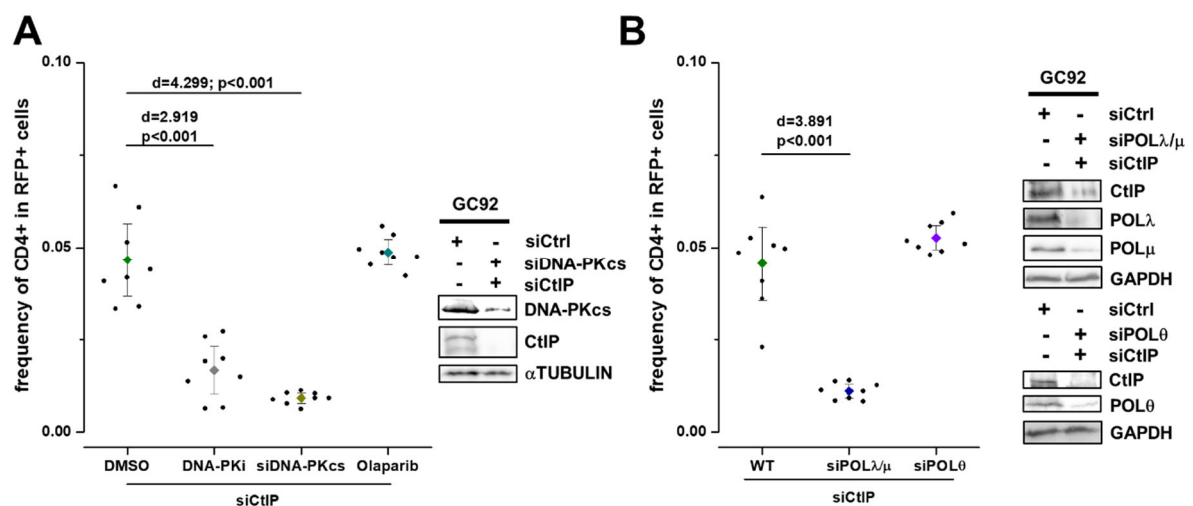


Figure 3.19 In the absence of CtIP, DNA-PK is required to misrejoin the remaining distant DSB ends, while POL θ and PARP are not

(A, B) Impact of inhibition or depletion of c-NHEJ factors, alt-EJ factors (A), or polymerases (B) on misrepair in CtIP-depleted GC92 cells. GC92 cells were treated with inhibitors and/or siRNAs against CtIP and DNA-PK (Nu7441), DNA-PKcs, PARP (Olaparib), POL θ , or POL λ/μ . As a control, cells were treated with DMSO. Harvest took place 72 h post-co-transfection with I-SceI and RFP plasmids. Downregulation by siRNA was confirmed by immunoblotting.

Cells were stained with anti-CD4, anti-RFP AB, and DAPI. Samples were scanned using Metafer software and only plasmid-transfected cells were analyzed. Data represent the mean of 8 independent experiments performed in duplicate ($n = 8$). RFP was used as a marker for cells with damage induction (see chapter 3.1.1). Error bars show the 95% CI. Effect size was calculated by Cohen's d and p -value was obtained by one-way ANOVA with Bonferroni correction.

As established in chapter 3.2.4, the nuclease ARTEMIS is crucial for misrepair of distant DSB ends. Therefore, CtIP was next depleted in GC92 ARTEMIS KO cells, which maintained the abolishment of misrepair events as was observed in GC92 ARTEMIS KO cells (Figure 3.20 A). The γ H2AX foci assay was conducted to investigate if the lack of misrepair events was due to the lack of repair, as GC92 ARTEMIS KO cells had a full repair defect of 3 γ H2AX foci (Figure 3.11 C). The mean γ H2AX foci were significantly reduced from 2.9 foci in GC92 ARTEMIS KO cells to 1.7 foci in CtIP-depleted GC92 ARTEMIS KO cells ($p < 0.001$) with an effect size of 5.69 (Figure 3.20 B). In comparison to the 0.9 γ H2AX foci in control cells, the mean 1.7 foci in CtIP-depleted GC92 ARTEMIS KO cells was significantly higher ($p = 0.013$) with an effect size of 3.52, which is consistent with a partial repair defect. In conclusion, the combination of proteins by which the remaining misrepair events in CtIP-depleted GC92 cells arise, indicates the requirement for c-NHEJ and not alt-EJ factors. However, the observed increase in additional deletions at the misrejoined break sites suggest a more detrimental mutagenic mechanism.

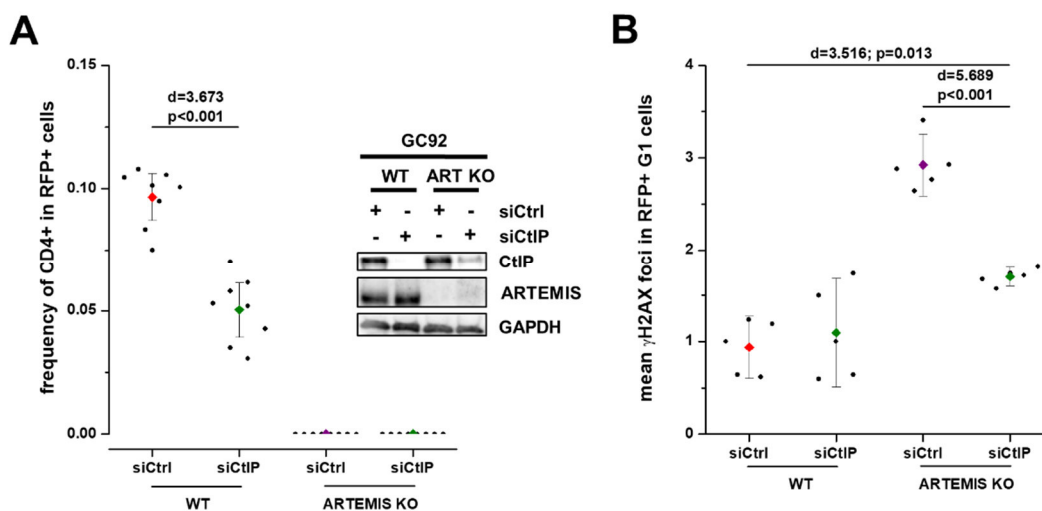


Figure 3.20 CtIP depletion in GC92 ARTEMIS KO cells partially rescues the ARTEMIS repair defect
(A, B) Impact of CtIP depletion on misrepair (A) or overall repair (B) in GC92 ARTEMIS KO cells. GC92 WT or ARTEMIS KO cells were treated with siRNA against CtIP. As a control, cells were treated with control siRNA. **(A)** Cells were harvested 72 h post-co-transfection with I-SceI and RFP plasmids. Downregulation by siRNA was confirmed by immunoblotting. Cells were stained with anti-CD4, anti-RFP AB, and DAPI. Samples were scanned using Metafer software and only plasmid-transfected cells were analyzed. Data represent the mean of 8 independent experiments performed in duplicates ($n = 8$). **(B)** Cells were co-transfected with the RFP and I-SceI plasmids and treated with EdU and nocodazole 30 min prior to harvest. Harvest took place 72 h post-plasmid transfection. Cells were stained with anti- γ H2AX, anti-RFP AB, and DAPI. Samples were scanned using Metafer software and only plasmid-transfected G₁ cells were analyzed. Data represent the mean of 5 independent experiments ($n = 5$). **(A, B)** RFP was used as a marker for cells with damage induction and exogenous protein (see chapter 3.1.1). Error bars show the 95% CI. Effect size was calculated by Cohen's d and p -value was obtained by one-way ANOVA with Bonferroni correction. Several data points were part of the analysis in Biehs et al. (2017).

Due to this interesting influence of CtIP in addition to ARTEMIS impairment and CtIPs major role in specifically impacting the misrejoining of distant DSB ends, other proteins associated with CtIP might be of interest. Strikingly, the damage-inducible ARTEMIS interaction partner PTIP (PAXIP1)⁴⁰⁰ was observed to be co-precipitated after damage induction with SFB-CtIP WT protein precipitated and purified from stably-transfected HEK293 cells (30 min post-5 Gy X-IR, analyzed by MS; Table 8.6). This result raises the question of how CtIP depletion would affect the misrejoining of distant DSBs in GC92 cells in the absence of the upstream PTIP factor 53BP1. The mean value of misrepair events in CtIP-53BP1 co-depleted GC92 cells was significantly reduced to 2.2% ($p < 0.001$) compared to CtIP depletion alone with an effect size of 2.16 (Figure 3.21 A). In contrast, co-depletion of CtIP and the pro-resection factor BRCA1 did not have any additional impact on misrepair events. The reduction in misrepair events upon CtIP-53BP1 co-depletion resulted from a repair defect, as evidenced by the γ H2AX foci assay (Figure 3.21 B). Next, CtIP and 53BP1 co-depleted GC92 cells were transfected with the WT CtIP plasmid, which resulted in overexpressed RFP-CtIP. It needs to be emphasized that in comparison to all other conditions this combination misrejoined distant DSBs most frequently, with nearly every-second RFP-positive cell resulting in a misrepair event (Figure 3.22 A).

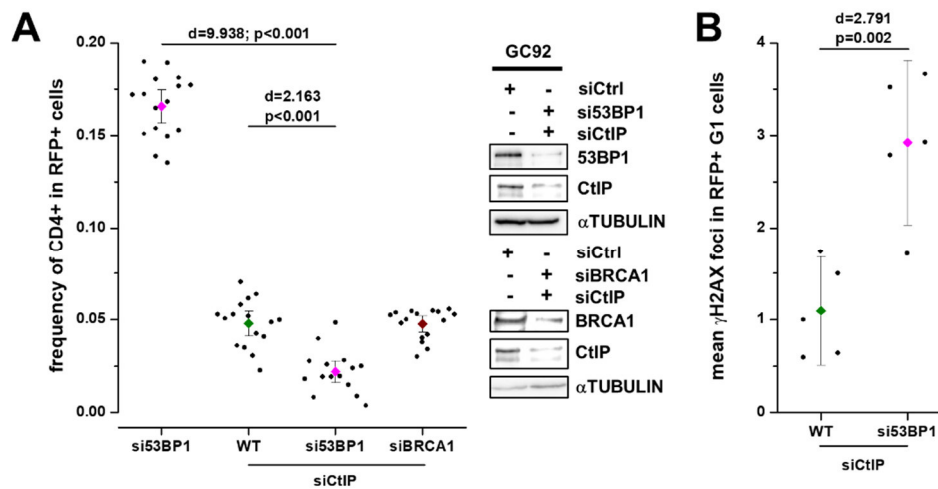


Figure 3.21 The increase of misrepair events in 53BP1-depleted GC92 cells is dependent on CtIP

(A, B) Impact of co-depletion of 53BP1 or BRCA1 with CtIP on misrepair (A) or overall repair (B) in GC92 cells. GC92 cells were treated with siRNAs against BRCA1, 53BP1, and/or CtIP. (A) Harvest took place 72 h post-co-transfection with I-SceI and RFP plasmids. Downregulation by siRNA was confirmed by immunoblotting. Cells were stained with anti-CD4, anti-RFP AB, and DAPI. Samples were scanned using Metafer software and only plasmid-transfected cells were analyzed. Data represent the mean of 16 independent experiments performed in duplicate ($n = 16$). (B) Cells were co-transfected with RFP and I-SceI plasmids and treated with EdU and nocodazole 30 min prior to harvest. Harvest took place 72 h post-plasmid transfection. Cells were stained with anti- γ H2AX, anti-RFP AB, and DAPI. Samples were scanned using Metafer software and only plasmid-transfected G₁ cells were analyzed. Data represent the mean of 5 independent experiments ($n = 5$). (A, B) RFP was used as a marker for cells with damage induction (see chapter 3.1.1). Error bars show the 95% CI. Effect size was calculated by Cohen's d and p -value was obtained by one-way ANOVA with Bonferroni correction (for A) or by two-sample Student's t -test (for B).

In the last part of this chapter, the influence of several CtIP domains on the misrejoining of distant DSBs was investigated. For this reason, CtIP-depleted GC92 cells were transfected with

CtIP plasmids encoding a variety of CtIP proteins, including the WT and mutants impaired in certain domains. Inhibition of ATM, an important Ser/Thr-protein kinase, resulted in the reduction of misrepair events in GC92 cells by 50% (Figure S8.14 a). ATM is known to phosphorylate CtIP at Ser664 and Ser745 subsequent to the aforementioned CDK phosphorylation in S/G₂ phase. This ATM-mediated CtIP phosphorylation is required to control resection during HR^{238,397}. Therefore, an exogenous CtIP phospho-mutant with Ser664 and Ser745 both mutated to Ala was transfected into CtIP-depleted GC92 cells, which resulted in the same frequency of elevated misrepair events as exogenous WT CtIP (Figure 3.22 B). Next, exogenous CtIP impaired in its endonuclease function by Asn289 and His290 both mutated to Ala was used in CtIP-depleted GC92 cells and misrepair events were still not impacted compared to the exogenous WT CtIP. Thus, both the ATM-dependent phosphorylation sites of CtIP and its endonuclease function are dispensable for misrejoining of distant DSBs. Surprisingly, exogenous endonuclease-impaired CtIP in combination with CtIP-53BP1 co-depletion caused a huge decrease in the frequency of misrepair events to 2.2% (Figure 3.22 A).

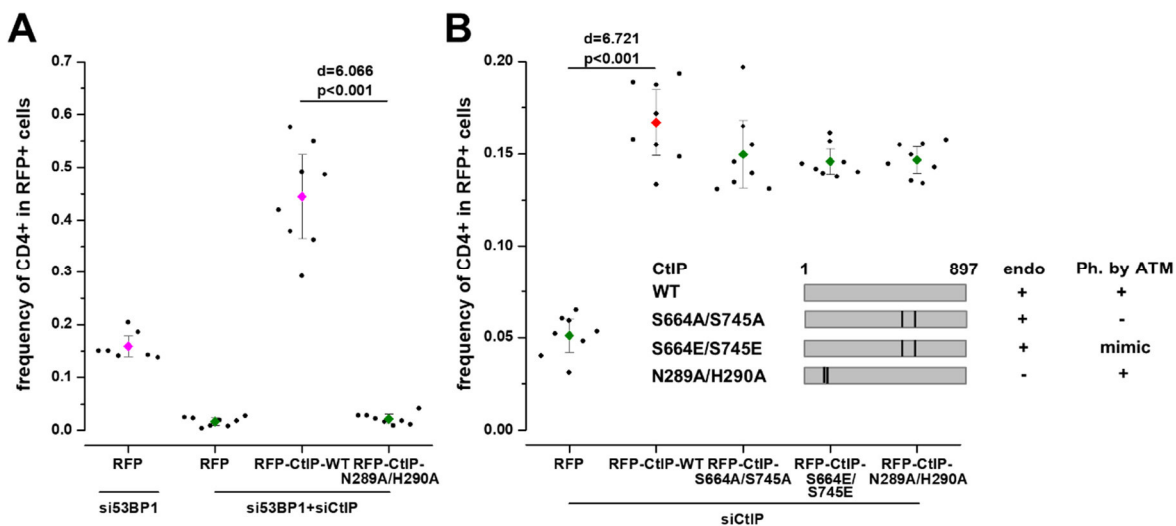


Figure 3.22 The endonuclease function of CtIP is dispensable for the misrejoining of distant DSB ends in WT cells but crucial in 53BP1-depleted cells

(A, B) Impact of WT and mutant CtIP complementation on misrepair in CtIP-depleted (B) or CtIP-53BP1 co-depleted (B) GC92 cells. GC92 cells were treated with siRNAs against 53BP1 and/or CtIP. Cells were transfected with the RFP or siRNA-resistant RFP-CtIP-WT, RFP-CtIP-S664A/S745A, RFP-CtIP-S664E/S745E, or RFP-CtIP-N289A/H290A plasmid. 36 h after plasmid transfection, cells were transfected with I-SceI and harvest occurred after an additional 72 h. Cells were stained with anti-CD4, anti-RFP AB, and DAPI. Samples were scanned using Metafer software and only plasmid-transfected cells were analyzed. Data represent the mean of 8 independent experiments performed in duplicate ($n = 8$). (B) Diagrams of the exogenous CtIP WT, the S664/S745 phospho-mimic- or phospho-mutant of the ATM-dependent phosphorylation sites, and the N289A/H290A endonuclease mutant are not drawn to scale. Of note, preliminary experiments with RFP-CtIP-S664A/S745A and RFP-CtIP-S664E/S745E were performed by C. Ruder and similar results were observed³³². (A, B) RFP was used as a marker for cells with damage induction and exogenous protein (see chapter 3.1.1). Error bars show the 95% CI. Effect size was calculated by Cohen's d and p -value was obtained by one-way ANOVA with Bonferroni correction.

As established earlier in this chapter, BRCA1 interacts with CtIP in G₁ phase in a damage-inducible manner dependent on CtIP phosphorylation at Ser327 (Figure S8.12 b). Thus far, the

possible involvement of CtIP phosphorylation at this site during misrejoining of distant DSBs has not been clarified. Therefore, CtIP-depleted GC92 cells were transfected with a CtIP plasmid encoding a CtIP phospho-mutant with Ser327 mutated to Ala. GC92 cells with this exogenous CtIP phospho-mutant retained the misrepair events at 4.6%, a similar level as CtIP-depleted cells (Figure 3.23 A). The difference in the mean values was significant ($p < 0.001$) compared to the exogenous CtIP WT, with an effect size of 8.16. The involvement of CtIP as a pro-resection factor in S/G₂ phase is mainly dependent on its phosphorylation at Thr847³¹⁵. Consequently, CtIP-depleted GC92 cells were next complemented with an exogenous CtIP phospho-mutant where Thr847 was mutated to Ala. The exogenous CtIP 847 phospho-mutant showed a similar phenotype as the 327 phospho-mutant and the CtIP-depleted situation (Figure 3.23 A). This result again links this novel repair pathway to resection.

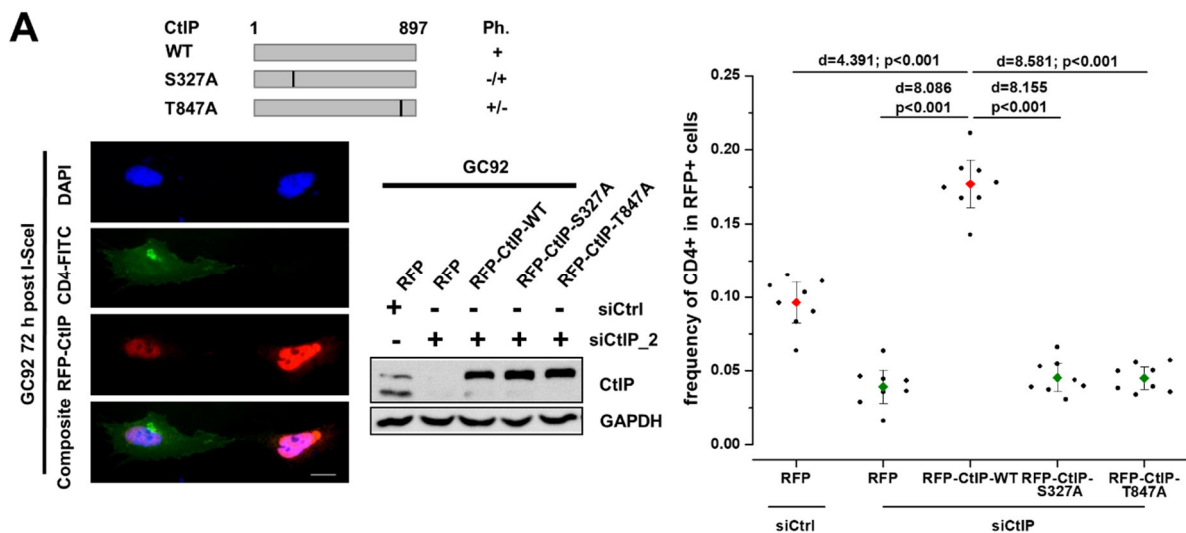


Figure 3.23 CtIP S327 and T847 phosphorylation sites are required for misrejoining of distant DSB ends (A) Impact of CtIP complementation with phospho-mutants S327A and T847A on misrepair in CtIP-depleted GC92 cells. GC92 cells were treated with siRNA against CtIP. Cells were transfected with the RFP or siRNA-resistant RFP-CtIP-WT, RFP-CtIP-S327A, or RFP-CtIP-T847A plasmid. 36 h after plasmid transfection, cells were transfected with I-SceI and harvest took place after an additional 72 h. Downregulation by siRNA and expression of exogenous plasmids were confirmed by immunoblotting. Representative images were obtained with a 63x objective using AxioVision software. Scale bar represents 10 μ m. Diagram of the exogenous CtIP WT and the S327A or T847A phospho-mutants are not drawn to scale. Cells were stained with anti-CD4, anti-RFP AB, and DAPI. Samples were scanned using Metafer software and only plasmid-transfected cells were analyzed. Data represent the mean of 8 independent experiments performed in duplicate ($n = 8$). RFP was used as a marker for cells with damage induction and exogenous protein (see chapter 3.1.1). Error bars show the 95% CI. Effect size was calculated by Cohen's d and p -value was obtained by one-way ANOVA with Bonferroni correction. Several data points were part of the analysis in Barton et al. (2014).

Next, overall repair was analyzed using the γ H2AX foci assay after CtIP depletion in GC92 ARTEMIS KO cells plus transfection with WT CtIP and the phospho-mutant plasmids (Ser327 or Thr847 mutated to Ala). As described in Figure 3.20 B, the depletion of CtIP in GC92 ARTEMIS KO cells resulted in a partial rescue of the ARTEMIS repair defect. Upon complementation with exogenous WT CtIP, the ARTEMIS repair defect was restored with a

mean value of 2.7 γ H2AX foci (Figure S8.14 b). This was a significant difference compared to the partial rescue in CtIP-depleted GC92 ARTEMIS KO cells ($p = 0.013$, $d = 2.23$). Usage of any of the two exogenous CtIP phospho-mutants in CtIP-depleted GC92 ARTEMIS KO cells again resulted in the partial rescue of the ARTEMIS repair defect. Finally, the effect of CtIP phospho-mimic mutants on the misrejoining of distant DSBs was tested. Exogenous CtIP with Ser327 and/or Thr847 mutated to Glu all resulted in elevated misrepair events comparable to the exogenous WT CtIP (Figure S8.15 a). However, when one of the two CtIP phosphorylation sites was mutated to Ala, misrepair events remained as low as in CtIP-depleted GC92 cells, independent of a phospho-mimic mutation at the other phosphorylation site.

In conclusion, CtIP is necessary for the misrejoining of distant DSB ends after I-SceI damage induction but is not required for repair. Both CtIP Ser327 and Thr847 phosphorylation sites are required to generate misrepair events in GC92 cells. Beyond its role in this particular pathway, CtIP is essential for the repair and misrejoining of distant DSBs by alt-EJ, as it occurs after 53BP1 depletion.

3.3.3. The kinase PLK3 activates CtIP for the misrejoining of distant DSBs

CtIP is constitutively active in S/G₂ phase through CDK complex-mediated phosphorylation at Ser327 and Thr847, which is required to initiate resection during HR^{176,177,339,428}. Accordingly, the impact of impaired CDK activity on the misrejoining of distant DSB ends in GC92 cells was examined next. Roscovitine is a selective CDK inhibitor (IC₅₀ for CDK1 = 0.65 μ M, for CDK2 = 0.7 μ M) with little effect on G₁-specific CDK complexes²⁶⁶. Neither CDK1/2 inhibition by roscovitine nor CDK2 depletion altered the frequency of misrepair events in GC92 cells (Figure 3.24 A). As expected, the same treatment did reduce frequencies of gene conversion events in HeLa pGC cells (Figure S8.16 a), which raised the question of which other kinase might influence misrejoining of distant DSB ends. Polo-like kinases can phosphorylate the same motifs as CDKs (an idea first introduced and pursued by O. Barton in her studies of slow DSB repair in G₁ phase). As PLK1 was observed to interact with CtIP in the MS analysis (Table 8.6), a PLK inhibitor that inhibits PLK1 and PLK3 was used in GC92 cells. GW843682X is a selective PLK inhibitor (IC₅₀ of PLK1 = 2.2 nM and PLK3 = 9.1 nM) with 100-fold selectivity over other kinases, including CDK1 and CDK2²⁶⁶. Indeed, this inhibitor significantly reduced the frequency of misrepair events to 4.6% ($p < 0.001$, $d = 2.58$; Figure 3.24 B). In contrast to the impairment of CDK2, PLK inhibition had no impact on gene conversion events in HeLa pGC cells (Figure S8.16 b). Astonishingly, PLK1 depletion had no impact on misrepair events in GC92 cells (Figure S8.16 c). Instead, depletion of PLK3 decreased misrepair events to the same frequency as the PLK inhibitor treatment, which was confirmed by several siRNAs (Figures 3.24 B). Similar

to the CtIP depletion in GCS5 cells, PLK inhibition did not have an impact on the misrepair of close DSBs (Figure 3.24 C).

The behavior of PLK3 differs greatly depending on the cell line. In thymidine-synchronized HeLa cells, PLK3 is specifically observed in G₁ phase and required for transition into S phase, while in several other cell lines, PLK3 is expressed throughout the cell cycle and even shows the strongest kinase activity in S/G₂ phase^{32,76,166,415,437}. Interestingly, PLK3 is phosphorylated and activated by ATM in a damage-inducible manner¹⁸, which could explain why ATM is required for the misrepair of distant DSBs (Figure S8.14 a). To further understand the role of PLK3 in the misrejoining of distant DSB ends, the influence of PLK and CDK inhibition on misrepair events was examined in synchronized GC92 cells. Similar to the situation in asynchronously grown cells, PLK inhibition reduced the misrepair events in G₁-synchronized cells by half while CDK inhibition (roscovitine) did not show any impact (Figure S8.16 d). A reduction of misrepair events to 1.5% from the already much lower frequency of 2.7% misrepair events in WT G₂-synchronized cells was also observed after PLK inhibition. Astonishingly, CDK inhibition by roscovitine in G₂-synchronized GC92 cells resulted in a significant increase to 8.2% misrepair events ($p < 0.001$) with an effect size of 4.58. This raises the question of why such an increase was not observed in asynchronous cells after CDK inhibition. Speculatively, this may be because these events preferentially arise in G₁ and that this type of repair is only observed in G₂-synchronized cells because of the synchronization procedure in which the specific CDK1 inhibitor RO-3306 is used to keep G₂ cells from progressing to mitosis. RO-3306 is an ATP competitive selective inhibitor of CDK1 (K_i for CDK1/cyclinB = 35 nM, CDK2/cyclinE = 340 nM), which binds the ATP pocket of CDK1³⁸⁹ more selectively than the ATP pocket of other CDKS such as CDK2. Even though the inhibitor has a 10-fold higher affinity for CDK1, a small impact on CDK2 is to be expected. This hypothesis is supported by the fact that the inhibition of HR by roscovitine, which completely inhibits CDK2, resulted in increased frequencies of misrepair events. Of note, double inhibition by roscovitine and PLK nearly abolished misrepair events, which confirms that the increase of misrepair events observed after CDK inhibition was dependent on PLK3. Furthermore, these results indicate that this kind of PLK3-dependent repair is usually prevented in S/G₂ phase in favor of HR. Indeed, Gelot et al. (2016) showed that the cohesin complex, which is required for chromosomal cohesion and therefore HR, suppresses the misrejoining of distant DSBs during S/G₂ phase.

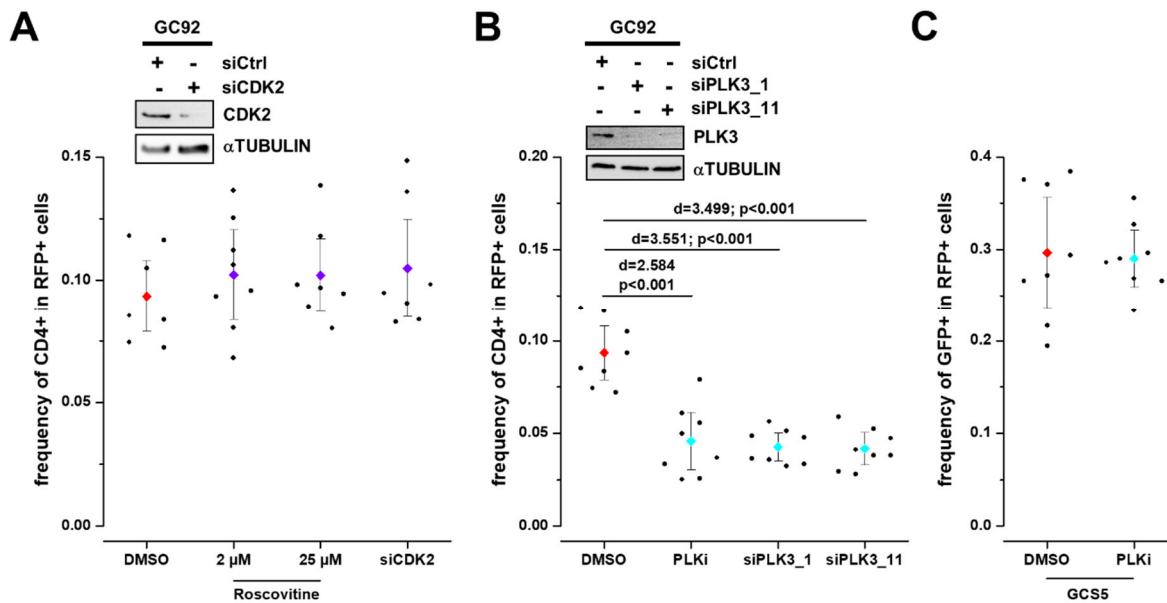


Figure 3.24 Misrejoining of distant DSB ends in GC92 cells is dependent on PLK3

(A, B, C) Impact of CDK1/2 inhibition, CDK2 depletion (A), PLK1/3 inhibition (B, C), or PLK3 depletion (B) on misrepair in GC92 or GCS5 (C) cells. GC92 or GCS5 cells were treated with inhibitors and/or siRNAs against CDK1/2 (roscovitrine), CDK2, PLK1/3 (GW843682X), or PLK3. As a control, cells were treated with DMSO or control siRNA. Harvest took place 72 h post-co-transfection with I-SceI and RFP plasmids. (A) Of note, the frequently used roscovitrine concentration of 25 μ M impairs cell cycle progression, and thus experiments were also performed at 2 μ M. (A, B) Downregulation by siRNA was confirmed by immunoblotting. (B) Immunoblotting was performed by C. Ruder. (A, B, C) Cells were stained with anti-CD4 or anti-GFP plus anti-RFP AB and DAPI. Samples were scanned using Metafer software and only plasmid-transfected cells were analyzed. Data represent the mean of 8 independent experiments performed in duplicate ($n = 8$). RFP was used as a marker for cells with damage induction (see chapter 3.1.1). Error bars show the 95% CI. Effect size was calculated by Cohen's d and p -value was obtained by one-way ANOVA with Bonferroni correction. Several data points were part of the analysis in Barton et al. (2014).

Comparable to the depletion of CtIP, impairment of PLK3 decreased the misrejoining of distant DSBs in GC92 cells by half and did not influence the misrejoining of close DSB ends in GCS5 cells. Therefore, it was interesting to determine whether additional similarities between these two factors could be found. PLK3 was overexpressed in PLK3-depleted GC92 cells by transfection with a plasmid encoding exogenous FLAG-PLK3 (Figure 3.25 A). Similarly to CtIP overexpression, a significant increase of misrepair events to 17.5% was observed in GC92 cells overexpressing exogenous PLK3 ($p < 0.001$, $d = 3.19$). A PLK3 mutant lacking the polo-box domain (PBD) retained the frequency of misrepair events at a level similar to PLK3-depleted cells, which implicates the polo-box domain in the misrejoining of distant DSB ends. Double depletion of PLK3 and CtIP in GC92 cells resulted in 4.5% misrepair events, a frequency that resembled the misrepair events after single PLK3 or CtIP depletion (Figure 3.25 B). This provides evidence, that CtIP and PLK3 are involved in the same mechanism. Additional depletion of PLK3 in 53BP1-depleted GC92 cells significantly reduced the misrepair events even further (compared to the single PLK3 depletion) to 2.2% ($p < 0.001$, $d = 1.98$, Figure S8.16 e). In addition, similar to CtIP depletion, PLK3 depletion in GC92 ARTEMIS KO cells did not affect the abolished misrepair events in GC92 ARTEMIS KO cells (Figure 3.25 B). Moreover, PLK3

depletion significantly decreased the repair defect, which was observed in GC92 ARTEMIS KO cells to 1.9 γ H2AX foci ($p = 0.002$, Figure 3.25 C). Compared to WT GC92 cells, this partial increase of γ H2AX foci in PLK3-depleted GC92 ARTEMIS KO cells was significant ($p = 0.011$) with an effect size of 2.11. PLK3 depletion in WT GC92 cells did not impact the mean number of γ H2AX foci. Together, these characteristics resemble the impact of CtIP depletion. Thus, both CtIP and PLK3 are necessary for the misrejoining of distant DSB ends after I-SceI damage induction, but are not required for repair. Similar to CtIP, PLK3 is essential for the repair and misrejoining of distant DSBs by alt-EJ, as it occurs after 53BP1 depletion. In addition, depletion of CtIP or PLK3 partly rescues the ARTEMIS repair defect, while misrepair events remain abolished. Of note, as PLK3 is involved in this novel end-joining mechanism and alt-EJ (both capable of producing misrepair events), it is not clear which mechanism is responsible for the increase of misrepair events in G₂-synchronized GC92 cells after impairment of HR (Figure S8.16 d).

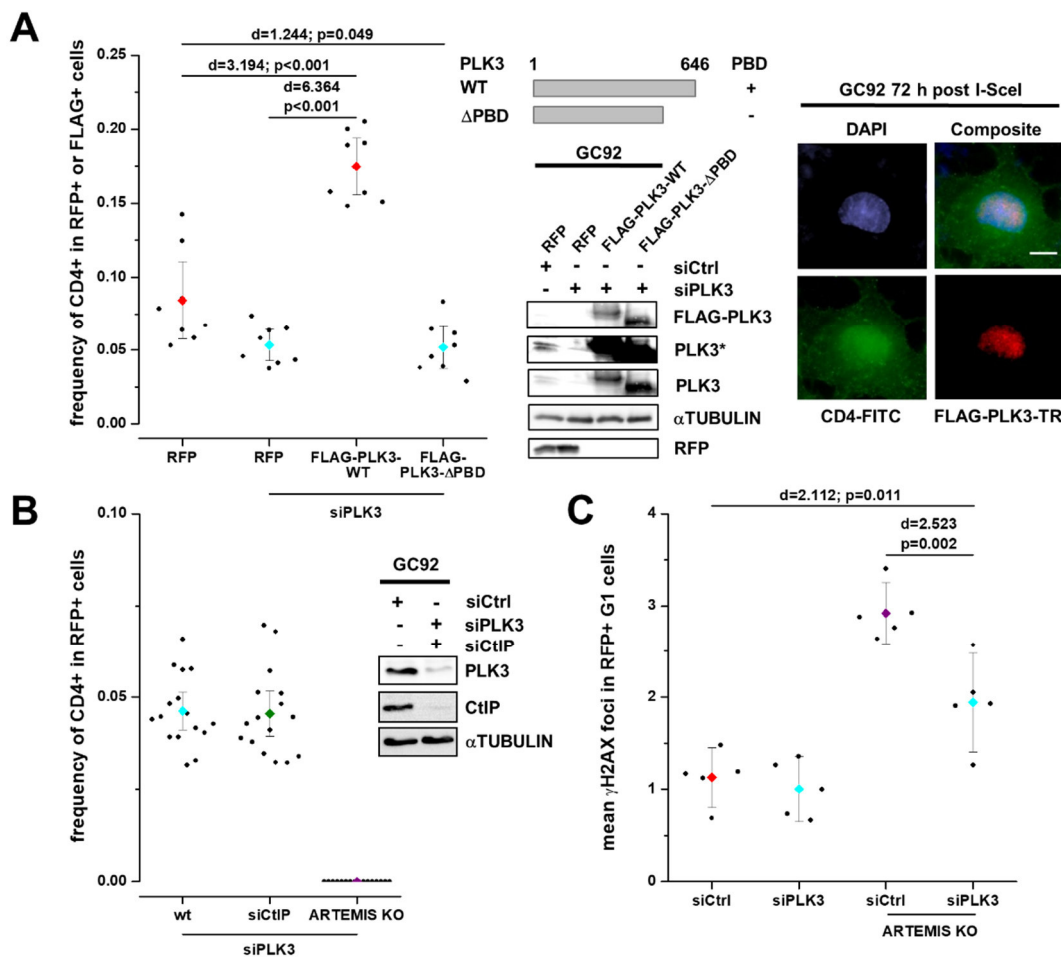


Figure 3.25 The PLK3 depletion phenotype in GC92 cells resembles the CtIP depletion phenotype

(A, B, C) Impact of PLK3 WT and mutant complementation (A) or CtIP (B) depletion on misrepair (A, B) or overall repair (C) in PLK3-depleted GC92 WT (A, B, C) or ARTEMIS KO (B, C) cells. GC92 WT or ARTEMIS KO cells were treated with siRNAs against PLK3 and/or CtIP. As a control, cells were treated with control siRNA. (A) GC92 cells were transfected with the RFP or siRNA-resistant FLAG-PLK3-WT or FLAG-PLK3- Δ PBD plasmid. 36 h after plasmid transfection, cells were transfected with I-SceI and harvested after an additional 72 h. Representative images were

obtained with a 63x objective using Metafer Isis software. Scale bar represents 10 μ m. Diagrams of the exogenous PLK3 WT and the PBD mutant are not drawn to scale. (B) Harvest took place 72 h post-co-transfection with I-SceI and RFP plasmids. (A, B) Downregulation by siRNA and expression of exogenous plasmids were confirmed by immunoblotting. Cells were stained with anti-RFP or anti-FLAG plus anti-CD4 AB and DAPI. Samples were scanned using Metafer software and only plasmid-transfected cells were analyzed. Data represent the mean of 8 or 16 independent experiments performed in duplicate ($n = 8$ for A; $n = 16$ for B). (C) Cells were co-transfected with RFP and I-SceI plasmids and treated with EdU and nocodazole 30 min prior to harvest. Harvest took place 72 h post-plasmid transfection. Cells were stained with anti- γ H2AX, anti-RFP AB, and DAPI. Samples were scanned using Metafer software and only plasmid-transfected G₁ cells were analyzed. Data represent the mean of 5 independent experiments ($n = 5$). (A, B, C) RFP and FLAG were used as a marker for cells with damage induction and exogenous protein (see chapter 3.1.1). Error bars show the 95% CI. Effect size was calculated by Cohen's d and p -value was obtained by one-way ANOVA with Bonferroni correction. (B) Several data points were part of the analysis in Barton et al. (2014).

PLK3 expression differs depending on the cell type¹⁶⁶. To investigate the PLK3 protein level relative to the cell cycle phase, GC92 cells were synchronized by double thymidine block (Figure 3.26 A) and PLK3, CtIP, and BRCA1 protein levels were analyzed (figure 3.26 B). Both, CtIP and BRCA1 protein levels were higher in G₂ and lower in G₁-synchronized cells compared to asynchronously grown cells. In contrast, the protein level of PLK3 remained steady throughout the cell cycle. The aim of the experiments conducted in this chapter was not just to find the Ser/Thr-protein kinase involved in the misrejoining of distant DSB ends, but to also find the specific kinase that phosphorylates and activates CtIP. Since CtIP phosphorylation was observed in a damage-inducible manner post-X-IR in G₁ phase (Figure S8.12 b), GC92 cells were synchronized in G₁ by double thymidine block (Figure 3.26 A) and CtIP was immunoprecipitated (Figures 3.26 C). Upon damage induction, phosphorylation of CtIP at Ser327 was observed 1 h post-5 Gy X-IR. However, PLK inhibition abolished the damage-inducible phosphorylation of CtIP at Ser327. As established in chapter 3.3.2, BRCA1 interacts with CtIP in a damage-inducible manner dependent on CtIP phosphorylation at Ser327 (Figure S8.12 b). Therefore, BRCA1 protein levels were also investigated in the immunoprecipitation experiment (Figures 3.26 C). Analogous to the abolished CtIP phosphorylation at Ser327 post-damage induction and PLK inhibitor treatment, BRCA1 interaction with CtIP was greatly reduced. The reverse BRCA1 co-immunoprecipitation experiment confirmed these findings. Additionally, the results of this experiment were confirmed in further cell systems (HeLa, 82-6 hTert, data not shown) and with additional ABs by other members of the working group³⁶.

BRCA1 is rapidly recruited to the DSB by KU80 in G₁ phase and the subsequent interaction is required for the stabilization of KU80 at the break end^{197,336}. To investigate the effect of PLK inhibition on that interaction, KU80 or BRCA1 was co-immunoprecipitated from GC92 cells synchronized in G₁ phase by double thymidine block (Figure 3.26 D). Both, the experimental and published data in Jiang et al. (2013) revealed a BRCA1-KU80 interaction, even before damage induction. In Jiang et al. (2013), this interaction increased several hours after transfection with the I-SceI plasmid. In Figure 3.26 D, the BRCA1-KU80 interaction increased

30 min after damage induction by X-IR and decreased 1 h post-irradiation. Interestingly, the BRCA1-KU80 interaction remained visible 1 h post-irradiation when the GC92 cells were treated with the PLK inhibitor. In conclusion, PLK3 phosphorylates CtIP post-damage induction at Ser327 to promote its interaction with BRCA1. The BRCA1-KU80 interaction lessens in favor of the BRCA1-CtIP interaction, and thus BRCA1 can no longer stabilize KU.

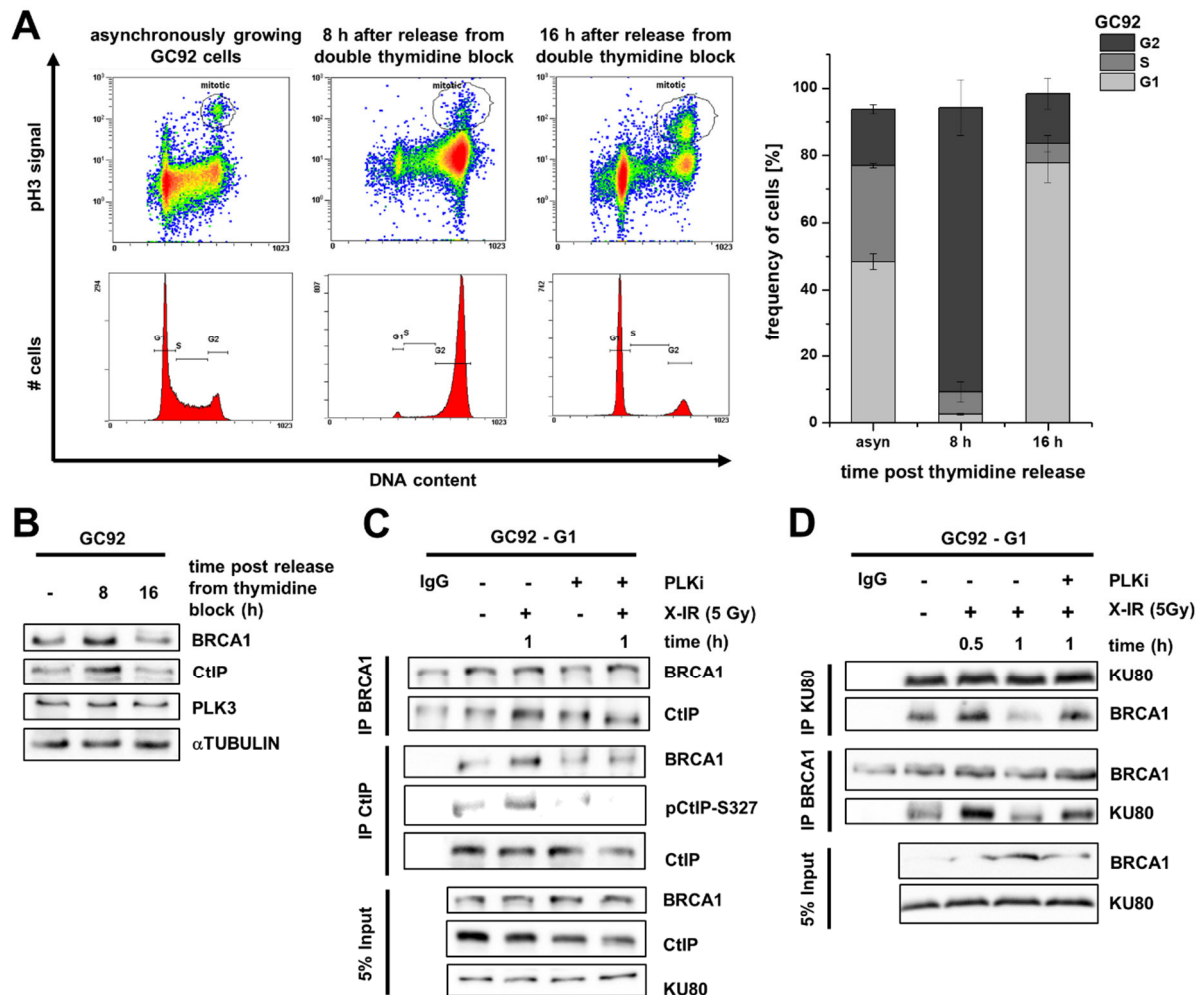


Figure 3.26 PLK3 is required for the damage-inducible BRCA1-CtIP-pS327 interaction and for the fading BRCA1-KU80 interaction after damage induction in G₁ phase
(A, B) Cell cycle distribution **(A)** and protein levels **(B)** in synchronized GC92 cells. GC92 cells were synchronized by double thymidine block and reached G₂ phase 8 h post-second thymidine release and G₁ phase 16 h post-second thymidine release. **(A)** Cells were harvested and stained with anti-pH3 AB and PI. (left) Samples were analyzed by flow cytometry. (right) Data represent the mean of 3 independent experiments ($n = 3$). Error bars show the SD. **(B)** Cells were harvested and protein levels were analyzed after immunoblotting of the samples. **(C, D)** BRCA1 and CtIP **(C)** or BRCA1 and KU80 **(D)** co-immunoprecipitation in G₁-synchronized GC92 cells. BRCA1, CtIP, or KU80 was immunoprecipitated with anti-CtIP, anti-KU80, or anti-BRCA1 ABs from G₁-synchronized GC92 cells 30 min and/or 1 h post-5 Gy X-IR or from unirradiated controls treated with or without PLK inhibitor 1 h prior to X-IR. Protein levels were analyzed after immunoblotting of the samples.

As established in chapter 3.3.2, phosphorylation of CtIP at both Ser327 and Thr847 is required for misjoining of distant DSBs in GC92 cells. To verify that PLK3 is able to phosphorylate CtIP at these two sites, SFB-CtIP WT was immunoprecipitated and purified from stably-transfected HEK293 cells with or without *in vitro* incubation with recombinant PLK3. Likely CtIP

phosphorylation events at Ser, Thr, or Tyr sites were analyzed by MS and the probability-based approach Ascore²⁷. An Ascore value greater than 19 suggests likely phosphorylation at a given site, less than 19 indicates an unlikely phosphorylation site. CtIP WT incubated with recombinant PLK3 resulted in the likely phosphorylation of CtIP at Ser327 and Thr847 (Table 8.7). Thus, PLK3 is able to phosphorylate CtIP at these two phosphorylation sites, which are required for misrepair events. CtIP showed high basal phosphorylation and incubation with recombinant PLK3 increased the phosphorylation levels. Therefore, an experiment was conducted to test if misrejoining of distant DSB ends only requires PLK3-dependent phosphorylation of CtIP at Ser327 and Thr847. CtIP-PLK3 double-depleted GC92 cells were transfected with a plasmid encoding RFP-CtIP WT (Figure 3.27 A). As PLK3 was depleted, and thus could not phosphorylate Ser327 and Thr847, unsurprisingly, the misrepair events remained at low levels, comparable to the PLK3-CtIP co-depleted GC92 cells. As a reminder, the expression of exogenous WT CtIP in CtIP-depleted GC92 cells elevated misrepair events, as did the usage of phospho-mimic mutants at sites 327 and/or 847 (Figure S8.15 a). Surprisingly, even the exogenous CtIP double phospho-mimic mutant did not increase the frequency of misrepair events (Figure 3.27 A). Thus, phosphorylation of CtIP at Ser327 and Thr847 by PLK3 is not sufficient to fully activate CtIP for the misrejoining of distant DSB ends. Obviously, activation of CtIP by PLK3 is different than phosphorylation of CtIP by the CDK2 complex in S/G₂ phase. Since PLK3 was involved in the increase of misrepair events in the absence of CDKs in G₂ phase (as per figure S8.16 d), PLK3 and CDK2 may compete to phosphorylate CtIP and PLK3 loses in S/G₂ phase because CDK complexes constitutively phosphorylate CtIP. In G₁ phase, PLK3 succeeds, as the CDK2 complex required to phosphorylate CtIP is not present.

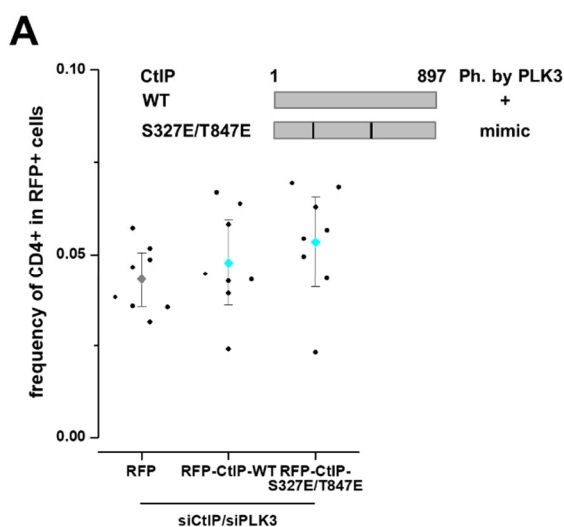


Figure 3.27 Phosphorylation at S327 and T847 by PLK3 is not sufficient for misrejoining of distant DSB ends

(A) Impact of CtIP complementation with the double phospho-mimic-mutant on misrepair in CtIP-PLK3 double-depleted GC92 cells. GC92 cells were treated with siRNAs against PLK3 and CtIP. Cells were transfected with RFP or siRNA-resistant RFP-CtIP-WT or RFP-CtIP-S327E/T847E plasmids. 36 h after plasmid transfection, cells were

transfected with I-SceI and harvested after an additional 72 h. Diagrams of the exogenous CtIP WT and the S327E/T847E phospho-mimic-mutant are not drawn to scale. Cells were stained with anti-CD4, anti-RFP AB, and DAPI. Samples were scanned using Metafer software and only plasmid-transfected cells were analyzed. Data represent the mean of 8 independent experiments performed in duplicate ($n = 8$). RFP was used as a marker for cells with damage induction and exogenous protein (see chapter 3.1.1). Error bars show the 95% CI.

To investigate which additional CtIP sites might get phosphorylated by PLK3, further MS data were analyzed. Two approaches were used: (1) the aforementioned exogenous WT CtIP immunoprecipitation and purification from stably-transfected HEK293 cells with or without *in vitro* incubation with recombinant PLK3 (Table 8.7 a) and (2) exogenous WT CtIP immunoprecipitation and purification from stably-transfected HEK293 cells 30 min or 2 h after X-IR with or without PLK3 inhibitor treatment prior to irradiation (Table 8.7 b). Importantly, the experimental procedures of these experiments were conducted by J. Wang. To identify which other PLK3-mediated CtIP phosphorylations could be involved in this novel pathway, results were of interest that showed an increase in the Ascore (from less than 19 to greater than 19) after *in vitro* incubation with recombinant PLK3 and when the Ascore was reduced in irradiated samples only after pretreatment with the PLK inhibitor (e.g. Ser326, Ser327). Interestingly, these two CtIP phosphorylation sites were only observed at 30 min but not 2 h post-X-IR, which is consistent with the observed phosphorylation of CtIP at Ser327 30 min or 1 h post-irradiation in immunoprecipitation experiments (Figures 3.26, S8.12). Nevertheless, results where an Ascore increase was only observed post-damage induction and vanished upon PLK inhibitor treatment prior to irradiation (Ser608, Ser641) were also of interest. This situation was especially noteworthy because the observed phosphorylation only occurred upon damage induction. In conclusion, PLK3 phosphorylates CtIP at Ser327, Thr847, and at least one other site following DNA damage induction, and thus induces a mechanism that results in the misrejoining of distant DSB ends. Consequently, PLK3 impairment or overexpression showed a similar phenotype compared to CtIP impairment or overexpression.

3.3.4. Nucleases conducting resection in this novel repair pathway

From the beginning of this results section, resection was mentioned as the cause for misrejoining of distant DSB ends. In this final chapter, the nucleases executing the resection that results in the misrejoining of distant DSB ends were examined. Resection is also the initial step of HR (Figure 2.3). In a simplified HR model, the endonuclease function of MRE11 in concert with CtIP makes a single cut several bases away from the DSB end¹⁰. From there, MRE11 exonuclease activity, together with EXD2, drives resection in a 3' to 5' direction towards the DSB end⁵³. Long-range 5' to 3' resection is performed by EXO1 in concert with BLM or by BLM/DNA2^{287,382} to produce long strands of ssDNA, which are protected by RPA coating³⁷. In Rass et al. (2009), MRE11 was already found to be involved in the misrejoining of distant DSB

ends, which is consistent with the previously described data (as MRE11 also acts in concert with CtIP to conduct resection in S/G₂ phase). This finding was confirmed by MRE11 depletion and MRE11 inhibition (Figures 3.28 A).

Thanks to the recent development of specific inhibitors³⁵⁴, the contribution of MRE11 to the misrejoining of distant DSBs could further be analyzed. Mirin is a small-molecule inhibitor of the MRN complex. It inhibits MRE11-associated exonuclease activity and prevents MRN-dependent activation of ATM without affecting ATM protein kinase activity¹²⁰. In contrast, PFM39 is an altered derivate of mirin which blocks 3' exonuclease activity specifically without interfering with the MRE11-dependent activation of ATM³⁵⁴. PFM01, on the other hand, is a derivate of mirin that specifically blocks the endonuclease activity of MRE11 without affecting its exonuclease function or ability to activate ATM³⁵⁴. All MRE11 inhibitors bind in proximity to the pocket of the active site (hydrophobic Leu59/Leu60 and Mn-ligand Asp58), which includes a His at site 61, a nearby loop starting at Asn93, and a groove for ssDNA-binding. For dsDNA exonuclease activity, rotation of the DNA phosphate backbone (controlled by His61) is necessary. For endonuclease activity, the Asn93 loop interacts with a base extending from the groove binding the ssDNA. While the endonuclease inhibitor is positioned to disrupt the ssDNA binding loop from Asn93 to Phe102, exonuclease inhibitors restrict dsDNA access and disrupt end opening by His61³⁵⁴. Treatment of GC92 cells with an MRE11 endonuclease inhibitor did not alter the frequency of misrepair events (Figure 3.28 A). In contrast, inhibition of MRE11 with an exonuclease-specific inhibitor significantly reduced the mean value of misrepair events to 4.9% compared to the control ($p < 0.001$, $d = 2.56$).

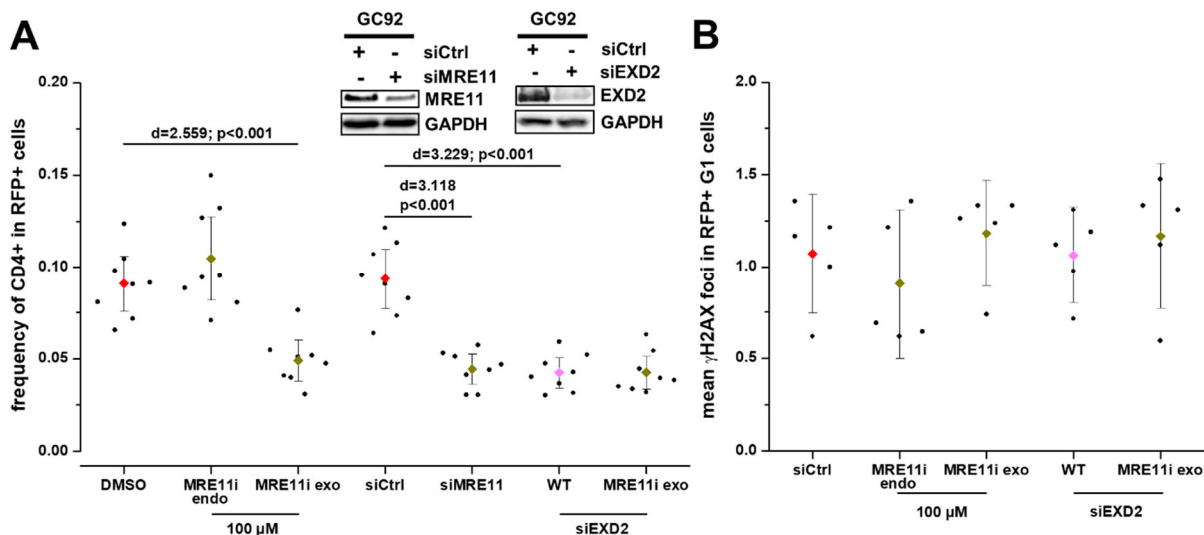


Figure 3.28 MRE11 and EXD2 are required for misrejoining of distant DSBs but MRE11 endonuclease function is dispensable

(A, B) Impact of MRE11 impairment and EXD2 depletion on misrepair (A) or overall repair (B) in GC92 cells. GC92 cells were treated with inhibitors and/or siRNAs against MRE11 endonuclease activity (PFM01), MRE11 exonuclease activity (PFM39), MRE11, and/or EXD2. As a control, cells were treated with DMSO or control siRNA. (A) Harvest

took place 72 h post-co-transfection with I-SceI and RFP plasmids. Downregulation by siRNA was confirmed by immunoblotting. Cells were stained with anti-CD4, anti-RFP AB, and DAPI. Samples were scanned using Metafer software and only plasmid-transfected cells were analyzed. Data represent the mean of 8 independent experiments performed in duplicate ($n = 8$). (B) Cells were co-transfected with the RFP and I-SceI plasmids and treated with EdU and nocodazole 30 min prior to harvest. Harvest took place 72 h post-plasmid transfection. Cells were stained with anti- γ H2AX, anti-RFP AB, and DAPI. Samples were scanned using Metafer software and only plasmid-transfected G₁ cells were analyzed. Data represent the mean of 5 independent experiments ($n = 5$). (A, B) RFP was used as a marker for cells with damage induction (see chapter 3.1.1). Error bars show the 95% CI. Effect size was calculated by Cohen's d and p -value was obtained by one-way ANOVA with Bonferroni correction. (A) Several data points were part of the analysis in Biehs et al. (2017).

Both inhibitors were confirmed to impair gene conversion events in HeLa pGC cells, and thus their functionality was validated (Figure S8.17 a). As MRE11 exonuclease functions together with EXD2 in HR, EXD2 was depleted in GC92 cells. EXD2 depletion resulted in a reduction of misrepair events to 4.2% (Figure 3.28 A). Moreover, treatment with the MRE11 exonuclease-specific inhibitor in addition to EXD2 depletion resulted in a similar frequency of misrepair events. All of these aforementioned factors did not have an impact in the γ H2AX foci assay (Figure 3.28 B).

The double depletion of MRE11 and CtIP did not further influence the frequency of misrepair events in comparison to single depletions (Figure S8.17 b). Next, misrepair events were investigated in 53BP1-depleted GC92 cells. Inhibition of the MRE11 endo- or exonuclease function reduced misrepair events to 1.5% and 2.4%, respectively (Figure 3.29 A). Accordingly, γ H2AX foci increased to 2.5 or 3.2 (Figure 3.29 B). MRE11 inhibition by the endo- or exonuclease-specific inhibitor did not alter the abolished misrepair events in GC92 ARTEMIS KO cells (Figure 3.29 A). Similar to CtIP depletion, depletion of EXD2 and/or MRE11 exonuclease inhibitor treatment in GC92 ARTEMIS KO cells resulted in 1.6 to 1.7 γ H2AX foci (Figure 3.29 C). Compared to the repair defect in GC92 ARTEMIS KO cells, the mean value was significantly lower ($p \leq 0.001$) with effect sizes between 3.43 and 3.71. The mean value compared to the control was not significantly different at the 0.05 level, though the effect size ranged between 1.24 and 1.95. To summarize, MRE11 exonuclease function and EXD2 are both required for the misrejoining of distant DSB ends but not essential for repair. Impairment of either one or both factors partly rescued the ARTEMIS repair defect. In contrast, MRE11 endonuclease function is dispensable for misrepair in GC92 cells. However, both MRE11 endo- and exonuclease activities are required for misrepair and overall repair in alt-EJ, as it occurs in 53BP1-depleted cells.

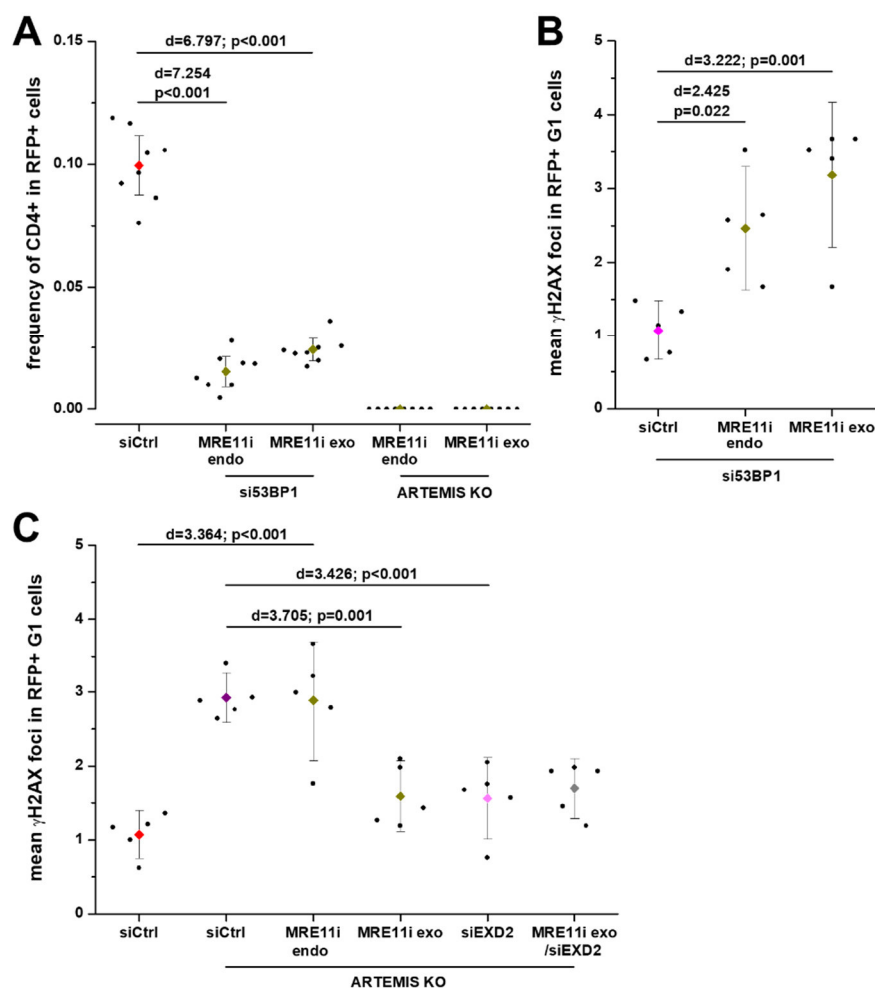


Figure 3.29 MRE11 endo- and exonuclease activities are required for misrepair in 53BP1-depleted GC92 cells

(A, B, C) Impact of MRE11 inhibitors on misrepair (A) or overall repair (B, C) in 53BP1-depleted GC92 cells (A, B) or in GC92 ARTEMIS KO cells (A, C). GC92 WT or ARTEMIS KO cells were treated with inhibitors and/or siRNAs against MRE11 endonuclease activity (PFM01), MRE11 exonuclease activity (PFM39), EXD2, and/or 53BP1. As a control, cells were treated with control siRNA. (A) Harvest took place 72 h post-co-transfection with the I-SceI and RFP plasmids. Cells were stained with anti-CD4, anti-RFP AB, and DAPI. Samples were scanned using Metafer software and only plasmid-transfected cells were analyzed. Data represent the mean of 8 independent experiments performed in duplicate ($n = 8$). (B, C) Cells were co-transfected with the RFP and I-SceI plasmids and treated with EdU and nocodazole 30 min prior to harvest. Harvest took place 72 h post-plasmid transfection. Cells were stained with anti- γ H2AX, anti-RFP AB, and DAPI. Samples were scanned using Metafer software and only plasmid-transfected G₁ cells were analyzed. Data represent the mean of 5 independent experiments ($n = 5$). (A, B, C) RFP was used as a marker for cells with damage induction (see chapter 3.1.1). Error bars show the 95% CI. Effect size was calculated by Cohen's d and p -value was obtained by one-way ANOVA with Bonferroni correction.

Next, EXO1 was depleted in GC92 cells, which significantly reduced misrepair events compared to the mean value of control cells to 4.4 ($p < 0.001$) with an effect size of 4.34 (Figure 3.30 A, 3.30 B). The impact of EXO1 impairment on misrepair events in GC92 cells was confirmed by CRISPR/Cas9 viral transduction (Figure S8.18 a). Furthermore, transfection of EXO1-depleted GC92 cells with an EXO1 plasmid encoding WT EXO1, restored the frequency of misrepair events to a level comparable to the control (Figure 3.30 B). In contrast, BLM and/or DNA2 depletion did not alter the misrepair events in GC92 cells although they are involved in 5' to 3'

resection during HR (Figure 3.30 A). Notably, previous studies have shown that BLM influences sequence alterations at misrejoined distant DSB sites, where BLM is involved in the protection against long-range deletions¹⁴⁸. EXO1 depletion in combination with CtIP depletion (Figure S8.18 b) or inhibition of MRE11 by the exonuclease-specific inhibitor (Figure 3.30 C) did not further influence the frequency of misrepair events compared to single EXO1 depletion. Thus, all three proteins are involved in the same mechanism to misrejoin distant DSB ends. In contrast, concurrent depletion of EXO1 and 53BP1 in GC92 cells resulted in numbers of misrepair events being elevated to 15.3%, which is a similar frequency to the single 53BP1 depletion (Figure 3.30 C). EXO1 depletion did not affect the abolished misrepair events in GC92 ARTEMIS KO cells. Despite EXO1's role in the misrejoining of distant DSB ends, EXO1 depletion did not show an impact in the γ H2AX foci assay (Figure S8.18 c). However, EXO1 depletion in GC92 ARTEMIS KO cells reduced the repair defect observed in GC92 ARTEMIS KO cells to 1.7 γ H2AX foci. Depletion of EXO1 in combination with MRE11 exonuclease inhibition in GC92 ARTEMIS KO cells also resulted in a reduced mean value of γ H2AX foci ($M = 1.7$). The difference between the mean values of both conditions was not significant at the 0.05 level compared to the control, but effect sizes were 1.5 and 2.79, respectively.

In conclusion, EXO1 is required for the misrejoining of distant DSB ends but is not necessary for overall repair. Depletion of EXO1 alone or in combination with MRE11 exonuclease inhibition resulted in the same frequency of misrepair events, and thus both factors act in a single mechanism. This suggests that CtIP-dependent misrejoining requires both, MRE11 and EXO1. Depletion of EXO1 alone or in combination with MRE11 exonuclease inhibition in GC92 ARTEMIS KO cells partly rescued the ARTEMIS repair defect. This further proves that both are required for the same mechanism to misrejoin distant DSB ends. In contrast to MRE11 inhibition, EXO1 depletion did not influence the misrepair in 53BP1-depleted cells. Therefore, EXO1 does not seem to be required for alt-EJ, as it occurs in 53BP1-depleted cells. In the literature, EXO1 is described as being prevented from accumulating at DSBs by KU80^{218,373,382}. To further link EXO1 to the misrejoining of distant DSBs, which is dependent on KU, SFB-EXO1 WT protein was precipitated and purified from stably-transfected HEK293 cells after no irradiation or 30 min post-5 Gy X-IR. Proteins that co-precipitated with EXO1 were analyzed by MS (Table 8.8). Interestingly, the CtIP-interacting protein EXD2⁵³ was observed to increasingly interact with EXO1 post-irradiation. Despite reports of EXO1 being segregated from DSBs by KU^{218,373,382}, KU80 (XRCC5) was co-precipitated with EXO1 in both unirradiated and irradiated samples. Moreover, KU70 (XRCC6) also co-precipitated with EXO1 and this interaction increased 30 min after irradiation. An even stronger post-irradiation EXO1 interaction was

observed with DNA-PKcs (PRKDC), thus linking all proteins of the DNA-PK complex to EXO1, mostly in a damage-inducible manner.

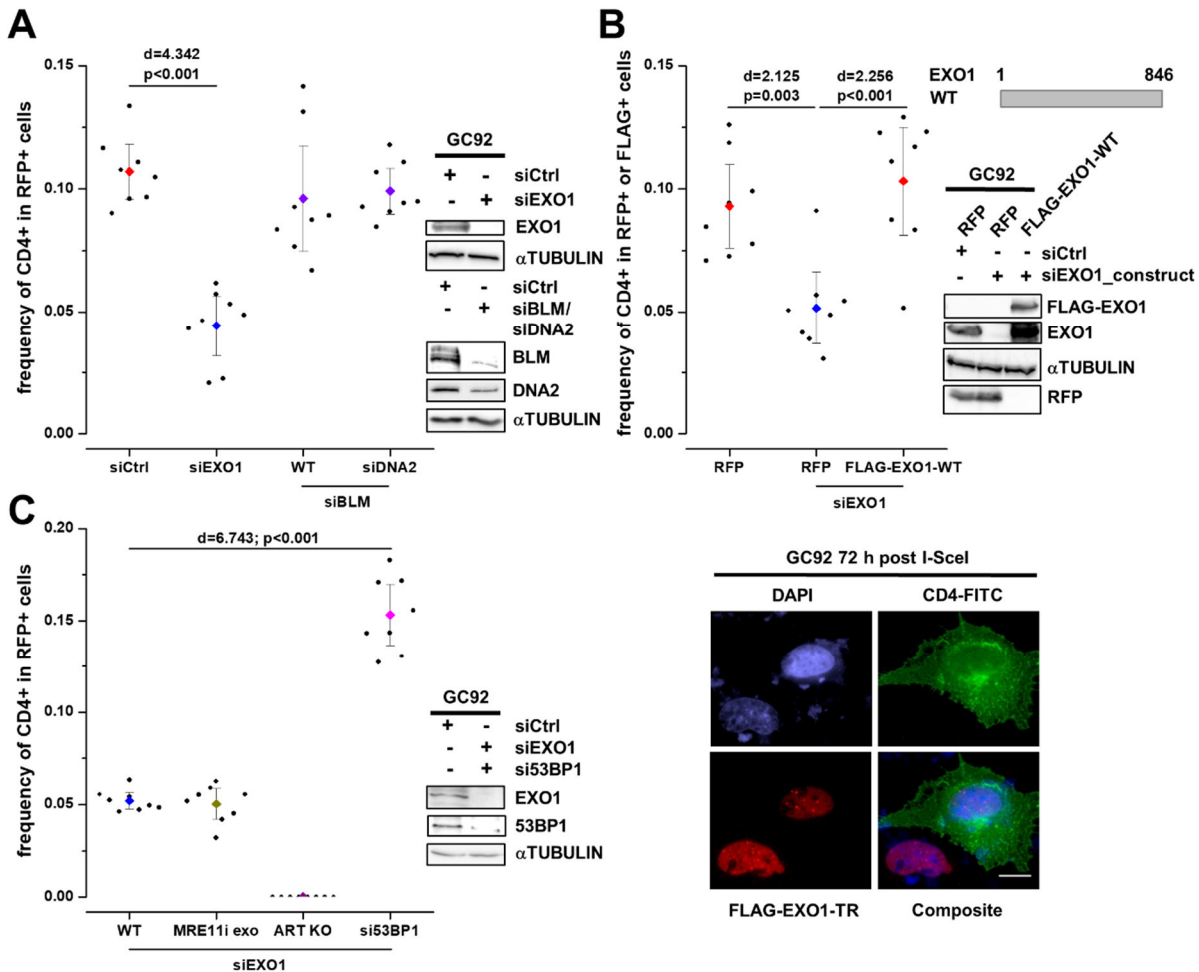


Figure 3.30 EXO1 is required for misrejoining of distant DSB ends

(A, B, C) Impact of EXO1 complementation (B), MRE11 inhibition (C), BLM/DNA2 (A), 53BP1 (C), and/or EXO1 depletion on misrepair in GC92 WT (A, B, C) or ARTEMIS KO (C) cells. GC92 WT or ARTEMIS KO cells were treated with inhibitors and/or siRNAs against MRE11 exonuclease activity (PFM39), 53BP1, and/or EXO1. As a control, cells were treated with control siRNA. (A, C) Cells were harvested 72 h post-co-transfection with I-SceI and RFP plasmids. (B) Cells were transfected with the RFP or siRNA-resistant FLAG-EXO1-WT plasmid. 36 h after plasmid transfection, cells were transfected with I-SceI and harvested after an additional 72 h. Representative images were obtained with a 63x objective using Metafer Isis software. Scale bar represents 10 μ m. Diagram of the exogenous EXO1 WT is not drawn to scale. (A, B, C) Downregulation by siRNA and expression of exogenous plasmids were confirmed by immunoblotting. Cells were stained with anti-RFP or anti-FLAG plus anti-CD4 AB and DAPI. Samples were scanned using Metafer software and only plasmid-transfected cells were analyzed. Data represent the mean of 8 independent experiments performed in duplicate ($n = 8$). RFP and FLAG were used as markers for cells with damage induction and exogenous protein (see chapter 3.1.1). Error bars show the 95% CI. Effect size was calculated by Cohen's d and p -value was obtained by one-way ANOVA with Bonferroni correction. (A, B) Several data points were part of the analysis in Biehs et al. (2017).

In conclusion, several nucleases involved in HR during resection are also observed in the misrejoining of distant DSBs. However, for the limited resection observed in the misrejoining of distant DSBs, these factors are orchestrated in a different way.

4. Discussion

Mutagenic error-prone end-joining of DNA DSBs in WT human cells is poorly understood but important to comprehend, as it endangers genomic stability and hence, initiates carcinogenesis^{51,161,413}. Previous studies on this subject have provided contradicting results. Some studies suggest that alt-EJ plays a role in the error-prone end-joining repair pathway in WT human cells^{148,302,322}. In contrast, other studies have reported that c-NHEJ factors prevent alt-EJ and are associated with generating genomic rearrangements^{142,357}. To study the mechanism of error-prone repair in human cells, mutagenic end-joining events were investigated in this work with a primary focus on the misrejoining of two 3.2 kb distant I-SceI-induced DSBs. In this study, evidence was provided that:

- All I-SceI-induced DSBs are repaired and in approximately 10% repair results in the misrejoining of the distant DSBs (chapter 3.1);
- This misrejoining is associated with additional deletions at the misrejoined break site and caused by limited resection (chapter 3.1, 3.3);
- The underlying error-prone repair mechanism is specific for G₁ phase of the cell cycle and is responsible for the misrepair of distant, but not close, DSBs (chapters 3.1, 3.3);
- This error-prone repair mechanism relies on c-NHEJ factors, involves PARP1, but does not require alt-EJ factors such as LIG1/3 (chapter 3.2);
- This error-prone resection-dependent c-NHEJ pathway is initiated by PLK3-dependent CtIP activation and subsequent CtIP interaction with BRCA1 to antagonize the anti-resection factor 53BP1 (chapter 3.3);
- The resection mechanism in this error-prone c-NHEJ pathway differs from that in alt-EJ and HR (chapter 3.3) and is characterized by (1) limited resection (chapters 3.1, 3.2); (2) resection being executed by EXO1; (3) resection involving EXD2 and MRE11; and (4) resection not requiring MRE11s endonuclease function (chapter 3.3);
- The impairment of factors initiating or executing resection in this error-prone c-NHEJ pathway enables a repair pathway switch, but once resection took place both DNA-PKcs and ARTEMIS are indispensable for repair completion (chapters 3.2, 3.3);
- The break sites are mostly misrejoined using microhomologies, and thus resection-dependent c-NHEJ depends on a variety of polymerases, including POL λ , POL μ , and POL θ (chapter 3.2);
- The absence of resection-dependent c-NHEJ results in less intrachromosomal genomic rearrangements, but more detrimental mutagenic sequence alterations at the remaining misrejoined break sites (chapter 3.3).

Therefore, this work describes a novel error-prone resection-dependent c-NHEJ repair pathway in WT human cells. This repair pathway was characterized in its initiation and execution. What makes resection-dependent c-NHEJ so unique is the involvement of resection in combination with c-NHEJ factors, which were hitherto thought to be mutually exclusive. This is why the name resection-dependent c-NHEJ³⁶ describes it so well (henceforth abbreviated as res-cNHEJ). Although the reporter assay, which was the main focus in this study, does not represent a physiological situation, it was essential for the characterization of the newly discovered repair pathway and could answer questions classical assays could not. The following chapters deal with (1) the strengths and weaknesses of the reporter assay employed; (2) the detailed mechanism of res-cNHEJ; (3) how the initiation of res-cNHEJ impacts DSB repair pathway choice; and (4) the physiological relevance of res-cNHEJ with the focus on open questions and future directions.

4.1. The repair of endonuclease-induced DSBs

The end-joining reporter assay in GC92 cells allows the investigation of mutagenic DSB repair (see Figure 3.1 A for the structure of the reporter assay). The endonuclease I-SceI introduces two DSBs 3.2 kb apart and the misrejoining of the distant DSBs can be measured with the help of a reporter protein. A disadvantage of most reporter assays is that only events that result in the expression of a reporter can be measured. This means that there is no information about how often DSBs are induced before misrepair occurs because accurate repair is not monitored. Thus, the statement that 10% of cells with damage induction undergo misrepair (chapter 3.1) needs to be considered as the frequency of misrepair over the entire repair time. However, this disadvantage was not a problem for this study, as the aim of this work was to characterize the underlying novel mutagenic repair pathway.

4.1.1. Enhancing the accuracy of reporter assay analysis

In this study, detailed consideration was given to clarify when and how DSBs are induced, repaired, and misrepaired in the reporter system (Figure 3.2 A). Furthermore, the protocol was adjusted to ensure sufficient downregulation of endogenous protein levels at the time I-SceI expression began (Figure 5.2). Another important adjustment to the protocol was the reduction of background fluctuations by changing the measurement method from the typical flow cytometry to immunofluorescence microscopy (chapter 3.1.1). In addition, analysis quality was enhanced by only analyzing cells transfected with the I-SceI plasmid, and thus cells in which damage was induced (chapter 3.1.1). This was achieved by using RFP as a marker. With the established protocol, more than 95% of RFP-positive cells were also positive for the endonuclease I-SceI (Figures 3.2 B). Of course, this means that some I-SceI-positive cells escape

the analysis. However, on average, 10% of distant DSBs are misrejoined and express the reporter in approximately 30% of RFP-positive cells. Therefore, misrepair events in all cells were approximately 3%, which is consistent with results in other studies^{35,154,155,322}. The frequency of undetected I-SceI-positive cells was much higher in cells where a tagged exogenous protein was used instead of RFP due to the transfection efficiency of larger proteins being lower (Figure S8.2 b). Nevertheless, the benefit of this analysis is a normalization of the reporter-positive cells to RFP or the exogenous protein-positive cells. Thus, the frequency of misrepair events remained stable at approximately 10%. In Biehs et al. (2017), the common reporter assay analysis method was used wherein misrepair events of treated samples are normalized relative to control samples (example in Figure S8.9 a). As described in chapter 3.1.1, this normalization is not sufficient. However, even for experiments where RFP was not mentioned in Biehs et al. (2017), all experiments were conducted by co-transfection of I-SceI and RFP plasmids to exclude all data in which transfection efficiencies differed by more than 5% between samples. Importantly, some treatments generally seemed to influence transfection efficiencies, which resulted in lower frequencies of RFP-positive cells compared to controls. Consequently, these treatments appeared to have higher frequencies of misrepair events than was actually the case when normalizing treated samples to controls. This problem was solved with the new analysis method used in this dissertation. In conclusion, the first benefit and strength of this study is the adjustment of the experimental procedure and analysis of the reporter assay, which enhances the accuracy of the results.

4.1.2. Beyond the reporter assay: the γ H2AX foci assay in GC92 cells

A major disadvantage of reporter assays is that only events resulting in the expression of the reporter after the misrejoining of DSBs can be measured. They, therefore, fail to provide information about overall DSB repair. This shortcoming was solved in this study by combining the GC92 reporter assay with the γ H2AX foci assay (Figures 3.1 A, C, 3.2 A). With this method, the repair of I-SceI-induced DSBs could be investigated by using γ H2AX as a DSB marker²⁴⁷. Therefore, this study provides information about the quality and the quantity of endonuclease-induced DSB repair. An interesting aspect of γ H2AX foci in this assay was how they increased in relation to the I-SceI protein levels. Although I-SceI was already overexpressed in many cells 24 h post-I-SceI plasmid transfection, a rise of DSBs, as indicated by the γ H2AX foci, was only observed at 36 h and remained high until 48 h post-I-SceI transfection (Figure 3.2 A). To interpret this finding, it is important to remember that DSB induction occurs over the entire duration that I-SceI is present in the cells (approximately 60 h) and that DSBs can be induced repeatedly as long as they are repaired accurately and the I-SceI recognition site is not disrupted. Therefore, this indicates that DSBs are repaired quickly in the beginning and only

start persisting long enough to be detectable at later timepoints. Interestingly, the frequency of misrepair events only rises after DSBs begin to persist. Thus, in the beginning, fast repair results in accurate rejoining, which is not detectable in the assay and misrepair occurs when repair is slow. Therefore, studies that do not include such kinetics and adjust their experimental procedure accordingly, might miss out on a certain type of repair and obtain different results.

As two DSBs are induced, the γ H2AX foci would theoretically increase by 2 foci in an unrepaired situation. Indeed, the impairment of major DSB repair factors resulted in an increase of 2 γ H2AX foci (e.g. Figure S8.6 b). However, as discussed in chapter 3.1.2, the γ H2AX signal extends beyond the distance of the two I-SceI recognition sites, suggesting that an increase of 2 foci would only be observed if the unrepaired breaks are not held in proximity. An increase of 2 foci could also mean that the reporter construct has integrated more than once. Understanding the meaning of an increase of 2 γ H2AX foci is crucial for the interpretation of results showing a partial repair defect with an increase by 1 γ H2AX focus (e.g. Figure S8.6 c). If 2 γ H2AX foci were visible because the DSB ends were not held in proximity, a partial repair defect (increase by 1 focus) could occur when the break ends are held together to only allow the formation of 1 γ H2AX focus. A second model for a partial repair defect involves repair taking place in some cells but not in others. Although this question should be possible to answer by analyzing the median of γ H2AX foci in each experiment (as displayed for cells that repaired the DSBs in Figure S8.5 c), the number of experiments was too small for a conclusive statement. Thus, the interpretation of a partial repair defect remains speculative and in this study, may indeed have different interpretations depending on the factor investigated. In conclusion, the expansion of the reporter assay with the γ H2AX foci assay enhances the quality of the analysis by filling the gap in the overall repair analyses, which are usually associated with reporter assays.

4.1.3. Radiation-induced DSBs in comparison to endonuclease-induced DSBs

Although the main focus of this study was the misrepair of distant endonuclease-induced DSBs, additional experimental procedures were included to analyze other areas where res-cNHEJ might play a role. In addition, these methods were used to further analyze how the factors involved in res-cNHEJ contribute to DSB repair pathway choice. Damage in these experiments was generally induced by X-IR. DSBs are repaired with biphasic kinetics after X-IR²⁷². The fast repair component is executed by c-NHEJ throughout the cell cycle, while slow repair during G₂ phase is performed by HR³⁴. Although several factors have been associated with the slow repair process during G₁ phase^{34,327}, until recently³⁶, the underlying repair pathway for slowly repairing G₁ phase DSBs was unclear. Based on data from the working group, the slow DSB repair pathway in G₁ phase likely is the same as the repair of distant endonuclease-induced

DSBs. Furthermore, studies investigating the repair of complex DNA damage following high-LET irradiation ^{15,343}, also showed a dependency on resection and error-prone repair. Therefore, the radiation-based assays used during this study are typically used to investigate HR during S/G₂ phase but modified to specifically investigate slow DSB repair and resection in G₁ phase. High doses of X-IR were used to generate clustered DNA damage by increasing the number of DSBs. To investigate the impact of res-cNHEJ factors on DSB repair pathway choice, protein interactions were studied in immunoprecipitation experiments with G₁-synchronized cells. To expand this approach, the interactome of key res-cNHEJ factors was investigated by tandem affinity purification mass spectrometry (TAP-MS) ^{129,418} to identify possible new interaction partners and analyze how the entire interactome is affected after DNA damage. The obtained results will direct future analyses of this repair pathway.

4.2. Resection-dependent c-NHEJ (res-cNHEJ)

This chapter is dedicated to the mechanics of the novel error-prone res-cNHEJ. The first distinction between a c-NHEJ pathway involving resection and alt-EJ was introduced by Goodarzi and Jeggo (2013) to describe how DSBs persisting in G₁ phase might be repaired. The persisting DSB ends were described as originating from non-ligatable ends or from chromatin complexity. Due to previous studies, it is known that the repair of persisting DSBs in G₁ phase involves ARTEMIS and ATM ³⁴. Other studies have shown that CtIP is required for error-prone end-joining during G₁ ⁴²⁹, that the repair of complex DSB ends during G₁ phase is dependent on CtIP and MRE11 ^{15,319,322}, and that complex DSBs from high-LET irradiation additionally require EXO1 ¹⁵. Importantly, DSB complexity can either mean chemically complex at the DSB ends or complex due to clustered damage. The misrejoining of distant endonuclease-induced DSBs might involve chemically complex breaks if I-SceI needs to be actively removed before the breaks can be repaired, as has been observed for other complex break ends ¹². However, this theory can be refuted because I-SceI-induced DSBs can cause different repair pathway responses from simple rejoining to resection-dependent repair. These DSB pathway responses are dependent on the distance of the DSB ends (chapter 4.3.1), and thus similar to clustered DSB ends, as both fail to rejoin the accurate break ends.

4.2.1. Barriers to resection during res-cNHEJ

A key protein in preventing any kind of DNA degradation is the KU heterodimer ¹⁸⁸. The misrejoining of distant (3.2 kb) DSBs was enhanced in KU-depleted GC92 cells (Figures 3.5 B), and this increase was dependent on alt-EJ factors (Figures 3.7 B). Therefore, KU-binding protects the DSB ends and prevents a pathway switch to alt-EJ. In other studies, reporter constructs were incorporated in KU-deficient Chinese hamster ovary (CHO) cell lines ^{155,156,258}.

Although no increase in misrepair events was observed in these studies, sequence analyses revealed an increase in the size of the additional deletions at the misrejoined break site. This supports the model wherein misrepair switches to alt-EJ in the absence of KU. The larger deletions observed in these studies might also explain why the misrejoining of close (34 bp) DSBs decreased in this study after KU depletion (Figures S8.6 a); the proximity of the DSB site probably harms the reporter gene. This has also been observed in other studies^{197,293}. Therefore, KU-binding of the DSB ends is essential to ensure DSB repair by res-cNHEJ can take place (Figure 4.1). Prevention of uncontrolled resection or a switch to alt-EJ is also provided by 53BP1. In the absence of 53BP1, the misrejoining of distant DSB ends increased (Figures 3.12 A, B), which was entirely dependent on alt-EJ factors (Figures 3.13 C, D). Thus, 53BP1 is an additional factor required to allow DSB repair by res-cNHEJ (Figure 4.1).

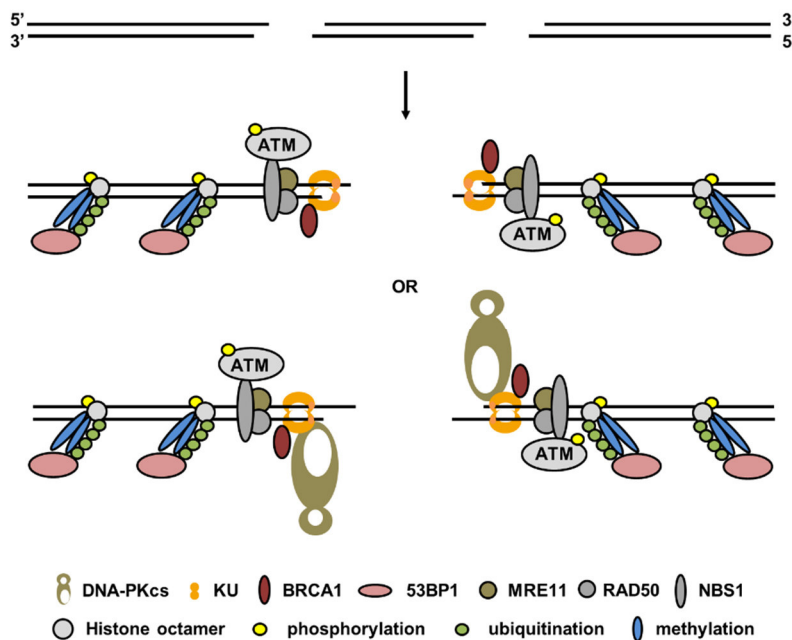


Figure 4.1 Model for the failure of accurate DSB repair

I-SceI induces two 3.2 kb separated DSBs in GC92 cells with 4 nt 3' overhangs. KU binds and protects the DSB ends while BRCA1 stabilizes KU. 53BP1 binds to histone octamers to prevent resection. KU translocates one helical turn inwards to allow DNA-PKcs-binding. The accurate repair of the DSB ends by c-NHEJ fails, which could occur for many reasons. Of note, Sibanda et al. (2017) speculate that because of the vicinity of the BRCA1 and DNA-PKcs-binding sites on KU80, BRCA1 and DNA-PKcs compete with each other for KU80-binding. Based on Jiang et al. (2013); Grundy et al. (2014); Saha and Davis (2016); Chang et al. (2017); Sibanda et al. (2017), and data herein (chapters 3.2, 3.3).

BRCA1 stabilizes KU during G₁ phase of the cell cycle, through its interaction with KU80, to promote high-fidelity rejoining of break ends^{197,336}. Jiang et al. (2013) found that the BRCA1-KU80 interaction was present in undamaged G₁ cells and increased after I-SceI damage induction. Herein, this observation was broadened by validating that KU80 interacts with BRCA1 in G₁ phase following DNA damage induction by X-IR (Figure 3.26 D). This interaction was present with no damage induction, increased 30 min post-irradiation, and was lower than

in undamaged cells 1 h post-irradiation. The absence of BRCA1 reduced the frequency of the misrejoining of distant and close DSBs (Figures 3.15 A, S8.11 c). Jiang et al. (2013) observed longer deletions in BRCA1-depleted cells. Thus, the reduction of close misrepair events likely has a similar origin as KU depletion, through longer deletions, which harm the reporter gene. In contrast, the reduction of misrejoining of distant DSBs is caused by the requirement of BRCA1 for the initiation of the res-cNHEJ pathway (further details in chapter 4.2.2). Importantly, BRCA1-bound KU might prevent proper DNA-PKcs-binding as Sibanda et al. (2017) suggest that the close proximity of the BRCA1 and DNA-PKcs-binding sites on KU80 sterically exclude simultaneous binding.

Translocation of KU during res-cNHEJ

In the literature, it is generally accepted that KU prevents resection^{239,273,362}. Indeed, biochemical studies showed that KU needs to be actively removed from the break ends before resection can take place³⁷³. Nevertheless, studies of single-ended DSBs have shown that resection is executed during HR while KU is bound to the DSB end and needs to be removed before the strand invasion takes place⁷⁴. Importantly, these studies all investigated extensive resection, which produces the long 3' overhangs necessary for repair by HR. The results of the sequence analysis in this study indicated a much more limited resection (Figures 3.3 A, B) associated with the misrejoining of distant DSBs. In addition, KU80 co-localized with pRPA during G₁ phase after 10 and 20 Gy X-IR (Figures 3.6 F, G). RPA requires approximately 30 nt ssDNA to coat and protect ssDNA stably⁴². As only high doses of X-IR resulted in pRPA foci during G₁ phase and the frequency of pRPA foci increased with increasing radiation doses, it can be assumed that only these high doses produce ssDNA regions long enough for pRPA to bind. This is supported by the sequence analysis, where 90% of the additional deletions at the misrejoined break sites ranged between no deletion and 50 nt deletions, with the majority of deletions less than 10 nt (Figures 3.3 A, B). Nevertheless, if KU remains bound to the break ends during the resection process in res-cNHEJ, it needs to be moved. This movement likely is very limited due to the very stable binding of KU to the DNA (Figure 4.2). Indeed, this is a favored model because it would explain why resection remains so limited during res-cNHEJ. The inwards translocation of KU by one helical turn (10 nt) to allow DNA-PKcs-binding is well-described^{271,321,424}. Furthermore, in biochemical studies, KU was able to translocate inwards stepwise to allow the binding of up to 5 KU molecules on duplex DNA³⁸⁵. The question then is: if (1) the translocation of KU inwards is something that happens when DSBs persist; (2) the inwards translocation of KU beyond 1 helical turn is inhibited right after damage induction to first prioritize accurate repair by c-NHEJ; and/or (3) the translocation of KU is promoted by an enzymatic activity to actively promote resection.

The most likely scenario is a combination of these mechanisms. For example, the inward translocation of KU might be actively promoted. Lee et al. (2016) showed that the phosphorylation of KU in the pillar and bridge region of KU70 leads to a conformational change, which leads to less stringent binding of KU to the DNA. This promotes the release of KU from the DSB ends through a combination of the low binding affinity of KU and possibly the assistance of the MRN complex with CtIP. The authors state that this phosphorylation is limited to S/G₂ phase, but only because in their study this phosphorylation allows the removal of KU and long-range 5' to 3' resection to produce large 3' overhangs. Perhaps KU is also phosphorylated in G₁ to lower its binding affinity to the DNA, and thus promote the translocation of KU inwards (for further details on how the same KU phosphorylation could have a different outcome in G₁ compared to S/G₂, see chapter 4.2.3). Even the removal of KU and subsequent rebinding of KU upon completion of resection in G₁ phase cannot be excluded, but such a model is unfavorable because it would raise the question of how resection remains so limited. In addition, the translocation of KU might be inhibited right after DSB induction by a stabilizing interaction with BRCA1. This would raise the question as to how the initiation of res-cNHEJ disrupts the BRCA1-KU interaction. In S/G₂ phase of the cell cycle, CtIP is constitutively phosphorylated at Ser327 by S/G₂-specific CDK complexes, which causes its interaction with BRCA1⁴²⁸. During this study, it was established that in G₁ phase, BRCA1 interacts with CtIP following DNA damage induction, in a CtIP Ser327 phosphorylation-dependent manner (Figures 3.26 C, S8.12 b). Indeed, the phosphorylation of CtIP at Ser327 was required for the misrejoining of distant DSB ends (Figure 3.23 A). Interestingly, at the time the BRCA1-CtIP-pSer327 interaction was strongest, the BRCA1-KU80 interaction was weaker than in unirradiated samples (Figures 3.26 C, D). Moreover, the BRCA1-KU80 interaction remained strong when the damage-dependent CtIP phosphorylation was prevented, and thus the subsequent BRCA1-CtIP interaction could not occur. This indicates that the damage-dependent formation of the BRCA1-CtIP interaction is involved in the disruption of the BRCA1-KU80 interaction (Figure 4.2).

Overcoming the resection barrier posed by 53BP1 during res-cNHEJ

The BRCA1-CtIP interaction is important for the movement of 53BP1 away from the break end (Figure 4.2). The movement of 53BP1 is essential during S/G₂ phase to enable HR and is achieved by several mechanisms. This includes the BRCA1-promoted dephosphorylation of 53BP1, and thus disruption of the 53BP1 interaction with RIF1 and PTIP^{96,127,178,186,353}, as well as the BRCA1-dependent ubiquitination of H2A Lys217 to allow SMARCAD1 to reposition nucleosomes including the bound 53BP1^{89,105}. The extent of 53BP1 movement in G₁ is unclear, as is the exact mechanism because resection remains so limited. However, Figure 3.15 B shows

that BRCA1 is no longer required in the absence of 53BP1, supporting the notion that BRCA1 plays a role in relocating 53BP1 during res-cNHEJ as it does in HR. In conclusion, the data suggest that the damage-dependent phosphorylation of CtIP results in its interaction with BRCA1 and disrupts BRCA1's interaction with KU80 (Figure 4.2). In addition, both the BRCA1 BRCT and RING domain are required for the misrejoining of distant DSB ends (Figure 3.16 A). This was not surprising for the BRCT domain, as it is necessary for BRCA1 to interact with phosphorylated CtIP. The requirement for the BRCA1 RING domain indicates that the E3 ubiquitin ligase activity of BRCA1 is necessary for res-cNHEJ, as it is for the initiation of HR¹²⁷. Furthermore, the BRCA1-CtIP interaction is clearly required for the initiation of this novel repair pathway (Figures 3.23 A, 3.26 C). Importantly, the roles of BRCA1 and CtIP differed during res-cNHEJ. The overexpression of CtIP, but not BRCA1, resulted in an increase of misrejoining of distant DSB ends (Figures 1.17 C, S8.11 e). This indicates that phosphorylated CtIP initiates resection by removing BRCA1 to destabilize KU, which could indeed be the primary reason for the BRCA1-CtIP interaction.

4.2.2. Initiation of resection during res-cNHEJ

As described, CtIP is phosphorylated at Ser327 upon damage induction in G₁ phase (Figures 3.26 C, S8.12 b). In Barton et al. (2014), PLK3 was identified as the kinase mediating this phosphorylation (Figure 4.2). Indeed, PLK3 is required for the misrejoining of distant, but not close, DSBs (just like CtIP; Figures 3.17 A, 3.24 B, C). In Barton et al. (2014), the possibility that PLK3 may be exclusive to G₁ phase is mentioned because that was the case in thymidine-synchronized HeLa cells⁴³⁷. However, the protein levels of PLK3 in GC92 cells are similar in all cell cycle phases (Figure 3.26 B). In fact, this is also observed in multiple other cell lines, including several fibroblast cell lines^{32,76,166,402,415}. Nevertheless, the damage-inducible phosphorylation of CtIP by PLK3 is specific for G₁ phase of the cell cycle²⁵. Furthermore, the CDK complexes responsible for constitutive CtIP phosphorylation during S/G₂ phase¹⁷⁷ have no impact on the misrejoining of distant DSB ends (Figure 3.24 A). This indicates that the misrejoining of distant DSB ends, and thus res-cNHEJ is a G₁-specific mechanism. However, PLK3-dependent misrejoining of distant DSBs was observed in G₂ phase after the inhibition of HR by the impairment of S/G₂-specific CDK complexes (Figure S8.16 d). Thus, PLK3 may be able to phosphorylate CtIP in G₂ in the absence of these CDK complexes. Therefore, the damage-inducible CtIP phosphorylation by PLK3 is probably suppressed by the constitutive CtIP phosphorylation by CDK complexes during S/G₂ phase.

In S/G₂ phase, BRCA1 forms a complex with CtIP and the MRN complex⁷⁸. The requisite phosphorylation of CtIP at Thr847¹⁰ is also present in G₁ following DNA damage induction and necessary for the misrejoining of distant DSB ends (Figure 3.23 A). This phosphorylation is also

performed by PLK3²⁵. Therefore, BRCA1-CtIP likely interacts with the MRN complex in G₁ phase (further discussed in chapter 4.2.3). In Barton et al. (2014), CtIP Ser327 was phosphorylated 30 to 90 min following 5 Gy X-IR, whereas the phosphorylation of Thr847 increased 120 min post-irradiation. In addition, the necessity of the PLK3 PBD to activate PLK3 by interaction with Ser327-phosphorylated CtIP was observed to subsequently phosphorylate CtIP at Ser327 and Thr847 (Figure 4.2). Indeed, the PLK3 PBD was required for the misrejoining of distant DSB ends (Figure 3.25 A). Therefore, a model was proposed where PLK3 binds via the PBD to Ser327-phosphorylated CtIP. It is unclear how this initial phosphorylation is accomplished. Based on models in the literature^{122,325} the phosphorylation of CtIP at Ser327 might be conducted by PLK3 in a self-priming mechanism, performed by an unknown kinase, or present in a fraction of the CtIP molecules from S/G₂ phase residues²⁵. In any case, PLK3 bound to CtIP-pSer327 then phosphorylates other CtIP molecules at Ser327 (Figure 4.2). Subsequently, PLK3 phosphorylates other sites such as Thr847 of the CtIP molecule to which PLK3 is bound and/or neighboring CtIP molecules.

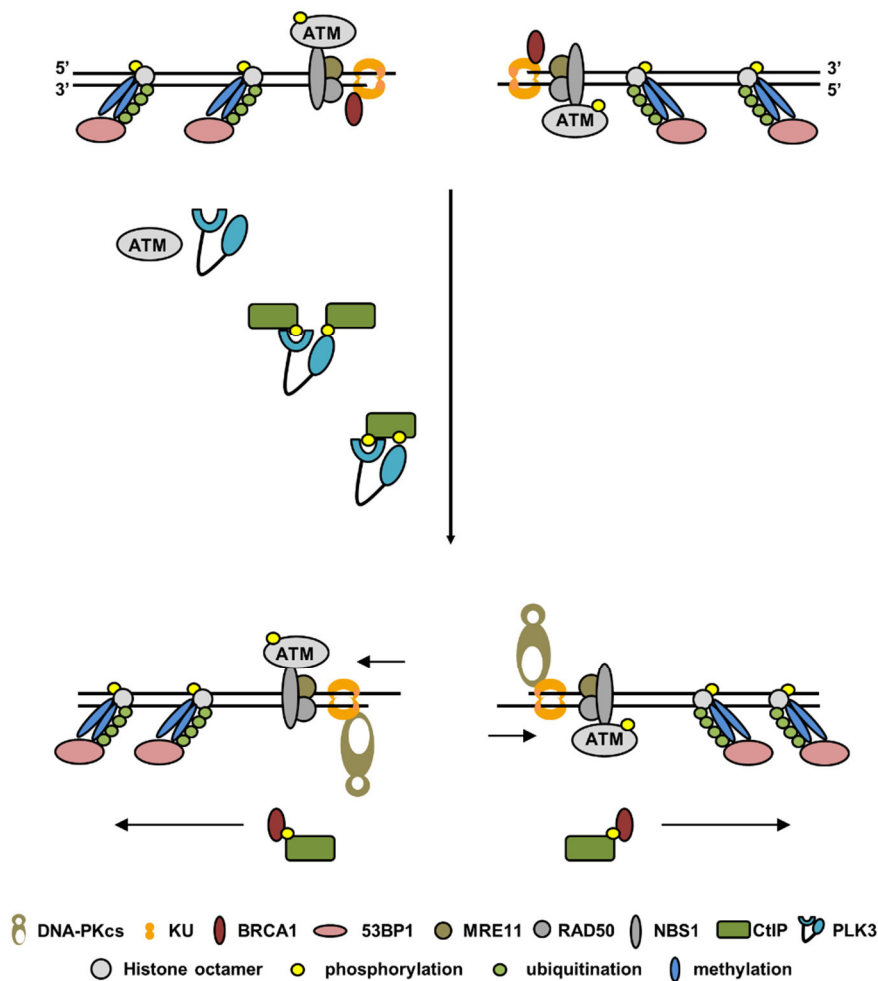


Figure 4.2 Model for overcoming resection barriers by the resection initiation mechanism during res-cNHEJ

After the failure of accurate repair, resection is initiated. PLK3 is phosphorylated by ATM and binds to CtIP-pS327 via its PBD domain. The origin of this initial CtIP-pS327 remains speculative. Subsequently, the CtIP phosphorylation

at S327 is amplified by PLK3 through the phosphorylation of neighboring CtIP molecules. Furthermore, PLK3 phosphorylates CtIP at T847 and additional sites. CtIP-pS327 interacts with BRCA1, which antagonizes the anti-resection function of 53BP1. This potentially involves the movement of 53BP1 away from the DSB end. Importantly, the KU80-BRCA1 interaction is no longer observed during this time. This might be caused by the BRCA1-CtIP-pS327 interaction to (1) destabilize KU and allow further KU translocation inwards or (2) to disrupt KU80-BRCA1 to allow DNA-PKcs-binding to KU (if steric competition exists as described in Sibanda et al. (2017)). Of note, it is plausible that the BRCA1-CtIP interaction forms a complex with MRN as is the case in S/G₂ phase. Based on Barton et al. (2014); Panier and Boulton (2014); Saha and Davis (2016); Shibata (2017), and data herein (chapter 3.3).

Hyper-phosphorylation of CtIP does not seem to play a role in G₁-specific res-cNHEJ (Table 8.7). However, the question arises as to whether phosphorylation of CtIP at Ser327 and Thr847 by PLK3 is sufficient to initiate res-cNHEJ. Expressing a CtIP phospho-mimic mutant at these two sites in CtIP/PLK3-depleted cells was not sufficient for the misrejoining of distant DSB ends (Figure 3.27 A). Therefore, additional phosphorylation of CtIP by PLK3 is necessary for res-cNHEJ. Importantly, in experiments with high-LET irradiation, resection was possible with this CtIP double phospho-mimic mutant ²⁵. This indicates that phosphorylation of Ser327 and Thr847 is sufficient to initiate resection, but that res-cNHEJ is impaired at a subsequent step without complete phosphorylation of CtIP by PLK3. Based on the biochemical studies, strong candidate CtIP sites that might be phosphorylated by PLK3 are Ser326, Ser608, and Ser641 (Table 8.7). In addition, several phosphorylation sites were identified that meet the criteria to be potentially phosphorylated by PLK3 but had a low probability for a phosphorylation in the one experiment performed during this study (e.g. Ser305, Ser555, Thr859).

4.2.3. Nucleases conducting resection during res-cNHEJ

An important characteristic of res-cNHEJ in G₁ phase is that if resection is not initiated, a pathway switch can occur and still repair the DSBs. This may be one reason why res-cNHEJ has not been discovered thus far ^{25,36}. After establishing how res-cNHEJ is initiated and how KU might translocate inwards to allow limited resection, the question remains as to which nucleases drive resection during res-cNHEJ. Resection is conducted in two steps during HR: short-range and long-range resection ³⁵⁴. During HR, resection is initiated by MRE11 endonuclease activity, which cleaves the ssDNA internally from the break end (Figure 2.3). This incision requires the presence of RAD50 and, for conformational reasons, NBS1 and Thr847-phosphorylated CtIP ¹⁰. Rass et al. (2009) showed that MRE11 is involved in the misrejoining of distant DSBs and, as described in chapter 4.2.2, so is CtIP-pThr847 (Figure 3.23 A). However, the use of an MRE11 endonuclease-specific inhibitor ³⁵⁴ during this study showed that the endonuclease activity of MRE11 is dispensable for the misrejoining of distant DSB ends (Figure 3.28 A). Ultimately, it is unsurprising that resection in G₁ is not initiated by an endonucleolytic MRE11-dependent cut, as that mechanism allows other resection processes to circumvent the protection of the DSB ends by KU. The lack of an endonucleolytic cut during res-cNHEJ indicates that resection is initiated from the DSB end, which again supports the notion that KU limits the extent of

resection in G₁. Moreover, resection from the DSB ends could move phosphorylated KU, which would be bound less stringently to the DNA (as per the model introduced in chapter 4.2.1) ²²⁹. Thus, if KU is phosphorylated in G₁ and S/G₂ phase, the movement of KU would be determined by the direction of the resection process. This would explain different outcomes of KU phosphorylation in G₁ (enabling limited resection that would not be visible with the experiments performed by Lee et al. (2016)) versus S/G₂ phase (removal of KU and enabling extensive resection during HR).

Another important aspect to consider regarding the lack of an endonucleolytic cleavage by MRE11 during res-cNHEJ, is an observation by Anand et al. (2016). In this study, this cut was possible in biochemical studies simply by the presence of the MRN complex in concert with CtIP-pThr847. This implies that there is a mechanism during G₁ phase, which inhibits the endonucleolytic function of MRE11. This inhibition is likely connected to 53BP1, because in the absence of 53BP1, the endonuclease function of MRE11 plays a role (Figure 3.29 A). As described in chapter 4.2.2, it is to be expected that BRCA1-CtIP may form a complex with MRN during res-cNHEJ, as is observed during S/G₂ phase ⁷⁸. This might be another process by which MRE11 activity could be inhibited, as BRCA1 is known to suppress the nucleolytic activity of MRE11 during G₁ phase ^{336,412}. This is achieved through BRCA1s interaction with NBS1 ^{336,412}. Thus, this interaction might change the conformation of the complex to prevent the endonucleolytic cut by MRE11, as NBS1 is required during S/G₂ phase during the incision by MRE11 for conformational reasons ¹⁰. However, the continued persistence of DSBs might change the way in which resection takes place during res-cNHEJ, as slow repair during G₁ phase also repairs blocked ends, which likely require MRE11 endonucleolytic activity ^{12,241,319}. Hence, the resection process during res-cNHEJ could be adjustable depending on the structure of the DSB end, just like the processing of the DSBs and the factors involved differ during resection-independent c-NHEJ ^{71,72,145,302,326,370}.

The endonuclease I-SceI introduces DSBs under the formation of 4 nt 3' ssDNA overhangs. Thus, 5' to 3' resection factors, which are usually responsible for long-range resection during HR, came into focus during this study. 5' to 3' resection during HR produces extensive 3' overhangs, which are necessary for strand invasion and requires the initiation of resection internally to the break end to overcome the block of the DSB ends ³⁵⁴. Resection in the 5' to 3' direction is either conducted by EXO1/BLM and/or BLM/DNA2 ^{67,287,382}. BLM is a helicase, which unwinds the dsDNA by translocating along ssDNA in a 3' to 5' direction ⁹². However, BLM also has a role in promoting DSB protection through the 53BP1/RIF1 pathway ¹⁴⁸, which makes it difficult to investigate. Although BLM depletion had no impact on the frequency of misrepair events (Figure 3.30 A), Grabarz et al. (2013) showed that the lack of BLM results in large deletions at

the misrejoined break sites. More importantly, the combined impairment of BLM with DNA2 also did not impact the misrejoining of distant DSB ends (Figure 3.30 A). This was not surprising, as 5' to 3' resection by BLM/DNA2 is stimulated during S/G₂ phase by RPA¹⁶, which binds to the generated ssDNA to protect it from digestion³⁷. RPA then directs the DNA2 endonucleolytic activity towards a stepwise degradation of the 5' DNA strand^{16,240,282}. As described previously, resection is generally too limited during G₁ phase for RPA-binding, and thus would not allow the DNA2/BLM-dependent 5' to 3' resection.

In the literature, EXO1 is described as a factor, which is prevented from accumulating at DSBs by KU80^{218,373,382}. Nevertheless, the misrejoining of distant DSBs was dependent on EXO1 to the same extent as CtIP (Figures 3.30 A, B, S8.18 b). This was unexpected but would be a favorable combination to ensure that resection during G₁ remains limited by creating a hostile environment. However, KU is not the only factor that counteracts EXO1-dependent resection. In fact, RPA also restricts EXO1-mediated resection by removing and/or blocking it from binding to ssDNA^{62,218,282}. To overcome this restriction in S/G₂ phase, EXO1 requires support. Several studies suggest that full EXO1 exonuclease activity, EXO1 recruitment, and/or the extent of EXO1 resection requires its stimulation by the MRN complex or factors such as MRE11, CtIP, BRCA1, BLM, and/or additional unknown proteins^{16,62,121,169,170,209,282,373,381,382}. In fact, EXO1 only is able to conduct resection on its own in the absence of KU80, when EXO1 is overexpressed, and/or when the DSB ends in a long 3' ssDNA tail^{240,260,382}. As EXO1 is required for resection in res-cNHEJ (Figure 4.3), further factors that might support EXO1 to allow DSB resection from the end despite KU80s presence were analyzed. As described, MRE11 has already been shown to be involved in the misrejoining of distant DSB ends³²². This was confirmed by this study and specified by the exonuclease-specific inhibition of MRE11 (Figure 3.28 A). This result suggested a dependency of misrejoining events on the 3' to 5' MRE11 exonuclease function. In Biehs et al. (2017), it is suggested that resection during G₁ phase is either conducted by EXO1 or MRE11, depending on whether 3' to 5' or 5' to 3' resection is required. However, the DSBs generated by I-SceI always generate the same DSB end structures with 3' overhangs. Another result, which speaks strongly against this model, is that the combined impairment of EXO1 and MRE11 exonuclease function did not further decrease the misrepair events (Figure 3.30 C). In addition, Rass et al. (2009) observed that an MRE11 mutant, which displayed impaired nuclease activity (both endo- and exonuclease activity), had no impact on the misrejoining of distant DSB ends in GC92 cells. Furthermore, BRCA1 has been shown to suppress the MRE11 nucleolytic activity during G₁ phase through its interaction with NBS1^{336,412}. Closer inspection of the endo- and exonuclease-specific inhibitor functionalities provided a possible explanation (also see chapter 3.3.4 for more details on the effect of the inhibitors).

Mirin and PFM39 both inhibit the 3' exonuclease activity of MRE11³⁵⁴. However, mirin is known to prevent MRN-dependent ATM activation¹²⁰. In contrast, PFM39 does not prevent MRN-dependent ATM activation^{36,354} but speculatively, may instead impair MRE11s support of EXO1-mediated resection. Importantly, EXO1/BLM-dependent resection during S/G₂ phase works in cells treated with the PFM39 exonuclease-specific MRE11 inhibitor³⁵⁴. This can be easily explained by BLM assuming the supporting role toward EXO1 in S/G₂ phase, which would only be possible in the presence of RPA¹⁶, and thus not an option during the limited resection in G₁ phase. Another factor, which might be required to support EXO1-dependent resection during res-cNHEJ, is the nuclease and RecQ helicase WRN. In biochemical experiments, the 5' to 3' dsDNA exonuclease activity of EXO1 is stimulated by WRN³⁵¹. In addition, WRN promotes c-NHEJ with its helicase and exonuclease activity and prevents large deletions by protecting the DSBs from 5' resection in error-prone end-joining³⁵⁰. Thus, WRN is a strong candidate to be involved in res-cNHEJ.

A major reason, why the model of both MRE11 exonuclease activity and EXO1-mediated resection during res-cNHEJ was included in Biels et al. (2017), was the observation that EXD2 was required for the misrejoining of distant DSBs (Figure 3.28 A). EXD2 conducts 3' to 5' resection in concert with MRE11 following the endonucleolytic cleavage by MRE11 during HR⁵³. However, the biochemical studies in Broderick et al. (2016) strongly suggest that the role of EXD2 in res-cNHEJ is different than HR. Although EXD2 can resect ssDNA in a 3' to 5' direction, the resection of dsDNA in the 3' to 5' resection is only possible from nicks or gaps, and thus requires MRE11 endonuclease activity. As the MRE11 endonuclease activity is not involved in res-cNHEJ, EXD2 is not able to perform 3' to 5' dsDNA resection in concert with MRE11 from the break end. This raises the question of what is the role of EXD2 in res-cNHEJ? As I-SceI generates 3' ssDNA overhangs, which are further expanded by EXO1 through its 5' to 3' exonuclease activity on dsDNA^{227,230}, EXD2 might process the ssDNA in the 3' to 5' direction. Thus, EXD2 could be responsible for the loss of nucleotides at the misrejoined break sites. Another possibility for an involvement of EXD2 might be found through its homolog CG6744 in *Drosophila melanogaster*. The exonuclease domain in EXD2 was predicted due to this gene containing homology to the WRN exonuclease domain^{91,358}. In addition, the same gene also shares homology with the helicase ATP-binding domain of WRN⁹¹. Therefore, the involvement of EXD2 in res-cNHEJ could be independent of its nuclease activity. Indeed, EXD2 might support EXO1, as was suggested for other proteins such as MRE11 and CtIP. This hypothesis is supported by the possible interaction of EXD2 with EXO1 (Table 8.8). Importantly, the interaction increased following DNA damage induction. In general, EXD2 might also be involved in the 3' to 5' dsDNA resection at DSBs with 5' overhangs, as it has weak nuclease activity at such

structures⁵³. However, this possibility is irrelevant for the repair of DSBs with 3' overhang in all assays with damage induction by I-SceI.

4.2.4. Processing of resection intermediates during res-cNHEJ

The ssDNA generated during resection in res-cNHEJ is too short for RPA to stably bind⁴², and thus is not protected. The structure of DNA-PKcs forms a “head” region and a “palm” region¹⁵⁹. The “head” of DNA-PKcs has a small cavity, which allows ssDNA to enter and is believed to promote end-processing⁴⁰⁸. Therefore, it was speculated in Biehs et al. (2017) that the generated ssDNA might be captured in the small cavity of DNA-PKcs to protect it from degradation (Figure 4.3).

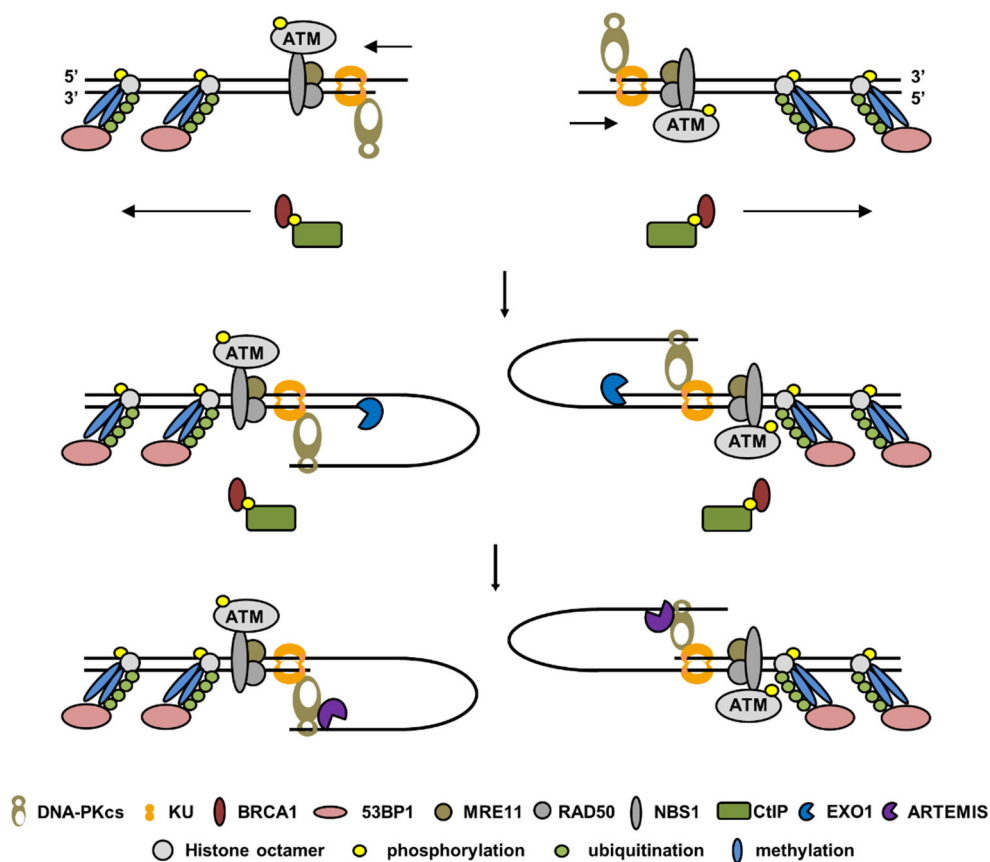


Figure 4.3 Model for resection and the processing of resection intermediates during res-cNHEJ

As KU translocates inwards, resection can take place. Speculatively, the generated ssDNA is captured by DNA-PKcs to prevent the degradation of the overhang. Resection is conducted by EXO1 in a 5' to 3' direction. Although MRE11 exonuclease activity may contribute by resecting in 3' to 5' direction, it is more likely that MRE11 only plays a supportive role in allowing EXO1 resection. Furthermore, EXD2 was observed to be involved. However, its role is unclear, as it can only resect dsDNA in S/G₂ in the 3' to 5' direction following the endonuclease cut by MRE11, which does not play a role during res-cNHEJ. Nevertheless, EXD2 was observed to have 3' to 5' exonuclease activity on 3' ssDNA, which could be one explanation for the involvement of EXD2. Of note, it is plausible that BRCA1-CtIP complexes with MRN, as is the case in S/G₂ phase, especially considering that BRCA1 is known to interact with NBS1 during G₁ phase to inhibit the nuclease activity of MRE11. Importantly, DNA-PKcs likely hangs on the “arm” of KU80 during the resection process (different compared to the model in Biehs et al. (2017)). Following resection, the endonuclease ARTEMIS cuts the hairpin-like structure of the DNA formed by DNA-PKcs. These cuts could be guided, and thus generate different sizes of deletions (as suggested in Biehs et al. (2017)). However, it is more likely that the size of generated ssDNA is controlled by the resection machinery, as ARTEMIS cuts hairpins and hairpin-like

structures (formed from ssDNA overhangs) an equivalent of 1 nt from the dsDNA-ssDNA transition in the 5' direction to produce 3' overhangs. This is why the capture of the ssDNA by DNA-PKcs is an attractive model: it would explain why ARTEMIS is crucial to process this hairpin-like structure. Based on Williams et al. (2008); Rass et al. (2009); Hammel et al. (2010); Panier and Boulton (2014); Williams et al. (2014); Chang et al. (2015); Broderick et al. (2016); Chang and Lieber (2016); Saha and Davis (2016), and data herein (chapters 3.2, 3.3).

The putative DNA-binding domain is located between the “head” and the “palm” region of DNA-PKcs. This is within an area where dsDNA enters (approximately one helical turn of dsDNA) and which includes a gap at the bottom of the “palm” region^{291,408}. The binding of DNA-PKcs to KU and the helical turn of dsDNA, therefore, stabilizes the position of the DNA-PK molecule. Thus, the model displayed in Biehs et al. (2017) where DNA-PKcs is bound to KU and the dsDNA, is unfavorable, as it would likely prevent further KU translocation inwards. Consequently, resection beyond 10 nt would be prevented in such a model^{267,285,388,409}. Therefore, it is likely that DNA-PKcs is not bound to KU and the DNA during resection in res-cNHEJ. This is additionally supported by the fact that upon autophosphorylation of DNA-PKcs, a conformational change broadens the area between the “head” and the “palm” region, which allows the flexible gap to open, and thus release the dsDNA^{159,291,409}. Thus, the formation of a mature DNA-PK molecule, including the contact of DNA-PKcs with KU, the dsDNA, and the DNA-PK molecule on the other DSB end might be prevented to allow KU translocation and avoid DNA-PKcs autophosphorylation before resection is complete. Instead, DNA-PKcs might be linked to the “arm” of KU80⁴⁰⁹ until a structure that allows DNA-PKcs-binding to the DNA is generated (Figure 4.4).

The misrejoining of distant DSBs is entirely dependent on the endonuclease ARTEMIS (Figures 3.11 A, B). The capture of the ssDNA in the small cavity of DNA-PKcs would form a loop or hairpin-like structure (Figure 4.3). In fact, the formation of such a structure is the main reason behind this model, as ARTEMIS is the only vertebrate nuclease in WT cells that is able to process hairpins⁷⁰. ARTEMIS processes hairpins or hairpin-like structures under the binding of the DNA at the ssDNA-dsDNA transition and performs an endonucleolytic cut an equivalent of 1 nt in the 5' direction, which forms 3' overhangs (except if the hairpin-like structure is formed from a 5' overhang)⁷⁰. Importantly, the endonuclease function of ARTEMIS is dependent on its interaction with DNA-PKcs^{70,114,198,251,286}. The necessity of ARTEMIS was also observed in other studies employing reporter assays^{278,293}. An important observation supporting the model is that in experiments with high-LET irradiation pRPA foci formation was reduced in cells lacking ARTEMIS³⁶. Another result supporting the necessity for ARTEMIS during res-cNHEJ is the observation that without ARTEMIS, DSBs remain unrepaired (Figures 3.11 C). However, whenever resection was not initiated or executed, the repair defect was partially rescued, indicating that ARTEMIS was not required if repair switched from res-cNHEJ to another

pathway (Figures 3.20 B, 3.25 C, 3.29 C, S8.11 d, S8.14 b, S8.18 c). Therefore, ARTEMIS resolves resection intermediates during res-cNHEJ.

4.2.5. Completion of repair during res-cNHEJ

The endonucleolytic cut by ARTEMIS produces ssDNA regions, which expose MHs and DSB ends for DNA-PKcs-binding (Figure 4.4). Sequence analysis of the misrejoined site confirmed that the majority of breaks are misrejoined using MHs (Figures 3.3 C, D). The annealing of the MHs requires the subsequent fill-in of the ssDNA gaps, and thus res-cNHEJ involves polymerases (Figure 4.4). Res-cNHEJ uses the polymerases POL λ , POL μ , and POL θ (Figures 3.10 A, B). Short MHs or high-fidelity misrepair events are likely associated with POL λ and POL μ . In contrast, the observation that the majority of misrejoined breaks used 3 or 4 nt MHs (Figures 3.3 C, D) fits well with the involvement of POL θ , which preferably uses these MH sizes⁴¹⁴. This aspect of res-cNHEJ seems to be closely related to MMEJ. In fact, the existence of res-cNHEJ answers the question of whether MMEJ is solely an alt-EJ mechanism or if the misrejoining under the usage of MHs exists as an error-prone mechanism in WT human cells (see also chapter 2.2.4). Yes, DSBs are rejoined using MHs in WT human cells in the form of res-cNHEJ, which involves c-NHEJ and not alt-EJ-associated factors. POL θ uses the annealed short sequence on the 3' ssDNA overhang as a primer while binding to the 5' terminal phosphate of the opposing DNA end to extend the annealed 3' overhang under the displacement of the 5' strand (Figure 4.4)^{207,414}. Therefore, additional nucleases might be required to dispose of the generated flap. The described mechanism entails that POL θ requires 3' overhangs. This supports the model that resection is conducted 5' to 3' and/or that the resection intermediates, which need to be resolved by ARTEMIS, are indeed hairpin-like and mainly result in 3' overhangs.

The autophosphorylation of DNA-PKcs can take place at any timepoint after DNA-PKcs contacts the DNA and DNA-PK is in contact with the DNA-PK molecule at the other DSB end^{40,108,267,271}. Thus, just like during c-NHEJ (see also chapter 2.2.3 for further details), the autophosphorylation and subsequent release of DNA-PKcs could be conducted before or after the fill-in of the gaps and/or further processing, but needs to be executed before ligation can take place¹⁹⁷.

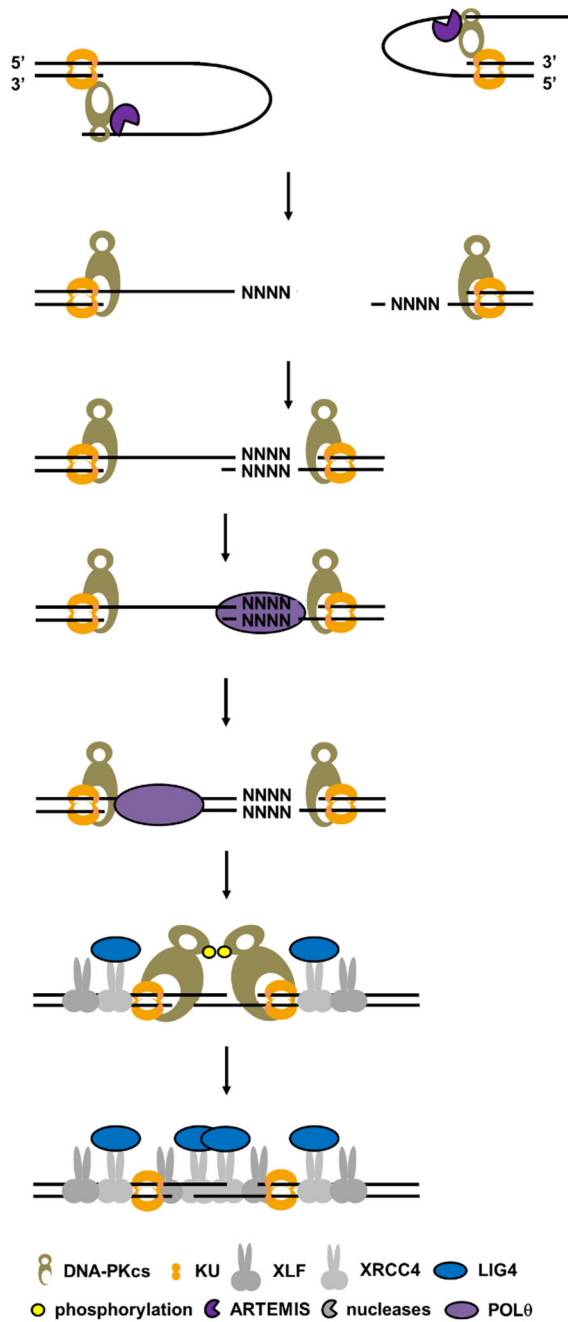


Figure 4.4 Model for completion of res-cNHEJ

The endonucleolytic cut by ARTEMIS produces 3' ssDNA overhangs (see Figure 4.3). The majority of the misrejoined break sites revealed MHs (N), allowing the annealing of the DNA strands. All three polymerases POL λ , POL μ , and POL θ play a role in the misrejoining of distant DSBs. This model proposes how POL θ could conduct the fill-in of the gaps during res-cNHEJ. Of note, further end-joining-associated nucleases might be involved, as POL θ produces 5' flaps, which would need to be removed. The limited resection and the short MHs allow ligation by LIG4, likely in a complex with XRCC4 and XLF, which are required for LIG4 to ligate sequences with MHs, gaps, and ssDNA overhangs. Speculatively, LIG4 is already present from the beginning of the process (Figure 4.1) and probably contributes to bringing the two DSB ends in proximity, as it does in c-NHEJ. Based on Gu, Lu, Tsai, et al. (2007); Gu, Lu, Tippin, et al. (2007); Lieber (2010); Kent et al. (2015); Reid et al. (2015); Brouwer et al. (2016); Wyatt et al. (2016); Jaafar et al. (2016), and data herein (chapter 3.2).

In MMEJ as an alt-EJ mechanism, ligation is conducted by the alt-EJ ligase LIG3 and in its absence, by LIG1^{116,346,347}. However, the impairment of LIG1/3 had little to no influence on the misrejoining of distant DSBs or the sequence alterations at the misrejoined sites (Figures 3.8 A,

3.9 A, B, C, D). This has recently been confirmed by Gelot et al. (2016). This difference between MMEJ as an alt-EJ mechanism and res-cNHEJ might be due to the much larger resection during alt-EJ processes, which are caused by the lack of DSB end-protection and/or the lack of factors able to recruit the c-NHEJ ligation complex. The misrejoining of distant DSB ends by res-cNHEJ was dependent on the c-NHEJ ligase LIG4 (Figure 3.5 B), which is consistent with other studies¹³⁶. Despite LIG4s involvement in the misrejoining of distant DSB ends and LIG4 acting downstream of ARTEMIS, the absence of LIG4 only resulted in a partial repair defect (Figure S8.6 c). Of course, as discussed in chapter 4.1.2, this could be due to a partial defect or because the break ends remain in proximity in contrast to ARTEMIS-deficient cells, where a full repair defect was observed (Figure 3.11 C). The observation of a full repair defect after the combined impairment of LIG4 with either LIG1/3 or the alt-EJ factor PARP1 (Figures 3.8 A, B, S8.8 c), implies that some breaks can be ligated in the absence of LIG4 by LIG1/3 in a PARP1-dependent manner. Importantly, this situation appears to be different than ligation after irradiation, where no switch to LIG1/3 was observed in hypomorph LIG4 mutant cells³⁶. However, this might be due to the partial loss of the LIG4 function in hypomorphic cells, which might result in differences compared to the depletion of LIG4 herein.

Although the other components of the LIG4 complex, XRCC4 and XLF, were not investigated during this study, it can be expected that they are also involved in the ligation process (Figure 4.4). This is due to the fact that LIG4 would not be able to ligate DSB ends, which have overhangs, MHs, and/or nucleotide gaps on its own^{152,153,242}. The involvement of these factors in res-cNHEJ was confirmed in radiation-based experiments in Biehs et al. (2017). However, the SFPQ/NONO complex could also play a role²¹³. SFPQ/NONO promotes the sequence-independent pairing of DNA substrates via a side-by-side alignment and loop formation, which differs from the XLF-dependent pairing of the break ends¹⁸⁷. During this study, ARTEMIS was found to likely interact with SFPQ and NONO in a DNA damage-dependent manner (Table 8.4). This novel interaction might indicate a possible involvement of SFPQ and NONO in res-cNHEJ and further investigation into the regulation of this damage-inducible interaction would be an interesting future study.

4.2.6. Additional factors involved in res-cNHEJ

Additional barriers to resection during res-cNHEJ

Res-cNHEJ is a DSB repair pathway that requires factors, which prevent excessive resection during G₁ phase of the cell cycle. Thus, factors limiting resection are crucial to ensure efficient res-cNHEJ. Some of these factors, including KU, 53BP1, RIF1, REV7, and RAP80 were identified during this study (Figures 3.5 B, 3.12 A, 3.14 B, C). The impairment of RAP80, RIF1, or REV7

resulted in increased misrejoining of distant DSBs (Figures 3.14 B, C), indicating that they are all involved in limiting resection during res-cNHEJ. These proteins are also involved in preventing DSB resection during S/G₂ phase. During S/G₂ phase, RAP80 poses a resection barrier, which is removed by POH1 after the priming of 53BP1 by BRCA1²⁰³. RIF1 directly interacts with ATM-phosphorylated 53BP1. Resection only can be initiated during HR after the dephosphorylation of 53BP1, and thus subsequent disruption of the 53BP1-RIF1 complex, which is promoted by BRCA1^{186,353}. REV7 is a downstream interaction partner of RIF1⁴¹⁷. Thus, much like 53BP1, all of these factors pose resection barriers. Hence, they might not have a direct impact on res-cNHEJ but their presence is crucial to prevent excessive and/or uncontrolled resection. Different behavior was observed for the 53BP1-interacting protein PTIP, the impairment of which reduced the frequency of misrepair events (Figure 3.14 B). ARTEMIS interacts with PTIP⁴⁰⁰. Thus, ARTEMIS is the major downstream effector of the 53BP1 pathway, which means that this reduction in misrepair events might be indirectly caused by restriction of the ARTEMIS protein. However, the reduction of misrepair events in the absence of PTIP is only half compared to the complete abolishment of misrepair events in ARTEMIS-deficient cells (Figures 3.11 B, 3.14 B). Thus, a more likely explanation is a direct effect of PTIP on res-cNHEJ. PTIP is required for long-range chromatin interactions by loop formation, and thus guaranteeing the closeness of distant DSBs for joining during CSR, which is disturbed in the absence of PTIP^{97,344}. Therefore, PTIP might be required to ensure the proximity of the distant DSBs during res-cNHEJ to allow misrejoining to occur. Interestingly, during this study, it was observed that CtIP is a likely interaction partner of PTIP following damage induction (Table 8.6). The investigation of this possible interaction might help to further characterize the res-cNHEJ pathway in future studies. More factors are likely involved in limiting resection, including HELB, as it was shown that HELB limits long-range resection during S/G₂ phase and is available in the nucleus in much higher concentration during G₁ phase³⁸⁰.

Chromatin remodeling during res-cNHEJ

The final protein investigated during this study was PARP1. PARP1 was initially linked to the repair of SSBs and the alt-EJ pathway in KU-deficient cells^{102,116,404}. Therefore, it was surprising that PARP inhibition by Olaparib or PARP1 depletion resulted in less misrejoining of distant DSBs (Figures 3.7 A, B). It was even more surprising, as the treatment of human fibroblasts with the PARP inhibitor PJ34 had no impact on res-cNHEJ in radiation-based assays³⁶. PJ34 could not be used in this study, as it induces side effects such as mitotic arrest and induction of apoptosis^{20,252}, which makes it unsuitable for experiments such as the reporter assay that lasts several days. Instead, the PARP inhibitor Olaparib was used in this study, as it does not trap PARP on the DNA like the majority of PARP inhibitors. Olaparib affects the PARylation dynamics

by enhancing PARP1 mobility (conference contribution Liu et al. (2017)). This might explain the different observations. To validate the observed effect, the results were confirmed by PARP1 depletion (Figure 3.7 B). This raised the question of what PARP1s role in res-cNHEJ is, as res-cNHEJ is not an alt-EJ pathway but involves c-NHEJ factors. PARP1 regulates and promotes c-NHEJ by a number of processes (for further details see chapter 2.2.3). One example is that PARP1 contributes to c-NHEJ by rapid chromatin expansion in concert with CHD2, which is required for efficient spreading of the LIG4 interaction partner XRCC4²⁵⁰. Indeed, this would be a favorable explanation since during S/G₂ phase, chromatin remodeling is also an important aspect of HR that allows resection¹⁹². A strong argument for this is made by the fact that PARP1 impairment behaved similarly to other factors involved in the initiation of resection. For example, PARP1 depletion or inhibition in combination with the impairment of other factors resulted in similar phenotypes as CtIP depletion, supporting the notion that PARP1 is required for the initiation of res-cNHEJ. Other possible roles for PARP1 during res-cNHEJ could be the stimulation of the kinase activity of DNA-PKcs³³⁴ or the damage-inducible rapid recruitment of MRE11¹⁵⁸. In any case, the involvement of PARP1 explains why res-cNHEJ could go unnoticed so long and why confusion regarding the possibility of an alt-EJ pathway in WT human cells prevailed. Therefore, it was important to distinguish between PARP1s role in res-cNHEJ and alt-EJ. An important difference was that PARP1 is crucial for alt-EJ and without it, a repair defect is observed (Figures 3.7 B, C, 3.13 C, D). In contrast, in the absence of PARP1 during res-cNHEJ, the misrejoining of distant DSBs is reduced but the DSBs are still repaired (Figures 3.7 A, B, C). For now, the role of PARP1 in res-cNHEJ remains unclear. However, since the role of PARP1 during res-cNHEJ might be linked to chromatin expansion as described for c-NHEJ by Luijsterburg et al. (2016) in concert with CHD2, chromatin remodeling might be required for res-cNHEJ (also discussed in chapter 4.4.1). For example, ARTEMIS was found to increasingly interact with the heterochromatin building factor KAP1 following DNA damage induction in this study (Table 8.4).

Statement on future studies on res-cNHEJ

In conclusion, this study reveals how res-cNHEJ is initiated, which nucleases conduct resection, and that the c-NHEJ pathway is related to res-cNHEJ. However, many questions remain open: (1) how does KU translocate inwards to allow resection?; (2) how does PARP1 contribute to res-cNHEJ?; (3) how is the endonuclease activity of MRE11 inhibited in G₁ phase?; (4) what is the role of EXD2?; (5) is the MRE11 exonuclease activity of relevance for res-cNHEJ?; (6) how does EXO1 act in the presence of KU80?; (7) if the resection intermediates do not involve the capture of the ssDNA by DNA-PKcs, why is ARTEMIS indispensable for res-cNHEJ?; (8) why are different polymerases required for the misrejoining of distant DSBs?; and (9) what determines

the extent of resection during res-cNHEJ? Although many of these questions could be addressed with speculative models in this chapter (4.2), based on the data in this study and other studies, these questions will help to further characterize res-cNHEJ in the future.

4.3. Repair pathway choice for the misrejoining of distant nuclease-induced DSBs

A major force in DSB repair pathway choice is the initiation of resection, which is dependent on factors such as the location of the break, the structure of the break ends, the cell cycle phase, and the complexity of the break^{13,15,17,71,72,74,75,140,145,147,202,288,302,312,326,370}. This chapter discusses which other repair pathways contribute to the misrejoining of distant DSB ends and under which circumstances they are employed.

4.3.1. Cell cycle-specific misrepair of distant DSB ends

The first indication that the resection process involved in the misrepair of distant DSBs is not limited to S/G₂ phase, was the observation that CtIP activation is dependent on PLK3 and not on S/G₂-specific CDK complexes as is the case during HR (Figures 3.24 A, B, 3.26 C). Although PLK3 expression differs depending on the cell line, in GC92 cells, PLK3 was observed throughout the cell cycle (Figure 3.26 B). In Barton et al. (2014), the CtIP activation by PLK3 was shown for G₁ phase, and thus the misrepair in the end-joining reporter assay in GC92 cells likely is also G₁-specific. This was confirmed by cell cycle-specific experiments in GC92 cells (Figure S8.3 c). Misrepair of distant DSBs was barely observed in G₂-synchronized cells. However, misrepair events in G₁-synchronized cells were nearly identical compared to asynchronously grown cells. Nevertheless, it remains unclear why the misrepair of distant DSB ends is a G₁-specific event. As discussed in chapter 4.2.2, the impairment of HR by inhibition of S/G₂-specific CDKs caused an increase in misrepair events in G₂-synchronized GC92 cells to nearly the same frequency observed in asynchronously grown cells (Figure S8.16 d). Therefore, HR might suppress res-cNHEJ during S/G₂ phase. Indeed, Gelot et al. (2016) recently found that the presence of the cohesin complex suppresses distant (3.2 kb), but not close (34 bp), misrepair of two endonuclease-induced DSBs during S/G₂ phase in favor of HR. The cohesin complex is responsible for the coupling of the sister chromatids from the moment of replication until the segregation during mitosis, and thus imperative for the invasion of the sister chromatid during HR. Gelot et al. (2016) used mimosine for synchronization in G₁ phase and observed a 2-fold increase in misrepair events. Mimosine synchronizes cells in late G₁ phase. This might explain why they observed an increase in misrepair events compared to Figure S8.3 c of this study (where misrepair events in early/mid G₁-synchronized cells were nearly identical compared to asynchronously grown cells). Resection factors such as CtIP are upregulated in late G₁ phase and with enhanced resection, misrepair increases (as observed in Figure 3.17 C)

⁴²⁸. In conclusion, the misrejoining of distant DSB ends is suppressed during S/G₂ phase in favor of HR, and thus specific for G₁ phase.

The frequency of misrepair events from the misrejoining of close DSBs in GCS5 cells was higher in comparison to the misrepair events in GC92 and GCSH14 cells (Figures 3.4 B, C). This indicates that the misrepair of two close endonuclease-induced DSBs occurs more frequently, which was also observed in other publications ^{136,154}. During this study, evidence was found that close DSBs do not require resection factors such as CtIP (Figure 3.17 A), and thus are not repaired by the G₁-specific res-cNHEJ. That would explain the observation by Gelot et al. (2016) that close endonuclease-induced DSBs are not affected by the cell cycle phase. Interestingly, misrepair in another end-joining reporter assay in which two I-SceI recognition sites are separated by a puromycin resistance gene (approximately 600 bp), was not dependent on CtIP either ²⁷⁸. This indicates that the endonuclease-induced DSBs are still not far enough apart from one another to be misrepaired by G₁-specific res-cNHEJ. In yet another reporter system, which only has one I-SceI restriction site but specifically investigates misrejoining using MHs, the frequency of misrepair events was also resection-dependent and involved factors such as CtIP. However, these events specifically arose in S/G₂ phase and the CtIP activation was dependent on S/G₂-specific CDK complexes ³⁸⁴. In Ahrabi et al. (2016), where they use a similar reporter assay, this type of repair was described as a backup for abrogated HR.

Importantly, sequence alterations at misrejoined break sites behave similarly, even in reporter assays with different structures, as was first described in detail by comparing the misrepair of a single I-SceI recognition site reporter to a reporter with two I-SceI recognition sites spaced 300 bp apart ¹⁷³. However, the number of cells, showing no additional alterations at the misrejoined break site, so-called high-fidelity misrepair events, differed greatly, with close DSBs producing more high-fidelity events. This was also observed in Guirouilh-Barbat et al. (2016) where the end-joining reporter construct with close DSBs (GCS5 cells) was used. Therefore, G₁-specific res-cNHEJ may also contribute to the misrepair of close DSBs, but the frequencies are too low to be detected. Another possibility is that even breaks that are not misrepaired by the G₁-specific res-cNHEJ pathway can produce similar kinds of sequence alterations by other processing mechanisms. This is supported by the observation that the misrepair of close DSBs is not associated with res-cNHEJ but mostly dependent on DNA-PKcs and ARTEMIS (Figures 3.5 A, 3.11 A). Thus, the key element for misrepair of all distant and most close DSBs seems to be the presence of intermediate structures, which need to be processed by the endonuclease activity of ARTEMIS in concert with DNA-PKcs. Speculatively, these structures do not only arise by the controlled resection mechanism during res-cNHEJ but also by the minimal processing of the DSBs, as described for c-NHEJ (for further details see chapter 2.2.3) ^{71,72,145,302,326,370}. As this

resection-independent process that requires ARTEMIS seems to be exclusive for close DSBs, it is not G1-specific as res-cNHEJ. However, an important indication that such a process might also contribute to the misrejoining of distant DSB ends is that the prevention of resection by the impairment of resection-initiating factors during res-cNHEJ only resulted in a partial rescue of the ARTEMIS repair defect (Figures 3.20 B, 3.25 C, 3.29 C, S8.11 d, S8.14 b, S8.18 c). This indicates that half of the ARTEMIS repair defect is independent of res-cNHEJ. However, in radiation-based assays, the rescue of the ARTEMIS repair defect was not always partial ³⁶. In any case, res-cNHEJ is a G₁-specific end-joining pathway that specifically misrejoins distant DSB ends.

DSBs induced by the endonuclease I-SceI have a curious behavior; despite their location and structure being the same, they are not only repaired with different outcomes (as observed by sequence analysis in this study and others) but also by different factors. Although the distance of the DSBs influences the pathway choice, this neither explains why res-cNHEJ is initiated for the misrejoining of distant DSB ends nor why only half of the misrejoined distant DSB ends are repaired by res-cNHEJ. An important indication during this study was that γ H2AX foci only persist long enough to be monitored several hours after I-SceI is already present and able to induce DSBs (Figure 3.2 A). In addition, res-cNHEJ repairs DSBs with slow kinetics (Figure S8.7 a) ³⁶ and accurate repair cannot be monitored in the reporter assay. Together, this indicates that the fast accurate repair of the I-SceI-induced DSBs impacts the decision for res-cNHEJ as time progresses. One model that could explain such a behavior is that DSB response factors accumulate at the accurately repaired DSB. After a DSB is accurately repaired, I-SceI induces the next DSB before the repair machinery is dissolved, and thus gives the impression of a persistent DSB, which induces res-cNHEJ. An additional aspect strongly supporting such a process, is the model introduced in chapter 4.2.1, where BRCA1 is introduced as a possible factor that could influence the decision for res-cNHEJ based on its interaction with KU80 (Figure 3.26 D). As a downstream factor in DSB recognition (for further details see chapter 2.2.1), BRCA1 may be present in the proximity of the accurately repaired DSB when the next DSB is induced by I-SceI. This could promote the BRCA1-KU interaction at previously accurately repaired breaks and subsequently prevent the accurate repair of the newly induced DSB. In consideration with the differences between the repair of close and distant DSBs (see chapter 4.3.1 for details), finding the wrong DSB end for misrepair takes longer for distant DSB ends, and thus explains the involvement of the time component in the initiation of res-cNHEJ in reporter assays.

4.3.2. Contribution of res-cNHEJ to the misrepair of distant endonuclease-induced DSBs

In this study, experiments were conducted to investigate what happens if res-cNHEJ is not available. Partly, this was already described in chapter 4.2, as the absence of factors involved in res-cNHEJ resulted in less misrejoining of distant DSB ends. Therefore, the absence of res-cNHEJ seemed to be beneficial to the cells, as less genomic rearrangements were observed. This was not only observed for intrachromosomal but also for interchromosomal genomic rearrangements (translocations) ²⁵. Therefore, a repair pathway switch to resection-independent c-NHEJ might occur if resection is not initiated and res-cNHEJ does not take place ^{25,36,245}. In the absence of CtIP, the misrejoining of distant DSBs was dependent on DNA-PK, the c-NHEJ-associated polymerases, and ARTEMIS (Figures 3.19 A, C, 3.20 A). Moreover, the alt-EJ factors PARP1 and LIG1/3 were not involved, nor were PLK3, MRE11, or EXO1 required (Figures 3.19 A, 3.25 B, S8.13 b, S8.17 b, S8.18 b). This fits with the model of resection-independent c-NHEJ occurring in the absence of CtIP ²⁴⁵.

Loss of genetic information in CtIP-depleted cells

However, the mean additional deletion size at misrejoined sites in CtIP-depleted GC92 cells increased nearly 4-fold after CtIP depletion (Figures 3.18 B). Indeed, deletions > 50 nt increased in frequency and length (Figures 3.18 A, Tables 8.1, 8.5). Moreover, it was revealed that the high-fidelity events remained consistent in CtIP-depleted cells compared to the control, while additional deletions between 1 and 10 nt decreased nearly 3-fold and 30 to 50 nt deletions decreased approximately 7-fold. In contrast, the additional deletions between 10 to 30 nt, 50 to 200 nt, and 250 to 550 nt increased between 3 and 5-fold. The longest deletions were either near or actually affecting the reporter gene or the promoter. Importantly, due to the location of the primers in the gene and the promoter region, the presence of longer deletions would go unnoticed. Of note, an increase in long deletions after CtIP depletion was also observed by Rass et al. (2009) and Grabarz et al. (2013). Since these studies use primers located closer to each other, it is not surprising that the increase in the deletion size is observed to a lesser extent in comparison to this study. In contrast, Guirouilh-Barbat et al. (2016) did not observe an increase in the deletion size after CtIP depletion. A major problem in sequence analysis remains the categorization of the distribution of deletion sizes observed at the misrejoined break sites. Categories are usually implemented based on DNA repair models. In Biehs et al. (2017) a commonly used categorization for the distribution of additional deletions was implemented, as this is the norm when publishing sequence analysis data. Based on this categorization the increase in the deletion size after CtIP depletion would have gone unnoticed.

Moreover, in comparison to this study, Guirouilh-Barbat et al. (2016) and Rass et al. (2009) used a different I-SceI plasmid.

To summarize, certain sizes of additional deletions increased significantly and therefore a shift took place in the remaining misrepair events after CtIP depletion. This shift in sequence alterations proves that in the absence of CtIP most of the remaining misrepair events are affected, which challenges the model where in the absence of res-cNHEJ, DSBs switch to resection-independent c-NHEJ. Indeed, the increase in deletion sizes challenges the dogma that the reduced frequency of misrepair events is caused by repair of the accurate DSB ends (which cannot be monitored in the assay). Instead the reduced frequency of misrepair events might be caused by enhanced deletion sizes, which go unnoticed because they harm either the reporter gene and/or the promoter (and extend beyond the primer). Strikingly, the misrepair of distant DSB ends in a reporter system where the reporter gene is located closer to the DSB than the construct in GC92 cells (GCSH14 cells) had less frequent misrepair events (Figure 3.4 A, B). This was likely caused by some of the misrepair events in control cells not being monitored due to deletions above a certain size harming the reporter. In addition, the reduction of misrepair events in CtIP-depleted GCSH14 cells was larger than in GC92 cells (with double the effect size, Figure 3.17 A). This further indicates that indeed, very large deletions might be the cause for reduced misrepair events in CtIP-depleted cells and not a switch to accurate end break repair by c-NHEJ. This would make the comparison of intrachromosomal and interchromosomal genomic rearrangements more difficult since translocations are reduced following CtIP depletion²⁵. Importantly, the remaining translocations and the seemingly accurately rejoined breaks may have large alterations, which cannot be monitored when investigating translocation formation by any kind of staining procedure²⁵. In any case, an increase in longer deletions in CtIP-depleted cells contradicts the model in which cells switch to resection-independent c-NHEJ in the absence of res-cNHEJ. However, it has to be noted that the reporter assay selects for misrejoining events, and thus how the presence or absence of res-cNHEJ affects other experimental setups (for example, after X-IR) can only be speculated. In conclusion, in the absence of res-cNHEJ, a havoc form of end-joining takes over and creates worse mutagenic events. Havoc end-joining seems to be related to c-NHEJ or at least involves c-NHEJ factors.

Misrejoining by microhomologies during res-cNHEJ

Additional information about the sequence analysis regarded the way break sites were misrejoined. While control cells predominantly used MHs of 3 or 4 nt, the majority of DSBs were rejoined without the use of MHs after CtIP depletion (Figure 3.18 D). Importantly, the largest category (4 nt) was completely abolished in CtIP-depleted cells. This is consistent with POL θ not being required in CtIP-depleted cells (Figure 3.19 B) since POL θ preferentially uses

MHs of at least 3 nt⁴¹⁴. Notably, POL θ was associated with additional deletions of mostly 5 to 50 nt in WT cells and with much larger deletion sizes in cells that underwent hyper-resection⁴¹⁴. These POL θ -associated deletion sizes in WT cells are consistent with deletion sizes observed for res-cNHEJ (Figures 3.18 A, Tables 8.1, 8.5) and with the model wherein MHs and POL θ contribute to both res-cNHEJ and MMEJ (Figure 4.5). Furthermore, POL θ has been linked to the prevention of genomic havoc and the suppression of chromosomal instability^{214,426}. Indeed, POL θ was described as an important factor when canonical pathways fail in maintaining genome stability. POL θ protects the cells from translocation formation and helps to remain on the same chromosome for rejoining, which is the second indication that interchromosomal and intrachromosomal genomic rearrangements might have a different outcome for res-cNHEJ (also see chapter 4.4.3)⁴¹⁴. Together, these data confirm that res-cNHEJ reduces genomic information loss by employing short deletions and MHs to prevent worse mutagenic events, at least on an intrachromosomal scale. Furthermore, CtIP prevents long resection in G₁ phase. The big question is which nucleases are involved in this process (which causes genomic havoc) and how they can operate in a situation where KU and 53BP1 prevent resection? Importantly, this process likely does not involve the endonucleolytic cut by MRE11 to overcome the resection barrier since Anand et al. (2016) showed that the MRE11-mediated endonucleolytic cut requires CtIP. Here, it again needs to be stressed that the data from this study specifically refer to a situation where screening for misrepair takes place. Nevertheless, other studies also speak of a mechanism preventing chromosomal instability or genomic havoc by allowing limited mutagenesis^{156,214,426}. In conclusion, these observations provide evidence that although res-cNHEJ is an error-prone end-joining mechanism, the absence of res-cNHEJ is not beneficial for the cells and results in worse mutagenic events. The prevention of such havoc end-joining might be the physiological relevance of res-cNHEJ.

4.3.3. Alternative end-joining of nuclease-induced DSBs

In chapter 4.2, wherein the res-cNHEJ pathway was introduced, many comparisons were drawn to the resection process during HR in S/G₂ phase. In contrast, this chapter describes the circumstances under which alt-EJ contributes to the misrejoining of distant DSB ends and how alt-EJ differs compared to res-cNHEJ, especially in the resection process. In chapter 4.2.1, the way in which alt-EJ takes over in the absence of KU or 53BP1 was described (Figures 3.7 B, C, 3.13 C, D). Although some aspects of repair by alt-EJ in the absence of KU have been investigated, the main focus of this study was how alt-EJ as it occurs in 53BP1-depleted cells differs from res-cNHEJ (Figure 4.5). The alt-EJ mechanism relies on PARP1 in both KU and 53BP1-depleted cells (Figures 3.7 B, C, 3.13 C, D). However, this dependency on PARP1 is different to res-cNHEJ (chapter 4.2.6). While PARP1 is required for the misrejoining of distant

DSB ends by res-cNHEJ, cells are still able to repair DSBs in its absence (Figures 3.7 A, B). In contrast, the overall repair of I-SceI-induced DSBs is entirely dependent on PARP1 in the absence of KU80 or 53BP1 (Figures 3.7 B, C, 3.13 C, D). This indicates that the role of PARP1 in alt-EJ is different than in res-cNHEJ. This is likely because, in alt-EJ, PARP1 is required to recruit downstream alt-EJ factors that are necessary for repair ⁴⁰⁴.

The situation in KU and 53BP1-depleted cells differs greatly; the absence of KU leaves the DSB ends unprotected. Therefore, all it takes for the initiation of resection is the recruitment of resection factors. The misrejoining of distant DSB ends in KU-depleted cells was largely dependent on EXO1 in preliminary data. However, the observation that misrejoining of distant DSB ends still partially occurs in the absence of EXO1, suggests that further nucleases are involved or can take over in the absence of EXO1. Radiation-based studies confirmed that resection in KU-depleted cells is associated with EXO1 ³⁸². In contrast, the DSB ends are still protected by KU in 53BP1-depleted cells. Nevertheless, 53BP1-depleted cells show excessive resection, not only in S/G₂ phase ²⁹² but also in the G₁-specific misrejoining of distant DSB ends ^{148,154}. Thus, the absence of 53BP1 somehow allows resection despite the protection of the DSB ends by KU and the resection is much larger than observed in res-cNHEJ.

In contrast to res-cNHEJ, the resection in 53BP1-depleted cells was not dependent on EXO1 (Figure 3.30 C). Instead, resection in 53BP1-depleted cells relied on the endonuclease and exonuclease functions of MRE11 (Figures 3.29 A, B) as well as the endonuclease function of CtIP (Figures 3.22 A). When compared to resection during S/G₂ phase in HR, this indicates that resection in 53BP1-depleted cells resembles the short-range resection process, where MRE11 introduces an endonucleolytic cut internally to the DSB end and then resects the DNA in a 3' to 5' direction ³⁵⁴. This might explain why the endonuclease activity of CtIP is required for alt-EJ but not res-cNHEJ (Figures 3.22 A, B). CtIP is responsible for removing the flap produced by MRE11 during 3' to 5' resection and likely they assist with the removal of KU ^{74,229}. Since resection in 53BP1-depleted cells was not depend on EXO1 (Figure 3.30 C), the resection process might be limited to the 3' to 5' direction and executed in a stepwise manner to produce large resected regions, as was observed in biochemical studies ¹⁰. Radiation-based studies confirmed that resection in 53BP1-depleted cells depends on MRE11 but not EXO1 ²². In addition, the MMEJ reporter assay, which was observed by Truong et al. (2013) to be S/G₂-specific, is also dependent on MRE11 and its nuclease function but not dependent on EXO1 ^{7,384}. In contrast to the prevention of the endonucleolytic cut during res-cNHEJ, the importance of the MRE11 endonucleolytic cut in 53BP1-depleted cells is further emphasized by the following observation: after the inhibition of DNA-PK with the Nu7441 inhibitor, WT cells lack misrepair events (Figures 3.5 A), while the misrejoining of distant DSB ends is undisturbed in

53BP1-depleted cells (Figures 3.13 A, B). The DNA-PK inhibitor Nu7441 causes a block by the DNA-PK molecules at the DSB ends due to the inhibition of DNA-PKcs at its active site, which prevents autophosphorylation⁹⁹, and thus the release of DNA-PKcs and completion by c-NHEJ or res-cNHEJ. Therefore, an endonucleolytic cut by MRE11 can overcome this block, which is only observed in WT S/G₂ phase cells. In this context, DNA-PK inhibition results in increased frequencies of HR²⁷⁸. In addition, the DNA-PK block after Nu7441 inhibitor treatment was overcome in a reporter assay investigating MMEJ frequencies²⁷⁸, which was similar to the S/G₂-specific reporter assay in Truong et al. (2013).

These observations further explain how resection in res-cNHEJ is limited, while alt-EJ mechanisms produce larger resected regions. The interesting question remains how the endonucleolytic cut of MRE11 is prevented in WT human cells during G₁ phase, as biochemical studies confirmed that the presence of the MRN complex in concert with CtIP-pThr847 is sufficient to perform the endonucleolytic cut¹⁰. As the cut is possible in 53BP1-depleted cells, 53BP1 or one of its downstream factors might be responsible. Moreover, BRCA1 is known to suppress the nuclease activity of MRE11 during G₁ phase (also see chapter 4.2.3)^{336,412}. In the absence of 53BP1, BRCA1 was not required for the misrejoining of distant DSB ends (Figure 3.15 B). The antagonism between CtIP-BRCA1 and 53BP1-RIF1 is believed to control the DSB repair pathway choice in a cell cycle-dependent manner^{96,123,178}. The CtIP-BRCA1 interaction, which requires phosphorylation of CtIP at Ser327, is crucial for res-cNHEJ (Figure 3.23 A) but not for MMEJ⁴²⁹. Interestingly, this interaction is constitutively active during S/G₂ phase but disrupted approximately 1 h post-damage induction by the hyper-phosphorylation of CtIP^{238,281,397}. Furthermore, the lack of the CtIP-BRCA1 interaction impacts the resection rate and speed during S/G₂ phase but not resection in general⁹³. Hence, this interaction in concert with 53BP1 might not only ensure efficient and accurate resection but also specifically control the MRE11 nuclease function, and thus DSB repair pathway choice (Figure 4.5). In the MMEJ reporter assay, CtIP activity is dependent on S/G₂-specific CDK complexes³⁸⁴. In contrast, CtIP is activated by PLK3 in the G₁-specific misrejoining of distant DSB ends (Figures 3.23 A, 3.26 C). This was also observed in the absence of 53BP1 (Figures 3.21 A, B, S8.16 e). Thus, resection in alt-EJ mechanisms is dependent on CtIP and PLK3 outside of S/G₂ phase, which has also been observed in radiation-based studies^{22,25}. Of note, the overexpression of CtIP in 53BP1-depleted cells caused a significant increase in misrepair events (Figure 3.22 A), emphasizing that the imbalance of pathway choice proteins is a driving force for alt-EJ mechanisms.

The misrejoining of distant DSB ends in 53BP1-depleted cells is dependent on ARTEMIS (Figures 3.14 A). The involvement of ARTEMIS in alt-EJ has also been observed by Moscariello et al. (2015). ARTEMIS might be required for the removal of either DNA-PK, the MRN complex,

and/or the flap generated by the MRE11 exonuclease activity after the 3' to 5' resection took place ^{74,164,229}. Furthermore, the misrejoining of distant DSB ends in 53BP1-depleted cells was entirely dependent on POL θ (Figures S8.10 b, c). Several publications distinguish between alt-EJ, which involves POL θ and uses MHs for rejoining (MMEJ) and an alt-EJ, which does not use MHs ^{102,116}. Microhomology-mediated rejoining was observed after both KU and 53BP1 depletion ^{7,155,414,427} and involved POL θ ⁴¹⁴. However, Mansour et al. (2010) observed that in the absence of KU, the MHs were shorter, which indicates that the rejoining process differs under these two conditions. In contrast to ligation during res-cNHEJ, ligation in 53BP1-depleted cells is dependent on LIG1/LIG3 (Figures 3.13 C, D). As described in chapter 4.2.5, in the absence of LIG4, a fraction of distant DSBs, which misrejoin by res-cNHEJ can switch to a LIG1/LIG3-dependent ligation (Figure 3.8 A, B). Speculatively, this is possible because PARP1 is involved in res-cNHEJ (as described in chapter 4.2.6 with a different function compared to alt-EJ) and its presence likely allows the recruitment of LIG1/3 in the absence of LIG4. Importantly, Dorsett et al. (2014) observed that resection in cells without LIG4 is still limited and the distribution of deletions in their study was similar to the distribution of additional deletions in WT GC92 cells herein (Figures 3.3 A). This indicates that the resection process in LIG4-depleted cells remains unaltered compared to alt-EJ in KU or 53BP1-depleted cells and therefore, res-cNHEJ still occurs in LIG4-depleted cells with only an alteration in the ligation step. Interestingly, Gelot et al. (2016) showed that in the absence of the pro-HR cohesin complex, the increase in misrejoining of distant DSB ends (in this case, no longer limited to G₁ phase, see chapter 4.3.1), is dependent on all three ligases, LIG1/3 and LIG4.

This confirms that MMEJ functions as a backup mechanism for abrogated HR during S/G₂ phase ^{7,136,384} and indeed works differently than microhomology-mediated misrejoining in G₁ phase by the res-cNHEJ pathway (Figure 4.5). Importantly, both are microhomology-mediated, and thus the use of MHs during res-cNHEJ can be termed MM-cNHEJ (as opposed to MMEJ that describes the use of MHs during an alt-EJ mechanism). In conclusion, alt-EJ takes over in the absence of certain c-NHEJ factors and involves a variety of mechanisms to conduct repair and overcome the deficits imposed by the absence of a factor (Figures 4.5). In contrast, res-cNHEJ is a distinct repair pathway for certain DSBs in G₁ phase of the cell cycle ³⁶. Thus, two resection regulation mechanisms exist: DSBs that do not undergo resection or undergo limited resection (fast repair versus slow repair, which is dependent on location, structure, and complexity of the DSB end) and DSBs that undergo limited or excessive resection (WT human cells versus deficient cells; Figure 4.5). As there is an overlap of several repair factors in the different pathways, publications referring to alt-EJ and/or MMEJ need to be carefully examined, as the pathway they investigate in WT cells could be res-cNHEJ.

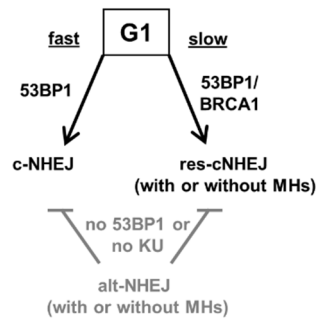


Figure 4.5 Alt-EJ in relation to WT end-joining pathways in G₁ phase

The fast repair component during all cell cycle phases is resection-independent c-NHEJ. In G₁ phase, 53BP1 needs to be antagonized by BRCA1 to initiate res-cNHEJ, a pathway that rejoins breaks with or without MHs. The absence of 53BP1 or KU results in excessive resection and the use of alt-EJ mechanisms, which can entail microhomologies. Of note, this model, with some alterations, was part of Biehs et al. (2017).

4.4. Rationale for res-cNHEJ

In the previous chapters, res-cNHEJ was introduced and its role in misrejoining distant DSBs discussed in the context of other DSB repair pathways. However, the majority of experiments in this study was performed with reporter assays and therefore, not physiological. In this final chapter, the physiological relevance of res-cNHEJ will be discussed with a focus on open questions and future directions. Res-cNHEJ is an error-prone repair mechanism in WT human cells, which prevents worse mutagenic events. Thus, the mutagenic events associated with res-cNHEJ can be considered collateral damage in preventing genomic havoc. However, under which circumstances is res-cNHEJ required?

4.4.1. Relevance of the location, structure, and complexity of the DSB ends

The DSB repair pathway choice is largely dependent on factors such as the cell cycle phase, the location, structure, and complexity of the DSB end^{13,15,17,71,72,74,75,140,145,147,202,288,302,312,326,370}. As res-cNHEJ is a G₁-specific pathway, the choice of res-cNHEJ is likely connected to the other factors mentioned. In Biehs et al. (2017), slow repair of DSBs induced by X-IR in G₁ phase was observed to be conducted by res-cNHEJ, as are DSBs induced by high-LET irradiation. While the prevention of resection resulted in a pathway switch after damage induction by X-IR, DSBs induced by high-LET irradiation required resection and subsequent res-cNHEJ or remained unrepaired^{15,25,36}. Importantly, the post-high-LET irradiation resection products were long enough to allow pRPA-binding, as was observed after high doses of X-IR (Figure 3.6 F). This indicates that the resection process in these situations was less limited than the resection observed at misrejoined break sites in GC92 cells (Figure 3.3 A). Thus, one biological reason for res-cNHEJ is the repair of complex DSBs after high-LET irradiation. In this case, complexity refers to clustered DSBs.

An interesting observation in the KU80 foci analysis in this study was that slowly repairing DSBs at 8 h post-4 Gy X-IR often showed a localized reduction in the DAPI intensity (Figure 3.6 A, C). This indicates a reduction in the chromatin density in the vicinity of these DSBs. Kruhlak et al. (2006) observed a local expansion, and thus reduced density of the chromatin immediately after DNA damage, which was also described as a local decondensation of heterochromatic regions in a study using heavy ion irradiation¹. This suggests that res-cNHEJ is employed in heterochromatic regions and/or regions where the chromatin structure needs to be altered. This was not surprising since DSBs in heterochromatic regions are known to be repaired with slow kinetics^{23,34,145,411} and res-cNHEJ is the slow repair process during G₁ phase³⁶. Indeed, this supports the claim that res-cNHEJ could require chromatin remodeling factors (chapter 4.2.6).

In conclusion, DSBs that are repaired with slow kinetics during G₁ phase employ res-cNHEJ. Resection and the use of res-cNHEJ is a necessity for DSBs, which cannot be repaired by resection-independent c-NHEJ during G₁ phase due to their complexity. However, DSBs that are repaired even if resection of res-cNHEJ is not initiated (e.g. after X-IR), indicate that the speed of repair determines which DSBs are repaired by res-cNHEJ in WT cells. Thus, persisting DSBs are repaired by res-cNHEJ. Therefore, DSBs located in heterochromatic regions are repaired by res-cNHEJ, as they first require chromatin remodeling. The most challenging question is why two I-SceI-induced DSBs in the same reporter assay are repaired differently in different cells. Speculatively, the availability of slow repair factors plays a role. If a second I-SceI cut is induced after the first accurately repaired and before the repair machinery disassembles, the cell might perceive a persistent DSB (for further details see chapter 4.3.2).

4.4.2. How error-prone is res-cNHEJ?

Res-cNHEJ is a DSB repair pathway, which specifically prevents extensive resection during G₁ phase of the cell cycle. In S/G₂ phase, extensive resection is required for accurate repair by HR, which is not possible during G₁ phase because HR in human cells requires the presence of a sister chromatid as a template for repair^{138,200}. A key step in preventing extensive resection is the prevention of short-range resection, which might sound counterintuitive at first. However, the internal endonucleolytic cut by MRE11, which induces short-range resection during HR³⁵⁴ and which is also required for alt-EJ (Figures 3.29 A, B), allows resection in both 3' to 5' (short-range) and 5' to 3' (long-range) resection irrespective of the DSB ends being protected^{10,354}. Therefore, prevention of the endonucleolytic cut by MRE11 is the key step in ensuring that resection remains limited during res-cNHEJ. Preventing the endonucleolytic cut by MRE11 during G₁ phase comes at a price; RPA cannot protect the generated ssDNA since resection is too limited for stable RPA-binding⁴². However, the absence of RPA-binding enables microhomology-mediated rejoining²⁶⁴, which the cell uses to limit the sequence loss during res-

cNHEJ and prevent worse mutagenic events. Importantly, this means that there could be differences in res-cNHEJ after high-LET irradiation because the ssDNA regions are large enough for RPA to bind^{15,25,36}. Indeed, the presence of RPA raises the question of how error-prone res-cNHEJ truly is. In the reporter-based sequence analysis of the misrejoined break sites, the mutagenicity of res-cNHEJ was visualized (Table 8.1). However, in the reporter system, the cells are selected for misrepair events and therefore these data are biased toward error-prone repair results. Thus, the frequency and extent to which res-cNHEJ is error-prone, could not be answered in this study.

Therefore, the mechanism by which res-cNHEJ might contribute to error-free repair events comes into question. One indication is that transcriptionally active regions in S/G₂ phase are repaired with slow kinetics by HR^{17,312}. As described in chapter 4.4.1, slow DSB repair in G₁ is performed by res-cNHEJ, and thus transcriptionally active regions might be repaired by res-cNHEJ during G₁ phase. Transcriptionally active regions are associated with RNA-DNA hybrids and with template-guided DSB repair^{69,175,236}. Chakraborty et al. (2016) found an error-free cNHEJ pathway, which uses RNA-DNA hybrids in transcriptionally active regions to ensure sequence integrity. In contrast, Ohle et al. (2016) associated RNA-DNA hybrids with HR in *Schizosaccharomyces pombe* and the stabilization of such hybrids impaired the recruitment of RPA. This implies that RNA-DNA hybrids form at short ssDNA regions to guide the resection process and RPA-binding. A major factor in template-guided repair by RNA-DNA hybrids is DDX1 (DEAD box 1) since it is crucial for the clearance of the RNA²³⁶. DDX1 forms foci after irradiation-induced damage induction, which co-localize with γ H2AX, phosphorylated ATM, and RIF1^{236,237}. The accumulation of DDX1 requires RNA-DNA hybrids and ATM-mediated phosphorylation of DDX1²³⁷. Importantly, RIF1 interacts with DDX1 to load BLM on chromatin (a 53BP1-independent role of RIF1), which is required at a subset of DSBs associated with transcriptionally active regions and/or where resection has been initiated²³⁷. In this study, a likely interaction of ARTEMIS with DDX1 following DNA damage induction was discovered (Table 8.4). Therefore, DDX1 might play a role in res-cNHEJ, and thus could link template-guided repair to res-cNHEJ.

However, template-guided repair still does not provide evidence for an error-free DSB repair pathway, as RNA-DNA hybrids are in fact, associated with genomic instability^{5,294}. Therefore, even if res-cNHEJ would be associated with template-guided repair, it might still be error-prone. Interestingly, the repair of DNA damage associated with certain RNA-DNA hybrids requires BRCA1¹⁶³. In any case, the idea that res-cNHEJ might not be as error-prone as this study indicates remains highly speculative. Future studies will have to investigate if res-cNHEJ plays a role in the DSB repair of transcriptionally active regions and if there is any indication that res-

cNHEJ might not be as mutagenic as observed in this study. Res-cNHEJ is involved in generating interchromosomal and intrachromosomal genomic rearrangements^{25,36} that are reduced in the absence of res-cNHEJ. However, the sequence alterations of the remaining intrachromosomal rearrangements in the absence of res-cNHEJ were of worse quality than those formed by res-cNHEJ (Figures 3.18 A, Table 8.1). Therefore, if inhibiting resection during G₁ phase, and thus targeting res-cNHEJ could be a beneficial situation for the cell remains an open question. Less than 2% of the human genome codes for proteins and a biochemical function has been predicted for up to 80% of the genome (of note, this claim is highly disputed due to a very loose definition of the word function in the respective study; it is predicted that the actual number probably lies between 10 and 20%)^{69,80,300}. Thus, limiting the loss of genetic information by slightly error-prone repair to reduce the probability of mutagenesis in a functional region might indeed be the physiological relevance for res-cNHEJ.

4.4.3. Genetic recombination as the physiological origin of res-cNHEJ?

The structure of the reporter construct containing two distant DSBs with 3' overhangs is reminiscent of the situation in CSR (for details see chapter 2.2.5). CSR aims to misrejoin distant DSBs to allow immunoglobulin gene diversification in mature B cells^{4,115}. During CSR, lesions induced by AID are first transformed into SSBs and then into DSBs^{24,196,365}. The AID-induced lesions are limited to transcriptionally active guanine and cytosine-rich switch regions of repetitive DNA sequences and initiated by cytokine-activated promoters^{4,115,365}. Interestingly, such regions were associated with difficult to repair RNA-DNA hybrids^{115,276}, again proving that the presence of such structures does not necessarily imply error-free repair but is associated with deliberate misrepair during CSR (also see chapter 4.4.2). Importantly, the expression of the lymphoid-specific AID induces CSR in fibroblast cell lines^{115,296,425}. Thus, only the induced lesions are specific for mature B cells, while the CSR repair process is present in all cells.

Since CSR aims to misrejoin distant DSB ends, this is a strong indication of where error-prone res-cNHEJ might originate. Indeed, many CSR factors were observed to be involved in res-cNHEJ in this study (Figures 3.5 B, 3.10 A, 3.11 A, 3.12 A, 3.14 B, 3.17 A, 3.28 A, 3.30 A): EXO1 and POL θ are involved in generating the DSBs during CSR via the formation of 3' overhangs^{24,364,365,419}; ATM and the MRN complex are involved in the stabilization of the broken DNA ends during CSR, along with γ H2AX⁴²³; 53BP1 and RIF1 promote CSR and protect the DSB ends from resection, while 53BP1 and PTIP facilitate long-range chromatin interactions to favor long-range intrachromosomal rejoining and avoid intra-switch recombination^{47,48,97,157,324,344,392}; the c-NHEJ factors KU70/80, DNA-PKcs, XLF/XRCC4/LIG4, and ARTEMIS are all involved in repair during CSR^{4,46,254,328,330,331,391}; CtIP is associated with CSR²²⁶; and some junctions of the distant DSBs are rejoined using MHs during CSR^{131,226,289,421}. Therefore,

the repair process during CSR might not only be the origin or closely related to res-cNHEJ but indeed could represent res-cNHEJ. Thus, CSR might be a lymphoid-specific type of res-cNHEJ where the DSBs are induced endogenously by AID.

CSR studies are also an important indicator for a difference in the repair outcome of interchromosomal (translocations) and intrachromosomal genomic rearrangements. Several studies on genetic recombination found different impacts on interchromosomal versus intrachromosomal genomic rearrangements. Genomic stability was linked to POL θ by preventing translocation formation and facilitating intrachromosomal rejoining to minimize the loss of genetic information ^{414,426}. Differences in interchromosomal and intrachromosomal genomic rearrangements were also observed in 53BP1-deficient cells ^{48,107}. Translocations are frequently observed in cells utilizing alt-EJ, which indicates that non-canonical repair pathways result in the imbalance of both genomic recombination outcomes ^{226,335,432}. Therefore, res-cNHEJ might be necessary to maintain the balance between interchromosomal and intrachromosomal genomic rearrangements since the disequilibrium causes a shift in one direction or the other.

4.4.4. A role for res-cNHEJ in checkpoint control?

After DNA damage, cell cycle checkpoints are initiated to allow the cell to repair the damage before progressing into the next cell cycle phase. The G₁/S checkpoint is initiated by ATM in a p53-dependent and a p53-independent manner ^{246,349}. Both result in an inactive CyclinE/CDK2 complex, and thus prevent the progression in S phase. In S/G₂ phase, large ssDNA regions are produced during DNA repair, which activates ATR. ATR also triggers p53-dependent and -independent response ^{101,310,338}. Therefore, ATM and ATR are the key factors of cell cycle checkpoint induction ². TOPBP1 is important for ATR activation but also interacts with 53BP1 to mediate the G₁ DNA damage checkpoint ^{68,222,355}. In addition, TOPBP1 is an established interaction partner of ARTEMIS ⁴⁰⁰, the interaction of which increased after DNA damage induction herein (Table 8.4). Furthermore, BRCA1 is required for the G₁/S checkpoint activation ⁴¹². The link between these res-cNHEJ factors (ARTEMIS, BRCA1, and ATM; Figures 3.11 A, 3.15 A, S9.14 a) and cell cycle checkpoint control in G₁ post-DNA damage induction, raises the question of whether res-cNHEJ has a role in cell cycle checkpoint control during G₁ phase. Indeed, Gamper et al. (2013) showed that ATR is activated in irradiated G₁ phase cells and this activation is associated with limited resection. The authors assume that CtIP is not required for this resection since the S/G₂-specific CtIP-activating CDK complex is not available in G₁ phase. However, by now CtIP was linked to small resection during G₁ phase, and thus the resection during res-cNHEJ may be required for checkpoint control during G₁ ^{25,36}. Another important aspect is the maintenance of cell cycle checkpoints ^{216,217,349}. As Kousholt et al. (2012)

observed that CtIP is required for ATR-dependent checkpoint maintenance but not activation, the initiation of resection during res-cNHEJ might be linked to maintaining the G₁/S checkpoint and allowing the cell more time to slowly repair DSBs before the DNA is replicated during S phase.

4.5. Final statement

The significance of this work lies in the discovery of a novel error-prone resection-dependent c-NHEJ pathway in WT human cells. Res-cNHEJ was characterized not only in its execution but also in its initiation. Thus, this work provides valuable insight into DSB repair pathway choice. Res-cNHEJ contributes to generating intrachromosomal genomic rearrangements by the repair of distant DNA DSBs during G₁ phase. Together with the results from the publications Barton et al. (2014) and Biehs et al. (2017), res-cNHEJ was identified in functioning during the slow repair component in G₁ phase, in repairing complex DSBs during G₁ phase, and in contributing to translocation formation.

Res-cNHEJ unifies the, until now, contradicting observations in other studies that genomic rearrangements arise from c-NHEJ^{142,357} but require certain pro-resection factors, which were thus far associated with the loss of genetic information in alt-EJ^{148,302,322}. Indeed, the unique feature of this pathway is the limited resection in combination with c-NHEJ factors, which was hitherto thought to be mutually exclusive. Importantly, the resection process in res-cNHEJ differs from other known resection processes to limit resection. Thus, the characterization of res-cNHEJ also helped to distinguish it from error-prone repair by alt-EJ, the role of which was clarified in human cells as a variety of backup mechanisms to compensate for missing repair factors. Therefore, published studies need to be reevaluated to assess when an investigated error-prone end-joining mechanism was, in fact, res-cNHEJ and not alt-EJ.

The absence of res-cNHEJ resulted in fewer genomic rearrangements. However, the remaining rearrangements featured more severe mutagenic sequence alterations at the misrejoined break site. Thus, it remains unclear if the inhibition of res-cNHEJ would be a beneficial situation for the cell to maintain genomic stability. Inhibiting res-cNHEJ in order to avoid genomic rearrangements in WT human cells is an interesting consideration for cancer patients undergoing radiation treatment. The question arises as to whether the inhibition of res-cNHEJ is more beneficial than harmful because res-cNHEJ indeed seems to be beneficial for genomic stability by limiting the loss of genomic information although at the cost of generating genomic rearrangements. Therefore, its characterization in comparison to alt-EJ and the resection process during HR is an important step for advanced tumor treatment options that target DNA repair proteins via inhibitors. When developing such inhibitors, the characterization of this novel repair pathway helps to specifically target tumor cells, which utilize alt-EJ, without interfering with WT cells and the repair pathways they utilize. In any case, the characterization of res-cNHEJ contributes to the broadening of therapeutic options to treat cancer patients in the future.

5. Materials & Methods

5.1. Materials

5.1.1. Consumable materials and appliances

Blotting paper, 703		VWR
Cell culture dishes (100 x 20 mm)		Biochrom
Cell culture dishes (35 x 10 mm, 60 x 15 mm, 100 x 20 mm)		nunc VWR
Cell culture flasks (25 cm ² , 75 cm ²)		TPP
Cell culture well plates (96, 24, 12, 6 well)		TPP
Coverslips (15 mm)		Roth
Centrifuge tubes (15 ml, 50 ml)		Greiner, TPP
Nunc cryogenic tubes		Thermo Scientific
Disposable pipettes (5 ml, 10 ml, 25 ml)		Sarstedt
Flow cytometry tubes with filter caps		Falcon
MACS separation columns MS		Miltenyi Biotec
SafeSeal reaction tubes (2 ml, 1.5 ml, 0.2 ml)		Roth
Microscope slides, superfrost (76 x 26 mm)		Roth
Pasteur pipettes, glass, plastic		Roth
Pipette tips (10 μ l, 200 μ l, 1000 μ l), filtered		Sarstedt, Roth
Plastic cuvettes		Roth
PVDF (polyvinylidene difluoride) membrane		Thermo Scientific
Round bottom flow cytometry tubes		BD Bioscience
Syringes (10 ml, 20 ml, 50 ml)		Braun
Syringe filters (0.45 μ m)		Roth
Agarose gel electrophoresis set	Horizon 58; 11-14	Life Technologies
	Wide Mini-Sub GT cell	Bio Rad
Camera system	AxioCam MRm	Zeiss
Centrifuge	5415 R; 5804 R	Eppendorf
	Biofuge pico	Heraeus
Cell counting chamber	Neubauer	Marienfeld
Cell sorter	S3e Cell Sorter	Bio Rad
Chemiluminescence detection	ChemiSmart 5000	Vilber Lourmat
	Fusion FX	Vilber Lourmat
Confocal laser scanning microscope	TCS SP5 II	Leica
Electrophoresis set	Mini-Protean Tetra Cell	Bio Rad
	Midi	Hofer
Fluorescence microscope	Axiovert 200M	Zeiss
	Imager.Z2	Zeiss
	Observer.D1	Zeiss
MACS system	MultiStand; Separator	Miltenyi Biotec
Microscope	Eclipse TS100	Nikon
Micropipette	1000, 200, 100, 20, 10, 2	Gilson
	1000, 200, 20, 10	Eppendorf
Nano Photometer	P-Class	Implen
pH detection	pMX2000	WTW
Power supply	PowerPac HC	Bio Rad
	EV 243; EPS 3500	Pharmacia Biotech
Scale	TE 1502S; TE 153S-DS	Sartorius
Thermocycler	peqStar	VWR
	C1000; T100	Bio Rad
	T-personal 48	Biometra
Thermomixer	Comfort	Eppendorf
Ultracentrifuge	Sorvall	Thermo Scientific
Ultrasound bath	Sonorex	Bandelin
Western blotting system	Mini Trans-Blot Cell	Bio Rad
	Midi	Hofer

Semi-dry blotting system	Trans-Blot	Bio Rad
X-Ray biological irradiator	MCN 165/796704	Philips
	X-RAD 320	Precision X-Ray

5.1.2. Software and external facilities

AxioVision V4.6.3.0	Zeiss Imaging Solutions	
BLAST	Open Source, NCBI	
ChemiCapt	Vilber Lourmat	
CLC Sequence Viewer 6	CLC bio A/S	
CXP Analysis	Beckman Coulter	
CXP Cytometer V2.2	Beckman Coulter	
FusionCapt Advance FX7	Vilber Lourmat	
G*Power V3.1.9.2	Open Source	
ImageJ	Open Source	
Isis	MetaSystems	
LAS AF Lite	Leica	
MEGA5.1	Open Source ³⁷⁶	
Micro-Manager	Open Source	
Metafer4 V3.4.109	MetaSystems	
OriginPro 8.5	OriginLab Corporation	
Serial Cloner 2.6	Serial Basics	
Cytometry Core Facility		MD Anderson Cancer Center
Cellular Imaging Core Facility		MD Anderson Cancer Center
The Taplin Biological Mass Spectrometry Facility		Harvard Medical School

5.1.3. Chemicals

Acetic acid (CH ₃ COOH)	Roth
Accutase	Sigma-Aldrich
Agar	Roth
Agarase	Thermo Scientific
Agarose	Roth
Ampicillin	Sigma-Aldrich
APS (Ammonium persulfate, (NH ₄) ₂ S ₂ O ₈)	Roth
β-Mercaptoethanol (C ₂ H ₆ OS)	Sigma-Aldrich
Biotin	Thermo Scientific
Bromophenol blue (C ₁₉ H ₁₀ Br ₄ O ₅ S)	USB
BSA (Bovine serum albumin)	AppliChem
Calcium chloride (CaCl ₂)	Roth
Coomassie brilliant blue R-250	Bio Rad
DAPI (4',6-diamidino-2-phenylindole)	Sigma-Aldrich
DMEM (Dulbecco's Modified Eagle Medium)	Sigma-Aldrich
DMSO (Dimethyl sulfoxide, C ₂ H ₆ OS)	Sigma-Aldrich
EDTA (Ethylenediaminetetraacetic acid, C ₁₀ H ₁₆ N ₂ O ₈)	Roth
Ethanol, pure (CH ₃ CH ₂ OH, ≥ 99.5%)	Roth
Ethidium bromide (C ₂₁ H ₂₀ BrN ₃)	Bio Rad
FBS (Fetal bovine serum; also FCS (Fetal calf serum))	Biochrom
Formaldehyde (CH ₂ O)	Roth
G418 (Geneticin)	Sigma-Aldrich
Glacial acetic acid (CH ₃ COOH, ≥ 99.85%)	Roth
Glycerol (C ₃ H ₈ O ₃)	Roth
Glycine (C ₂ H ₅ NO ₂)	Roth
Hydrogen chloride (HCl)	Roth
Immersion oil	Zeiss
IPTG (Isopropyl β-D-1-thiogalactopyranoside, C ₉ H ₁₈ O ₅ S)	Sigma-Aldrich
Isopropanol (Isopropyl alcohol, C ₃ H ₈ O)	Roth
Kanamycin	Sigma-Aldrich
Low melting point agarose, UltraPure	Thermo Scientific

MEM (Minimum Essential Medium)	Sigma-Aldrich
MES (2-(<i>N</i> -morpholino)ethanesulfonic acid, C ₆ H ₁₃ NO ₄ S)	Roth
Methanol (CH ₃ OH)	Roth
Magnesium chloride (MgCl ₂)	Roth
Magnesium sulfate (MgSO ₄)	Roth
Manganese(II) chloride (MnCl ₂)	Roth
Mounting medium	Vectashield
NP-40 (Nonidet P-40)	Sigma-Aldrich
Opti-MEM (Reduced serum MEM)	Life Technologies
NEAA (Non-essential amino acids)	Biochrom
Paraformaldehyde (OH(CH ₂ O) _n ; n = 8-100)	Roth
Peptone	Roth
PIPES (piperazine- <i>N,N'</i> -bis(2-ethanesulfonic acid))	Roth
Potassium acetate (CH ₃ COOK)	Sigma-Aldrich
Potassium chloride (KCl)	Roth
Potassium dihydrogen phosphate (KH ₂ PO ₄)	Roth
ProLong gold antifade	Invitrogen
PI (Propidium iodide, C ₂₇ H ₃₄ I ₂ N ₄)	Sigma-Aldrich
Puromycin	Sigma-Aldrich
Rubidium chloride (RbCl)	Sigma-Aldrich
RNase A	Sigma-Aldrich
Roti-Safe GelStain	Roth
Rotiphorese Gel 30 (37, 5:1)	Roth
SDS (Sodium dodecyl sulfate, C ₁₂ H ₂₅ NaO ₄ S)	Roth
Skim milk (Non-fat dry milk)	Frema
Sodium chloride (NaCl)	Roth
Sodium deoxycholate (C ₂₄ H ₃₉ NaO ₄)	Roth
Sodium hydrogen phosphate (Na ₂ HPO ₄)	Roth
Sodium hydroxide (NaOH)	Roth
Sucrose (Saccharose, C ₁₂ H ₂₂ O ₁₁)	Roth
TEMED (Tetramethylethylenediamine, C ₆ H ₁₆ N ₂)	Roth
Tris-HCl (Tris hydrochloride)	Roth
TritonX-100 (C ₁₄ H ₂₂ O(C ₂ H ₄ O) _n)	Roth
Trypsin	Roth
Tryptone	Roth
Tween20 (Polysorbate 20, C ₂₆ H ₅₀ O ₁₀)	Roth
X-Gal (5-bromo-4-chloro-3-indolyl-β-D-galactopyranoside)	Roth
Xylen-Cyanol FF (C ₂₅ H ₂₇ N ₂ NaO ₆ S ₂)	USB
Yeast extract	Roth

5.1.4. Solutions, buffers, and media

PCR, enzymatic digestion, ligation, and agarose gel electrophoresis

dNTP mix (10 mM)	Thermo Scientific	
10x Herc buffer	Agilent Genomics	
5x Phusion buffer HF	Thermo Scientific	
10x Phu turbo buffer	Agilent Genomics	
10x Thermopool buffer	BioLabs	
10x T4 ligase buffer	Thermo Scientific	
10x T4 ligation buffer with ATP	NEB	
50% PEG 4000 solution	Thermo Scientific	
10x Fast digest buffer	Fermentas	
6 x DNA loading dye	0.25% Bromophenol blue	
	0.25% Xylen-Cyanol FF	
	30% Glycerin	
TAE (Tris-acetate-EDTA)	4.84 g/l Tris-HCl	pH 8.0
	1.142 g/l Acetic acid	
TE (Tris-EDTA)	10 mM Tris-HCl	pH 8.0

	1 mM EDTA	
Bacteria		
LB (lysogeny broth) medium	10 g/l Peptone 5 g/l Yeast extract 5 g/l NaCl	
LB agar	1.5% (w/v) Agar	in LB media
SOB (super optimal broth) medium	2% (w/v) Tryptone 0.5% (w/v) yeast extract 10 mM NaCl 2.5 mM KCl 10 mM MgCl ₂ 10 mM MgSO ₄	
Competent bacteria solution 1	30 mM Potassium acetate 50 mM MnCl ₂ 100 mM RbCl 10 mM CaCl ₂ 15% (w/v) Glycerin	pH 5.8
Competent bacteria solution 2	10 mM RbCl 75 mM CaCl ₂ 10 mM MOPS 15% (w/v) Glycerin	pH 6.8
Cell culture, purification, and staining		
PBS (phosphate-buffered saline)	137 mM NaCl 2.7 mM KCl 8 mM Na ₂ HPO ₄ 1.5 mM KH ₄ PO ₄	pH 7.4
TBS (Tris-buffered saline)	20 mM Tris-HCl 137 mM NaCl	pH 7.6
Trypsin/EDTA	0.5 M EDTA 2.5% (v/v) Trypsin	pH 8.0 in PBS
CSK (cytoskeletal) buffer	10 mM PIPES pH 7 100 mM NaCl 300 mM Sucrose 3 mM MgCl ₂ 0.7% TritonX-100 0.3 mg/ml RNase	
PI solution	10 µg/ml PI 0.5 mg/ml RNase	in PBS
PBS-T	PBS 0.1% Tween20	
Fixative	3:1 Methanol/glacial acetic acid	
Biotin solution	2 mg/ml Biotin	in NETN buffer
Coomassie blue staining solution	0.1% Coomassie brilliant blue R-250 50% Methanol 10% Glacial acetic acid	
Coomassie destaining solution	40% Methanol 10% Glacial acetic acid	
Cell lysis		
RIPA (radio-immunoprecipitation assay) buffer	50 mM Tris-HCl 150 mM NaCl 0.5% Sodium deoxycholate 1% TritonX-100 0.1% SDS	pH 8.0
Lysis buffer	20 mM Tris-HCl	pH 8.2

2x SDS loading buffer	150 mM NaCl 1% TritonX-100 100 mM Tris-HCl 4% (w/v) SDS 0.2% (w/v) Bromophenol blue 20% (v/v) Glycerol	pH 6.8
NETN buffer	200 mM β -Mercaptoethanol 20 mM Tris-HCl 100 mM NaCl 0.5 mM EDTA 0.5% (v/v) Nonidet P-40	pH 8.0
Chelsky buffer	10 mM Tris-HCl 10 mM NaCl 3 mM MgCl ₂ 30 mM Sucrose	pH 7.5
NP-40 buffer	Chelsky buffer 0.5% Nonidet P-40	

SDS-PAGE (polyacrylamide gel electrophoresis) and immunoblotting

Electrophoresis buffer	25 mM Tris-HCl 0.2 M Glycine 0.5% (w/v) SDS	pH 8.8
5x SDS loading buffer (Laemmli)	60 mM Tris-HCl 2% (w/v) SDS 5% (v/v) β -Mercaptoethanol 10% (v/v) Glycerin 0.01% Bromophenol blue	pH 6.8
Stacking gel buffer	0.5 M Tris-HCl 1% SDS	pH 6.8
Stacking gel (4 gels)	2.2 ml RotiphoreseGel30 3.8 ml Stacking gel buffer 9 ml Aqua dest. 100 μ l 10% APS 40 μ l TEMED	
Running gel buffer	1.5 M Tris-HCl 1% SDS	pH 8.8
Running gel (4 gels)	7.5% 10% 12.5%	
RotiphoreseGel30	18 ml 12 ml 15 ml	
Running gel buffer	9 ml 9 ml 9 ml	
Aqua dest.	9 ml 15 ml 12 ml	
10% APS	200 μ l 200 μ l 200 μ l	
TEMED	20 μ l 20 μ l 20 μ l	
Transfer buffer	20 mM Tris-HCl 150 mM Glycine	pH 8.3
TBS-T	0.1% Tween20	in TBS

5.1.5. Reagents, kits, ladders, and enzymes

Transfection reagents

HiPerFect transfection reagent	Qiagen
jetPEI transfection reagent	Polyplus
PEI (Polyethylenimine)	Sigma-Aldrich
MATra-A reagent	IBA

Chemiluminescence detection reagents

LumiLight western blotting substrate	Roche
ChemiGlow	Biozym
WesternBright Quantum	Advansta

WesternBright Sirius

Advansta

Kits

peqGold Xchange plasmid maxi EF kit	peqLab
ZR plasmid mini prep classic	Zymo Research
QIAPrep spin miniprep kit	Qiagen
peqGold MicroSpin cycle pure kit	peqLab
MasterPure Complete DNA & RNA Purification Kit	Epicentre
PureLink genomic DNA mini kit	Thermo Scientific
Gateway cloning system	Life Technologies
EdU Click-iT (Cy5, TexasRed)	baseclick
MACS separation column	Miltenyi Biotec

Protein and DNA ladders

PageRuler plus prestained protein ladder	Fermentas
HiMark prestained standard	Thermo Scientific
ProSieve quad color protein ladder	biozym
Precision plus protein all blue standards	Bio Rad
GeneRuler 1kb DNA ladder	Thermo Scientific
GeneRuler 100 bp plus DNA ladder	Thermo Scientific

Enzymes

Fast alkaline phosphatase	Fermentas
Fast BsmBI	Fermentas
Fast DpnI	Fermentas
Fast SmaI	Fermentas
Gateway BP clonase	Life Technologies
Gateway LR clonase	Life Technologies
Herc polymerase	Agilent Genomics
KOD Hot Start DNA polymerase	Novagen
Pfu turbo polymerase	Agilent Genomics
Phusion polymerase	Thermo Scientific
Proteinase K	Epicentre
Q5 polymerase	Thermo Scientific
RNase A	Epicentre
RNase A	Sigma-Aldrich
T4 DNA ligase	Thermo Scientific
T4 PNK	NEB
Taq polymerase	BioLabs

5.1.6. Primers, siRNAs, and gRNAs

Table 5.1 Primers

Primers were maintained as 100 pmol/ μ l stocks and diluted to 10 pmol/ μ l as a working solution.

Primer name	Sequence
ARTEMIS gRNA1 fw	5'-GAACTCTGGGCGACACAGCAAGACTCCATTTCACAA-3'
ARTEMIS gRNA1 rev	5'-ACAAGGAACATCTATTACAAACTGGGTAGCATCTC-3'
ARTEMIS gRNA3 fw	5'-AGATTTTACCAAATCCAAGTCGGG-3'
ARTEMIS gRNA3 rev	5'-AGAATCAACAGACTGGGAACACTG-3'
BRCA1 gRNA9 fw	5'-TGAGTGGTTTTCCAGAAGTG-3'
BRCA1 gRNA9 rev	5'-GTTTGGTTAGTTCCTGATT-3'
CD4int	5'-GCTGCCCCAGAATCTTCCTCT-3'
CMV2	5'-ATATATGGAGTCCGCGTTACAT-3'
EXO1 mutP73P fw	5'-CTCATGGGATCAAGCCAATTCTCGTATTTGATGG-3'
EXO1 mutP73P rev	5'-CCATCAAATACGAGAATTGGCTTGATCCCATGAG-3'
T7 fw	5'-TAATACGACTCACTATAGGGCGA-3'

Table 5.2 siRNAs (small interfering RNAs)

siRNA	Sequence/number	Conc.	Vendor
53BP1	5'-GAGAGCAGATGATCCTTTA-3'	25 nM	Dharmacon
53BP1 (construct)	5'-AGAACGAGGAGACGGUAAUAGUGGG-3'	50 nM	Qiagen
ARTEMIS	5'-AACTGAAGAGAGCTAGAACAG-3'	25 nM	Qiagen
BRCA1	5'-GGAACCTGTCTCCACAAAGTG-3'	15 nM	Qiagen
BRCA1_14	5'-CAGGAAATGGCTGAACTAGAA-3'	25 nM	Qiagen
BRCA1 (construct)	5'-AATCACAGTGTCTTTTATGTA-3'	50 nM	Qiagen
BLM	5'-AAGCTAGGAGTCTGCGTGCGA-3'	50 nM	Qiagen
CDK2	SI02654631	25 nM	Qiagen
CtIP	5'-TCCACAACATAATCCTAATTT-3'	50 nM	Qiagen
CtIP (construct)	5'-AAGCTAAAACAGGAACGAATC-3'	50 nM	Qiagen
Ctrl (negative)	5'-AATTCTCCGAACGTGTCACGT-3'	10-50 nM	Qiagen
DNA2	5'-AAATAGCCAGTAGTATTCGAT-3'	20 nM	Qiagen
DNA-PKcs	5'-CTCGTGTATTACAGAAGGAAA-3'	15 nM	Qiagen
EXD2	L-020899-02	25 nM	Dharmacon
EXO1 (construct)	5'-CAAGCCTATTCTCGTATTTTT-3'	50 nM	Qiagen
EXO1_7	5'-ATGGATGTACTTTACCTTCTA-3'	20 nM	Qiagen
KU70	5'-GGAAGAGATAGTTTGATTTTT-3'	20 nM	Qiagen
KU80	5'-AAGACAGACACCCTTGAAGAC-3'	20 nM	Qiagen
LIG I	5'-GGCATGATCCTGAAGCAGA-3'	25 nM	Qiagen
LIG III	5'-CCACAAAAAAATCGAGGA-3'	25 nM	Qiagen
LIG IV	5'-CAAGATGTTTACAGAAAGGAA-3'	20 nM	Qiagen
MRE11	5'-ACAGGAGAAGAGATCAACTAA-3'	20 nM	Qiagen
MRE11_2	5'-AAGAAAGGCTCTATCGAATGT-3'	20 nM	Qiagen
PARP1	M-06656-01-0005	25 nM	Dharmacon
PLK1_2	SI00071624	20 nM	Qiagen
PLK1_6	SI02223837	20 nM	Qiagen
PLK3	5'-CTGCATCAAGCAGTTCACTA-3'	25 nM	Qiagen
PLK3_1	SI00059388	20 nM	Qiagen
PLK3_11	SI05056450	20 nM	Qiagen
POL λ	sc-43729	10 nM	Santa Cruz
POL μ	sc-105304	10 nM	Santa Cruz
POL θ	S100090062	25 nM	Qiagen
RAP80	UMC1 (51720)	20 nM	Dharmacon

Table 5.3 gRNAs (guide RNAs)

gRNA	Sequence
53BP1 gRNA #4 (kindly provided by Z. Gong)	5'-ATCGGAAAGCATCAGGAGA-3'
ARTEMIS gRNA #1 ⁴⁰⁰	5'-GAGACTTCAGATTGGCGCA-3'
ARTEMIS gRNA #3 ⁴⁰⁰	5'-GAGCCCGTACCATGTTGTG-3'
BRCA1 gRNA #3 (kindly provided by Z. Gong)	5'-GTAAGAATGATATAACCAAA-3'
BRCA1 gRNA #9 (kindly provided by Z. Gong)	5'-AGGCTTGCCTTCTCCGAT-3'
CtIP gRNA #2 (kindly provided by Z. Gong)	5'-GTTAACGCCAGAAAATGAGA-3'
EXO1 gRNA #4 (kindly provided by Z. Gong)	5'-GGAAAGCAACTTCTTCGTGA-3'
PTIP gRNA #1 ⁴⁰⁰	5'-TGTGAGGCTAGTGCATTGT-3'
REV7 gRNA #4 (kindly provided by Z. Gong)	5'-TGTGCTCTGCGAGTTCCTGG-3'
RIF1 gRNA #1 (kindly provided by Z. Gong)	5'-CACAAAAGGTACATTTGCG-3'

5.1.7. Inhibitors, nucleotides, and nucleotide analogues

Table 5.4 Inhibitors

Inhibitor (name)	Conc. or dilution	Vendor/Reference
ATM (Ku60019)	0.5 μM	Tocris Bioscience
CDK1 (RO-3306)	1 μM, 10 μM	Selleckchem
CDK1/2 (Roscovitine)	2 μM, 25 μM	Sigma-Aldrich
DNA-PK (Nu7441)	7.5 μM	Tocris Bioscience
MRE11 (mirin)	500 μM	Tocris Bioscience

MRE11 endonuclease (PFM01)	50 μ M, 100 μ M	354
MRE11 exonuclease (PFM39)	100 μ M, 300 μ M	354
Nocodazole	100 μ g/ml	Sigma-Aldrich
PARP (PJ34)	15 μ M	Calbiochem
PARP (Olaparib)	0.5 to 2.5 μ M	Selleckchem
PhosphoStop	10x	Roche
PLK1/3 (GW843682X)	0.5 μ M	Tocris Bioscience
Protease	25x	Roche
Protease (pepstatin)	1:500	Sigma-Aldrich
Protease (aprotinin)	1:500	Sigma-Aldrich

Table 5.5 Nucleotides and nucleotide analogs

Inhibitor (name)	Conc. or dilution	Vendor
BrdU (5-bromo-2-deoxyuridine)	10 μ g/ml	Sigma-Aldrich
EdU (5-ethynyl-2-deoxyuridine)	1 μ M	Baseclick
EdU	1 μ M	Invitrogen
Thymidine	2 mM	Sigma-Aldrich

5.1.8. Antibodies and beads

Table 5.6 Primary antibodies

Primary antibodies (ABs) with vendor, dilution, and application. Where the AB was used for immunoblotting, the AB solution and the solvent is named instead of the application.

Antibody	Vendor (number)	Dilution (application)
mouse-anti-53BP1 (BP13)	Millipore (#05-726)	1:1,000 (5% BSA)
rabbit-anti-53BP1	Bethyl (A300-272A)	1:2,000 (5% BSA)
mouse-anti- β -ACTIN	Santa Cruz (sc47778)	1:1,000 (5% BSA)
rabbit-anti-ARTEMIS	Abcam (ab35648)	1:2,000 (5% BSA)
rabbit-anti-ARTEMIS	GenTex (GTX100128)	1:3,000 (5% milk)
rabbit-anti-ARTEMIS	Novus Biologicals (100-542)	1:1,000 (3% milk)
rabbit-anti-ARTEMIS	Thermo Scientific (14241)	1:1,000 (5% BSA)
rabbit-anti-BLM	Abcam (ab2179)	1:1,000 (5% BSA)
mouse-anti-BRCA1 (MS13)	Abcam (ab16781)	10 μ g (IP)
mouse-anti-BRCA1 (D9)	Santa Cruz (sc6954)	1:100 (3% milk)
rabbit-anti-BRCA1 (C20)	Santa Cruz (sc642)	1:200 (5% BSA)
rabbit-anti-BRCA1 (I20)	Santa Cruz (sc646)	1:500 (5% BSA)
mouse-anti-BrdU	Becton Dickinson (347580)	1:500 (IFM)
rabbit-anti-CDK2 (D12)	Santa Cruz (sc6248)	1:400 (1% milk)
rabbit-anti-CtIP	Bethyl (A300-488A)	1:1,000 (5% BSA)
rabbit-anti-CtIP	Abcam (ab70163)	1:1,000 (3% milk)
mouse-anti-CtIP (D-4)	Santa Cruz (sc271339)	2 μ g (IP)
mouse-anti-CtIP (E-2)	Santa Cruz (sc48415)	1:800 (5% BSA)
rabbit-anti-phospho-CtIP-Ser327	Kindly provided by T. Paull	1:1,100 (5% BSA)
rabbit-anti-DNA2	Abcam (ab96488)	1:1,000 (5% BSA)
rabbit-anti-DNA-PKcs	Novus Biologicals (100658)	1:1,000 (1% milk)
rabbit-anti-EXD2	Sigma (HPA005848)	1:1,000 (5% BSA)
mouse-anti-EXO1	Abcam (ab3307)	1:800 (5% BSA)
rabbit-anti-EXO1	Bethyl (A302-640)	1:1,000 (5% BSA)
rabbit-anti-EXO1	Santa Cruz (sc33194)	1:400 (5% BSA)
mouse-anti-FLAG (M2)	Sigma (F3165)	1:1,000 (5% BSA)
rabbit-anti-GAPDH	Santa Cruz (sc25778)	1:1,000 (1% milk)
mouse-anti-GFP	Roche (11 814 460 001)	1:500 (1% milk)
rabbit-anti-GFP	Santa Cruz (sc8334)	1:500 (3% milk)
rabbit-anti-GFP	Abcam (ab6556)	1:500 (3% milk)
mouse-anti-phospho-H2A.X-Ser139	Millipore (#05-636)	1:2,000 (IFM)
rabbit-anti-phospho-H2A.X-Ser139	Abcam (ab81299)	1:1,000 (IFM)
rabbit-anti-phospho-H2A.X-Ser139	Epitomics (mono 2212-1)	1:2,000 (IFM)
mouse-anti-phospho-H3-Ser10	Cell signaling (9706)	1:200 (FACS)

mouse-anti-HA (HA.C5)	Abcam (ab18181)	1:1,000 (5% BSA)
mouse-anti-KU70 (A9)	Santa Cruz (sc5309)	1:1,000 (1% milk)
mouse-anti-KU80 (B4)	Santa Cruz (sc515736)	1:1,000 (1% milk)
mouse-anti-KU80 (B4)	Santa Cruz (sc515736)	5 μ g (IP)
mouse-anti-KU80 (111)	Abcam (ab79220)	1:100 (IFM)
mouse-anti-LIG1 (1A9)	Santa Cruz (sc47703)	1:1,000 (1% milk)
mouse-anti-LIG3	Santa Cruz(sc56089)	1:1,000 (1% milk)
rabbit-anti-LIG4	Acris (SP1275)	1:2,000 (5% BSA)
mouse-anti-MRE11	Abcam (ab214)	1:1,000 (1% milk)
mouse-anti-cMyc (9E10)	Novus Biologicals (600302)	1:1,000 (5% BSA)
mouse-anti-cMyc (9E10)	Santa Cruz (sc40)	1:1,000 (5% milk)
mouse-anti-OctA-Probe (H5)	Santa Cruz (sc166355)	1:1,000 (1% milk)
rabbit-anti-PARP1	Abcam (ab137653)	1:1,000 (5% BSA)
rabbit-anti-PLK1	AB online (ABIN1527406)	1:800 (1% milk)
rabbit-anti-PLK3	Abcam (ab33119)	1:1,000 (2.5% milk)
rabbit-anti-POL μ	Abcam (ab157465)	1:1,000 (5% BSA)
rabbit-anti-POL λ	Abcam (ab82919)	1:1,000 (5% BSA)
rabbit-anti-POL θ (M09)	Abnova (H000107 21-M09)	1:500 (5% BSA)
rabbit-anti-PTIP	Generated by Z. Gong	1:1,000 (5% BSA)
rabbit-anti-PTIP (H167)	Santa Cruz (sc367459)	1:400 (5% milk)
rabbit-anti-RAP80	Abcam (ab124763)	1:400 (5% BSA)
rabbit-anti-tRFP	Evrogen (AB233)	1:1,000 (1% milk)
rabbit-anti-RIF1	Novus Biologicals (1001587)	1:1,000 (5% BSA)
rabbit-anti-RPA2 (phosphoT21)	Abcam (ab109394)	1:10,000 (IFM)
rabbit-anti-RAD51	Abcam (ab63801)	1:15,000 (IFM)
rabbit-anti-I-SceI (FL-86)	Santa Cruz (sc98269)	1:1,000 (IFM)
mouse-anti- α -TUBULIN (TU-02)	Santa Cruz (sc8035)	1:2,000 (5% BSA)

Table 5.7 Tagged primary antibodies

Antibody	Vendor (number)	Dilution
mouse-anti-CD4-FITC	BioLegends (100510)	1.5 μ g (IFM)
FITC rat anti-mouse CD4	BD Pharmingen (553047)	1.5 μ g (IFM, MACS)
FITC rat anti-mouse CD8	BioLegends (100706)	2 μ g (IFM)

Table 5.8 Secondary antibodies

Secondary ABs with vendor, dilution, and application. Where the AB was used for immunoblotting, the AB solution and the solvent is named instead of the application.

Antibody	Vendor (number)	Dilution
goat anti-mouse AlexaFluor 488	Molecular Probes (A11001)	1:1,000 (IFM)
goat anti-rabbit AlexaFluor 488	Molecular Probes (A1008)	1:1,000 (IFM)
goat anti-mouse AlexaFluor 594	Molecular Probes (A11005)	1:1,000 (IFM)
goat anti-rabbit AlexaFluor 594	Molecular Probes (A1012)	1:1,000 (IFM)
goat anti-mouse IgG-HRP	Santa Cruz (sc2031)	1:10,000 (1% milk)
goat anti-mouse IgG-HRP	Generated by Z. Gong	1:4,000 (5% milk)
goat anti-rabbit IgG-HRP	Santa Cruz (sc2030)	1:30,000 (1% milk)
goat anti-rabbit IgG-HRP	Generated by Z. Gong	1:3,000 (5% milk)

Table 5.9 Beads

Antibody	Vendor (number)	Dilution
Dynabeads protein G	Thermo Scientific (10004D)	20 to 50 μ l
S protein agarose beads	EMD Millipore (69704)	120 μ l
Streptavidin coupled Dynabeads	Thermo Scientific (11206D)	300 μ l
anti-rat IgG MicroBeads	Miltenyi Biotec (130-048-501)	20 μ l

5.1.9. Plasmids

HA-53BP1-WT: Plasmid encoding HA-tagged siRNA-resistant (A231G, A234G, A237C silent point mutations) human WT 53BP1 construct; pCMH6K-53BP1, 10.1 kb, ampicillin resistance, kindly provided by P. Jeggo ²⁸⁸.

cMyc-ARTEMIS-WT, cMyc-ARTEMIS-D37N: Plasmid encoding cMyc-tagged siRNA-resistant (K376K, R377R, A378A) human WT ARTEMIS or ARTEMIS endonuclease mutant with Asp37 mutated to Asn; pCleo-cMyc-ARTEMIS-WT or -D37N, 7.43 kb, ampicillin resistance, original plasmid kindly provided by P. Jeggo ³⁴, mutations for siRNA resistance by O. Barton.

SFB-ARTEMIS: *N*-terminal triple epitope tag destination vector (S protein, FLAG epitope tag, and streptavidin-binding peptide tag) with human ARTEMIS WT; SFB-ARTEMIS-N-LR, 2079 bp, ampicillin and puromycin resistance, kindly provided by Z. Gong ⁴⁰⁰.

FLAG-BRCA1-WT, FLAG-BRCA1-I26A, FLAG-BRCA1-C61G, FLAG-BRCA1-S1655A: Plasmid encoding FLAG-tagged siRNA-resistant (C186T, C187T, G189A, C191G, C192T) human WT BRCA1, BRCA1 hypomorphic RING domain mutant with Ile26 mutated to Ala with residual E3 ligase activity ¹²⁷, BRCA1 RING domain mutant with Cys61 mutated to Gly, or BRCA1 BRCT mutant with Ser1655 mutated to Ala; FLAG-BRCA1-WT, -I26A, -C61G, or -S1655A, ampicillin resistance, kindly provided by A. Shibata ³⁴⁸.

SFB-BRCA1: *N*-terminal triple epitope tag destination vector (S protein, FLAG epitope tag, and streptavidin-binding peptide tag) with human BRCA1 WT; SFB-BRCA1-N-LR, 5592 bp, ampicillin and puromycin resistance, kindly provided by Z. Gong.

Cas9: Plasmid encoding Cas9; gRNA vector needs to be transfected simultaneously; hSpCas9-blast, blasticidin resistance, vendor: GeCKO.

psPAX2 & pMD2.G: Envelope and packaging plasmids for second-generation lentiviral plasmid, gRNA-V2 plasmid acts as transfer plasmid; psPAX2, vendor: AddGene (#12260).

gRNA-V0: Plasmid encoding chimeric gRNA; lentiGuide-puro, 13 kb, kanamycin and puromycin resistance, vendor: GeCKO.

gRNA-V2: Viral plasmid encoding hSpCas9 and the chimeric gRNA; the vector can be digested by BsmBI and a pair of annealed oligo nucleotides can be cloned into the region to alter the gRNA sequence; lentiCRISPRv2, 13 kb, ampicillin and puromycin resistance, vendor: GeCKO.

FLAG-CtIP: *N*-terminal triple epitope tag destination vector (S protein, FLAG epitope tag, and streptavidin-binding peptide tag) with siRNA-resistant (C133T silent point mutation) human CtIP WT; SFB-CtIP-N-LR, 2691 bp, ampicillin and puromycin resistance, original plasmid kindly provided by Z. Gong.

GFP-CtIP-WT, GFP-CtIP-S327A: Plasmid encoding *C*-terminal GFP-tagged siRNA-resistant (C133T, A135G, A138G silent point mutations) human WT CtIP or CtIP phospho-mutant with Ser327 mutated to Ala; pEGFP-CtIP-WT-C1 or -S327A-C1, 7416 bp, kanamycin and neomycin resistance, original plasmid kindly provided by S. Takeda ²⁵.

RFP-CtIP-WT, RFP-CtIP-S327A, RFP-CtIP-S327E, RFP-CtIP-T847A, RFP-CtIP-T847E: Plasmid encoding *C*-terminal RFP-tagged siRNA-resistant (C133T, A135G, A138G silent point mutations) human WT CtIP, CtIP phospho-mutant with Ser327 or Thr 847 mutated to Ala, or CtIP phospho-mimic mutant with Ser327 or Thr 847 mutated to Glu; ptagRFP-CtIP-WT-C1, -S327A-C1, -S327E-C1, -T847A-C1, or -T847E-C1, 7416 bp, kanamycin resistance, generated by graduate student F. Lörch ²⁵ from original GFP-tagged version kindly provided by S. Takeda.

RFP-CtIP-S327A/T847A, RFP-CtIP-S327E/T847E, RFP-CtIP-S327E/T847A, RFP-CtIP-S327A/T847E: Plasmid encoding *C*-terminal RFP-tagged siRNA-resistant (C133T, A135G, A138G silent point mutations) human CtIP phospho-mutant with Ser327 and Thr847 mutated to Ala, CtIP phospho-mimic mutant with Ser327 and Thr847 mutated to Glu, CtIP mixed phospho-mimic and phospho-mutant with Ser327 and Thr847 mutated to Glu or Ala; ptagRFP-CtIP-S327A/T847A-C1, -S327E/T847E-C1, -S327E/T847A-C1,

or -S327A/T847E-C1, 7416 bp, kanamycin resistance, generated by undergraduate student C. Ruder from original GFP-tagged version generated by O. Barton.

RFP-CtIP-S664A/S745A, RFP-CtIP- S664E/S745E, RFP-CtIP-N289A/H290A: Plasmid encoding C-terminal RFP-tagged siRNA-resistant (C133T, A135G, A138G silent point mutations) human CtIP phospho-mutant with Ser664 and 745 mutated to Ala, CtIP phospho-mimic mutant with Ser664 and 745 mutated to Glu, CtIP nuclease mutant with Asn289 and His290 mutated to Ala; ptagRFP-CtIP-S664A/S745A-C1, -S664E/S745E-C1, or -N289A/H290A-C1, 7416 bp, kanamycin resistance, generated by graduate student F. Lörch from original GFP-tagged version generated by O. Barton.

SFB-CtIP: N-terminal triple epitope tag destination vector (S protein, FLAG epitope tag, and streptavidin-binding peptide tag) with human CtIP WT; SFB-CtIP-N-LR, 2691 bp, ampicillin and puromycin resistance, kindly provided by Z. Gong.

FLAG-EXO1-WT: C-terminal triple epitope tag destination vector (S protein, FLAG epitope tag, and streptavidin-binding peptide tag) with human siRNA-resistant (P73P) EXO1 WT; SFB-EXO1-C-LR, ampicillin resistance, original plasmid kindly provided by Z. Gong.

SFB-EXO1: C-terminal triple epitope tag destination vector (S protein, FLAG epitope tag, and streptavidin-binding peptide tag) with human EXO1 WT; SFB-EXO1-C-LR, ampicillin and puromycin resistance, kindly provided by Z. Gong.

GFP: C-terminal GFP plasmid for mammalian cells; pEGFP-C1, 4.7 kb, kanamycin and neomycin resistance, vendor: Clontech (#632470).

CMV-EGFP: Plasmid encoding EGFP; suitable for viral production as positive control; pCMV-EGFP, vendor: AddGene (#19319).

FLAG-PLK3-WT, FLAG-PLK3-PBD: N-terminal triple epitope tag destination vector (S protein, FLAG epitope tag, and streptavidin-binding peptide tag) with siRNA-resistant human WT PLK3 or PLK3 deletion mutant (aa 1 to 480); SFB-PLK3-WT-N-LR or - Δ PBD-N-LR, ampicillin and puromycin resistance, original plasmid kindly provided by J. Wang ²⁵, mutations for siRNA resistance by O. Barton.

RFP: RFP expressing plasmid for human cells; ptagRFP-C1, 4643 bp, kanamycin resistance, vendor: Takara Bio Inc.

I-SceI: Plasmid encoding the meganuclease I-SceI for expression in human cells; pBL464-pCBA-Sce, 5661 bp, ampicillin resistance, kindly provided by W. Mansour ²⁵⁸.

pGEM-T easy: Vector from pGEM-T easy vector system I, which is suitable for α -complementation; vector is included in its linearized form (EcoRV); pGEM-T easy vector, 3015 bp, ampicillin resistance, vendor: Promega (#A1360).

pUC19: Vector that is suitable for α -complementation with a SmaI restriction site within the multiple cloning site; pUC19, 2686 bp, ampicillin resistance, vendor: New England Biolabs (#N3041S).

5.1.10. Cell lines and bacteria

82-6 hTERT: hTERT-immortalized human WT fibroblast cell line; cells were cultivated in MEM with 20% FCS and 1% NEAA and passaged twice per week (1:8 or 1:10); kindly provided by P. Jeggo ³²⁷.

GC92: SV40-transformed GM639 human fibroblast control cell line isolated from a 8-year-old female (National Institute of General Medical Sciences Human Genetic Mutant Cell Repository (Camden, NJ)) ¹³² containing a stable intrachromosomal integrated reporter substrate (see Figures 3.1 A, S9.2 a); cells were cultivated in DMEM plus 10% FCS and 1% NEAA and passaged twice per week (1:10 or 1:15); kindly provided by B. Lopez ³²².

GC92 ARTEMIS KO: GC92 ARTEMIS knock-out cell line generated with CRISPR/Cas9; cells were cultivated in DMEM plus 10% FCS and 1% NEAA and passaged twice per week (1:10 or 1:15); ³⁶.

GC92 BRCA1 KO: GC92 BRCA1 mutant cell line with a depleted BRCT domain generated with CRISPR/Cas9; cells were cultivated in DMEM plus 10% FCS and 1% NEAA and passaged twice per week (1:10 or 1:15).

GCS5: Variant of the GC92 reporter cell line but with a second reporter substrate, which has G418 resistance (see Figure 3.4 A); cells were cultivated in DMEM plus 10% FCS and 1% NEAA plus 350 $\mu\text{g/ml}$ G418 and passaged twice per week (1:8 or 1:10); kindly provided by B. Lopez ¹⁵⁴.

GCSH14: Variant of the GC92 reporter cell line with a second reporter substrate, which has G418 resistance (see Figure 3.4 A); cells were cultivated in DMEM plus 10% FCS and 1% NEAA plus 350 $\mu\text{g/ml}$ G418 and passaged twice per week (1:8 or 1:10); kindly provided by B. Lopez ¹⁵⁴.

HEK293T: Human epithelial embryonic kidney cell line; cells were cultivated in DMEM plus 10% FCS or DMEM plus 10% FCS and 1% Glutathione and passaged twice per week (1:8 or 1:10); vendor: ATCC (#ATCC-CRL-3216).

HeLa-S3: Human epithelial cervix tumor cell line isolated in 1951 from 31 year old Henrietta Lacks suffering from adenocarcinoma; cells were cultivated in DMEM plus 10% FCS and 1% NEAA and passaged twice per week (1:8 or 1:10); vendor: ATCC (#ATCC-CCL-2.2).

HeLa pGC: HeLa cells containing a gene conversion reporter construct with puromycin resistance; cells were cultivated in DMEM plus 10% FCS and 1% NEAA plus 2 $\mu\text{g/ml}$ puromycin and passaged twice per week (1:8 or 1:10); kindly provided by W. Mansour ²⁵⁸.

***Escherichia coli* DH5 α :** *E. coli* strain used for cloning; suitable for α -complementation due to an incomplete *lacZ* gene, which makes blue-white colony screening possible after transformation with a vector coding for the missing *lacZ*- α (*N*-terminal α fragment of β -galactosidase)

5.2. Cellular biological methods

5.2.1. Cell culture, transfections, and treatments

Cell culture

Cells were cultured at 37°C in a 5% CO₂ incubator in either 75 cm² cell culture flasks or 10 cm cell culture dishes. Sterile solutions, media, and materials were used. For thawing, cells were taken from the liquid nitrogen storage and incubated for 1 min in a 37°C water bath. The cell suspension was mixed with 5 ml of medium and centrifuged for 3 min at 300 \times g. The pellet was resuspended in 1 ml of fresh medium and incubated for 24 h in either 6 or 10 cm cell culture dishes. The first passage after thawing was executed at a 1:3 ratio. Passaging was performed at 80 or 90% optical confluence. Medium was discharged and cells were washed with PBS. Cells were incubated with trypsin/EDTA solution until cells could be shaken off the cell culture dish or flask (after 3 to 10 min, depending on the cell line). Trypsinization was stopped by medium addition, cells were singularized by resuspension and transferred into new cell culture dishes or flasks containing fresh medium (for passaging ratios see chapter 5.1.13). Cells were harvested at 70% confluence, washed with PBS, trypsinized and transferred into a tube. The suspension was centrifuged at 300 \times g for 3 min and cells were resuspended in fresh medium. After another centrifugation, cells from one 10 cm cell culture dish were resuspended in 2 ml FBS/10% DMSO and transferred into cryogenic tubes 1 ml each. Samples were frozen at -80°C or in liquid nitrogen tanks.

After stopping the trypsinization, cells were centrifuged at $300 \times g$ for 3 min and resuspended in fresh medium. The cell number was determined with a Neubauer counting chamber and cells were seeded in cell culture dishes. For microscopy assays, cells were seeded in either 35 or 60 mm cell culture dishes on coverslips with 1.5×10^5 cells in 2.2 ml medium or 2.5×10^5 cells in 5.5 ml medium, respectively. For protein analysis, 2.5×10^5 cells were seeded in 35 mm dishes with 2.2 ml medium. For cell sorting with flow cytometry, cells were seeded in 6-well plates in a 1:100 ratio. For cell sorting with MACS, 2×10^5 cells were seeded with 5.5 ml medium in 60 mm dishes. For immunoprecipitation and purification, cells were seeded in 10 cm dishes at a 1:10 ratio. Cells were first transfected with small interfering RNA (siRNA) during seeding and all additional transfections or other treatments took place between 24 and 72 h after seeding.

RNA interference

Transfection of siRNA was performed with HiPerFect transfection reagent (for target sequences and applied concentrations see Table 5.2). The composition was dependent on the desired siRNA concentration and the medium volume the cells were seeded in. For cells seeded in 2.2 ml medium, a total volume of 100 μ l Opti-MEM with siRNA (1.2 to 3 μ l) was mixed with 12 μ l of HiPerFect in a 1.5 ml reaction tube and vortexed for 1 min. For cells seeded in 5.5 ml medium, a total volume of 250 μ l Opti-MEM with siRNA (2.88 to 7.2 μ l) was mixed with 28.8 μ l of HiPerFect in a tube and vortexed for 1 min. After incubation for 10 min at RT, the solution was added dropwise under pivoting. The first siRNA transfection was executed during the seeding of the cells. A second siRNA transfection took place 24 to 36 h after the first. Downregulation was confirmed by immunoblotting and the strongest downregulation was detected 72 h after the first transfection. After a third siRNA transfection, which took place 72 h after cell seeding, protein levels remained low for an additional 72 h, providing enough time to conduct the experiments.

Plasmid transfection

Plasmid transfection was performed with gentle jetPEI transfection reagent for reporter assay experiments. For cells seeded in 2.2 ml medium, 1 μ g plasmid DNA and 4 μ l jetPEI were each mixed and briefly vortexed with 100 μ l 150 mM NaCl. For cells seeded in 5.5 ml medium, 4 μ g plasmid DNA and 8 μ l jetPEI were each mixed and briefly vortexed with 250 μ l 150 mM NaCl. The jetPEI solution was then added to the DNA solution and the mixture was briefly vortexed again. After 15 min incubation at RT, the solution was added dropwise under pivoting. The medium was changed 8 to 12 h after adding the plasmid DNA and the second or third siRNA

transfection was subsequently performed. Plasmid transfection was performed with PEI or MATra-A for all other experiments following the manufacturer's instructions.

Viral Transduction

Viral transduction was used to establish gRNAs. HEK293T cells were seeded in 60 mm dishes with 3 ml medium and were transfected with PEI after 24 h, using 200 μ l Opti-MEM with 40 μ l PEI solution and 200 μ l Opti-MEM containing 10 μ g DNA. The DNA was mixed in a 4:3:1 ratio: 4.8 μ g gRNA-V2 vector, 3.6 μ g psPAX2, and 1.2 μ g pMD2.G. The virus was collected 48 h after transfection with a syringe and a 0.45 μ m filter and 6 μ l enhancer was added. 1 ml of virus solution was added to cells seeded 24 h prior in 6-well plates after medium was removed. 1 ml fresh medium was added. After 72 h, the medium was changed to selection medium containing 2 μ g/ml puromycin. Fresh selection medium was added after 24 h and cells were harvested after an additional 48 h for immunoblotting. Viral transduction was also used in some experiments instead of siRNA downregulation.

Generation of KO cell lines

CRISPR/Cas9 technology was used to generate knock-out (KO) cell lines. GC92 or MCF10A cells were simultaneously transfected with gRNA-V0 plasmids, a Cas9-encoding plasmid, and a GFP plasmid using PEI following the manufacturer's instructions. GFP-positive cells were singularized in 96-well plates by cell sorting and transferred to two 24-well plates after reaching confluence. One 24-well plate was used to screen for knock-out at the protein level by immunoblotting. Clones were transferred to two 12-well plates and after reaching confluence, one 12-well plate was used to verify protein levels by immunoblotting. Potential KO cells were transferred to 6-well plates and genomic DNA was extracted with pure link genomic DNA mini kit following the manufacturer's instructions. The targeted region was amplified by PCR using KOD hot start DNA polymerase (for primer sequences see Table 5.1). PCR products were cloned into pGEM-T easy vector and transformed into competent *E. coli* DH5 α . α -complementation was used to identify colonies containing the plasmid. Plasmid preparation was performed with QIAprep spin mini prep kit according to the manufacturer's instruction. To confirm the KO, the isolated DNA of at least 10 colonies was sent for sequencing to verify frameshift mutations in the targeted region.

Generation of stable cell lines

HEK293T cells were seeded in 6-well plates and plasmid transfection with 3 μ g DNA was performed after 24 h using PEI following the manufacturer's instructions. After another 24 h, the transfected cells were seeded in 10 cm cell culture dishes with DMEM/15% FBS at 1:5, 1:10, and 1:40 ratios. After 48 h, the medium was changed to selection medium containing 2 μ g/ml

puromycin. Fresh selection medium was added every 72 h and after a total of 12 to 15 days, single clones were picked and transferred to 24 or 12-well plates. After reaching confluence, cells were transferred into 6-well plates with coverslips. Cell-covered coverslips were used for immunofluorescence microscopy analysis to identify clones showing homogenous expression levels roughly equal to the endogenous protein level. Protein level was also tested by immunoblotting.

Inhibitor treatment

Chemical inhibitors were added 1 h before IR or 8 h after I-SceI transfection in reporter assay experiments when the medium was changed. To maintain inhibition over the entire repair time for reporter assay experiments, the medium and inhibitor were replaced 24 h after initial treatment. Negative controls were treated with DMSO. For concentrations used see Table 5.4.

Cell synchronization

For synchronization, proliferating GC92 cells were treated with 2 mM thymidine. 16 h after the first treatment with thymidine, cells were washed 3x with PBS and incubated in medium to release the cells from their block in S phase and at the G₁/S transition. To fully synchronize all cells at the G₁/S transition, thymidine was re-added 10 h after release. After 14 h pulse treatment with thymidine, cells were washed 3x with PBS and fresh medium was added. To obtain synchronized G₂ cells, experiments were conducted 8 h after release and to obtain synchronized G₁ cells, experiments were conducted 16 to 18 h after release. Cell synchronization was controlled using propidium iodide flow cytometry analysis.

To maintain GC92 cells synchronized in G₁ phase for the duration of the entire repair time in reporter assay experiments, serum-free medium (or starvation medium with 0.5% FCS) was added to the cells 12 h after release from the second thymidine block. Additionally, EdU was added. To maintain GC92 cells in G₂ phase for the duration of the repair time, the CDK1 inhibitor RO-3306 was added 8 h after the second thymidine release to keep cells from progressing from G₂ into G₁ phase. Additionally, EdU was added. EdU incorporation was used to exclude the small number of cells which continued to progress in the cell cycle. Of note, both procedures without previous thymidine block were unsuccessful in GC92 cells.

DSB induction

Damage induction by I-SceI expression was initiated in cells containing a reporter substrate by transient transfection of an I-SceI plasmid. The first sign of I-SceI expression was detected in very few cells after 12 h and was observed in roughly 30% of all cells after 48 h. In the first step of I-SceI DSB induction, the two β -sheets interact directly with the DNA to recognize the 18 bp I-SceI recognition site on one DNA strand. Next, the endonucleolytic cut is performed by the

Asp-rich active region cradled between the two β -sheets^{205,279}. The *N*-terminal loop of I-SceI is coiled around the DNA to maintain position while the nuclease moves to also disrupt the second DNA strand, which produces a DSB with a 4 nt 3' ssDNA overhang (also see Table 9.1).

Damage induction by X-IR was performed at 90 kV and 39 mA for immunoprecipitation and purification experiments and at 90 kV and 19 mA for all other experiments. The dose doubling effect was taken into account when cells were seeded on glass coverslips, thus exposure times were reduced to obtain the indicated dose²⁰⁶. The X-ray machine uses a tungsten anode and a beryllium window and the samples were irradiated on a 1 mm aluminum plate which filters low energy X-rays.

5.2.2. Flow cytometry and magnetic-activated cell sorting (MACS)

For flow cytometry experiments, cells were washed twice with PBS then trypsinized for 5 min at 37°C. Trypsinization was stopped with medium. All further steps were conducted on ice and with cold solutions. Cells were resuspended and transferred into falcon tubes or reaction tubes. After centrifugation at $300 \times g$ for 3 min at 4°C, cells were resuspended in 1 ml of PBS and transferred to a fresh 1.5 ml reaction tube. After another centrifugation, cells were fixed by dropwise addition of -20°C cold ethanol under constant vortexing of the cell pellet. Fixed cells were stored at -20°C. Cells were centrifuged at $400 \times g$ for 3 min at 4°C. After two washing steps with PBS, cells were permeabilized with 0.25% TritonX-100/PBS by incubation for 15 min on ice. After centrifugation, cells were washed twice with 1% BSA/PBS. Cells were incubated for at least 1 h at RT or overnight at 4°C in 1% BSA/PBS. Cells were resuspended in primary antibody diluted in 1% BSA/PBS and incubated at 4°C overnight. After centrifugation at $400 \times g$ for 3 min at 4°C, cells were washed twice with 1% BSA/PBS. Following secondary antibody treatment in 1% BSA/PBS for 1 h at RT in the dark, cells were centrifuged and washed once more. Cells were resuspended in PI solution and incubated for 30 min at RT in the dark. Cells were detected by flow cytometry after gating on forward and side scatter to exclude cell debris. Cells were scanned and plotted for secondary antibody signal and PI signal. Data were analyzed using CXP analysis software.

MACS was used to enrich CD4-positive cells for sequence analysis. Cells were washed twice with PBS and incubated in 50 mM EDTA solution for 10 min at 37°C. All further steps were conducted on ice and with cold solutions. Cells were carefully resuspended in PBS to singularize them. After centrifugation at $300 \times g$ for 3 min at 4°C, cells were stained and separated on miniMACS MS columns following the manufacturer's instructions.

5.2.3. Immunofluorescence

For immunofluorescence experiments, cells were grown on coverslips. In experiments where the endogenous protein was depleted, transfection with plasmids coding for exogenous protein occurred 24 h after cell seeding and transfection with the I-SceI plasmid took place 60 h after cell seeding to initiate DNA damage induction from roughly 72 h after cell seeding. In experiments where downregulation of an endogenous protein was not necessary, I-SceI transfection occurred 24 h after cell seeding. Cells were harvested 72 h after I-SceI was first detected. Cells were treated with EdU and nocodazole 30 min prior to IR or cell harvest. EdU is a thymidine analog, and thus marks cells that progress through S phase, while nocodazole disrupts the spindle apparatus, and thus prevents cells from successfully completing mitosis and therefore progressing into G₁ phase. This procedure permits the analysis of cells damaged during G₁ phase and maintained in G₁ throughout repair time in IR-based experiments and the recognition of G₁ phase cells in reporter assay-based experiments.

For KU foci detection, cells were pre-extracted twice for 3 min with CSK buffer supplemented with 0.3 mg/ml RNase. Cells were then fixed for 15 min at RT with 2.5% formaldehyde/PBS or 4% paraformaldehyde and washed 3x with PBS. Cells were permeabilized for 10 min at 4°C with 0.2% TritonX-100/PBS/1% FCS and washed 3x with PBS/1% FCS. Cells were blocked for at least 1 h in 3% BSA/PBS/1% FCS or overnight in 0.5% BSA/PBS-T for detection of KU foci. Cells were stained with the primary AB in humid chambers overnight at 4°C or 2 to 4 h at RT for KU foci analysis (for primary antibody dilutions see Table 5.6, 5.7) in blocking solution. After 3x washing with PBS/1% FCS or 0.5% BSA/PBS-T, cells were stained for 1 h at RT in the dark with the secondary AB in PBS/1% FCS or 0.5% BSA/PBS-T (see Table 5.8). For KU foci, the stained samples were fixed with 2% paraformaldehyde for 10 min at RT to fix the secondary AB. Cells were washed 3x in PBS/1% FCS or 0.5% BSA/PBS-T. EdU incorporation was detected with EdU click kit following the manufacturer's instructions using Cy5 diluted at a 1:40 ratio. Cells were washed 3x in PBS and once in Aqua dest. before DAPI staining with 0.4 µg/ml DAPI/PBS for 4 min at RT. The coverslips were transferred to a microscope slide with mounting medium and sealed with nail polish. For KU foci analysis, mounting was performed with ProLong gold and images were captured within 48 h.

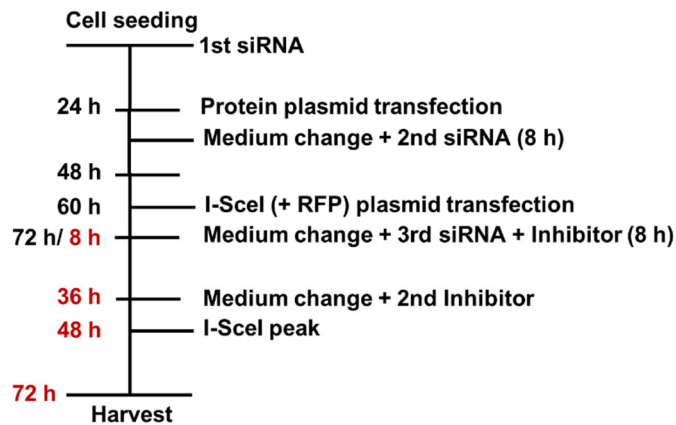


Figure 5.1 Workflow for reporter assay experiments

The first siRNA transfection took place during cell seeding. The exogenous protein plasmid was transfected 24 h after cell seeding. To reduce toxicity from the transfection reagent, the medium was changed and a second siRNA treatment was conducted to ensure downregulation of the endogenous protein. The I-SceI plasmid was transfected at 60 h after cell seeding and the first signs of I-SceI were detected 12 h later in a few cells. Cells were harvested for immunoblotting experiments to confirm downregulation by siRNA since DSB induction begins at this point. For all other experiments, the medium was changed 8 h (red) after I-SceI plasmid transfection and a third siRNA transfection and/or the first inhibitor treatment occurred. In experiments with inhibitor treatment, another medium change plus second inhibitor treatment was conducted 36 h (red) after I-SceI transfection. I-SceI expression peaked at 48 h (red) after I-SceI plasmid transfection and was observed in roughly 30% of cells. Cells were harvested 72 h after I-SceI transfection.

Cells were analyzed with a Zeiss microscope and Metafer software. The DAPI and EdU content were scanned and plotted, making it possible to select G₁ phase cells for further analysis. In experiments with exogenous tagged protein, cells were also scanned for the tag to facilitate the analysis of G₁ cells positive for the tagged protein. For foci analysis, the number of foci per cell was analyzed in at least 40 G₁ cells per sample. For reporter assay data, up to 10,000 cells (with a minimum of 2,000 cells) were scanned per condition. The intensities of DAPI, RFP (or a tag), and CD4 were detected and the quantity of cells positive for the reporter protein was analyzed in plasmid-transfected cells (see chapter 3.1.1). Alterations due to experimental conditions are mentioned where applicable. Images were captured with Metafer Isis or AxioVision software and analyzed with ImageJ. For KU foci, Z stacks were acquired by confocal laser scanning microscopy using a 100x immersion objective. Co-localization of KU80 with γ H2AX, pRPA, or RAD51 foci was analyzed using LAS AF lite software (dx < 20 nm for co-localization of signal intensity in line profile).

5.3. Biochemical methods

5.3.1. Protein extracts, immunoprecipitation, and immunoblotting

Protein extracts

All steps were conducted on ice and with cold solutions. Cells were washed twice with PBS, harvested with a cell scraper, and transferred into a falcon or reaction tube after resuspension.

After centrifugation at $300 \times g$ for 3 min at 4°C , cells were lysed using RIPA buffer to confirm knockdown efficiency and exogenous protein levels or lysis buffer for immunoprecipitation experiments together with sonification in an ultrasound bath twice for 1 min. The buffers were mixed with PhosphoStop and protease inhibitor following the manufacturer's instructions. The supernatant was transferred into a new reaction tube after centrifugation at $16,000 \times g$ for 30 min at 4°C . Protein concentration was determined using Bradford protein assay (absorption at 595 nm). Alternatively, 2x SDS buffer was used for cell lysis when testing the protein levels in generated KO cell lines.

Immunoprecipitation

$30 \mu\text{l}$ of protein G Dynabeads were washed with PBS and then incubated with 2 to $10 \mu\text{g}$ AB for 2 to 4 h at 4°C . The beads-AB complex was washed 3x with 0.1% BSA/PBS. After incubation with the cell extracts for 2 to 4 h at 4°C , the suspension was washed 3x with 0.1% Tween20/PBS, transferred to a new tube and washing buffer was removed after brief centrifugation. The beads-AB-protein complex was resuspended in $20 \mu\text{l}$ RIPA buffer with PhosphoStop and protease inhibitor and Laemmli buffer was added. Proteins were eluted by boiling at 99°C for 10 min. After brief centrifugation, the supernatant was used in SDS-PAGE.

Immunoblotting

Samples were prepared with 5x Laemmli buffer (unless they were harvested with 2x SDS buffer) and boiled for 5 min at 95°C or for 10 min at 80°C for large proteins ($> 250 \text{ kDa}$). SDS-PAGE was performed to separate the proteins according to size. Electrophoresis buffer was used and gels were run at 180 V or alternatively at 25 to 50 mA. For western blotting, a PVDF membrane was activated in methanol and then equilibrated in transfer buffer. After completion of the SDS-PAGE, the gel was fixed on a membrane and placed in between filter paper and sponges soaked in transfer buffer. The stack was sealed after removing air bubbles and the blotting aperture was assembled with the membrane facing the anode. The western blot was conducted at 300 mA for 90 min, 3 h, or 4 h or at 80 mA overnight depending on the size of the target protein. When using the semi-dry western blot aperture, blotting was performed at 0.8 A for 1 to 2 h. The membrane was blocked in 5% milk/TBS-T for experiments where knockdown efficiencies and exogenous protein levels were confirmed or for immunoprecipitation experiments. After brief washing in TBS-T, the membrane was incubated in primary AB (AB solutions see Table 5.6) in 1, 3, or 5% milk/TBS-T or 5% BSA/TBS-T overnight at 4°C . After 3 wash steps, the membrane was incubated in secondary IgG-HRP-coupled AB in 1% milk/TBS-T for 1 h at RT. The membrane was washed 3x. For detection, western blotting substrates were mixed and incubated on the membrane following the manufacturer's instructions. The emitted

chemiluminescent signal was detected using ChemiSmart5000 or Fusion FX imaging system. Images were analyzed using ImageJ.

5.3.2. Tandem affinity purification mass spectrometry (TAP-MS)

HEK293T cells stably expressing exogenous SFB-tagged protein were collected on ice with cell scrapers and centrifuged at $400 \times g$ for 4 min at 4°C . The pellet was washed with PBS and centrifugation repeated. Cells were lysed in NETN/pepstatin/aprotinin for 30 min with rotation at 4°C . The suspension was centrifuged at $22,000 \times g$ for 20 min at 4°C . The supernatant was transferred into a clean falcon tube and the chromatin fraction was collected in 1.5 ml reaction tubes and frozen at -80°C . Streptavidin beads were washed twice with NETN buffer, added to the supernatant and incubated overnight at 4°C on a shaker. The suspension was centrifuged at $400 \times g$ for 3 min, beads were resuspended in 1 ml of fresh lysis buffer, and transferred to a 1.5 ml reaction tube. Samples were centrifuged at $1,000 \times g$ for 1 min and beads washed twice with the buffer. After the remaining buffer was completely removed, the bound protein was eluted by incubation of the beads in 1 ml of 2 mg/ml biotin in lysis buffer on a shaker at 4°C for 2 h. After centrifugation at $1,000 \times g$ for 2 min, the supernatant was transferred to a fresh tube and the elution step was repeated with another $800 \mu\text{l}$ of biotin solution. $120 \mu\text{l}$ of S beads were washed twice with NETN buffer, the first eluate was added and beads were incubated at 4°C for 2 h with rotation. The second eluate was added and S beads were incubated again at 4°C for 2 h with rotation. Beads were centrifuged at $1,000 \times g$ for 1 min and washed 4x with lysis buffer. The lysis buffer was completely removed and $30 \mu\text{l}$ 2x SDS buffer was added to elute the protein from the beads with boiling for 10 min at 99°C . Samples were briefly run on SDS-PAGE for a quarter of the running gel. The gel was stained overnight with Coomassie blue staining solution and subsequently destained for several hours with Coomassie destaining solution. Protein bands were excised and transferred to a fresh 1.5 ml reaction tube for analysis at the Taplin Mass Spectrometry Facility, Harvard Medical School.

For phosphorylation MS data, the statistical analysis (Ascore calculation) was performed by the Taplin Mass Spectrometry Facility²⁷ and the provided probabilities were analyzed to determine certain (Ascore = 1,000), likely (Ascore > 18), unlikely (Ascore > 0), and no phosphorylation at Ser, Thr, and Tyr sites. For analysis, sites showing no phosphorylation under a certain condition were given the value 0.1 (rationale: no phosphorylation is less than the smallest value Ascore of 1 but even when no phosphorylation was detected, phosphorylation is still generally possible). For each condition, the highest provided Ascore was used. For interaction MS data⁸⁴, associated proteins and likely interaction partners were determined. The number of minimum interacting peptides of a protein identified by MS to have been co-precipitated with the purified protein of interest was used for analysis because the maximum interacting peptide

number can be highly inaccurate (especially for large proteins). Conditions where no interaction was observed were assigned 0.1 for further analysis (rationale: no interaction is smaller than 1 interacting molecule). Next, the ratio of the irradiated sample compared to the unirradiated condition was calculated. The calculated ratios were used to compare conditions and to observe the development of an interaction depending on the different experimental conditions.

5.4. Molecular biological methods

5.4.1. DNA purification, amplification, digestion, and ligation

DNA extraction, PCR, and agarose gel electrophoresis

DNA isolation and purification after MACS enrichment of CD4-positive cells was performed using a MasterPure complete DNA & RNA purification kit, following the manufacturer's instructions. All other DNA isolation was conducted using the PureLink genomic DNA mini kit. To amplify the DNA, polymerase chain reaction (PCR) was conducted using polymerase kits following the manufacturer's instructions. Phusion polymerase or Q5 polymerase were used for error-free DNA amplification after MACS with annealing temperatures ascertained using the software on the vendor's homepage. Taq polymerase was used for colony PCR screening. Pfu turbo or Herc polymerases were used for mutagenesis PCR at annealing temperatures of 54°C and 56°C, respectively. KOD hot start polymerase was used for all other applications with annealing temperatures ranging from 50°C to 56°C. Agarose gels of 1% were used to separate DNA fragments according to their size. After heating 100 ml TAE buffer with 1 g agarose in the microwave, 5 μ l RotiSafe or ethidium bromide was added. Electrophoresis was performed at 10 V per 1 cm of gel length. ChemiSmart5000 aperture was used for the detection of DNA bands.

Mutagenesis, digestion, ligation, and Gateway cloning

Mutagenesis PCR was performed using Pfu turbo polymerase following the manufacturer's instructions. After mutagenesis PCR, template plasmid was removed by Dpn1 digestion for 1 h at 37°C. For linearization of vectors, dephosphorylation and digestion were performed simultaneously with restriction enzymes and alkaline phosphatase following the manufacturer's instructions. Ligation was performed using T4 DNA ligase or pGEM-T easy cloning system following the manufacturer's instructions. The molar insert/vector ratio of 3:1 was used to calculate the components of the ligation for most ligation reactions but was adjusted to a higher insert amount if necessary. The gateway cloning system was used following the manufacturer's instructions. BP donor vectors were created for ARTEMIS, BRCA1, CtIP, and EXO1. C-terminal

SFB-tagged LR plasmids were generated for CtIP, BRCA1, and ARTEMIS. An *N*-terminal SFB-tagged LR plasmid was generated for EXO1.

Interchanging gRNA sequences in the GeCKO CRISPR/Cas9 system

The CRISPR gRNA plasmid was digested with BsmBI and the 11 kb plasmid was purified using agarose gel electrophoresis. Oligonucleotides encoding the target gRNA sequence were phosphorylated and annealed with T4 PNK in the thermocycler at 37°C for 30 min, then at 95°C for 5 min with a ramp down to 25°C (5°C per min). Linearized plasmid and annealed oligonucleotides were ligated with T4 ligase for at least 2 h at RT.

5.4.2. Bacteria preparation, transformation, plasmid isolation, and sequence analysis

Competent *E. coli* DH5 α were prepared by the rubidium chloride method. RbCl-competent DH5 α cells were grown overnight at 37°C with rotation at 220 rpm in 5 ml SOB medium. 1 ml of overnight culture was used to inoculate 100 ml SOB medium. During incubation at 37°C and rotation at 220 rpm, absorption at 550 nm was regularly measured until an OD of 0.5 was reached. All further steps were conducted on ice using ice-cold solutions. Cells were centrifuged at 2,000 \times *g* for 10 min at 4°C and the pellet was resuspended in 12.5 ml solution 1. After a second centrifugation step, the pellet was resuspended in 8 ml solution 2. 1.5 ml reaction tubes were prepared with 100 μ l cell suspension and snap frozen in liquid nitrogen for storage at –80°C.

For bacteria transformation, DH5 α were thawed on ice and 10 ng plasmid DNA or 10 μ l ligation sample were added, resuspended, and incubated on ice for 30 min. After 90 sec heat shock at 42°C, a 5 min incubation on ice followed. 900 μ l LB medium was added and the cells were incubated for 1 h at 37°C with rotation at 220 rpm or in a water bath. After centrifugation for 1 min at 10,000 \times *g*, the medium was removed. Cells were resuspended in 25 μ l 0.4 M IPTG and 20 μ l 50 μ g/ μ l X-Gal in DMSO was added for α -complementation or cells were resuspended in 50 μ l LB medium for all other experiments. Cells were plated on 30 mg/ml kanamycin or 50 mg/ml ampicillin agar and incubated at 37°C overnight. Colonies were picked and incubated in 10 μ l LB medium at 4°C for short-term storage or a glycerol stock was prepared with 850 μ l 30% glycerol and 150 μ l of a 10 ml bacterial culture grown overnight at 37°C with rotation at 220 rpm for long term storage at –80°C. Plasmid maxi-preparation was conducted using peqGold Xchange plasmid maxi EF kit and plasmid mini-preparation was conducted using either ZR plasmid mini prep classic or QIAPrep spin mini prep kit following the manufacturer's instructions. DNA concentration was determined at absorption of 260 nm with Implem's nano photometer.

For sequencing, samples were mixed with the corresponding primer according to instructions and sent for sequencing to Eurofins. For sequencing after cloning into pGEM-T easy vector, the T7 forward primer was used. The sequences were analyzed with MEGA5.1 for sequence analysis after MACS separation or with BLASTN for CRISPR/Cas9 generated KOs.

5.5. Analysis

For general analysis, procedure, and presentation of the results, the guidelines of Cumming et al. (2007) were followed. All plots were created with Origin8.5. Key experiments are shown in the results part of this thesis (chapter 3) while supporting data, preliminary experiments, and raw data can be found in the appendix (chapters 9.1). Experiments within one cell line were treated as independent in statistical analyses because cellular biology on the laboratory scale aims to propose a model based on the findings within a cell line³⁹⁰. Therefore, the experimental procedure was performed independently: experiments were performed at least one week apart, fresh chemicals/reagents were prepared, cells were used at different passaging stages, and cell lines were freshly thawed regularly for experiments.

5.5.1. Quantification and descriptive statistics

For reporter assay analysis, between 2,000 and up to 10,000 cells were scanned with the microscope software Metafer4 and only damage-induced cells were analyzed (meaning I-SceI-positive cells, identified by RFP or a tagged protein; for details see chapters 3.1.1, 5.2.5). Each experiment was performed in duplicate to counteract the variability frequently observed in reporter assay experiments. For foci assay analyses, at least 40 cells were analyzed per experiment (for details see chapters 3.1.2, 5.2.5).

The majority of the data in this study compares untreated and treated samples. To describe the magnitude of the effect between a treated and an untreated sample, the effect size was utilized^{284,372}. The effect size was determined by Cohen's *d* with GPower 3.1, which was calculated to estimate the difference of the means over the common standard deviation (*SD*) of two samples. Additionally, the effect size was used to estimate the sample size *a priori* (power > 0.9) with data obtained during the master's thesis³⁵, preliminary data, and published data utilizing the same reporter assay³²²(for further details see chapter 3.1.1). According to the *a priori* sample size calculations, all reporter assay data were obtained from $n = 8$ or $n = 16$ independent experiments. For foci analysis, data were obtained from $n = 5$ independent experiments. Sequence analysis was conducted with data from $n = 4$ or $n = 5$ experiments and a total of at least 39 sequences per condition. All other data were derived from at least $n = 3$ independent experiments.

The majority of the data are displayed in dot plots, which show the mean value of all independent experiments as well as the individual data points. Error bars in the dot plots show the confidence interval at the 95% confidence level (95% CI) or the *SD*. Background data were generally not subtracted (for details see chapter 3.1.2). For $n > 20$ samples, the data were additionally displayed in box plots to allow easy interpretation of the distribution ²²⁰. The boxplots show the median, mean, and 25th and 75th quartile. The whiskers represent the 1st and 99th percentile, while plotted data points are the outliers. Additionally, histograms were used for large sample sizes to visualize normal distribution.

5.5.2. Inferential statistics

Origin8.5 was used for all inferential statistic calculations. The confidence interval of the mean was calculated with a confidence level of 95% using the *t*-distribution. All confidence intervals were calculated this way, even if the data was not normally distributed. Wang (2001) shows that this approach is still advantageous for small sample sizes compared to the Bootstrap method, which would typically be used for confidence interval calculations of non-normally distributed data. For small sample sizes, the Shapiro-Wilk test was performed to test data for a normal distribution, which would allow the usage of a parametric test. Analysis of all WT data obtained during this work revealed that the data generally follow a normal distribution (e.g. Figure S9.5 a). However, some samples at the significance level of 0.05 were not from a normally distributed population. Usually, this could be attributed to either one outlier in a data set or due to the application of a siRNA with varying efficiencies, which resulted in a bimodal distribution. Another reason for a non-normal distribution was an experimental condition where no positive events occurred. In any of these cases, nonparametric tests could not be performed either because such data sets were compared with normally distributed data sets. Therefore, statistical analysis was forgone for such samples, except to involve them in the overall analysis by ANOVA (see below) when comparing the WT to more than one normally-distributed condition to prevent an increase in α -error.

To compare the means of two independent normally distributed samples, two-sample Student's *t*-test was performed. For other normally distributed data sets of groups larger than two, a one-way ANOVA was performed to assess the relative size of variance among group means ²¹⁰. ANOVA was used for such groups larger than two to prevent an α -error increase relative to the pre-set α -level, which repeated multiple tests would lead to. Subsequently, Levene's test was performed to establish the homogeneity of the population variances. In many cases, the population variances were different at the 0.05 significance level. As ANOVA is robust to differing variances if n is equal ⁴³⁶, the sample sizes in the experiments were always identical

within a group. The one-way ANOVA was followed by stringent Bonferroni correction to examine which group means were significantly different.

6. References

1. Abdollahi E, Taucher-Scholz G, Durante M, Jakob B. Upgrading the GSI beamline microscope with a confocal fluorescence lifetime scanner to monitor charged particle induced chromatin decondensation in living cells. 2015;365:626–630.
2. Abraham RT. Cell cycle checkpoint signaling through the ATM and ATR kinases. 2001;15:2177–2196. doi:10.1101/gad.914401.DNA
3. Acs K, Luijsterburg MS, Ackermann L, Salomons F a, Hoppe T, Dantuma NP. The AAA-ATPase VCP/p97 promotes 53BP1 recruitment by removing L3MBTL1 from DNA double-strand breaks. 2011;18(12):1345–1350. doi:10.1038/nsmb.2188
4. Adams MM, Carpenter PB. Tying the loose ends together in DNA double strand break repair with 53BP1. 2006;1(February):19. doi:10.1186/1747-1028-1-19
5. Aguilera A, García-Muse T. R Loops: From Transcription Byproducts to Threats to Genome Stability. 2012;46(2):115–124. doi:10.1016/j.molcel.2012.04.009
6. Ahnesorg P, Smith P, Jackson SP. XLF interacts with the XRCC4-DNA ligase IV complex to promote DNA nonhomologous end-joining. 2006;124(2):301–13. doi:10.1016/j.cell.2005.12.031
7. Ahrabi S, Sarkar S, Pfister SX, Pirovano G, Higgins GS, Porter ACG, Humphrey TC. A role for human homologous recombination factors in suppressing microhomology-mediated end joining. 2016;44(12). doi:10.1093/nar/gkw326
8. Al-Hakim A, Escribano-Diaz C, Landry MC, Donnell L, Panier S, Szilard RK, Durocher D. The ubiquitous role of ubiquitin in the DNA damage response. 2010;9(12):1229–1240. doi:10.1016/j.dnarep.2010.09.011
9. Alagoz M, Katsuki Y, Ogiwara H, Ogi T, Shibata A, Kakarougkas A, Jeggo P. SETDB1, HP1 and SUV39 promote repositioning of 53BP1 to extend resection during homologous recombination in G2 cells. 2015;43(16):7931–7944. doi:10.1093/nar/gkv722
10. Anand R, Ranjha L, Cannavo E, Cejka P. Phosphorylated CtIP Functions as a Co-factor of the MRE11-RAD50-NBS1 Endonuclease in DNA End Resection. 2016;64:940–950. doi:10.1016/j.molcel.2016.10.017
11. Andrea J Hartlerode, Morgan MJ, Wu Y, Buis J, Ferguson DO. Recruitment and activation of the ATM kinase in the absence of DNA-damage sensors. 2015;22(9):736–743. doi:10.1038/nsmb.3072
12. Aparicio T, Baer R, Gottesman M, Gautier J. MRN, CtIP and BRCA1 mediate repair of Topoisomerase II-DNA adducts. 2016;212(4). doi:10.1083/jcb.201504005
13. Arnaudeau C, Lundin C, Helleday T. DNA double-strand breaks associated with replication forks are predominantly repaired by homologous recombination involving an exchange mechanism in mammalian cells. 2001;307(5):1235–45. doi:10.1006/jmbi.2001.4564
14. van Attikum H, Gasser SM. Crosstalk between histone modifications during the DNA damage response. 2009;19(5):207–17. doi:10.1016/j.tcb.2009.03.001
15. Averbeck NB, Ringel O, Herrlitz M, Jakob B, Durante M, Taucher-Scholz G. DNA end resection is needed for the repair of complex lesions in G1-phase human cells. 2014;13(16):2509–2516. doi:10.4161/15384101.2015.941743
16. Awate S, Brosh RM. Interactive roles of DNA helicases and translocases with the single-stranded DNA binding protein RPA in nucleic acid metabolism. 2017;18(6). doi:10.3390/ijms18061233
17. Aymard F, Bugler B, Schmidt CK, Guillou E, Caron P, Briois S, Iacovoni JS, Daburon V, Miller KM, Jackson SP, et al. Transcriptionally active chromatin recruits homologous recombination at DNA double-strand breaks. 2014;21(4):366–74. doi:10.1038/nsmb.2796
18. Bahassi EM, Conn CW, Myer DL, Hennigan RF, McGowan CH, Sanchez Y, Stambrook PJ. Mammalian Polo-like kinase 3 (Plk3) is a multifunctional protein involved in stress response pathways. 2002;21(43):6633–40. doi:10.1038/sj.onc.1205850
19. Bahassi EM, Ovesen JL, Riesenberga L, Bernstein WZ, Hasty PE, Stambrook PJ. The checkpoint kinases Chk1 and Chk2 regulate the functional associations between hBRCA2 and Rad51 in response to DNA damage. 2008;27(28):3977–3985. doi:10.1038/onc.2008.17
20. Bai XT, Moles R, Chaib-Mezrag H, Nicot C. Small PARP inhibitor PJ-34 induces cell cycle arrest and apoptosis of adult T-cell leukemia cells. 2015;8(1):117. doi:10.1186/s13045-015-0217-2
21. Bakkenist CJ, Kastan MB. DNA damage activates ATM through intermolecular autophosphorylation and dimer dissociation. 2003;421(6922):499–506. doi:10.1038/nature01368
22. Bakr A, Köcher S, Volquardsen J, Petersen C, Borgmann K, Dikomey E, Rothkamm K, Mansour WY. Impaired 53BP1/RIF1 DSB mediated end-protection stimulates CtIP-dependent end resection and switches the repair to PARP1-dependent end joining in G1. 2016. doi:10.18632/oncotarget.11023
23. Baldock RA, Day M, Wilkinson OJ, Cloney R, Jeggo PA, Oliver AW, Watts FZ, Pearl LH. ATM Localization and Heterochromatin Repair Depend on Direct Interaction of the 53BP1-BRCT2 Domain with γH2AX. 2015;13:2081–2089. doi:10.1016/j.celrep.2015.10.074
24. Bardwell PD, Woo CJ, Wei K, Li Z, Martin A, Sack SZ, Parris T, Edelmann W, Scharff MD. Altered somatic hypermutation and reduced class-switch recombination in exonuclease 1-mutant mice. 2004;5(2):224–229. doi:10.1038/ni1031
25. Barton O, Naumann SC, Diemer-Biehls R, Künzel J, Steinlage M, Conrad S, Makharashvili N, Wang J, Feng L, Lopez BS, et al. Polo-like kinase 3 regulates CtIP during DNA double-strand break repair in G1. 2014;206(7):877–94. doi:10.1083/jcb.201401146
26. Bassing CH, Swat W, Alt FW. The mechanism and regulation of chromosomal V(D)J recombination. 2002;109(2 SUPPL. 1):45–55. doi:10.1016/S0092-8674(02)00675-X
27. Beausoleil SA, Villén J, Gerber SA, Rush J, Gygi SP. A probability-based approach for high-throughput protein phosphorylation analysis and site localization. 2006;24(10):1285–1292. doi:10.1038/nbt1240
28. Beck A, Wurch T, Bailly C, Corvaia N. Strategies and challenges for the next generation of therapeutic antibodies. 2010;10(5):345–52. doi:10.1038/nri2747
29. Beckwitt EC, Kong M, Houten B Van. Studying protein-DNA interactions using atomic force microscopy. 2017.

doi:10.1016/j.semcd.2017.06.028

30. Bekker-Jensen S, Lukas C, Melander F, Bartek J, Lukas J. Dynamic assembly and sustained retention of 53BP1 at the sites of DNA damage are controlled by Mdc1/NFBD1. 2005;170(2):201–11. doi:10.1083/jcb.200503043
31. Bekker-Jensen S, Mailand N. Assembly and function of DNA double-strand break repair foci in mammalian cells. 2010;9(12):1219–1228. doi:10.1016/j.dnarep.2010.09.010
32. Bensimon A, Aebersold R, Shiloh Y. Beyond ATM: The protein kinase landscape of the DNA damage response. 2011;585(11):1625–1639. doi:10.1016/j.febslet.2011.05.013
33. Bétermier M, Bertrand P, Lopez BS. Is Non-Homologous End-Joining Really an Inherently Error-Prone Process? 2014;10. doi:10.1371/journal.pgen.1004086
34. Beucher A, Birraux J, Tchouandong L, Barton O, Shibata A, Conrad S, Goodarzi AA, Krempler A, Jeggo PA, Löbrich M. ATM and Artemis promote homologous recombination of radiation-induced DNA double-strand breaks in G2. 2009;28(21):3413–27. doi:10.1038/emboj.2009.276
35. Biehs R. Analyse NHEJ-induzierter genomischer Umlagerungen. 2013.
36. Biehs R, Steinlage M, Barton O, Juhasz S, Kunzel J, Spies J, Shibata A, Jeggo P, Löbrich M. DNA double-strand break resection occurs during non-homologous end-joining in G1 but is distinct to resection during homologous recombination in G2. 2017;65:1–14. doi:10.1016/j.molcel.2016.12.016
37. Binz SK, Sheehan AM, Wold MS. Replication protein A phosphorylation and the cellular response to DNA damage. 2004;3(8–9):1015–24. doi:10.1016/j.dnarep.2004.03.028
38. Black SJ, Kashkina E, Kent T, Pomerantz RT. DNA polymerase Theta: A unique multifunctional end-joining machine. 2016;7. doi:10.3390/genes7090067
39. Blanpain C, Mohrin M, Sotiropoulou PA, Passegué E. DNA-damage response in tissue-specific and cancer stem cells. 2011;8(1):16–29. doi:10.1016/j.stem.2010.12.012
40. Block WD, Yu Y, Merkle D, Gifford JL, Ding Q, Meek K, Lees-Miller SP. Autophosphorylation-dependent remodeling of the DNA-dependent protein kinase catalytic subunit regulates ligation of DNA ends. 2004;32(14):4351–7. doi:10.1093/nar/gkh761
41. Bochkareva E, Belegu V, Korolev S, Bochkarev A. Structure of the major single-stranded DNA-binding domain of replication protein A suggests a dynamic mechanism for DNA binding. 2001;20(3):612–8. doi:10.1093/emboj/20.3.612
42. Bochkareva E, Korolev S, Lees-Miller SP, Bochkarev A. Structure of the RPA trimerization core and its role in the multistep DNA-binding mechanism of RPA. 2002;21(7):1855–1863. doi:10.1093/emboj/21.7.1855
43. Bohgaki M, Bohgaki T, El S, Srikumar T, Maire G. RNF168 ubiquitylates 53BP1 and controls its response to DNA double-strand breaks. 2013;110(52):20982–20987. doi:10.1073/pnas.1320302111/-/DCSupplemental.www.pnas.org/cgi/doi/10.1073/pnas.1320302111
44. Bohgaki T, Bohgaki M, Hakem R. DNA double-strand break signaling and human disorders. 2010;1(1):15. doi:10.1186/2041-9414-1-15
45. van den Boom J, Wolf M, Weimann L, Schulze N, Li F, Kaschani F, Riemer A, Zierhut C, Kaiser M, Iliakis G, et al. VCP/p97 Extracts Sterically Trapped Ku70/80 Rings from DNA in Double-Strand Break Repair. 2016;64:189–198. doi:10.1016/j.molcel.2016.08.037
46. Bosma GC, Kim J, Urich T, Fath DM, Cotticelli MG, Ruetsch NR, Radic MZ, Bosma MJ. DNA-dependent protein kinase activity is not required for immunoglobulin class switching. 2002;196(11):1483–1495. doi:10.1084/jem.20001871
47. Bothmer A, Robbiani DF, Feldhahn N, Gazumyan A, Nussenzweig A, Nussenzweig MC. 53BP1 regulates DNA resection and the choice between classical and alternative end joining during class switch recombination. 2010;207(4):855–65. doi:10.1084/jem.20100244
48. Bothmer A, Robbiani DF, Di Virgilio M, Bunting SF, Klein IA, Feldhahn N, Barlow J, Chen HT, Bosque D, Callen E, et al. Regulation of DNA End Joining, Resection, and Immunoglobulin Class Switch Recombination by 53BP1. 2011;42(3):319–329. doi:10.1016/j.molcel.2011.03.019
49. Botuyan MV, Lee J, Ward IM, Kim JE, Thompson JR, Chen J, Mer G. Structural Basis for the Methylation State-Specific Recognition of Histone H4-K20 by 53BP1 and Crb2 in DNA Repair. 2006;127(7):1361–1373. doi:10.1016/j.cell.2006.10.043
50. Boutou E, Louka M, Pappa V, Stürzbecher H-W, Knippschild U, Vlachodimitropoulos D, Vorgias CE. Ubiquitination — An Evolving Role in DNA Repair. In: Advances in DNA repair. 2015. p. 81–94.
51. Boveri T. Concerning the Origin of Malignant Tumours by Theodor Boveri. Translated and annotated by Henry Harris. 2008;121:1–84. doi:10.1242/jcs.025742
52. Bretones G, Delgado MD, León J. Myc and cell cycle control. 2015;1849(5):506–516. doi:10.1016/j.bbagr.2014.03.013
53. Broderick R, Nieminuszczy J, Baddock HT, Deshpande RA, Gileadi O, Paull TT, Mchugh PJ, Niedzwiedz W. EXD2 promotes homologous recombination by facilitating DNA end resection. 2016;18:271–280. doi:10.1038/ncb3303
54. Brouwer I, Sitters G, Candelli A, Heerema SJ, Heller I, Melo de AJ, Zhang H, Normanno D, Modesti M, Peterman EJG, et al. Sliding sleeves of XRCC4–XLF bridge DNA and connect fragments of broken DNA. 2016;535:566–569. doi:10.1038/nature18643
55. Brown JS, Jackson SP. Ubiquitylation, neddylation and the DNA damage response. 2015;5. doi:10.1098/rsob.150018
56. Brown JS, Lukashchuk N, Sczaniecka-Clift M, Britton S, le Sage C, Calsou P, Beli P, Galanty Y, Jackson SP. Neddylation Promotes Ubiquitylation and Release of Ku from DNA-Damage Sites. 2015;11:704–714. doi:10.1016/j.celrep.2015.03.058
57. Bunting SF, Callén E, Wong N, Chen H-T, Polato F, Gunn A, Bothmer A, Feldhahn N, Fernandez-Capetillo O, Cao L, et al. 53BP1 Inhibits Homologous Recombination in Brca1-Deficient Cells by Blocking Resection of DNA Breaks. 2010;141(2):243–254. doi:10.1016/j.cell.2010.03.012
58. Burma S, Chen BP, Murphy M, Kurimasa A, Chen DJ. ATM phosphorylates histone H2AX in response to DNA double-strand breaks. 2001;276(45):42462–7. doi:10.1074/jbc.C100466200
59. Butler LR, Densham RM, Jia J, Garvin AJ, Stone HR, Shah V, Weekes D, Festy F, Beesley J, Morris JR. The proteasomal de-

- ubiquitinating enzyme POH1 promotes the double-strand DNA break response. 2012;31(19):3918–34. doi:10.1038/emboj.2012.232
60. Campisi J, d'Adda di Fagagna F. Cellular senescence: when bad things happen to good cells. 2007;8(9):729–740. doi:10.1038/nrm2233
61. Cannavo E, Cejka P. Sae2 promotes dsDNA endonuclease activity within Mre11-Rad50-Xrs2 to resect DNA breaks. 2014;514(7520):122–125. doi:10.1038/nature13771
62. Cannavo E, Cejka P, Kowalczykowski SC. Relationship of DNA degradation by *Saccharomyces cerevisiae* exonuclease 1 and its stimulation by RPA and Mre11-Rad50-Xrs2 to DNA end resection. 2013;110(18):E1661–8. doi:10.1073/pnas.1305166110
63. Capp J-P, Boudsocq F, Bertrand P, Laroche-Clary A, Pourquier P, Lopez BS, Cazaux C, Hoffmann J-S, Canitrot Y. The DNA polymerase lambda is required for the repair of non-compatible DNA double strand breaks by NHEJ in mammalian cells. 2006;34(10):2998–3007. doi:10.1093/nar/gkl380
64. Caron P, Choudhary J, Clouaire T, Bugler B, Daburon V, Aguirrebengoa M, Mangeat T, Iacovoni JS, Álvarez-Quilón A, Cortés-Ledesma F, et al. Non-redundant Functions of ATM and DNA-PKcs in Response to DNA Double-Strand Breaks. 2015;13(8):1598–1609. doi:10.1016/j.celrep.2015.10.024
65. Carson CT, Schwartz R a, Stracker TH, Lilley CE, Lee D V, Weitzman MD. The Mre11 complex is required for ATM activation and the G2/M checkpoint. 2003;22(24):6610–20. doi:10.1093/emboj/cdg630
66. Castillo A, Paul A, Sun B, Huang TH, Wang Y, Yazinski SA, Tyler J, Li L, You MJ, Zou L, et al. The BRCA1-Interacting Protein Abraxas Is Required for Genomic Stability and Tumor Suppression. 2014;8(3):807–817. doi:10.1016/j.celrep.2014.06.050
67. Cejka P. DNA End Resection: Nucleases Team Up with the Right Partners to Initiate Homologous Recombination. 2015;290(38):22931–22938. doi:10.1074/jbc.R115.675942
68. Cescutti R, Negrini S, Kohzaki M, Halazonetis TD. TopBP1 functions with 53BP1 in the G1 DNA damage checkpoint. 2010;29(21):3723–3732. doi:10.1038/emboj.2010.238
69. Chakraborty A, Tapryal N, Venkova T, Horikoshi N, Pandita RK, Sarker AH, Sarkar PS, Pandita TK, Hazra TK. Classical non-homologous end-joining pathway utilizes nascent RNA for error-free double-strand break repair of transcribed genes. 2016;7. doi:10.1038/ncomms13049
70. Chang HHY, Lieber MR. Structure-Specific nuclease activities of Artemis and the Artemis: DNA-PKcs complex. 2016. doi:10.1093/nar/gkw456
71. Chang HHY, Pannunzio NR, Adachi N, Lieber MR. Non-homologous DNA end joining and alternative pathways to double-strand break repair. 2017;18(8):495–506. doi:10.1038/nrm.2017.48
72. Chang HHY, Watanabe G, Gerodimos CA, Ochi T, Blundell TL, Jackson SP, Lieber MR. Different DNA end configurations dictate which NHEJ components are most important for joining efficiency. 2016. doi:10.1074/jbc.M116.752329
73. Chang HHY, Watanabe G, Lieber MR. Unifying the DNA end-processing roles of the artemis nuclease: Ku-dependent Artemis resection at blunt DNA ends. 2015;290(40):24036–24050. doi:10.1074/jbc.M115.680900
74. Chanut P, Britton S, Coates J, Jackson SP, Calsou P. Coordinated nuclease activities counteract Ku at single-ended DNA double-strand breaks. 2016;7. doi:10.1038/ncomms12889
75. Chapman JR, Taylor MRG, Boulton SJ. Playing the end game: DNA double-strand break repair pathway choice. 2012;47(4):497–510. doi:10.1016/j.molcel.2012.07.029
76. Chase D, Feng Y, Hanshaw B, Winkles JA, Longo DL, Ferris DK. Expression and phosphorylation of fibroblast-growth-factor-inducible kinase (Fnk) during cell-cycle progression. 1998;333:655–60.
77. Chen JJ, Silver S, Cantor S, Livingston DM, Scully R. BRCA1, BRCA2, and Rad51 operate in a common DNA damage response pathway. 1999;59(7 Suppl):1752s–1756s.
78. Chen L, Nievera CJ, Lee AY-LY-L, Wu X. Cell cycle-dependent complex formation of BRCA1.CtIP.MRN is important for DNA double-strand break repair. 2008;283(12):7713–20. doi:10.1074/jbc.M710245200
79. Cheng Q, Barboule N, Frit P, Gomez D, Bombarde O, Couderc B, Ren GS, Salles B, Calsou P. Ku counteracts mobilization of PARP1 and MRN in chromatin damaged with DNA double-strand breaks. 2011;39(22):9605–9619. doi:10.1093/nar/gkr656
80. Chi KR. The dark side of the human genome. 2016;538. doi:10.1038/538275a
81. Chi Y, Welcker M, Hizli AA, Posakony JJ, Aebersold R, Clurman BE. Identification of CDK2 substrates in human cell lysates. 2008;9(10):R149. doi:10.1186/gb-2008-9-10-r149
82. Cohen J. Statistical power analysis for the behavioral sciences. Seond Edit. Lawrence Erlbaum Associates; 1988.
83. Coleman KA, Greenberg RA. The BRCA1-RAP80 complex regulates DNA repair mechanism utilization by restricting end resection. 2011;286(15):13669–80. doi:10.1074/jbc.M110.213728
84. Collins MO, Choudhary JS. Mapping multiprotein complexes by affinity purification and mass spectrometry. 2008;19(4):324–330. doi:10.1016/j.copbio.2008.06.002
85. Collis SJ, DeWeese TL, Jeggo PA, Parker AR. The life and death of DNA-PK. 2005;24(6):949–961. doi:10.1038/sj.onc.1208332
86. Conaway RC, Conaway JW. The INO80 chromatin remodeling complex in transcription, replication and repair. 2009;34(2):71–77. doi:10.1016/j.tibs.2008.10.010
87. Connell-Crowley L, Harper JW, Goodrich DW. Cyclin D1/Cdk4 regulates retinoblastoma protein-mediated cell cycle arrest by site-specific phosphorylation. 1997;8(2):287–301.
88. Cooper MP, Machwe A, Orren DK, Brosh RM, Ramsden D, Bohr VA. Ku complex interacts with and stimulates the Werner protein. 2000;14(8):907–912. doi:10.1101/GAD.14.8.907
89. Costelloe T, Louge R, Tomimatsu N, Mukherjee B, Martini E, Khadaroo B, Dubois K, Wiegant WW, Thierry A, Burma S, et al. The yeast Fun30 and human SMARCAD1 chromatin remodellers promote DNA end resection. 2012:1–6. doi:10.1038/nature11353
90. Couto CAM, Wang HY, Green JCA, Kiely R, Siddaway R, Borer C, Pears CJ, Lakin ND. PARP regulates nonhomologous end

- joining through retention of Ku at double-strand breaks. 2011;194(3):367–375. doi:10.1083/jcb.201012132
91. Cox LS, Clancy DJ, Boubriak I, Saunders RDC. Modeling Werner syndrome in *Drosophila melanogaster*: Hyper-recombination in flies lacking WRN-like exonuclease. 2007;1119(1):274–288. doi:10.1196/annals.1404.009
92. Croteau DL, Popuri V, Opresko PL, Bohr VA. Human RecQ helicases in DNA repair, recombination, and replication. 2014;83:519–52. doi:10.1146/annurev-biochem-060713-035428
93. Cruz-García A, Lopez-Saavedra A, Huertas P. BRCA1 accelerates CtIP-mediated DNA-end resection. 2014;9(2):451–459. doi:10.1016/j.celrep.2014.08.076
94. Cumming G, Fidler F, Vaux DL. Error bars in experimental biology. 2007;177(1):7–11. doi:10.1083/jcb.200611141
95. D'Amours D, Jackson SP. The Mre11 complex: at the crossroads of dna repair and checkpoint signalling. 2002;3(5):317–27. doi:10.1038/nrm805
96. Daley JM, Sung P. 53BP1, BRCA1, and the choice between recombination and end joining at DNA double-strand breaks. 2014;34(8):1380–8. doi:10.1128/MCB.01639-13
97. Daniel JA, Santos MA, Wang Z, Zang C, Schwab KR, Jankovic M, Filsuf D, Chen H-T, Gazumyan A, Yamane A, et al. PTIP Promotes Chromatin Changes Critical for Immunoglobulin Class Switch Recombination. 2010;329(5994):917–923. doi:10.1126/science.1187942
98. Davidovic L, Bechara E, Gravel M, Jaglin XH, Tremblay S, Sik A, Bardoni B, Khandjian EW. The nuclear MicroSpherule protein 58 is a novel RNA-binding protein that interacts with fragile X mental retardation protein in polyribosomal mRNPs from neurons. 2006;15(9):1525–1538. doi:10.1093/hmg/ddl074
99. Davidson D, Amrein L, Panasci L, Aloyz R. Small molecules, inhibitors of DNA-PK, targeting DNA repair, and beyond. 2013. doi:10.3389/fphar.2013.00005
100. Davis AJ, Chi L, So S, Lee KJ, Mori E, Fattah K, Yang J, Chen DJ. BRCA1 modulates the autophosphorylation status of DNA-PKcs in S phase of the cell cycle. 2014. doi:10.1093/nar/gku824
101. Deckbar D, Jeggo P a, Löbrich M. Understanding the limitations of radiation-induced cell cycle checkpoints. 2011;46(4):271–83. doi:10.3109/10409238.2011.575764
102. Decottignies A. Alternative end-joining mechanisms: a historical perspective. 2013;4(April):48. doi:10.3389/fgene.2013.00048
103. DeFazio LG, Stansel RM, Griffith JD, Chu G. Synapsis of DNA ends by DNA-dependent protein kinase. 2002;21(12):3192–200. doi:10.1093/emboj/cdf299
104. Le Deist F, Poinsignon C, Moshous D, Fischer A, de Villartay J-P. Artemis sheds new light on V(D)J recombination. 2004;200:142–55. doi:10.1111/j.0105-2896.2004.00169.x
105. Densham RM, Garvin AJ, Stone HR, Strachan J, Baldock RA, Daza-Martin M, Fletcher A, Blair-Reid S, Beesley J, Johal B, et al. Human BRCA1-BARD1 ubiquitin ligase activity counteracts chromatin barriers to DNA resection. 2016;23:647–655. doi:10.1038/nsmb.3236
106. Deriano L, Roth DB. Modernizing the nonhomologous end-joining repertoire: alternative and classical NHEJ share the stage. 2013;47:433–55. doi:10.1146/annurev-genet-110711-155540
107. Difilippantonio S, Gapud E, Wong N, Huang C-Y, Mahowald G, Chen HT, Kruhlak MJ, Callen E, Livak F, Nussenzweig MC, et al. 53BP1 facilitates long-range DNA end-joining during V(D)J recombination. 2008;456:529–533. doi:10.1038/nature07476
108. Ding Q, Reddy Y, Wang W. Autophosphorylation of the catalytic subunit of the DNA-dependent protein kinase is required for efficient end processing during DNA double-strand break repair. 2003. doi:10.1128/MCB.23.16.5836
109. Dobbs TA, Tainer JA, Lees-Miller SP. A structural model for regulation of NHEJ by DNA-PKcs autophosphorylation. 2010;9(12):1307–14. doi:10.1016/j.dnarep.2010.09.019
110. Doil C, Mailand N, Bekker-Jensen S, Menard P, Larsen DH, Pepperkok R, Ellenberg J, Panier S, Durocher D, Bartek J, et al. RNF168 binds and amplifies ubiquitin conjugates on damaged chromosomes to allow accumulation of repair proteins. 2009;136(3):435–46. doi:10.1016/j.cell.2008.12.041
111. Dorsett Y, Zhou Y, Tubbs AT, Chen B-R, Purman C, Lee B-S, George R, Bredemeyer AL, Zhao J, Sodergren E, et al. HCoDES Reveals Chromosomal DNA End Structures with Single-Nucleotide Resolution. 2014;56(6):808–818. doi:10.1016/j.molcel.2014.10.024
112. Drané P, Brault M-E, Cui G, Meghani K, Chaubey S, Detappe A, Parmandi N, He Y, Zheng X-F, Botuyan MV, et al. TIRR regulates 53BP1 by masking its histone methyl-lysine binding function. 2017;543(7644):211–216. doi:10.1016/j.cell.2016.05.007.Mapping
113. Drouet J, Delteil C, Lefrançois J, Concannon P, Salles B, Calsou P. DNA-dependent protein kinase and XRCC4-DNA ligase IV mobilization in the cell in response to DNA double strand breaks. 2005;280(8):7060–7069. doi:10.1074/jbc.M410746200
114. Drouet J, Frit P, Delteil C, De Villartay JP, Salles B, Calsou P. Interplay between Ku, artemis, and the DNA-dependent protein kinase catalytic subunit at DNA ends. 2006;281(38):27784–27793. doi:10.1074/jbc.M603047200
115. Dudley DD, Chaudhuri J, Bassing CH, Alt FW. Mechanism and control of V(D)J recombination versus class switch recombination: similarities and differences. 2005;86(D):43–112. doi:S0065277604860024 [pii]r10.1016/S0065-2776(04)86002-4
116. Dueva R, Iliakis G. Alternative pathways of non-homologous end joining (NHEJ) in genomic instability and cancer. 2013;2(3):163–177. doi:10.3978/j.issn.2218-676X.2013.05.02
117. Dungal DA, Maginn EN, Stronach EA. Preventing Damage Limitation: Targeting DNA-PKcs and DNA Double-Strand Break Repair Pathways for Ovarian Cancer Therapy. 2015;5(October):240. doi:10.3389/fonc.2015.00240
118. Dunphy WG, Brizuela L, Beach D, Newport J. The *Xenopus cdc2* protein is a component of MPF, a cytoplasmic regulator of mitosis. 1988;54(3):423–31.
119. Dupré A, Boyer-Chatenet L, Gautier J. Two-step activation of ATM by DNA and the Mre11-Rad50-Nbs1 complex. 2006;13(5):451–7. doi:10.1038/nsmb1090

120. Dupré A, Boyer-Chatenet L, Sattler RM, Modi AP, Lee J-H, Nicolette ML, Kopelovich L, Jasin M, Baer R, Paull TT, et al. A forward chemical genetic screen reveals an inhibitor of the Mre11-Rad50-Nbs1 complex. 2008;4(2):119–125. doi:10.1038/nchembio.63
121. Eid W, Steger M, El-Shemerly M, Ferretti LP, Peña-Díaz J, König C, Valtorta E, Sartori A a, Ferrari S. DNA end resection by CtIP and exonuclease 1 prevents genomic instability. 2010;11(12):962–8. doi:10.1038/embor.2010.157
122. Elia AEH, Rellos P, Haire LF, Chao JW, Ivins FJ, Hoepker K, Mohammad D, Cantley LC, Smerdon SJ, Yaffe MB. The molecular basis for phosphodependent substrate targeting and regulation of Plks by the Polo-box domain. 2003;115(1):83–95.
123. Escribano-Díaz C, Orthwein A, Fradet-Turcotte A, Xing M, Young JTF, Tkáč J, Cook M a, Rosebrock AP, Munro M, Canny MD, et al. A Cell Cycle-Dependent Regulatory Circuit Composed of 53BP1-RIF1 and BRCA1-CtIP Controls DNA Repair Pathway Choice. 2013;1. doi:10.1016/j.molcel.2013.01.001
124. Fan W, Wu X. DNA polymerase λ can elongate on DNA substrates mimicking non-homologous end joining and interact with XRCC4-ligase IV complex. 2004;323(4):1328–1333. doi:10.1016/j.bbrc.2004.09.002
125. Fell VL, Schild-Poulter C. The Ku heterodimer: Function in DNA repair and beyond. 2015;763:15–29. doi:10.1016/j.mrrev.2014.06.002
126. Feng L, Chen J. The E3 ligase RNF8 regulates KU80 removal and NHEJ repair. 2012;19(2):201–6. doi:10.1038/nsmb.2211
127. Feng L, Li N, Li Y, Wang J, Gao M, Wang W, Chen J. Cell cycle-dependent inhibition of 53BP1 signaling by BRCA1. 2015;1. doi:10.1038/celldisc.2015.19
128. Ferretti LP, Lafranchi L, Sartori AA. Controlling DNA-end resection: a new task for CDKs. 2013;4(June):1–7. doi:10.3389/fgene.2013.00099
129. Figeys D, McBroom LD, Moran MF. Mass spectrometry for the study of protein-protein interactions. 2001;24(3):230–9. doi:10.1006/meth.2001.1184
130. Finnie NJ, Gottlieb TM, Blunt T, Jeggo P a, Jackson SP. DNA-dependent protein kinase activity is absent in xrs-6 cells: implications for site-specific recombination and DNA double-strand break repair. 1995;92(1):320–324.
131. Frit P, Barboule N, Yuan Y, Gomez D, Calsou P. Alternative end-joining pathway(s): Bricolage at DNA breaks. 2014;17:81–97. doi:10.1016/j.dnarep.2014.02.007
132. Fukuchi K, Martin GM, Monnat RJ. Mutator phenotype of Werner syndrome is characterized by extensive deletions. 1989;86(15):5893–7. doi:10.1073/pnas.86.15.5893
133. Gamper AM, Rofougaran R, Watkins SC, Greenberger JS, Beumer JH, Bakkenist CJ. ATR kinase activation in G1 phase facilitates the repair of ionizing radiation-induced DNA damage. 2013;41(22):10334–10344. doi:10.1093/nar/gkt833
134. Garcia-Exposito L, Bournique E, Bergoglio V, Bose A, Barroso-Gonzalez J, Zhang S, Roncaioli JL, Lee M, Wallace CT, Watkins SC, et al. Proteomic Profiling Reveals a Specific Role for Translesion DNA Polymerase η in the Alternative Lengthening of Telomeres. 2016;17(7):1858–1871. doi:10.1016/j.celrep.2016.10.048
135. Garcia V, Phelps SEL, Gray S, Neale MJ. Bidirectional resection of DNA double-strand breaks by Mre11 and Exo1. 2011;479(7372):241–244. doi:10.1038/nature10515.Bidirectional
136. Gelot C, Guirouilh-Barbat J, Le Guen T, Dardillac E, Chailleux C, Canitrot Y, Lopez BS. The Cohesin Complex Prevents the End Joining of Distant DNA Double-Strand Ends. 2016;61:15–26. doi:10.1016/j.molcel.2015.11.002
137. Genschel J, Bazemore LR, Modrich P. Human exonuclease I is required for 5' and 3' mismatch repair. 2002;277(15):13302–13311. doi:10.1074/jbc.M111854200
138. van Gent DC, Hoeijmakers JH, Kanaar R. Chromosomal stability and the DNA double-stranded break connection. 2001;2(3):196–206. doi:10.1038/35056049
139. van Gent DC, Mizuuchi K, Gellert M. Similarities between initiation of V(D)J recombination and retroviral integration. 1996;271(5255):1592–4.
140. Gerelchuluun A, Zhu J, Su F, Asaithamby A, Chen DJ, Tsuboi K. Homologous recombination pathway may play a major role in high-LET radiation-induced DNA double-strand break repair. 2014;55:i83–i84. doi:10.1093/jrr/rrt181
141. Geuting V, Reul C, Löbrich M. ATM Release at Resected Double-Strand Breaks Provides Heterochromatin Reconstitution to Facilitate Homologous Recombination. 2013;9(8). doi:10.1371/journal.pgen.1003667
142. Ghezraoui H, Piganeau M, Renouf B, Renaud J-B, Sallmyr A, Ruis B, Oh S, Tomkinson AE, Hendrickson EA, Giovannangeli C, et al. Chromosomal Translocations in Human Cells Are Generated by Canonical Nonhomologous End-Joining. 2014;55(6):829–842. doi:10.1016/j.molcel.2014.08.002
143. Ghosal G, Chen J. DNA damage tolerance: a double-edged sword guarding the genome. 2013;2(3):107–129. doi:10.3978/j.issn.2218-676X.2013.04.01.
144. Goodarzi A a, Yu Y, Riballo E, Douglas P, Walker S a, Ye R, Härer C, Marchetti C, Morrice N, Jeggo P a, et al. DNA-PK autophosphorylation facilitates Artemis endonuclease activity. 2006;25(16):3880–9. doi:10.1038/sj.emboj.7601255
145. Goodarzi AA, Jeggo PA. The heterochromatic barrier to DNA double strand break repair: How to get the entry visa. 2012;13(9):11844–11860. doi:10.3390/ijms130911844
146. Goodarzi AA, Jeggo PA. The Repair and Signaling Responses to DNA Double-Strand Breaks. 1st ed. Elsevier Inc.; 2013. doi:10.1016/B978-0-12-407676-1.00001-9
147. Goodarzi AA, Jeggo P, Lobrich M. The influence of heterochromatin on DNA double strand break repair: Getting the strong, silent type to relax. 2010;9(12):1273–1282. doi:10.1016/j.dnarep.2010.09.013
148. Grabarz A, Guirouilh-Barbat J, Barascu A, Pennarun G, Genet D, Rass E, Germann SM, Bertrand P, Hickson ID, Lopez BS. A Role for BLM in Double-Strand Break Repair Pathway Choice: Prevention of CtIP/Mre11-Mediated Alternative Nonhomologous End-Joining. 2013;5:21–8. doi:10.1016/j.celrep.2013.08.034
149. Graham TGW, Walter JC, Loparo JJ. Two-Stage Synapsis of DNA Ends during Non-homologous End Joining. 2016;61:850–858. doi:10.1016/j.molcel.2016.02.010

150. Grawunder U, Wilm M, Wu X, Kulesza P, Wilson TE, Mann M, Lieber MR. Activity of DNA ligase IV stimulated by complex formation with XRCC4 protein in mammalian cells. 1997;388(6641):492–5. doi:10.1038/41358
151. Grundy GJ, Moulding HA, Caldecott KW, Rulten SL. One ring to bring them all - The role of Ku in mammalian non-homologous end joining. 2014;17:30–38. doi:10.1016/j.dnarep.2014.02.019
152. Gu J, Lu H, Tippin B, Shimazaki N, Goodman MF, Lieber MR. XRCC4:DNA ligase IV can ligate incompatible DNA ends and can ligate across gaps. 2007;26(4):1010–1023. doi:10.1038/sj.emboj.7601729
153. Gu J, Lu H, Tsai AG, Schwarz K, Lieber MR. Single-stranded DNA ligation and XLF-stimulated incompatible DNA end ligation by the XRCC4-DNA ligase IV complex: Influence of terminal DNA sequence. 2007;35(17):5755–5762. doi:10.1093/nar/gkm579
154. Guirouilh-Barbat J, Gelot C, Xie A, Dardillac E, Scully R, Lopez BS. 53BP1 Protects against CtIP-Dependent Capture of Ectopic Chromosomal Sequences at the Junction of Distant Double-Strand Breaks. 2016;12(10). doi:10.1371/journal.pgen.1006230
155. Guirouilh-Barbat J, Huck S, Bertrand P, Pirzio L, Desmaze C, Sabatier L, Lopez BS. Impact of the KU80 pathway on NHEJ-induced genome rearrangements in mammalian cells. 2004;14(5):611–23. doi:10.1016/j.molcel.2004.05.008
156. Guirouilh-Barbat J, Rass E, Plo I, Bertrand P, Lopez BS. Defects in XRCC4 and KU80 differentially affect the joining of distal nonhomologous ends. 2007;104(52):20902–7. doi:10.1073/pnas.0708541104
157. Gupta A, Hunt CR, Chakraborty S, Pandita RK, Yordy J, Ramnarain DB, Horikoshi N, Pandita TK. Role of 53BP1 in the Regulation of DNA Double-Strand Break Repair Pathway Choice. 2014;181. doi:10.1667/RR13572.1.Role
158. Haince JF, McDonald D, Rodrigue A, Déry U, Masson JY, Hendzel MJ, Poirier GG. PARP1-dependent kinetics of recruitment of MRE11 and NBS1 proteins to multiple DNA damage sites. 2008;283(2):1197–1208. doi:10.1074/jbc.M706734200
159. Hammel M, Yu Y, Mahaney BL, Cai B, Ye R, Phipps BM, Rambo RP, Hura GL, Pelikan M, So S, et al. Ku and DNA-dependent protein kinase dynamic conformations and assembly regulate DNA binding and the initial non-homologous end joining complex. 2010;285(2):1414–23. doi:10.1074/jbc.M109.065615
160. Han L, Yu K. Altered kinetics of nonhomologous end joining and class switch recombination in ligase IV-deficient B cells. 2008;205(12):2745–2753. doi:10.1084/jem.20081623
161. Hanahan D, Weinberg RA. Hallmarks of cancer: The next generation. 2011;144(5):646–674. doi:10.1016/j.cell.2011.02.013
162. Harris JL, Khanna KK. BRCA1 A-Complex fine tunes repair functions of BRCA1. 2011;3(5):461–463.
163. Hatchi E, Skourti-Stathaki K, Ventz S, Pinello L, Yen A, Kamieniarz-Gdula K, Dimitrov S, Pathania S, McKinney KM, Eaton ML, et al. BRCA1 recruitment to transcriptional pause sites is required for R-loop-driven DNA damage repair. 2015;57(4):636–647. doi:10.1016/j.molcel.2015.01.011
164. Helmink B a, Tubbs AT, Dorsett Y, Bednarski JJ, Walker LM, Feng Z, Sharma GG, McKinnon PJ, Zhang J, Bassing CH, et al. H2AX prevents CtIP-mediated DNA end resection and aberrant repair in G1-phase lymphocytes. 2011;469(7329):245–9. doi:10.1038/nature09585
165. Helmink BA, Bredemeyer AL, Lee B-S, Huang C-Y, Sharma GG, Walker LM, Bednarski JJ, Lee W-L, Pandita TK, Bassing CH, et al. MRN complex function in the repair of chromosomal Rag-mediated DNA double-strand breaks. 2009;206(3):669–679. doi:10.1084/jem.20081326
166. Helmke C, Becker S, Strebhardt K. The role of Plk3 in oncogenesis. 2015. doi:10.1038/onc.2015.105
167. Henderson BR. The BRCA1 Breast Cancer Suppressor: Regulation of Transport, Dynamics, and Function at Multiple Subcellular Locations. 2012. doi:10.6064/2012/796808
168. Heyer W-D, Ehmsen KT, Liu J. Regulation of homologous recombination in eukaryotes. 2010;44:113–39. doi:10.1146/annurev-genet-051710-150955
169. Hoa NN, Akagawa R, Yamasaki T, Hirota K, Sasa K, Natsume T, Kobayashi J, Sakuma T, Yamamoto T, Komatsu K, et al. Relative contribution of four nucleases, CtIP, Dna2, Exo1 and Mre11, to the initial step of DNA double-strand break repair by homologous recombination in both the chicken DT40 and human TK6 cell lines. 2015;20(12):1059–1076. doi:10.1111/gtc.12310
170. Hoa NN, Kobayashi J, Omura M, Hirakawa M, Yang SH, Komatsu K, Paull TT, Takeda S, Sasanuma H. BRCA1 and CtIP are both required to recruit Dna2 at double-strand breaks in homologous recombination. 2015;10(4):1–17. doi:10.1371/journal.pone.0124495
171. Hogg M, Sauer-Eriksson AE, Johansson E. Promiscuous DNA synthesis by human DNA polymerase θ . 2012;40(6):2611–2622. doi:10.1093/nar/gkr1102
172. Hollick JJ, Golding BT, Hardcastle IR, Martin N, Richardson C, Rigoreau LJM, Smith GCM, Griffin RJ. 2,6-Disubstituted pyran-4-one and thiopyran-4-one inhibitors of DNA-dependent protein kinase (DNA-PK). 2003;13(18):3083–3086. doi:10.1016/S0960-894X(03)00652-8
173. Honma M, Sakuraba M, Koizumi T, Takashima Y, Sakamoto H, Hayashi M. Non-homologous end-joining for repairing I-SceI-induced DNA double strand breaks in human cells. 2007;6(6):781–8. doi:10.1016/j.dnarep.2007.01.004
174. Huen MSY, Grant R, Manke I, Minn K, Yu X, Yaffe MB, Chen J. RNF8 transduces the DNA-damage signal via histone ubiquitylation and checkpoint protein assembly. 2007;131(5):901–14. doi:10.1016/j.cell.2007.09.041
175. Huertas P, Aguilera A. Cotranscriptionally formed DNA:RNA hybrids mediate transcription elongation impairment and transcription-associated recombination. 2003;12(3):711–721. doi:10.1016/j.molcel.2003.08.010
176. Huertas P, Cortés-Ledesma F, Sartori A a, Aguilera A, Jackson SP. CDK targets Sae2 to control DNA-end resection and homologous recombination. 2008;455(7213):689–92. doi:10.1038/nature07215
177. Huertas P, Jackson SP. Human CtIP mediates cell cycle control of DNA end resection and double strand break repair. 2009;284(14):9558–65. doi:10.1074/jbc.M808906200
178. Hustedt N, Durocher D. The control of DNA repair by the cell cycle. 2017;19(1):1–9. doi:10.1038/ncb3452
179. Huyen Y, Zgheib O, DiTullio Jr RA, Gorgoulis VG, Zacharatos P, Petty TJ, Sheston EA, Mellert HS, Stavridi ES, Halazonetis TD. Methylated lysine 79 of histone H3 targets 53BP1 to DNA double-strand breaks. 2004;432(7015):406–411. doi:10.1038/nature03114

180. IJspeert H, Wentink M, van Zessen D, Driessen GJ, Dalm V a SH, van Hagen MP, Pico-Knijnenburg I, Simons EJ, van Dongen JJM, Stubbs AP, et al. Strategies for B-cell receptor repertoire analysis in primary immunodeficiencies: from severe combined immunodeficiency to common variable immunodeficiency. 2015;6. doi:10.3389/fimmu.2015.00157
181. Iliakis G, Murmann T, Soni A. Alternative end-joining repair pathways are the ultimate backup for abrogated classical non-homologous end-joining and homologous recombination repair: Implications for the formation of chromosome translocations. 2015;793:166–175. doi:10.1016/j.mrgentox.2015.07.001
182. De Ioannes P, Malu S, Cortes P, Aggarwal AK. Structural Basis of DNA Ligase IV-Artemis Interaction in Nonhomologous End-Joining. 2012;2(6):1505–1512. doi:10.1016/j.celrep.2012.11.004
183. Irminger-Finger I, Ratajska M, Pilyugin M. New concepts on BARD1: Regulator of BRCA pathways and beyond. 2016;72. doi:10.1016/j.biocel.2015.12.008
184. Ismail IH, Gagné J-P, Genois M-M, Strickfaden H, McDonald D, Xu Z, Poirier GG, Masson J-Y, Hendzel MJ. The RNF138 E3 ligase displaces Ku to promote DNA end resection and regulate DNA repair pathway choice. 2015;17(11):1446–57. doi:10.1038/ncb3259
185. Isobe S-Y, Nagao K, Nozaki N, Kimura H, Obuse C. Inhibition of RIF1 by SCAI Allows BRCA1-Mediated Repair. 2017;20(2):297–307. doi:10.1016/j.celrep.2017.06.056
186. Isono M, Niimi A, Oike T, Hagiwara Y, Sato H, Sekine R, Yoshida Y, Isobe S-Y, Obuse C, Nishi R, et al. BRCA1 Directs the Repair Pathway to Homologous Recombination by Promoting 53BP1 Dephosphorylation. 2017;18(2):520–532. doi:10.1016/j.celrep.2016.12.042
187. Jaafar L, Li Z, Li S, Dynan WS. SFPQ-NONO and XLF function separately and together to promote DNA double-strand break repair via canonical nonhomologous end joining. 2016. doi:10.1093/cercor/bhw393
188. Jackson SP. Sensing and repairing DNA double-strand breaks. 2002;23(5):687–96.
189. De Jager M, Van Noort J, Van Gent DC, Dekker C, Kanaar R, Wyman C. Human Rad50/Mre11 is a flexible complex that can tether DNA ends. 2001;8(5):1129–1135. doi:10.1016/S1097-2765(01)00381-1
190. Jansen A, Verstrepen KJ. Nucleosome positioning in *Saccharomyces cerevisiae*. 2011;75(2):301–320. doi:10.1128/MMBR.00046-10
191. Jeggo PA. Identification of genes involved in repair of DNA double-strand breaks in mammalian cells. 1998;150(5 Suppl):S80–S91.
192. Jeggo PA, Downs JA. Roles of chromatin remodellers in DNA double strand break repair. 2014;329(1):69–77. doi:10.1016/j.yexcr.2014.09.023
193. Jeggo PA, Löbrich M. How cancer cells hijack DNA double-strand break repair pathways to gain genomic instability. 2015;471(1):1–11. doi:10.1042/BJ20150582
194. Jeggo P, O'Neill P. The Greek Goddess, Artemis, reveals the secrets of her cleavage. 2002;1(9):771–7.
195. Jelinic P, Levine D a. New insights of PARP inhibitors' effect on cell cycle and homology-directed DNA damage repair. 2014;13(6):1645–54. doi:10.1158/1535-7163.MCT-13-0906-T
196. Jeppesen DK, Bohr VA, Stevnsner T. DNA repair deficiency in neurodegeneration. 2011;94(2):166–200. doi:10.1016/j.pneurobio.2011.04.013
197. Jiang G, Plo I, Wang T, Rahman M, Cho JHJH, Yang E, Lopez BS, Xia F. BRCA1-Ku80 protein interaction enhances end-joining fidelity of chromosomal double-strand breaks in the G1 phase of the cell cycle. 2013;288(13):8966–76. doi:10.1074/jbc.M112.412650
198. Jiang W, Crowe JL, Liu X, Nakajima S, Wang Y, Li C, Lee BJ, Dubois RL, Liu C, Yu X, et al. Differential phosphorylation of DNA-PKcs regulates the interplay between end-processing and end-ligation during nonhomologous end-joining. 2015;58(1):172–185. doi:10.1016/j.molcel.2015.02.024
199. Jimeno S, Fernandez-Avila MJ, Cruz-Garcia A, Cepeda-Garcia C, Gomez-Cabello D, Huertas P. Neddylation inhibits CtIP-mediated resection and regulates DNA double strand break repair pathway choice. 2015;43(2):987–999. doi:10.1093/nar/gku1384
200. Johnson RD, Jasin M. Sister chromatid gene conversion is a prominent double-strand break repair pathway in mammalian cells. 2000;19(13):3398–3407. doi:10.1093/emboj/19.13.3398
201. Kaidi A, Weinert BT, Choudhary C, Jackson SP. Human SIRT6 Promotes DNA End Resection Through CtIP Deacetylation. 2010;329:1348–1353. doi:10.1126/science.1133734
202. Kakarougkas A, Ismail A, Chambers A, Riballo E, Herbert A, Künzel J, Löbrich M, Jeggo P, Downs J. Requirement for PBAF in Transcriptional Repression and Repair at DNA Breaks in Actively Transcribed Regions of Chromatin. 2014;55(5):723–732. doi:10.1016/j.molcel.2014.06.028
203. Kakarougkas A, Ismail A, Katsuki Y, Freire R, Shibata A, Jeggo PA. Co-operation of BRCA1 and POH1 relieves the barriers posed by 53BP1 and RAP80 to resection. 2013;41(22):10298–10311. doi:10.1093/nar/gkt802
204. Kakarougkas A, Ismail A, Klement K, Goodarzi AA, Conrad S, Freire R, Shibata A, Lobrich M, Jeggo PA. Opposing roles for 53BP1 during homologous recombination. 2013;41(21):9719–9731. doi:10.1093/nar/gkt729
205. Katz SS, Gimble FS, Storic F. To nick or not to nick: Comparison of I-SceI single- and double-strand break-induced recombination in yeast and human cells. 2014;9(2). doi:10.1371/journal.pone.0088840
206. Kegel P, Riballo E, Kühne M, Jeggo PA, Löbrich M. X-irradiation of cells on glass slides has a dose doubling impact. 2007;6(11):1692–1697. doi:10.1016/j.dnarep.2007.05.013
207. Kent T, Chandramouly G, McDevitt SM, Ozdemir AY, Pomerantz RT. Mechanism of microhomology-mediated end-joining promoted by human DNA polymerase theta. 2015;22(3):230–237. doi:10.1038/nsmb.2961
208. Khalil H, Tummala H, Zhelev N. ATM in focus: A damage sensor and cancer target. 2012;(5):1–60. doi:10.7750/BioDiscovery.2012.5.1

209. Kijas AW, Lim YC, Bolderson E, Cerosaletti K, Gatei M, Jakob B, Tobias F, Taucher-Scholz G, Gueven N, Oakley G, et al. ATM-dependent phosphorylation of MRE11 controls extent of resection during homology directed repair by signalling through Exonuclease 1. 2015;43(17):8352–8367. doi:10.1093/nar/gkv754
210. Kim H. Analysis of variance (ANOVA) comparing means of more than two groups. 2014;7658:74–77. doi:10.5395/rde.2014.39.1.74
211. Kim J. Signaling networks controlled by the MRN complex and MDC1 during early DNA damage responses. 2006;408(May):403–408. doi:10.1002/mc
212. Kim J, Lee SK, Jeon Y, Kim Y, Lee C, Jeon SH, Shim J, Kim IH, Hong S, Kim N, et al. TopBP1 deficiency impairs V(D)J recombination during lymphocyte development. 2014;33(3):217–228. doi:10.1002/embj.201284316
213. Knott GJ, Bond CS, Fox AH. The DBHS proteins SFPQ, NONO and PSPC1: A multipurpose molecular scaffold. 2016;44(9):3989–4004. doi:10.1093/nar/gkw271
214. Koole W, van Schendel R, Karambelas AE, van Heteren JT, Okihara KL, Tijsterman M. A Polymerase Theta-dependent repair pathway suppresses extensive genomic instability at endogenous G4 DNA sites. 2014;5. doi:10.1038/ncomms4216
215. Kotnis A, Du L, Liu C, Popov SW, Pan-Hammarström Q. Non-homologous end joining in class switch recombination: the beginning of the end. 2009;364(1517):653–65. doi:10.1098/rstb.2008.0196
216. Kousholt AN, Fugger K, Hoffmann S, Larsen BD, Menzel T, Sartori AA, Sørensen CS. CtIP-dependent DNA resection is required for DNA damage checkpoint maintenance but not initiation. 2012;197(7):869–76. doi:10.1083/jcb.201111065
217. Kousholt AN, Menzel T, Sørensen C. Pathways for Genome Integrity in G2 Phase of the Cell Cycle. 2012;2:579–607. doi:10.3390/biom2040579
218. Krasner DS, Daley JM, Sung P, Niu H. Interplay between Ku and Replication Protein A in the Restriction of Exo1-mediated DNA Break End Resection. 2015;290(30):18806–18816. doi:10.1074/jbc.M115.660191
219. Kruhlak MJ, Celeste A, Dellaire G, Fernandez-Capetillo O, Müller WG, McNally JG, Bazett-Jones DP, Nussenzweig A. Changes in chromatin structure and mobility in living cells at sites of DNA double-strand breaks. 2006;172(6):823–834. doi:10.1083/jcb.200510015
220. Krzywinski M, Altman N. Designing comparative experiments. 2014;11(6):597–598. doi:10.1038/nmeth.2974
221. Kumagai A, Dunphy WG. The cdc25 protein controls tyrosine dephosphorylation of the cdc2 protein in a cell-free system. 1991;64(5):903–14.
222. Kumagai A, Lee J, Yoo HY, Dunphy WG. TopBP1 activates the ATR-ATRIP complex. 2006;124(5):943–955. doi:10.1016/j.cell.2005.12.041
223. Langelier M-F, Planck JL, Roy S, Pascal JM. Structural Basis for DNA Damage – Dependent Poly(ADP-ribosyl)ation by Human PARP-1. 2012;336:728–733.
224. Langerak P, Mejia-Ramirez E, Limbo O, Russell P. Release of Ku and MRN from DNA ends by Mre11 nuclease activity and Ctp1 is required for homologous recombination repair of double-strand breaks. 2011;7(9). doi:10.1371/journal.pgen.1002271
225. Lavia P, Jansen-Dürr P. E2F target genes and cell-cycle checkpoint control. 1999;21(3):221–30. doi:10.1002/(SICI)1521-1878(199903)21:3<221::AID-BIES6>3.0.CO;2-J
226. Lee-Theilen M, Matthews AJ, Kelly D, Zheng S, Chaudhuri J. CtIP promotes microhomology-mediated alternative end joining during class-switch recombination. 2011;18(1):75–9. doi:10.1038/nsmb.1942
227. Lee BI, Wilson DM. The RAD2 domain of human exonuclease 1 exhibits 5' to 3' exonuclease and flap structure-specific endonuclease activities. 1999;274(53):37763–37769. doi:10.1074/jbc.274.53.37763
228. Lee J-H, Paull TT. Direct activation of the ATM protein kinase by the Mre11/Rad50/Nbs1 complex. 2004;304(5667):93–96. doi:10.1126/science.1091496
229. Lee KJ, Saha J, Sun J, Fattah KR, Wang SC, Jakob B, Chi L, Wang SY, Taucher-Scholz G, Davis AJ, et al. Phosphorylation of Ku dictates DNA double-strand break (DSB) repair pathway choice in S phase. 2016;44(4):1732–1745. doi:10.1093/nar/gkv1499
230. Lee Bi B, Nguyen LH, Barsky D, Fernandes M, Wilson DM. Molecular interactions of human Exo1 with DNA. 2002;30(4):942–949. doi:10.1093/nar/30.4.942
231. Lees-Miller S. Repair of DNA double strand breaks by non-homologous end joining. 2003;85(11):1161–1173. doi:10.1016/j.biochi.2003.10.011
232. Lemée F, Bergoglio V, Fernandez-Vidal A, Machado-Silva A, Pillaire M-J, Bieth A, Gentil C, Baker L, Martin A-L, Leduc C, et al. DNA polymerase theta up-regulation is associated with poor survival in breast cancer, perturbs DNA replication, and promotes genetic instability. 2010;107(30):13390–5. doi:10.1073/pnas.0910759107
233. Lengsfeld BM, Rattray AJ, Bhaskara V, Ghirlando R, Paull TT. Sae2 is an endonuclease that processes hairpin DNA cooperatively with the Mre11/Rad50/Xrs2 complex. 2007;28(4):638–51. doi:10.1016/j.molcel.2007.11.001
234. Li G, Alt FW, Cheng HL, Brush JW, Goff PH, Murphy MM, Franco S, Zhang Y, Zha S. Lymphocyte-Specific Compensation for XLF/Cernunnos End-Joining Functions in V(D)J Recombination. 2008;31(5):631–640. doi:10.1016/j.molcel.2008.07.017
235. Li GM. Decoding the histone code: Role of H3K36me3 in mismatch repair and implications for cancer susceptibility and therapy. 2013;73(21):6379–6383. doi:10.1158/0008-5472.CAN-13-1870
236. Li L, Monckton E a, Godbout R. A role for DEAD box 1 at DNA double-strand breaks. 2008;28(20):6413–6425. doi:10.1128/MCB.01053-08
237. Li L, Poon HY, Hildebrandt MR, Monckton EA, Germain DR, Fahlman RP, Godbout R. Role for RIF1-interacting partner DDX1 in BLM recruitment to DNA double-strand breaks. 2017;55(May):47–63. doi:10.1016/j.dnarep.2017.05.001
238. Li S, Ting NS, Zheng L, Chen PL, Ziv Y, Shiloh Y, Lee EY, Lee WH. Functional link of BRCA1 and ataxia telangiectasia gene product in DNA damage response. 2000;406(6792):210–5. doi:10.1038/35018134
239. Liang F, Romanienko PJ, Weaver DT, Jeggo P a, Jasin M. Chromosomal double-strand break repair in Ku80-deficient cells. 1996;93(17):8929–33.

240. Liao S, Guay C, Toczylowski T, Yan H. Analysis of MRE11's function in the 5' - 3' processing of DNA double-strand breaks. 2012;40(10):4496–4506. doi:10.1093/nar/gks044
241. Liao S, Tamaro M, Yan H. The structure of ends determines the pathway choice and Mre11 nuclease dependency of DNA double-strand break repair. 2016;44(12):5689–5701. doi:10.1093/nar/gkw274
242. Lieber MR. The Mechanism of Double-Strand DNA Break Repair by the Nonhomologous DNA End Joining Pathway. 2010;(3):181–211. doi:10.1146/annurev.biochem.052308.093131.The
243. Liu L, Kong M, Gassman NR, Freudenthal BD, Prasad R, Zhen S, Watkins SC, Wilson SH, Van Houten B. Auto-PARylation switches PARP1 search mechanism from three-dimensional diffusion to anomalous one-dimensional sliding. In: *Keystone Symposia Genomic Instability and DNA Repair*. 2017.
244. Liu X, Shao Z, Jiang W, Lee BJ, Zha S. PAXX promotes KU accumulation at DNA breaks and is essential for end-joining in XLF-deficient mice. 2017. doi:10.1038/ncomms13816
245. Löbrich M, Jeggo P. A Process of Resection-Dependent Nonhomologous End Joining Involving the Goddess Artemis. 2017. doi:10.1016/j.tibs.2017.06.011
246. Löbrich M, Jeggo PPA. The impact of a negligent G2/M checkpoint on genomic instability and cancer induction. 2007;7(11):861–869.
247. Löbrich M, Shibata A, Beucher A, Fisher A, Ensminger M, Goodarzi AA, Barton O, Jeggo PA. gammaH2AX foci analysis for monitoring DNA double-strand break repair. 2010;9(4):662–669.
248. Lord CJ, Ashworth A. The DNA damage response and cancer therapy. 2012;481(7381):287–294. doi:10.1038/nature10760
249. Lovett ST. The DNA exonucleases of *Escherichia coli*. 2011;4(2). doi:10.1128/ecosalplus.4.4.7.The
250. Luijsterburg MS, de Krijger I, Wiegant WW, Shah RG, Smeenk G, de Groot AJL, Pines A, Vertegeal ACO, Jacobs JLL, Shah GM, et al. PARP1 Links CHD2-Mediated Chromatin Expansion and H3.3 Deposition to DNA Repair by Non-homologous End-Joining. 2016;61:547–562. doi:10.1016/j.molcel.2016.01.019
251. Ma Y, Pannicke U, Schwarz K, Lieber MR. Hairpin opening and overhang processing by an Artemis/DNA-dependent protein kinase complex in nonhomologous end joining and V(D)J recombination. 2002;108(6):781–94.
252. Madison DL, Stauffer D, Lundblad JR. The PARP inhibitor PJ34 causes a PARP1-independent, p21 dependent mitotic arrest. 2011;10(10):1003–1013. doi:10.1016/j.dnarep.2011.07.006
253. Mahajan KN, Nick McElhinny S a, Mitchell BS, Ramsden D a. Association of DNA polymerase mu (pol mu) with Ku and ligase IV: role for pol mu in end-joining double-strand break repair. 2002;22(14):5194–202. doi:10.1128/MCB.22.14.5194
254. Manis JP, Tian M, Alt FW. Mechanism and control of class-switch recombination. 2002;23(1):31–39. doi:10.1016/S1471-4906(01)02111-1
255. Mansilla-Soto J, Cortes P. VDJ Recombination: Artemis and Its In Vivo Role in Hairpin Opening. 2003;197(5):543–547. doi:10.1084/jem.20022210
256. Mansour WY, Borgmann K, Petersen C, Dikomey E, Dahm-Daphi J. The absence of Ku but not defects in classical non-homologous end-joining is required to trigger PARP1-dependent end-joining. 2013;12(12):1134–1142. doi:10.1016/j.dnarep.2013.10.005
257. Mansour WY, Rhein T, Dahm-Daphi J. The alternative end-joining pathway for repair of DNA double-strand breaks requires PARP1 but is not dependent upon microhomologies. 2010;38(18):6065–6077. doi:10.1093/nar/gkq387
258. Mansour WY, Schumacher S, Roskopf R, Rhein T, Schmidt-Petersen F, Gatzemeier F, Haag F, Borgmann K, Willers H, Dahm-Daphi J. Hierarchy of nonhomologous end-joining, single-strand annealing and gene conversion at site-directed DNA double-strand breaks. 2008;36(12):4088–98. doi:10.1093/nar/gkn347
259. Mari P-O, Florea BI, Persengiev SP, Verkaik NS, Brü Ggenwirth HT, Modesti M, Giglia-Mari G, Bezstarosti K, Demmers JAA, Luider TM, et al. Dynamic assembly of end-joining complexes requires interaction between Ku70/80 and XRCC4. 2006;103(49):18597–18602. doi:10.1073/pnas.0609061103
260. Mashimo T, Kaneko T, Sakuma T, Kobayashi J, Kunihiro Y, Voigt B, Yamamoto T, Serikawa T. Efficient gene targeting by TAL effector nucleases coinjected with exonucleases in zygotes. 2013;3. doi:10.1038/srep01253
261. Matsuoka S, Ballif BA, Smogorzewska A, McDonald ER, Hurov KE, Luo J, Bakalarski CE, Zhao Z, Solimini N, Lerenthal Y, et al. ATM and ATR substrate analysis reveals extensive protein networks responsive to DNA damage. 2007;316(5828):1160–1166. doi:10.1126/science.1140321
262. Mazón G, Mimitou EP, Symington LS. SnapShot: Homologous recombination in DNA double-strand break repair. 2010;142(4):646, 646.e1. doi:10.1016/j.cell.2010.08.006
263. McElhinny SAN, Snowden CM, Ramsden DA, Elhinny SANMC, Carville JMC. Ku Recruits the XRCC4-Ligase IV Complex to DNA Ends. 2000;20(9). doi:10.1128/MCB.20.9.2996-3003.2000.Updated
264. McVey M. RPA puts the brakes on MMEJ. 2014;21(4):348–9. doi:10.1038/nsmb.2802
265. McVey M, Lee SE. MMEJ repair of double-strand breaks (director's cut): deleted sequences and alternative endings. 2008;24(11):529–38. doi:10.1016/j.tig.2008.08.007
266. MedChem-Express. MedChem Express - Master of small molecules.
267. Meek K, Douglas P, Cui X, Ding Q, Lees-Miller SP. trans Autophosphorylation at DNA-dependent protein kinase's two major autophosphorylation site clusters facilitates end processing but not end joining. 2007;27(10):3881–90. doi:10.1128/MCB.02366-06
268. Meir M, Galanty Y, Kashani L, Blank M, Khosravi R, Fernández-Ávila MJ, Cruz-García A, Star A, Shochot L, Thomas Y, et al. The COP9 signalosome is vital for timely repair of DNA double-strand breaks. 2015;43(9):4517–4530. doi:10.1093/nar/gkv270
269. Menear KA, Adcock C, Boulter R, Cockcroft XL, Copsey L, Cranston A, Dillon KJ, Drzewiecki J, Garman S, Gomez S, et al. 4-[3-(4-Cyclopropanecarbonylpiperazine-1-carbonyl)-4-fluorobenzyl] -2H-phthalazin-1-one: A novel bioavailable inhibitor of poly(ADP-ribose) polymerase-1. 2008;51(20):6581–6591. doi:10.1021/jm8001263

270. Menon V, Povirk LF. End-processing nucleases and phosphodiesterases: An elite supporting cast for the non-homologous end joining pathway of DNA double-strand break repair. 2016;43:57–68. doi:10.1016/j.dnarep.2016.05.011
271. Merkle D, Douglas P, Moorhead GBG, Leonenko Z, Yu Y, Cramb D, Bazett-Jones DP, Lees-Miller SP. The DNA-dependent protein kinase interacts with DNA to form a protein - DNA complex that is disrupted by phosphorylation. 2002;41(42):12706–12714. doi:10.1021/bi0263558
272. Metzger L, Iliakis G. Kinetics of DNA double-strand break repair throughout the cell cycle as assayed by pulsed field gel electrophoresis in CHO cells. 1991;59(6):1325–39.
273. Mimitou EP, Symington LS. Ku prevents Exo1 and Sgs1-dependent resection of DNA ends in the absence of a functional MRX complex or Sae2. 2010;29(19):3358–69. doi:10.1038/emboj.2010.193
274. Mimitou EP, Symington LS. Sae2, Exo1 and Sgs1 collaborate in DNA double-strand break processing. 2008;455(7214):770–4. doi:10.1038/nature07312
275. Mitchell J, Smith GCM, Curtin NJ. Poly(ADP-Ribose) Polymerase-1 and DNA-Dependent Protein Kinase Have Equivalent Roles in Double Strand Break Repair Following Ionizing Radiation. 2009;75(5):1520–1527. doi:10.1016/j.ijrobp.2009.07.1722
276. Mizuta R, Iwai K, Shigeno M, Mizuta M, Uemura T, Ushiki T, Kitamura D. Molecular visualization of immunoglobulin switch region RNA/DNA complex by atomic force microscope. 2003;278(7):4431–4434. doi:10.1074/jbc.M209262200
277. Morrison C, Smith G, Stingl L, Jackson SP, Wagner E, ZQ W. Genetic interaction between PARP and DNA-PK in V(D)J recombination and tumorigenesis. 1997;17(4):479–82. doi:10.1038/ng1297-479
278. Moscariello M, Wieloch R, Kurosawa A, Li F, Adachi N, Mladenov E, Iliakis G. Role for Artemis nuclease in the repair of radiation-induced DNA double strand breaks by alternative end joining. 2015;31:29–40. doi:10.1016/j.dnarep.2015.04.004
279. Moure CM, Gimble FS, Quioco FA. Crystal structures of I-SceI complexed to nicked DNA substrates: snapshots of intermediates along the DNA cleavage reaction pathway. 2008;36(10):3287–96. doi:10.1093/nar/gkn178
280. Moynahan ME, Pierce AJ, Jasin M. BRCA2 is required for homology-directed repair of chromosomal breaks. 2001;7(2):263–272. doi:10.1016/S1097-2765(01)00174-5
281. Mullan PB, Quinn JE, Harkin DP. The role of BRCA1 in transcriptional regulation and cell cycle control. 2006;25(43):5854–5863. doi:10.1038/sj.onc.1209872
282. Myler LR, Finkelstein IJ. Eukaryotic resectosomes: A single-molecule perspective. 2016;127:119–129. doi:10.1016/j.pbiomolbio.2016.08.001
283. Nakada S. Opposing roles of RNF8/RNF168 and deubiquitinating enzymes in ubiquitination-dependent DNA double-strand break response signaling and DNA-repair pathway choice. 2016;57. doi:10.1093/jrr/rww027
284. Nakagawa S, Cuthill IC. Effect size, confidence interval and statistical significance: A practical guide for biologists. 2007;82(4):591–605. doi:10.1111/j.1469-185X.2007.00027.x
285. Neal JA, Sugiman-Marangos S, VanderVere-Carozza P, Wagner M, Turchi J, Lees-Miller SP, Junop MS, Meek K. Unraveling the complexities of DNA-dependent protein kinase autophosphorylation. 2014;34(12):2162–2175. doi:10.1128/MCB.01554-13
286. Niewolik D, Peter I, Butscher C, Schwarz K. Autoinhibition of the nuclease ARTEMIS is mediated by a physical interaction between its catalytic and C-terminal domains. 2017;292(8):3351–3365. doi:10.1074/jbc.M116.770461
287. Nimonkar A V., Genschel J, Kinoshita E, Polaczek P, Campbell JL, Wyman C, Modrich P, Kowalczykowski SC. BLM, DNA2, RPA, MRN and EXO1, BLM, RPA, MRN constitute two DNA end resection machineries for human DNA break repair. 2011;25(4):350–362. doi:10.1101/gad.2003811
288. Noon AT, Shibata A, Rief N, Löbrich M, Stewart GS, Jeggo PA, Goodarzi AA. 53BP1-dependent robust localized KAP-1 phosphorylation is essential for heterochromatic DNA double-strand break repair. 2010;12(2):177–184. doi:10.1038/ncb2017
289. Nussenzweig A, Nussenzweig MC. A backup DNA repair pathway moves to the forefront. 2007;131(2):223–5. doi:10.1016/j.cell.2007.10.005
290. Ochi T, Blackford AN, Coates J, Jhujh S, Mehmood S, Tamura N, Travers J, Wu Q, Draviam VM, Robinson C V, et al. PAXX, a paralog of XRCC4 and XLF, interacts with Ku to promote DNA double-strand break repair. 2015;347(6218):185–188. doi:10.1126/science.1261971
291. Ochi T, Sibanda BL, Wu Q, Chirgadze DY, Bolanos-Garcia VM, Blundell TL. Structural biology of DNA repair: spatial organisation of the multicomponent complexes of nonhomologous end joining. 2010;2010(August 2010):1–28. doi:10.4061/2010/621695
292. Ochs F, Somyajit K, Altmeyer M, Rask M-B, Lukas J, Lukas C. 53BP1 fosters fidelity of homology-directed DNA repair. 2016;23(8):714–21. doi:10.1038/nsmb.3251
293. Ogiwara H, Kohno T. Essential factors for incompatible DNA end joining at chromosomal DNA double strand breaks in vivo. 2011;6(12). doi:10.1371/journal.pone.0028756
294. Ohle C, Tesorero R, Schermann GG, Dobrev N, Sinning I, Fischer TT. Transient RNA-DNA Hybrids Are Required for Efficient Double-Strand Break Repair. 2016;167(4). doi:10.1016/j.cell.2016.10.001
295. Ohta T, Sato K, Wu W. The BRCA1 ubiquitin ligase and homologous recombination repair. 2011;585(18):2836–44. doi:10.1016/j.febslet.2011.05.005
296. Okazaki I, Kinoshita K, Muramatsu M, Yoshikawa K, Honjo T. The AID enzyme induces class switch recombination in fibroblasts. 2002;416(6878):340–345. doi:10.1038/nature727
297. Olive PL. The role of DNA single- and double-strand breaks in cell killing by ionizing radiation. 1998;150(5 Suppl):S42-51.
298. Orren DK, Machwe a, Karmakar P, Piotrowski J, Cooper MP, Bohr V a. A functional interaction of Ku with Werner exonuclease facilitates digestion of damaged DNA. 2001;29(9):1926–1934.
299. Orthwein A, Noordermeer SM, Wilson MD, Landry S, Enchev RI, Sherker A, Munro M, Pinder J, Salsman J, Dellaire G, et al. A mechanism for the suppression of homologous recombination in G1 cells. 2015;528(7582):422–426. doi:10.1038/nature16142
300. Palazzo AF, Gregory TR. The Case for Junk DNA. 2014;10(5). doi:10.1371/journal.pgen.1004351

301. Panier S, Boulton SJ. Double-strand break repair: 53BP1 comes into focus. 2014;15(1):7–18. doi:10.1038/nrm3719
302. Pannunzio NR, Li S, Watanabe G, Lieber MR. Non-homologous end joining often uses microhomology: Implications for alternative end joining. 2014;17. doi:10.1016/j.dnarep.2014.02.006
303. Paull TT. Mechanisms of ATM Activation. 2015;84:711–738. doi:10.1146/annurev-biochem-060614-034335
304. Paull TT, Gellert M. The 3' to 5' exonuclease activity of Mre 11 facilitates repair of DNA double-strand breaks. 1998;1(7):969–79.
305. Payne SL, Rodriguez-Aristegui S, Bardos J, Cano C, Golding BT, Hardcastle IR, Peacock M, Parveen N, Griffin RJ. Mapping the ATP-binding domain of DNA-dependent protein kinase (DNA-PK) with coumarin- and isocoumarin-derived inhibitors. 2010;20(12):3649–3653. doi:10.1016/j.bmol.2010.04.102
306. Pellegrini L, Yu DS, Lo T, Anand S, Lee M, Blundell TL, Venkitaraman AR. Insights into DNA recombination from the structure of a RAD51-BRCA2 complex. 2002;420(6913):287–293.
307. Pellegrino S, Altmeyer M. Interplay between ubiquitin, SUMO, and poly(ADP-Ribose) in the cellular response to genotoxic stress. 2016;7. doi:10.3389/fgene.2016.00063
308. Pellegrino S, Michelena J, Teloni F, Imhof R, Altmeyer M. Replication-Coupled Dilution of H4K20me2 Guides 53BP1 to Pre-replicative Chromatin. 2017;19(9):1819–1831. doi:10.1016/j.celrep.2017.05.016
309. Peña-Díaz J, Jiricny J. Mammalian mismatch repair: Error-free or error-prone? 2012;37(5):206–214. doi:10.1016/j.tibs.2012.03.001
310. Peng C. Mitotic and G2 Checkpoint Control: Regulation of 14-3-3 Protein Binding by Phosphorylation of Cdc25C on Serine-216. 1997;277(5331):1501–1505. doi:10.1126/science.277.5331.1501
311. Petrini J. The cellular response to DNA double-strand breaks: defining the sensors and mediators. 2003;13(9):458–462. doi:10.1016/S0962-8924(03)00170-3
312. Pfister SX, Ahrabi S, Zalmas LP, Sarkar S, Aymard F, Bachrati CZ, Helleday T, Legube G, LaThangue NB, Porter ACG, et al. SETD2-Dependent Histone H3K36 Trimethylation Is Required for Homologous Recombination Repair and Genome Stability. 2014;7(6):2006–2018. doi:10.1016/j.celrep.2014.05.026
313. Pines A, Mullenders LH, van Attikum H, Luijsterburg MS. Touching base with PARPs: Moonlighting in the repair of UV lesions and double-strand breaks. 2013;38(6):321–330. doi:10.1016/j.tibs.2013.03.002
314. Pines J. Cyclins and cyclin-dependent kinases: a biochemical view. 1995;308 (Pt 3):697–711.
315. Polato F, Callen E, Wong N, Faryabi R, Bunting S, Chen HT, Kozak M, Kruhlak MJ, Reczek CR, Lee W-H, et al. CtIP-mediated resection is essential for viability and can operate independently of BRCA1. 2014;211(6):1027–1036. doi:10.1084/jem.20131939
316. Polo SE, Jackson SP. Dynamics of DNA damage response proteins at DNA breaks: a focus on protein modifications. 2011;25(5):409–33. doi:10.1101/gad.2021311.critical
317. Postow L, Funabiki H. An SCF complex containing Fbx12 mediates DNA damage-induced Ku80 ubiquitylation. 2013;12(4):587–595. doi:10.4161/cc.23408
318. Postow L, Ghenoiu C, Woo EM, Krutchinsky AN, Chait BT, Funabiki H. Ku80 removal from DNA through double strand break-induced ubiquitylation. 2008;182(3):467–479. doi:10.1083/jcb.200802146
319. Quennet V, Beucher A, Barton O, Takeda S, Löbrich M. CtIP and MRN promote non-homologous end-joining of etoposide-induced DNA double-strand breaks in G1. 2011;39(6):2144–52. doi:10.1093/nar/gkq1175
320. Radhakrishnan SK, Lees-Miller SP. DNA requirements for interaction of the C-terminal region of Ku80 with the DNA-dependent protein kinase catalytic subunit (DNA-PKcs). 2017;57(May):17–28. doi:10.1016/j.dnarep.2017.06.001
321. Ramsden DA, Geliert M. Ku protein stimulates DNA end joining by mammalian DNA ligases: A direct role for Ku in repair of DNA double-strand breaks. 1998;17(2):609–614. doi:10.1093/emboj/17.2.609
322. Rass E, Grabarz A, Plo I, Gautier J, Bertrand P, Lopez BS. Role of Mre11 in chromosomal nonhomologous end joining in mammalian cells. 2009;16(8):819–824. doi:10.1038/nsmb.1641
323. Reid DA, Keegan S, Leo-Macias A, Watanabe G, Strande NT, Chang HH, Oksuz BA, Fenyo D, Lieber MR, Ramsden DA, et al. Organization and dynamics of the nonhomologous end-joining machinery during DNA double-strand break repair. 2015;112(20):E2575–E2584. doi:10.1073/pnas.1420115112
324. Reina-San-Martin B, Chen J, Nussenzweig A, Nussenzweig MC. Enhanced intra-switch region recombination during immunoglobulin class switch recombination in 53BP1^{-/-} B cells. 2007;37(1):235–239. doi:10.1002/eji.200636789
325. Reinhardt HC, Yaffe MB. Phospho-Ser/Thr-binding domains: navigating the cell cycle and DNA damage response. 2013;14(9):563–580. doi:10.1038/nrm3640
326. Reynolds P, Anderson JA, Harper J V., Hill MA, Botchway SW, Parker AW, O'Neill P. The dynamics of Ku70/80 and DNA-PKcs at DSBs induced by ionizing radiation is dependent on the complexity of damage. 2012;40(21):10821–10831. doi:10.1093/nar/gks879
327. Riballo E, Kühne M, Rief N, Doherty A, Smith GCM, Recio M-J, Reis C, Dahm K, Fricke A, Krempler A, et al. A pathway of double-strand break rejoining dependent upon ATM, Artemis, and proteins locating to gamma-H2AX foci. 2004;16(5):715–24. doi:10.1016/j.molcel.2004.10.029
328. Rivera-Munoz P, Soulas-Sprauel P, Guyader G Le, Abramowski V, Bruneau S, Fischer A, Paques F, Villartay J-P de. Reduced immunoglobulin class switch recombination in the absence of Artemis Reduced immunoglobulin class switch recombination in the absence of Artemis. 2009;114(17):3601–3610. doi:10.1182/blood-2008-11-188383
329. Rogakou EP, Pilch DR, Orr a H, Ivanova VS, Bonner WM. DNA double-stranded breaks induce histone H2AX phosphorylation on serine 139. 1998;273(10):5858–68.
330. Rooney S, Alt FW, Lombard D, Whitlow S, Eckersdorff M, Fleming J, Fugmann S, Ferguson DO, Schatz DG, Sekiguchi J. Defective DNA Repair and Increased Genomic Instability in Artemis-deficient Murine Cells. 2003;197(5):553–565. doi:10.1084/jem.20021891

331. Rooney S, Alt FW, Sekiguchi J, Manis JP. Artemis-independent functions of DNA-dependent protein kinase in Ig heavy chain class switch recombination and development. 2005;102(7):2471–2475. doi:10.1073/pnas.0409857102
332. Ruder C. Untersuchungen zur Rolle von CtIP-Phosphorylierungen anhand von NHEJ-Reporter-Assays. 2014.
333. Rulten SL, Fisher AEO, Robert I, Zuma MC, Rouleau M, Ju L, Poirier G, Reina-San-Martin B, Caldecott KW. PARP-3 and APLF function together to accelerate nonhomologous end-joining. 2011;41(1):33–45. doi:10.1016/j.molcel.2010.12.006
334. Ruscetti T, Lehnert BE, Halbros J, Trong H Le, Hoekstra MF, Chen DJ, Peterson SR. Stimulation of the DNA-dependent Protein Kinase by Poly(ADP-Ribose) Polymerase. 1998;273(23):14461–14467.
335. Rybanska-Spaeder I, Reynolds TL, Chou J, Prakash M, Jefferson T, Huso DL, Desiderio S, Franco S. 53BP1 Is Limiting for NHEJ Repair in ATM-deficient Model Systems That Are Subjected to Oncogenic Stress or Radiation. 2013;11(10):1223–1234. doi:10.1158/1541-7786.MCR-13-0252-T
336. Saha J, Davis AJ. Unsolved mystery: The role of BRCA1 in DNA end-joining. 2016;57. doi:10.1093/jrr/rrw032
337. San Filippo J, Sung P, Klein H. Mechanism of eukaryotic homologous recombination. 2008;77:229–57. doi:10.1146/annurev.biochem.77.061306.125255
338. Sanchez Y. Conservation of the Chk1 Checkpoint Pathway in Mammals: Linkage of DNA Damage to Cdk Regulation Through Cdc25. 1997;277(5331):1497–1501. doi:10.1126/science.277.5331.1497
339. Sartori A a, Lukas C, Coates J, Mistrik M, Fu S, Bartek J, Baer R, Lukas J, Jackson SP. Human CtIP promotes DNA end resection. 2007;450(7169):509–14. doi:10.1038/nature06337
340. Satyanarayana A, Kaldis P. A dual role of Cdk2 in DNA damage response. 2009;4(9). doi:10.1186/1747-1028-4-9
341. Savage KI, Harkin DP. BRCA1, a “complex” protein involved in the maintenance of genomic stability. 2015;282:630–646. doi:10.1111/febs.13150
342. Schiller CB, Lammens K, Guerini I, Coords B, Feldmann H, Schlauderer F, Möckel C, Schele A, Strässer K, Jackson SP, et al. Structure of Mre11-Nbs1 complex yields insights into ataxia-telangiectasia-like disease mutations and DNA damage signaling. 2012;19(7):693–700. doi:10.1038/nsmb.2323
343. Schipler A, Iliakis G. DNA double-strand-break complexity levels and their possible contributions to the probability for error-prone processing and repair pathway choice. 2013;41(16):7589–7605. doi:10.1093/nar/gkt556
344. Schwab KR, Patel SR, Dressler GR. Role of PTIP in Class Switch Recombination and Long-Range Chromatin Interactions at the Immunoglobulin Heavy Chain Locus. 2011;31(7):1503–1511. doi:10.1128/MCB.00990-10
345. Schwertman P, Bekker-Jensen S, Mailand N. Regulation of DNA double-strand break repair by ubiquitin and ubiquitin-like modifiers. 2016;17:379–394. doi:10.1038/nrm.2016.58
346. Seol J-H, Shim EY, Lee SE. Microhomology-mediated end joining: Good, bad and ugly. 2017. doi:10.1016/j.mrfmmm.2017.07.002
347. Sfeir A, Symington LS. Microhomology-Mediated End Joining: A Back-up Survival Mechanism or Dedicated Pathway? 2015;40(11):701–714. doi:10.1016/j.tibs.2015.08.006
348. Shakya R, Reid LJ, Reczek CR, Cole F, Egli D, Lin CS, deRooij DG, Hirsch S, Ravi K, Hicks JB, et al. BRCA1 tumor suppression depends on BRCT phosphoprotein binding, but not its E3 ligase activity. 2011;334(6055):525–528. doi:10.1126/science.1209909
349. Shaltiel IA, Krenning L, Bruinsma W, Medema RH. The same, only different - DNA damage checkpoints and their reversal throughout the cell cycle. 2015;128(4):607–20. doi:10.1242/jcs.163766
350. Shamanna RA, Lu H, de Freitas JK, Tian J, Croteau DL, Bohr VA. WRN regulates pathway choice between classical and alternative non-homologous end joining. 2016;7. doi:10.1038/ncomms13785
351. Sharma S, Sommers JA, Driscoll HC, Uzdilla L, Wilson TM, Brosh RM. The exonucleolytic and endonucleolytic cleavage activities of human exonuclease 1 are stimulated by an interaction with the carboxyl-terminal region of the Werner syndrome protein. 2003;278(26):23487–23496. doi:10.1074/jbc.M212798200
352. Shen J-C, Loeb LA. Werner syndrome exonuclease catalyzes structure-dependent degradation of DNA. 2000;28:3260–3268.
353. Shibata A. Regulation of repair pathway choice at two-ended DNA double-strand breaks. 2017. doi:10.1016/j.mrfmmm.2017.07.011
354. Shibata A, Moiani D, Arvai AS, Perry J, Harding SM, Genois M-M, Maity R, van Rossum-Fikkert S, Kertokallio A, Romoli F, et al. DNA Double-Strand Break Repair Pathway Choice Is Directed by Distinct MRE11 Nuclease Activities. 2014;53(1):7–18. doi:10.1016/j.molcel.2013.11.003
355. Shimada K, Gasser SM. A game of musical chairs : Pro- and anti-resection factors compete for TOPBP1 binding after DNA damage. 2017. doi:10.1083/jcb.201701038
356. Sibanda BL, Chirgadze DY, Ascher DB, Blundell TL. DNA-PKcs structure suggests an allosteric mechanism modulating DNA double-strand break repair. 2017;355(6324):520–524. doi:10.1126/science.aak9654
357. Simsek D, Jasin M. Alternative end-joining is suppressed by the canonical NHEJ component Xrcc4/ligaseIV during chromosomal translocation formation. 2010;17(4):410–416. doi:10.1038/nsmb.1773
358. Smogorzewska A, Desetty R, Saito TT, Schlabach M, Lach FP, Sowa ME, Clark AB, Kunkel TA, Harper JW, Colaiácovo MP, et al. A Genetic Screen Identifies FANL1, a Fanconi Anemia-Associated Nuclease Necessary for DNA Interstrand Crosslink Repair. 2010;39(1):36–47. doi:10.1016/j.molcel.2010.06.023
359. Soni a., Siemann M, Grabos M, Murmann T, Pantelias GE, Iliakis G. Requirement for Parp-1 and DNA ligases 1 or 3 but not of Xrcc1 in chromosomal translocation formation by backup end joining. 2014. doi:10.1093/nar/gku298
360. Soria-Bretones I, Cepeda-García C, Checa-Rodríguez C, Heyer V, Reina-San-Martin B, Soutoglou E, Huertas P. DNA end resection requires constitutive sumoylation of CtIP by CBX4. 2017;8(1):113. doi:10.1038/s41467-017-00183-6
361. Spagnolo L, Barbeau J, Curtin NJ, Morris EP, Pearl LH. Visualization of a DNA-PK/PARP1 complex. 2012;40(9):4168–4177. doi:10.1093/nar/gkr1231

362. Spagnolo L, Rivera-Calzada A, Pearl LH, Llorca O. Three-dimensional structure of the human DNA-PKcs/Ku70/Ku80 complex assembled on DNA and its implications for DNA DSB repair. 2006;22(4):511–9. doi:10.1016/j.molcel.2006.04.013
363. Starkman BG, Sakharkar AJ, Pandey SC. Epigenetics - beyond the genome in alcoholism. 2012;34(3):293–305.
364. Stavnezer J, Guikema JEJ, Schrader CE. Mechanism and Regulation of Class Switch Recombination. 2008;26(1):261–292. doi:10.1146/annurev.immunol.26.021607.090248
365. Stavnezer J, Schrader CE. IgH Chain Class Switch Recombination: Mechanism and Regulation. 2014;193(11):5370–5378. doi:10.4049/jimmunol.1401849
366. Steger M, Murina O, Hühn D, Ferretti LP, Walser R, Hänggi K, Lafranchi L, Neugebauer C, Paliwal S, Janscak P, et al. Prolyl isomerase PIN1 regulates DNA double-strand break repair by counteracting DNA end resection. 2013;50(3):333–343. doi:10.1016/j.molcel.2013.03.023
367. Stewart GS, Wang B, Bignell CR, Taylor a MR, Elledge SJ. MDC1 is a mediator of the mammalian DNA damage checkpoint. 2003;421(6926):961–6. doi:10.1038/nature01446
368. Stiff T, O'Driscoll M, Rief N, Iwabuchi K, Löbrich M, Jeggo PA, Driscoll MO, Rief N, Iwabuchi K, Lo M, et al. ATM and DNA-PK Function Redundantly to Phosphorylate H2AX after Exposure to Ionizing Radiation. 2004;64(7):2390–2396. doi:10.1158/0008-5472.CAN-03-3207
369. Stracker TH, Roig I, Knobel PA, Marjanović M. The ATM signaling network in development and disease. 2013;4. doi:10.3389/fgene.2013.00037
370. Strande NT, Waters CA, Ramsden D a. Resolution of complex ends by Nonhomologous end joining - better to be lucky than good? 2012;3. doi:10.1186/2041-9414-3-10
371. Sturzenegger A, Burdova K, Kanagaraj R, Levikova M, Pinto C, Cejka P, Janscak P. DNA2 cooperates with the WRN and BLM RecQ helicases to mediate long-range DNA end resection in human cells. 2014;289(39):27314–27326. doi:10.1074/jbc.M114.578823
372. Sullivan GM, Feinn R. Using Effect Size - or Why the P Value Is Not Enough. 2012;4(3):279–82. doi:10.4300/JGME-D-12-00156.1
373. Sun J, Lee K-J, Davis AJ, Chen DJ. Human Ku70/80 Protein Blocks Exonuclease 1-mediated DNA Resection in the Presence of Human Mre11 or Mre11/Rad50 Protein Complex. 2012;287(7):4936–4945. doi:10.1074/jbc.M111.306167
374. Sung P, Krejci L, Van Komen S, Sehorn MG. Rad51 recombinase and recombination mediators. 2003;278(44):42729–32. doi:10.1074/jbc.R300027200
375. Swindall AF, Stanley JA, Yang ES. PARP-1: Friend or foe of DNA damage and repair in tumorigenesis? 2013;5(3):943–958. doi:10.3390/cancers5030943
376. Tamura K, Peterson D, Peterson N, Stecher G, Nei M, Kumar S. MEGA5: molecular evolutionary genetics analysis using maximum likelihood, evolutionary distance, and maximum parsimony methods. 2011;28(10):2731–9. doi:10.1093/molbev/msr121
377. Tavecchio M, Munck JM, Cano C, Newell DR, Curtin NJ. Further characterisation of the cellular activity of the DNA-PK inhibitor, NU7441, reveals potential cross-talk with homologous recombination. 2012;69:155–164. doi:10.1007/s00280-011-1662-4
378. Taylor EM, Cecillon SM, Bonis A, Chapman JR, Povirk LF, Lindsay HD. The Mre11/Rad50/Nbs1 complex functions in resection-based DNA end joining in *Xenopus laevis*. 2010;38(2):441–54. doi:10.1093/nar/gkp905
379. Teo SH, Jackson SP. Lif1p targets the DNA ligase Lig4p to sites of DNA double-strand breaks. 2000;10(3):165–8.
380. Tkáč J, Xu G, Adhikary H, Young JTF, Gallo D, Escribano-Díaz C, Krietsch J, Orthwein A, Munro M, Sol W, et al. HELB Is a Feedback Inhibitor of DNA End Resection. 2016;61(3):405–418. doi:10.1016/j.molcel.2015.12.013
381. Tomimatsu N, Mukherjee B, Catherine Hardebeck M, Ilcheva M, Vanessa Camacho C, Louise Harris J, Porteus M, Llorente B, Khanna KK, Burma S. Phosphorylation of EXO1 by CDKs 1 and 2 regulates DNA end resection and repair pathway choice. 2014;5:3561. doi:10.1038/ncomms4561
382. Tomimatsu N, Mukherjee B, Deland K, Kurimasa A, Bolderson E, Khanna KK, Burma S. Exo1 plays a major role in DNA end resection in humans and influences double-strand break repair and damage signaling decisions. 2012;11(4):441–448. doi:10.1016/j.dnarep.2012.01.006
383. Trujillo KM, Yuan SS, Lee EY, Sung P. Nuclease activities in a complex of human recombination and DNA repair factors Rad50, Mre11, and p95. 1998;273(34):21447–50.
384. Truong LN, Li Y, Shi LZ, Hwang PY-H, He J, Wang H, Razavian N, Berns MW, Wu X, Truong LN, et al. Microhomology-mediated End Joining and Homologous Recombination share the initial end resection step to repair DNA double-strand breaks in mammalian cells. 2013;110(19):7720–5. doi:10.1073/pnas.1213431110/-/DCSupplemental.www.pnas.org/cgi/doi/10.1073/pnas.1213431110
385. Turchi JJ, Henkels KM, Zhou Y. Cisplatin-DNA adducts inhibit translocation of the Ku subunits of DNA-PK. 2000;28(23):4634–41.
386. Turinetto V, Giachino C. Multiple facets of histone variant H2AX: A DNA double-strand-break marker with several biological functions. 2015;43(5):2489–2498. doi:10.1093/nar/gkv061
387. Udayakumar D, Dynan WS. Characterization of DNA binding and pairing activities associated with the native SFPQ-NONO DNA repair protein complex. 2015;463(4):473–478. doi:10.1016/j.bbrc.2015.05.024
388. Valerie K, Povirk LF. Regulation and mechanisms of mammalian double-strand break repair. 2003;22(37):5792–5812. doi:10.1038/sj.onc.1206679
389. Vassilev LT, Tovar C, Chen S, Knezevic D, Zhao X, Sun H, Heimbrook DC, Chen L. Selective small-molecule inhibitor reveals critical mitotic functions of human CDK1. 2006;103(28):10660–10665. doi:10.1073/pnas.0600447103
390. Vaux DL, Fidler F, Cumming G. Replicates and repeats — what is the difference and is it significant? 2012;13(4):291–296.

- doi:10.1038/embor.2012.36
391. de Villartay J-P, Fischer A, Durandy A. The mechanisms of immune diversification and their disorders. 2003;3(12):962–72. doi:10.1038/nri1247
392. Di Virgilio M, Callen E, Yamane A, Zhang W, Jankovic M, Gitlin AD, Feldhahn N, Resch W, Oliveira TY, Chait BT, et al. Rif1 prevents resection of DNA breaks and promotes immunoglobulin class switching. 2013;339(6120):711–5. doi:10.1126/science.1230624
393. Vissers JHA, Lohuizen M van, Citterio E. The emerging role of Polycomb repressors in the response to DNA damage. 2012;125(17). doi:10.1128/mcb.01048-09
394. Walker JR, Corpina R a, Goldberg J. Structure of the Ku heterodimer bound to DNA and its implications for double-strand break repair. 2001;412(6847):607–14. doi:10.1038/35088000
395. Wang B, Matsuoka S, Ballif BA, Zhang D, Smogorzewska A, Gygi SP, Elledge SJ. Abraxas and RAP80 form a BRCA1 protein complex required for the DNA damage response. 2007;316(5828):1194–1198. doi:10.1126/science.1139476
396. Wang FK. Confidence Interval for the Mean of Non-Normal Data. 2001;17:257–267. doi:10.1002/qre400
397. Wang H, Shi LZ, Wong CCL, Han X, Hwang PY-H, Truong LN, Zhu Q, Shao Z, Chen DJ, Berns MW, et al. The interaction of CtIP and Nbs1 connects CDK and ATM to regulate HR-mediated double-strand break repair. 2013;9(2):e1003277. doi:10.1371/journal.pgen.1003277
398. Wang H, Wang M, Wang H, Böcker W, Iliakis G. Complex H2AX phosphorylation patterns by multiple kinases including ATM and DNA-PK in human cells exposed to ionizing radiation and treated with kinase inhibitors. 2005;202(2):492–502. doi:10.1002/jcp.20141
399. Wang H, Xu X. Microhomology-mediated end joining: new players join the team. 2017;7(1):6. doi:10.1186/s13578-017-0136-8
400. Wang J, Aroumougame A, Loblrich M, Li Y, Chen D, Chen J, Gong Z, Chen J, Gong Z. PTIP associates with Artemis to dictate DNA repair pathway choice. 2014;28(24):2693–8. doi:10.1101/gad.252478.114
401. Wang M, Wu W, Wu W, Rosidi B, Zhang L, Wang H, Iliakis G. PARP-1 and Ku compete for repair of DNA double strand breaks by distinct NHEJ pathways. 2006;34(21):6170–6182. doi:10.1093/nar/gkl840
402. Wang Q, Xie S, Chen J, Fukasawa K, Naik U, Traganos F, Darzynkiewicz Z, Jhanwar-Uniyal M, Dai W. Cell cycle arrest and apoptosis induced by human Polo-like kinase 3 is mediated through perturbation of microtubule integrity. 2002;22(10):3450–9. doi:10.1128/MCB.22.10.3450
403. Ward JF. Radiation mutagenesis: the initial DNA lesions responsible. 1995;142(3):362–368.
404. Wei H, Yu X. Functions of PARylation in DNA Damage Repair Pathways. 2016;14(3):131–139. doi:10.1016/j.gpb.2016.05.001
405. Wei L, Lan L, Hong Z, Yasui A, Ishioka C, Chiba N. Rapid recruitment of BRCA1 to DNA double-strand breaks is dependent on its association with Ku80. 2008;28(24):7380–93. doi:10.1128/MCB.01075-08
406. Weinberg R a. The retinoblastoma protein and cell cycle control. 1995;81(3):323–30.
407. West SC. Molecular views of recombination proteins and their control. 2003;4(6):435–445. doi:10.1038/nrm1127
408. Williams DR, Lee KJ, Shi J, Chen DJ, Stewart PL. Cryo-EM Structure of the DNA-Dependent Protein Kinase Catalytic Subunit at Subnanometer Resolution Reveals alpha Helices and Insight into DNA Binding. 2008;16(3):468–477. doi:10.1016/j.str.2007.12.014
409. Williams GJ, Hammel M, Radhakrishnan SK, Ramsden D, Lees-Miller SP, Tainer JA. Structural insights into NHEJ: Building up an integrated picture of the dynamic DSB repair super complex, one component and interaction at a time. 2014;17:110–120. doi:10.1016/j.dnarep.2014.02.009
410. Wood RD, Double S. DNA polymerase Theta (POLQ), double-strand break repair, and cancer. 2016;44:22–32. doi:10.1016/j.dnarep.2016.05.003
411. Woodbine L, Brunton H, Goodarzi AA, Shibata A, Jeggo PA. Endogenously induced DNA double strand breaks arise in heterochromatic DNA regions and require ataxia telangiectasia mutated and Artemis for their repair. 2011;39(16):6986–97. doi:10.1093/nar/gkr331
412. Wu J, Lu L-Y, Yu X. The role of BRCA1 in DNA damage response. 2010;1(2):117–123. doi:10.1007/s13238-010-0010-5
413. Wu J, Starr S. Low-fidelity compensatory backup alternative DNA repair pathways may unify current carcinogenesis theories. 2014;10(7):1239–53. doi:10.2217/fon.13.272
414. Wyatt DW, Feng W, Conlin MP, Yousefzadeh MJ, Roberts SA, Mieczkowski P, Wood RD, Gupta GP, Ramsden DA. Essential Roles for Polymerase Theta-Mediated End Joining in the Repair of Chromosome Breaks. 2016;63(4):662–673. doi:10.1016/j.molcel.2016.06.020
415. Xie S, Wu H, Wang Q, Kunicki J, Thomas RO, Hollingsworth RE, Cogswell J, Dai W. Genotoxic stress-induced activation of Plk3 is partly mediated by Chk2. 2002;1(6):424–429. doi:10.4161/cc.1.6.271
416. Xiong X, Du Z, Wang Y, Feng Z, Fan P, Yan C, Willers H, Zhang J. 53BP1 promotes microhomology-mediated end-joining in G1-phase cells. 2015. doi:10.1093/nar/gku1406
417. Xu G, Chapman JR, Brandsma I, Yuan J, Mistrik M, Bouwman P, Bartkova J, Gogola E, Warmerdam D, Barazas M, et al. REV7 counteracts DNA double-strand break resection and affects PARP inhibition. 2015;521(7553):541–4. doi:10.1038/nature14328
418. Xu X, Song Y, Li Y, Chang J, Zhang H, An L. The tandem affinity purification method: An efficient system for protein complex purification and protein interaction identification. 2010;72(2):149–156. doi:10.1016/j.pep.2010.04.009
419. Xu Z, Fulop Z, Zhong Y, Evinger AJ, Zan H, Casali P. DNA Lesions and Repair in Immunoglobulin Class Switch Recombination and Somatic Hypermutation. 2005;1050:146–162. doi:10.1196/annals.1313.119
420. Yamtich J, Sweasy JB. DNA polymerase Family X: Function, structure, and cellular roles. 2010:1136–1150. doi:10.1016/j.bbapap.2009.07.008

421. Yan CT, Boboila C, Souza EK, Franco S, Hickernell TR, Murphy M, Gumaste S, Geyer M, Zarrin AA, Manis JP, et al. IgH class switching and translocations use a robust non-classical end-joining pathway. 2007;449(7161):478–482. doi:10.1038/nature06020
422. Yano K, Morotomi-Yano K, Wang S-Y, Uematsu N, Lee K-J, Asaithamby A, Weterings E, Chen DJ. Ku recruits XLF to DNA double-strand breaks. 2008;9(1):91–6. doi:10.1038/sj.embor.7401137
423. Yin B, Savic V, Juntilla MM, Bredemeyer AL, Yang-Iott KS, Helmink B a, Koretzky G a, Sleckman BP, Bassing CH. Histone H2AX stabilizes broken DNA strands to suppress chromosome breaks and translocations during V(D)J recombination. 2009;206(12):2625–2639. doi:10.1084/jem.20091320
424. Yoo S, Dynan WS. Geometry of a complex formed by double strand break repair proteins at a single DNA end: recruitment of DNA-PKcs induces inward translocation of Ku protein. 1999;27(24):4679–86. doi:10.1093/nar/27.24.4679
425. Yoshikawa K, Okazaki I, Eto T, Kinoshita K, Muramatsu M, Nagaoka H, Honjo T. AID Enzyme-Induced Hypermutation in an Actively Transcribed Gene in Fibroblasts. 2002;296(5575):2033–2036. doi:10.1126/science.1071556
426. Yousefzadeh MJ, Wyatt DW, Takata K ichi, Mu Y, Hensley SC, Tomida J, Bylund GO, Doublié S, Johansson E, Ramsden DA, et al. Mechanism of Suppression of Chromosomal Instability by DNA Polymerase POLQ. 2014;10(10). doi:10.1371/journal.pgen.1004654
427. Yu AM, McVey M. Synthesis-dependent microhomology-mediated end joining accounts for multiple types of repair junctions. 2010;38(17):5706–5717. doi:10.1093/nar/gkq379
428. Yu X, Chen J. DNA damage-induced cell cycle checkpoint control requires CtIP, a phosphorylation-dependent binding partner of BRCA1 C-terminal domains. 2004;24(21):9478–86. doi:10.1128/MCB.24.21.9478-9486.2004
429. Yun MH, Hiom K. CtIP-BRCA1 modulates the choice of DNA double-strand-break repair pathway throughout the cell cycle. 2009;459(7245):460–3. doi:10.1038/nature07955
430. Zgheib O, Huyen Y, DiTullio RA, Snyder A, Venere M, Stavridi ES, Halazonetis TD. ATM signaling and 53BP1. 2005;76(2):119–122. doi:10.1016/j.radonc.2005.06.026
431. Zha S, Boboila C, Alt FW. Mre11: roles in DNA repair beyond homologous recombination. 2009;16(8):798–800. doi:10.1038/nsmb0809-798
432. Zhang Y, Jasin M. An essential role for CtIP in chromosomal translocation formation through an alternative end-joining pathway. 2011;18(1):80–4. doi:10.1038/nsmb.1940.An
433. Zhou B, Elledge S. The DNA damage response: putting checkpoints in perspective. 2000;408(November):433–439.
434. Zhou Y, Caron P, Legube G, Paull TT. Quantitation of DNA double-strand break resection intermediates in human cells. 2014;42(3):e19–e19. doi:10.1093/nar/gkt1309
435. Zhou Y, Lee J-H, Jiang W, Crowe JL, Zha S, Paull TT. Regulation of the DNA Damage Response by DNA-PKcs Inhibitory Phosphorylation of ATM. 2016;65:1–14. doi:10.1016/j.molcel.2016.11.004
436. Zimmerman DW. A note on preliminary tests of equality of variances. 2004;57:173–181. doi:10.1348/000711004849222
437. Zimmerman WC, Erikson RL. Polo-like kinase 3 is required for entry into S phase. 2007;104(6):1847–52. doi:10.1073/pnas.0610856104
438. Zimmermann M, de Lange T. 53BP1: pro choice in DNA repair. 2013;24(Figure 1):1–10. doi:10.1016/j.tcb.2013.09.003

7. Directories

7.1. Abbreviations

Abbreviations for chemical compounds and buffers not included in this abbreviation list, can be found in chapters 5.1.3 and 5.1.4.

53BP1	tumor suppressor p53-binding protein 1
95% CI	confidence interval at the 95% confidence level
aa	amino acid
AB	antibody
ABRAXAS	BRCA1-A complex subunit Abraxas 1
AID	activation-induced cytidine deaminase
Ala (A)	alanine
alt-EJ	alternative end-joining
APLF	aprataxin and PNK-like factor
ARTEMIS	DCLRE1C, DNA cross-link repair 1C protein
Asn (N)	asparagine
Asp (D)	aspartate
ATM	ataxia telangiectasia mutated
ATR	ATM- and Rad3-related
α -TUBULIN	Tubulin alpha-1A chain
β -actin	Actin, cytoplasmic 1
BARD1	BRCA1-associated RING domain protein 1
BLM	Bloom syndrome protein
bp	base pair
BRCA1	breast cancer susceptibility protein 1
BRCT	BRCA1 C-terminal domain
BrdU	5-bromo-2'-deoxyuridine
CD4	T cell surface glycoprotein CD4
CDK	cyclin-dependent kinase
CHD2	chromodomain-helicase-DNA-binding protein 2
CHK	checkpoint kinase
CLSM	confocal laser scanning microscopy
c-NHEJ	canonical non-homologous end-joining
CSR	class switch recombination
CtIP	CtBP-interacting protein
Cys (C)	cysteine
<i>d</i>	effect size (Cohen)
DAPI	4',6-diamidino-2-phenylindole
DDX1	ATP-dependent RNA helicase DEAD box protein 1
DMSO	dimethyl sulfoxide
DNA	deoxyribonucleic acid
DNA2	DNA replication ATP-dependent helicase/nuclease DNA2
DNA-PK	DNA-dependent protein kinase
DNA-PKcs	DNA-dependent protein kinase catalytic subunit
DSB	double-strand break
dsDNA	double-stranded DNA
<i>E. coli</i>	Escherichia coli
EdU	5-ethynyl-2'-deoxyuridine
EJ	end-joining
EXD2	exonuclease 3'-5' domain-containing protein 2
EXO1	exonuclease 1
FITC	fluorescein isothiocyanate

G ₁	gap phase 1
G ₂	gap phase 2
GAPDH	glyceraldehyde-3-phosphate-dehydrogenase
GC	gene conversion
GFP	green fluorescent protein
γH2AX	gamma H2AX; phosphorylated histone variant H2AX
Gln (Q)	glutamine
Glu (E)	glutamate
Gly (G)	glycine
gRNA	guide RNA
Gy	Gray
h	hour
H4 Lys20me2	Lys 20-dimethylated histone H4
HELB	DNA helicase B
His (H)	histidine
HR	homologous recombination
HRP	horseradish peroxidase
hTERT	human telomerase reverse transcriptase
IC50	half maximal inhibitory concentration
IgG	immunoglobulin G
Ile (I)	isoleucine
INO80	DNA helicase INO80
KAP1	KRAB domain associated protein 1; TRIM28, transcription intermediary factor 1-beta
kb	kilo base
kDa	kilo Dalton
Ki	inhibitory constant
KU70/80	XRCC6/5, X-ray repair cross-complementing protein 6/5
LET	linear energy transfer
Leu (L)	leucine
LIG	DNA ligase
Lys (K)	lysine
M	mean
MACS	magnetic-activated cell sorting
MDC1	mediator of DNA damage checkpoint protein 1
me	methylated
MH	microhomology
MMEJ	microhomology-mediated end-joining
MRE11	meiotic recombination 11
MRN	MRE11, RAD50, NBS1 complex
MS	mass spectrometry
<i>n</i>	sample size
NBS1	Nijmegen breakage syndrome 1
NONO	non-POU domain-containing octamer-binding protein
nt (N)	nucleotide
p	phosphorylated
p21	cyclin-dependent kinase inhibitor 1
p53	cellular tumor antigen p53
PARP1	poly(ADP-ribose) polymerase 1
PAXX	paralogue of XRCC4 and XLF
PBAF	chromatin remodeling complex
PBD	polo-box domain
PEI	polyethylenimine
Phe (F)	phenylalanine

PI	propidium iodide
PIKK	phosphatidylinositol 3-kinase-related kinases
PIN1	Peptidyl-prolyl cis-trans isomerase NIMA-interacting 1
PLK3	Serine/threonine-protein kinase PLK3
POH1	PSMD14, 26S proteasome non-ATPase regulatory subunit 14
POL λ	DNA polymerase lambda
POL μ	DNA-directed DNA/RNA polymerase mu
POL θ	DNA polymerase theta
Pro (P)	proline
PTIP	PAXIP1, PAX interacting protein 1
RAD50	radiation repair protein 50
RAD51	DNA repair protein RAD51 homolog 1
RAG1/2	recombination activating gene
RAP80	BRCA1-A complex subunit RAP80
res-cNHEJ	resection-dependent c-NHEJ
RFP	red fluorescent protein
RIF1	RAP1-interacting factor homolog
RING	really interesting new gene
RNA	ribonucleic acid
RNF	E3 ubiquitin protein ligase RING finger protein
RPA	replication protein A
RT	room temperature
S	synthesis phase
<i>S. cerevisiae</i>	<i>Saccharomyces cerevisiae</i>
SD	standard deviation
Ser (S)	serine
SFPQ	splicing factor, proline- and glutamine-rich
siRNA	small interfering RNA
SMARCAD1	SWI/SNF-related matrix-associated actin-dependent regulator of chromatin subfamily A containing DEAD/H box 1
SMART	single molecule analysis of resection tracks
SNM1B	5' exonuclease Apollo; DCLRE1B: DNA cross-link repair 1B protein
SSB	single-strand break
ssDNA	single-stranded DNA
TAP-MS	tandem affinity purification mass spectrometry
TexRed, TR	Texas Red; sulforhodamine 101 acid chloride
Thr (T)	threonine
TOPBP1	DNA topoisomerase 2-binding protein 1
Tyr (Y)	tyrosine
U	enzymatic activity unit
ub	ubiquitinated
VCP	valosin-containing protein
V(D)J	variable, diversity, joining
WRN	Werner syndrome ATP-dependent helicase
WT	wild-type
X-IR	X-ray irradiation
XLF	XRCC4-like factor; Cernunnos
XRCC1	X-ray repair cross-complementing protein 1
XRCC4	X-ray repair cross-complementing protein 4

7.2. List of figures

FIGURE 2.1 CELL CYCLE REGULATION	6
FIGURE 2.2 DSB RECOGNITION	9
FIGURE 2.3 HOMOLOGOUS RECOMBINATION (HR)	14
FIGURE 2.4 CANONICAL NON-HOMOLOGOUS END-JOINING (C-NHEJ)	18
FIGURE 2.5 MICROHOMOLOGY-MEDIATED END-JOINING (MMEJ)	21
FIGURE 3.1 MISREPAIR AND OVERALL REPAIR OF DISTANT I-SCEI-INDUCED DSBs CAN BE ASSESSED BY THE COMBINATION OF THE GC92 REPORTER ASSAY WITH THE γ H2AX FOCI ASSAY	28
FIGURE 3.2 MISREJOINING OF DISTANT DSB ENDS AND OVERALL REPAIR IN GC92 CELLS IN RELATION TO I-SCEI LEVELS	31
FIGURE 3.3 SEQUENCE ANALYSIS OF MISREJOINED BREAK SITES.....	34
FIGURE 3.4 MISREPAIR OF TWO RELATIVELY-CLOSE AND TWO RELATIVELY-DISTANT I-SCEI-INDUCED DSBs	35
FIGURE 3.5 C-NHEJ FACTORS ARE REQUIRED IN END-JOINING REPORTER SYSTEMS	37
FIGURE 3.6 KU80 FOCI CO-LOCALIZE WITH PRPA FOCI AFTER HIGH DOSES OF X-IR IN G ₁ PHASE	39
FIGURE 3.7 PARP1 HAS MULTIPLE ROLES IN DIFFERENT END-JOINING MECHANISMS.....	41
FIGURE 3.8 THE ROLE OF LIG1/3 IS LIMITED TO ALT-EJ	42
FIGURE 3.9 LIG1/3 DEPLETION BARELY INFLUENCES MISREJOINED SITES IN GC92 CELLS	43
FIGURE 3.10 MISREPAIR IN GC92 CELLS REQUIRES POL λ / μ AND POL θ	44
FIGURE 3.11 ARTEMIS IS REQUIRED FOR MISREJOINING OF DSB ENDS.....	45
FIGURE 3.12 53BP1 DEPLETION INCREASES MISREPAIR IN GC92 CELLS	48
FIGURE 3.13 MISREPAIR IN 53BP1-DEPLETED GC92 CELLS REQUIRES ALT-EJ FACTORS	49
FIGURE 3.14 THE ABSENCE OF THE KNOWN RESECTION BARRIER PROTEINS RIF1, REV7, AND RAP80 INCREASED, WHILE THE ABSENCE OF THE 53BP1-ASSOCIATED FACTOR PTIP REDUCED THE MISREPAIR OF DISTANT DSB ENDS	50
FIGURE 3.15 BRCA1 DEPLETION DECREASES MISREPAIR IN GC92 CELLS	52
FIGURE 3.16 THE RING AND BRCT DOMAINS OF BRCA1 ARE REQUIRED FOR THE MISREPAIR OF DISTANT DSBs	53
FIGURE 3.17 CTIP IS REQUIRED FOR MISREJOINING OF DISTANT DSB ENDS.....	55
FIGURE 3.18 CTIP DEPLETION RESULTS IN AN INCREASE IN THE DELETION SIZE AT THE MISREJOINED SITES OF THE REMAINING MISREPAIR EVENTS AND REJOINING IS PRIMARILY CONDUCTED WITHOUT MHS	56
FIGURE 3.19 IN THE ABSENCE OF CTIP, DNA-PK IS REQUIRED TO MISREJOIN THE REMAINING DISTANT DSB ENDS, WHILE POL θ AND PARP ARE NOT	57
FIGURE 3.20 CTIP DEPLETION IN GC92 ARTEMIS KO CELLS PARTIALLY RESCUES THE ARTEMIS REPAIR DEFECT	58
FIGURE 3.21 THE INCREASE OF MISREPAIR EVENTS IN 53BP1-DEPLETED GC92 CELLS IS DEPENDENT ON CTIP.....	59
FIGURE 3.22 THE ENDONUCLEASE FUNCTION OF CTIP IS DISPENSABLE FOR THE MISREJOINING OF DISTANT DSB ENDS IN WT CELLS BUT CRUCIAL IN 53BP1-DEPLETED CELLS	60
FIGURE 3.23 CTIP S327 AND T847 PHOSPHORYLATION SITES ARE REQUIRED FOR MISREJOINING OF DISTANT DSB ENDS	61
FIGURE 3.24 MISREJOINING OF DISTANT DSB ENDS IN GC92 CELLS IS DEPENDENT ON PLK3.....	64
FIGURE 3.25 THE PLK3 DEPLETION PHENOTYPE IN GC92 CELLS RESEMBLES THE CTIP DEPLETION PHENOTYPE	65
FIGURE 3.26 PLK3 IS REQUIRED FOR THE DAMAGE-INDUCIBLE BRCA1-CTIP-PS327 INTERACTION AND FOR THE FADING BRCA1-KU80 INTERACTION AFTER DAMAGE INDUCTION IN G ₁ PHASE.....	67
FIGURE 3.27 PHOSPHORYLATION AT S327 AND T847 BY PLK3 IS NOT SUFFICIENT FOR MISREJOINING OF DISTANT DSB ENDS	68
FIGURE 3.28 MRE11 AND EXD2 ARE REQUIRED FOR MISREJOINING OF DISTANT DSBs BUT MRE11 ENDONUCLEASE FUNCTION IS DISPENSABLE.....	70
FIGURE 3.29 MRE11 ENDO- AND EXONUCLEASE ACTIVITIES ARE REQUIRED FOR MISREPAIR IN 53BP1-DEPLETED GC92 CELLS	72
FIGURE 3.30 EXO1 IS REQUIRED FOR MISREJOINING OF DISTANT DSB ENDS.....	74
FIGURE 4.1 MODEL FOR THE FAILURE OF ACCURATE DSB REPAIR.....	80
FIGURE 4.2 MODEL FOR OVERCOMING RESECTION BARRIERS BY THE RESECTION INITIATION MECHANISM DURING RES-CNHEJ	84
FIGURE 4.3 MODEL FOR RESECTION AND THE PROCESSING OF RESECTION INTERMEDIATES DURING RES-CNHEJ	89
FIGURE 4.4 MODEL FOR COMPLETION OF RES-CNHEJ	92
FIGURE 4.5 ALT-EJ IN RELATION TO WT END-JOINING PATHWAYS IN G ₁ PHASE	105
FIGURE 5.1 WORKFLOW FOR REPORTER ASSAY EXPERIMENTS.....	129
FIGURE S8.1 SUPPLEMENT TO FIGURES 3.2 A	IX

FIGURE S8.2 SUPPLEMENT TO FIGURE 3.2 A, B	IX
FIGURE S8.3 SUPPLEMENT TO FIGURE 3.2 A	X
FIGURE S8.4 CELL CYCLE-DEPENDENT γ H2AX FOCI ANALYSIS IN PLASMID-TRANSFECTED CELLS	X
FIGURE S8.5 SUPPLEMENT TO FIGURE 3.2 A	XI
FIGURE S8.6 SUPPLEMENT TO FIGURE 3.5	XI
FIGURE S8.7 DNA-PK IS REQUIRED THROUGHOUT THE SLOW REPAIR MECHANISM IN G ₁	XIII
FIGURE S8.8 SUPPLEMENT TO FIGURE 3.7 AND 3.8	XIII
FIGURE S8.9 SUPPLEMENT TO FIGURE 3.11	XIV
FIGURE S8.10 SUPPLEMENT TO FIGURES 3.12, 3.13 AND 3.14	XV
FIGURE S8.11 SUPPLEMENT TO FIGURE 3.15 AND 3.16	XVI
FIGURE S8.12 BRCA1-CTIP INTERACTS IN G ₁ PHASE AFTER DAMAGE INDUCTION AND IS DEPENDENT ON CTIP PHOSPHORYLATION AT S327	XVII
FIGURE S8.13 SUPPLEMENT TO FIGURE 3.17 AND 3.19	XVII
FIGURE S8.14 SUPPLEMENT TO FIGURE 3.22 AND 3.23	XIX
FIGURE S8.15 BOTH CTIP S327 AND T847 PHOSPHORYLATION SITES NEED TO BE PHOSPHORYLATED FOR MISREPAIR IN GC92 CELLS	XIX
FIGURE S8.16 SUPPLEMENT TO FIGURE 3.24 AND 3.25	XX
FIGURE S8.17 SUPPLEMENT TO FIGURE 3.28	XXII
FIGURE S8.18 SUPPLEMENT TO FIGURE 3.30	XXII

7.3. List of tables

TABLE 5.1 PRIMERS	117
TABLE 5.2 siRNAs (SMALL INTERFERING RNAs)	117
TABLE 5.3 gRNAs (GUIDE RNAs)	118
TABLE 5.4 INHIBITORS	118
TABLE 5.5 NUCLEOTIDES AND NUCLEOTIDE ANALOGS	119
TABLE 5.6 PRIMARY ANTIBODIES	119
TABLE 5.7 TAGGED PRIMARY ANTIBODIES	120
TABLE 5.8 SECONDARY ANTIBODIES	120
TABLE 5.9 BEADS	120
TABLE 8.1 OVERVIEW OF THE SEQUENCE ANALYSES IN GC92 CELLS	XII
TABLE 8.2 SEQUENCE ANALYSIS IN GC92 CELLS	XII
TABLE 8.3 SEQUENCE ANALYSIS AFTER DEPLETION OF LIG1/3 IN GC92 CELLS	XIII
TABLE 8.4 ARTEMIS-ASSOCIATED FACTORS	XIV
TABLE 8.5 SEQUENCE ANALYSIS AFTER DEPLETION OF CTIP IN GC92 CELLS	XVIII
TABLE 8.6 CTIP-ASSOCIATED FACTORS	XVIII
TABLE 8.7 PLK3-DEPENDENT CTIP PHOSPHORYLATION SITES	XXI
TABLE 8.8 EXO1-ASSOCIATED FACTORS	XXIII

8. Appendix

8.1. Supplemental figures and raw data

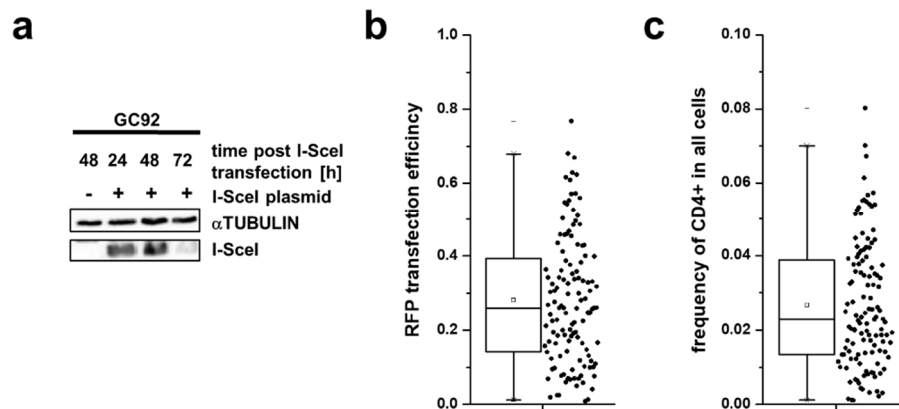


Figure S8.1 Supplement to Figures 3.2 A

(a) I-SceI protein levels in GC92 cells over time. GC92 cells were harvested at various timepoints post-I-SceI transfection and protein levels were analyzed by immunoblotting. Of note, this experiment was part of the master's thesis³⁵. (b, c) Data displayed in Figure S8.3 b in relation to all cells (b) and the RFP transfection efficiency of all experiments displayed in Figure S8.3 b (c).

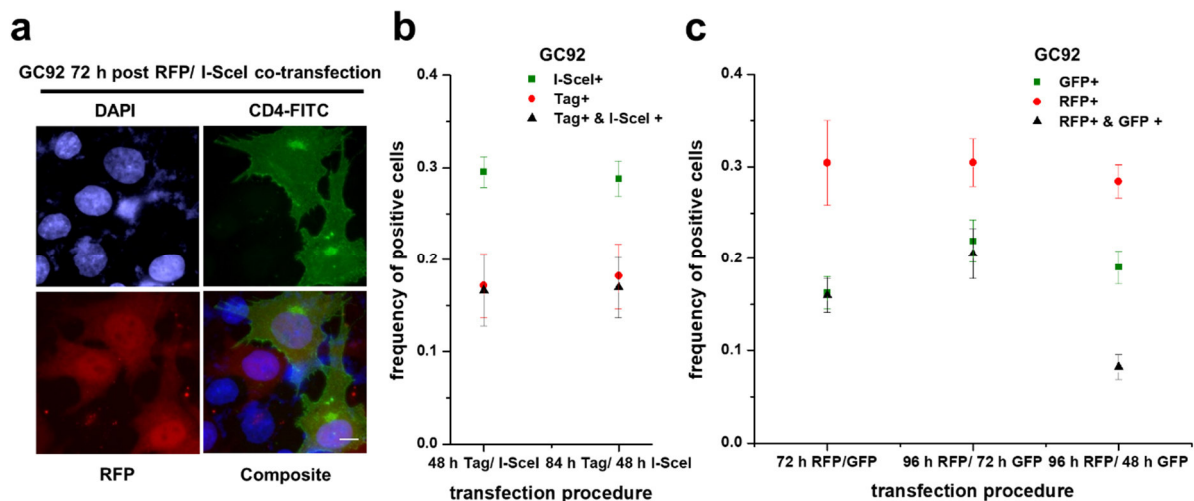


Figure S8.2 Supplement to Figure 3.2 A, B

(a) Representative image for Figure S8.3 b was captured with a 63x objective using Metafer Isis software. The scale bar represents 10 μm . (b, c) Multiple transfections at various timepoints in GC92 cells. GC92 cells were transfected either 24 h, 36 h, or 48 h apart with either the I-SceI plasmid plus a plasmid coding for the tagged 102 kDa protein (b) or with the RFP and GFP plasmids (c). Cells were harvested at the indicated timepoints post-plasmid transfection and either stained for RFP, the tag, I-SceI and the tag, or with anti-RFP and anti-GFP AB plus DAPI. Samples were scanned and analyzed using Metafer software. Data represent the mean of 4 independent experiments performed in duplicate ($n = 4$). Error bars show the *SD*.

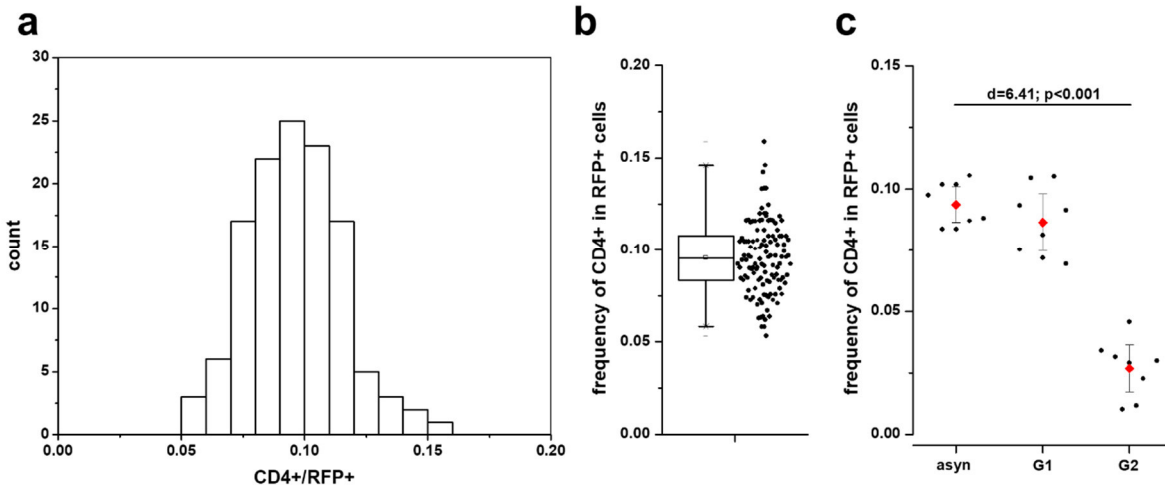


Figure S8.3 Supplement to Figure 3.2 A

(a) Histogram of data displayed in Figure S8.3 b revealing the data are derived from a normally distributed population ($n = 124$). (b) Misrepair events in GC92 cells. GC92 cells were co-transfected with the RFP and I-SceI plasmids and harvesting occurred 72 h post-I-SceI transfection. Cells were stained with anti-CD4, anti-RFP AB, and DAPI. Samples were scanned using Metafer software and plasmid-transfected cells were analyzed. (c) Cell cycle-dependent analysis of misrepair events in GC92 cells. GC92 cells were synchronized with double thymidine block and cells were subsequently held in G₁/G₀ by serum starvation or in G₂ by CDK inhibitor treatment (RO-3306). EdU was added and harvest took place 72 h post-co-transfection with the I-SceI and RFP plasmids. Cells were stained with anti-CD4, anti-RFP AB, and DAPI. Samples were scanned using Metafer software and only plasmid-transfected EdU-negative cells were analyzed. The treatment was very harmful to the cells and therefore only between 500 and 1,000 cells could be analyzed per experiment. (b, c) RFP was used as a marker for cells with damage induction (see chapter 3.1.1). Data represent the mean of 8 or 124 independent experiments performed in duplicates (for b $n = 124$; for c $n = 8$). (c) Error bars show the 95% CI. Effect size was calculated by Cohen's d and p -value was obtained by one-way ANOVA with Bonferroni correction. (b) Box plot shows the mean, median, 25th and 75th percentile (whiskers 1st and 99th percentile). Several data points were part of the analysis in Barton et al. (2014) or Biehs et al. (2017).

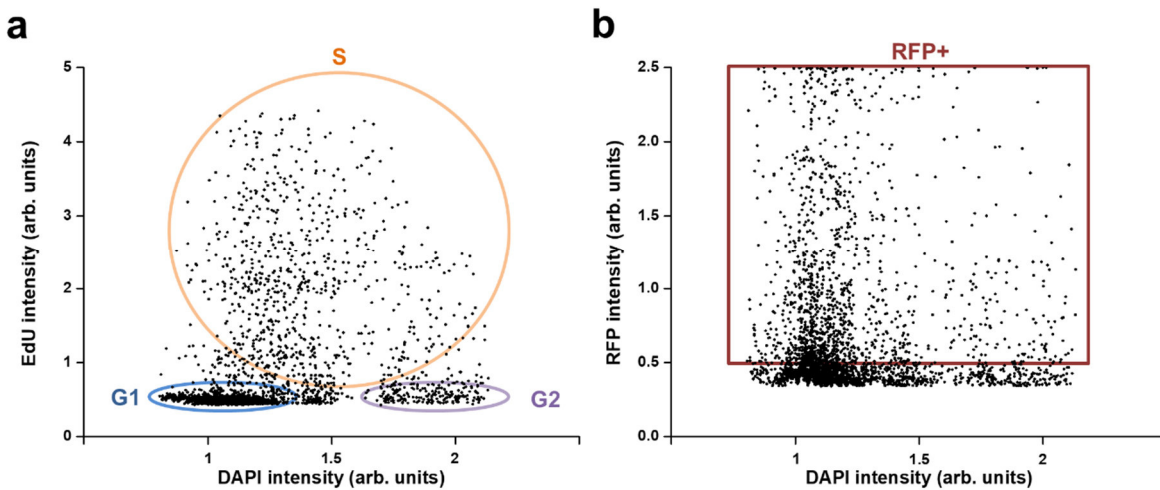


Figure S8.4 Cell cycle-dependent γ H2AX foci analysis in plasmid-transfected cells

(a, b) Cell selection by Metafer software. GC92 cells were treated with EdU and nocodazole 30 min prior to harvest. Harvest took place 72 h post-co-transfection with I-SceI and RFP plasmids. Cells were stained with anti-RFP, anti- γ H2AX ABs, and DAPI. Cells were scanned with Metafer software to select and analyze only RFP-positive cells (red box) in all experiments (b, $n = 1$; 3,291 cells) and to additionally select and only analyze G₁ phase cells (a, $n = 1$; 3,276 cells) in the γ H2AX foci assay (blue circle).

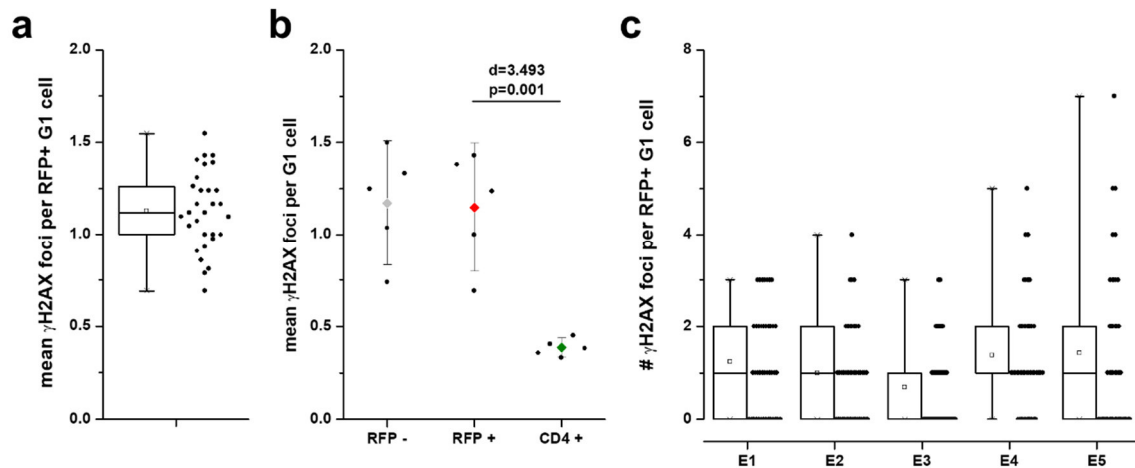


Figure S8.5 Supplement to Figure 3.2 A

(a) Background γ H2AX foci (RFP-negative), overall repair in plasmid-transfected cells (RFP-positive), and γ H2AX in cells that underwent misrepair (CD4-positive). (b) Overall repair in GC92 cells. (a, b) GC92 cells were co-transfected with the RFP and I-SceI plasmids and treated with EdU and nocodazole 30 min prior to harvest. Harvest took place 72 h post-plasmid transfection. Cells were stained with anti-RFP or anti-CD4 plus anti- γ H2AX AB and DAPI. Samples were scanned using Metafer software and non-transfected, plasmid-transfected, and/or CD4-positive G_1 cells were analyzed. RFP was used as a marker for cells with damage induction (see chapter 3.1.1). Data represent the mean of 5 or 30 independent experiments (for a $n = 5$, for b $n = 30$). (a) Error bars show the 95% CI. Effect size was obtained by Cohen's d and p -value was obtained by one-way ANOVA with Bonferroni correction. (c) 5 exemplary experiments from data displayed in Figure S8.5 b. In each experiment at least 40 cells were analyzed. (b, c) Box plots show the mean, median, 25th and 75th percentile (whiskers 1st and 99th percentile). (a, b, c) Several data points were part of the analysis in Biehs et al. (2017).

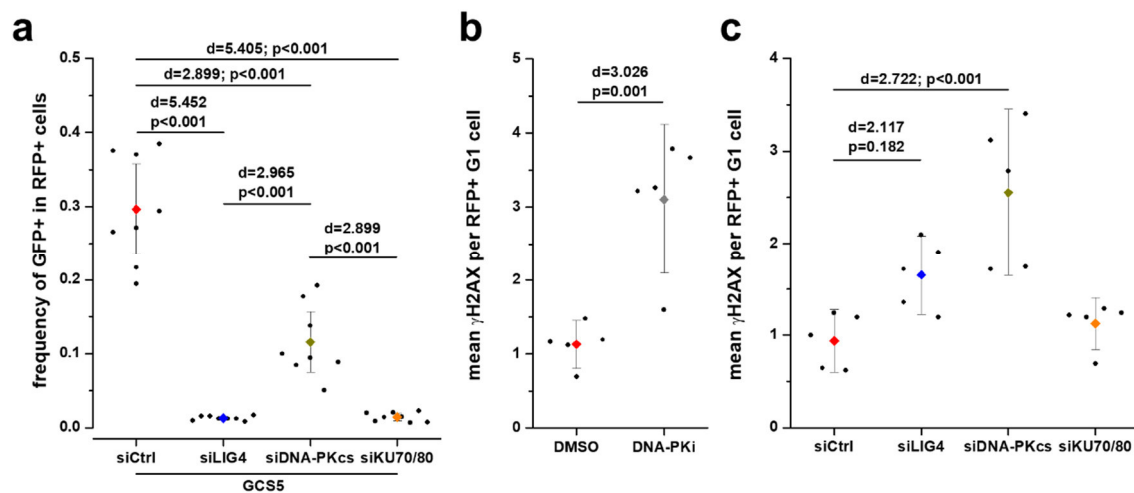


Figure S8.6 Supplement to Figure 3.5

(a, b, c) Impact of inhibition or depletion of core c-NHEJ factors on misrepair in GCS5 (a) or overall repair in GC92 (b, c) cells. GCS5 or GC92 cells were treated with inhibitors or siRNAs against DNA-PK (Nu7441), LIG4, KU70/80, or DNA-PKcs. As a control, cells were treated with DMSO or control siRNA. (a) Cell harvest occurred 72 h post-co-transfection with I-SceI and RFP plasmids. Cells were stained with anti-GFP, anti-RFP AB, and DAPI. Samples were scanned using Metafer software and only plasmid-transfected cells were analyzed. Data represent the mean of 8 independent experiments performed in duplicate ($n = 8$). (b, c) GC92 cells were co-transfected with RFP and I-SceI plasmids and treated with EdU and nocodazole 30 min prior to harvest. Harvesting occurred 72 h post-plasmid transfection. Cells were stained with anti- γ H2AX, anti-RFP AB, and DAPI. Samples were scanned using Metafer software and only plasmid-transfected G_1 cells were analyzed. Data represent the mean of 5 independent experiments ($n = 5$). (a, b, c) RFP was used as a marker for cells with damage induction (see chapter 3.1.1). Error bars show the 95% CI. Effect size was calculated by Cohen's d and p -value was obtained by one-way ANOVA with Bonferroni correction (a,c) or by two-sample Student's t -test (b). (c) Several data points were part of the analysis in Biehs et al. (2017).

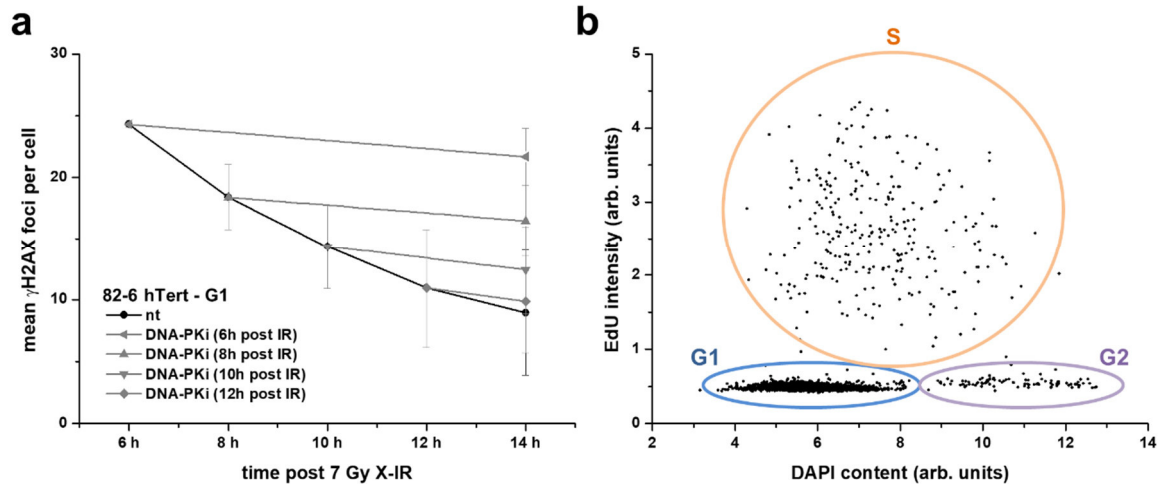


Figure S8.7 DNA-PK is required throughout the slow repair mechanism in G₁
 (a) 82-6 hTERT cells were treated with EdU and nocodazole 30 min prior to 7 Gy X-IR. DMSO or DNA-PK inhibitor (Nu7441) treatment took place at 6 h, 8 h, 10 h, or 12 h post-X-IR and cells were harvested at the indicated timepoints. Cells were stained with anti- γ H2AX AB and DAPI. Samples were scanned using Metafer software and only G₁ cells were analyzed, as identified by EdU intensity and DAPI content (b, $n = 1; 4,191$ cells). Data represent the mean of 4 independent experiments ($n = 4$). Error bars show the *SD*. Experiments were conducted together with R. Weimer and analysis was shared. (a) The kinetics were included in Biehs et al. (2017).

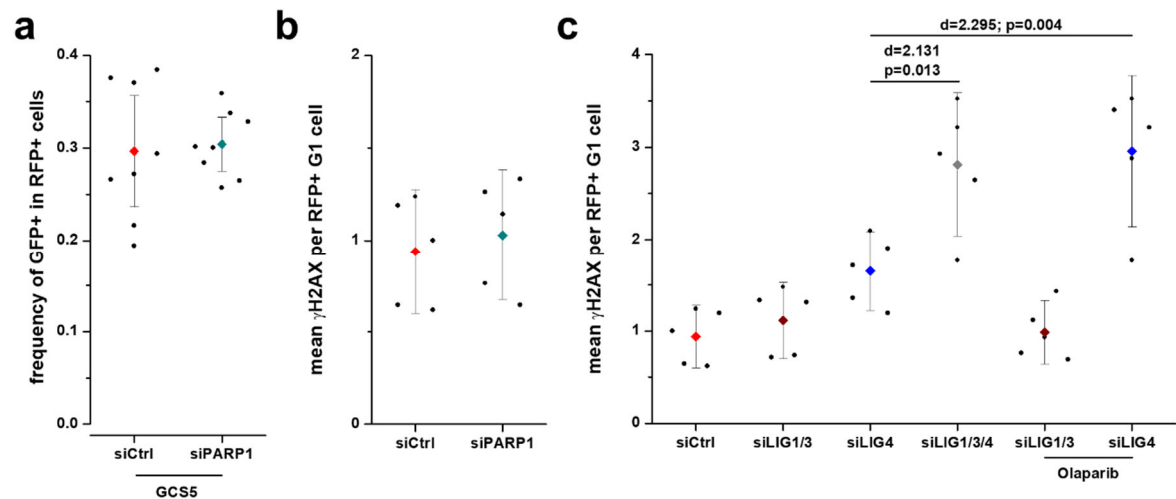


Figure S8.8 Supplement to Figure 3.7 and 3.8
 (a, b, c) Impact of inhibition or depletion of alt-EJ factors on misrepair in GCS5 (a) or overall repair in GC92 (b, c) cells. GCS5 or GC92 cells were treated with inhibitors and/or siRNAs against PARP (Olaparib), PARP1, LIG1/3, and/or LIG4. As a control, cells were treated with DMSO or control siRNA. (a) GCS5 cells were harvested 72 h post-co-transfection with I-SceI and RFP plasmids. Cells were stained with anti-GFP, anti-RFP AB, and DAPI. Samples were scanned using Metafer software and only plasmid-transfected cells were analyzed. Data represent the mean of 8 independent experiments performed in duplicate ($n = 8$). (b, c) GC92 cells were co-transfected with RFP and I-SceI plasmids and treated with EdU and nocodazole 30 min prior to harvest. Harvesting occurred 72 h post-plasmid transfection. Cells were stained with anti- γ H2AX, anti-RFP AB, and DAPI. Samples were scanned using Metafer software and only plasmid-transfected G₁ cells were analyzed. Data represent the mean of 5 independent experiments ($n = 5$). (a, b, c) RFP was used as a marker for cells with damage induction (see chapter 3.1.1). Error bars show the 95% CI. Effect size was calculated by Cohen's *d* and *p*-value was obtained by one-way ANOVA with Bonferroni correction.

Table 8.3 Sequence analysis after depletion of LIG1/3 in GC92 cells

All 39 sequences analyzed after depletion of LIG1/3 from 4 independent experiments ($n = 4$) with the I-SceI recognition site (bold), the I-SceI restriction site (red), MHs (yellow), and insertions (blue). The numbers indicate if sequences were observed more than once. Most sequences were part of the analysis in Biehs et al. (2017).

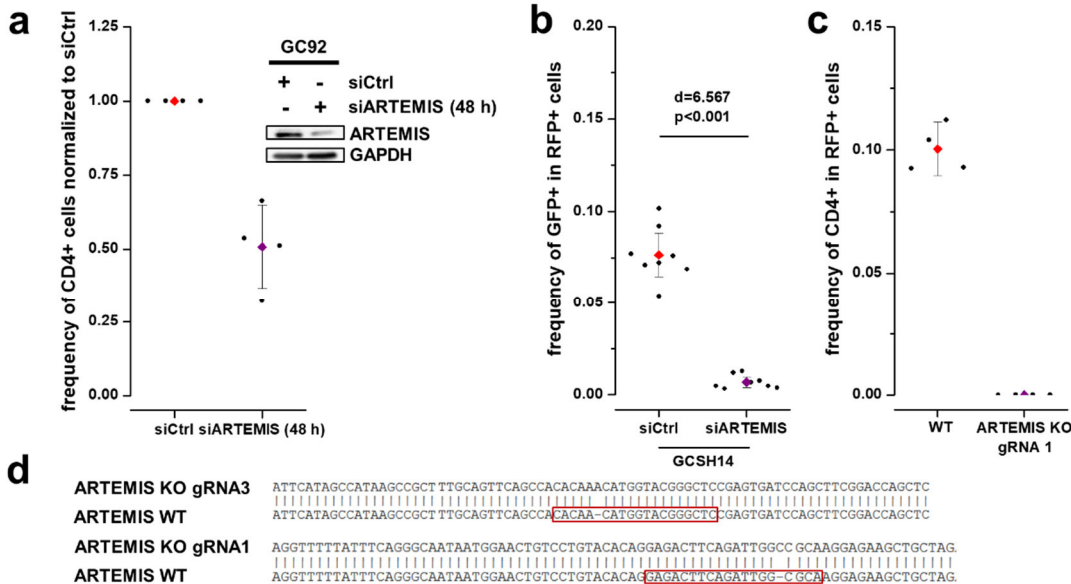
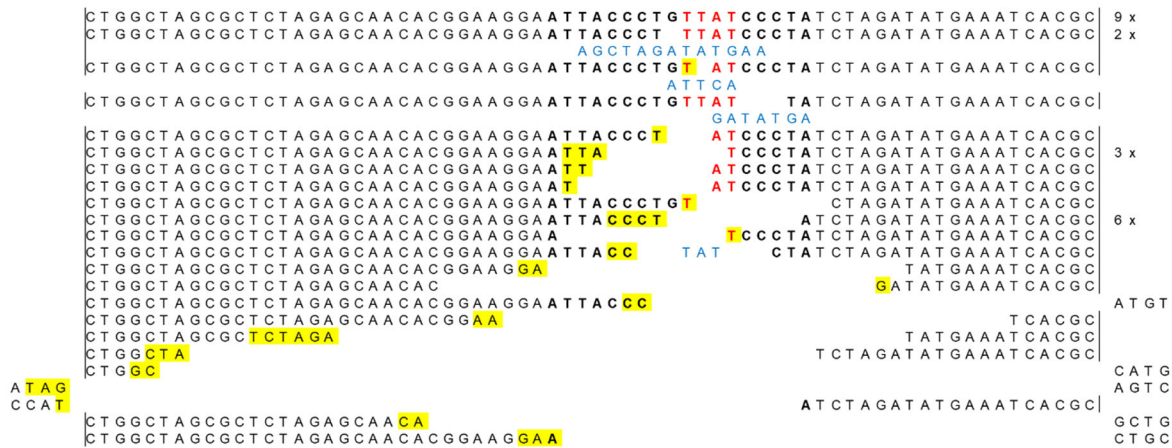


Figure S8.9 Supplement to figure 3.11

(a, b, c) Impact of the absence of ARTEMIS on the misrepair in GC92 (a, c) or GCSH14 (b) cells. GC92 or GCSH14 cells were treated with inhibitors and/or siRNA against ARTEMIS. As a control, cells were treated with DMSO or control siRNA. (a) Based on data published in the master's thesis³⁵. The protocol during these experiments did not allow sufficient time for ARTEMIS downregulation (48 h instead of 72 h) although downregulation by siRNA measured by immunoblotting showed a strong reduction in ARTEMIS protein levels. Each experiment was normalized to cells treated with control siRNA and all cells were analyzed. (b, c) Cells were harvested 72 h post-co-transfection with the I-SceI and RFP plasmids. Cells were stained with anti-GFP or anti-CD4 plus anti-RFP AB and DAPI. Samples were scanned using Metafer software and only plasmid-transfected cells were analyzed. (a, b, c) Data represent the mean of 4 or 8 independent experiments performed in duplicate ($n = 4$ for a, c; $n = 8$ for b). (b, c) RFP was used as a marker for cells with damage induction and exogenous protein (see chapter 3.1.1). Error bars show the 95% CI (b, c) or the SD (a). Effect size was calculated by Cohen's d and p -value was obtained by two-sample Student's t -test. (d) Generation of GC92 ARTEMIS KO cells by CRISPR/Cas9 technology with gRNAs #3 and #1 (red boxes). KO was confirmed by sequencing. Both GC92 ARTEMIS KO cell lines show a 1 nt insertion resulting in a premature termination of the amino acid sequence. Of note, in all experiments labeled ARTEMIS KO, GC92 ARTEMIS KO cells generated with gRNA #3 were used.

Table 8.4 ARTEMIS-associated factors

SFB-ARTEMIS-WT was precipitated and purified from stably-transfected HEK293 cells with streptavidin beads. Precipitation took place in unirradiated controls, 30 min, or 2 h post-5 Gy X-IR (all conditions $n = 1$). MS was performed by the Taplin Mass Spectrometry Facility, Harvard Medical School. Conditions where no interaction was observed were given a value of 0.1 for further analysis. The minimum amount of interacting peptides of a potential interaction partner was used to calculate the ratio of the irradiated sample compared to the unirradiated condition. Therefore, values greater than 1 show an interaction increase while values less than 1 show an interaction decrease following X-IR. Interesting possible novel interacting proteins and some established interacting proteins are included in this table. Of note, observed interactions may be unspecific or may not only result from a direct interaction, but also an indirect protein-protein or indirect DNA-protein interaction.

ARTEMIS TAP-MS Protein	min # pep.			Ratio	
	0 Gy	5Gy 30 min	2 h	30 min	2 h
DCLRE1C	51	62	59	1.216	1.157
DDX1	2	4	6	2	3
LIG4	3	3	6	1	2
MCRS1	0.1	4	5	40	50
MRE11A	10	11	12	1.1	1.2
NBN	14	21	21	1.5	1.5
NONO	1	3	13	3	13
PAXIP1	0.1	3	3	30	30
PRKDC	312	339	337	1.087	1.08
PSMD14	1	0.1	3	0.1	3
RAD50	18	27	24	1.5	1.33
RBBP4	5	3	4	0.6	0.8
RBBP7	3	3	7	1	2.333
RNF138	3	2	1	0.667	0.333
SFPQ	1	5	12	5	12
TOPBP1	7	30	30	4.28571	4.28571
TRIM28	9	16	15	1.778	1.667
XRCC4	3	3	4	1	1.33333
XRCC5	9	3	11	0.333	1.222
XRCC6	9	10	13	1.111	1.444

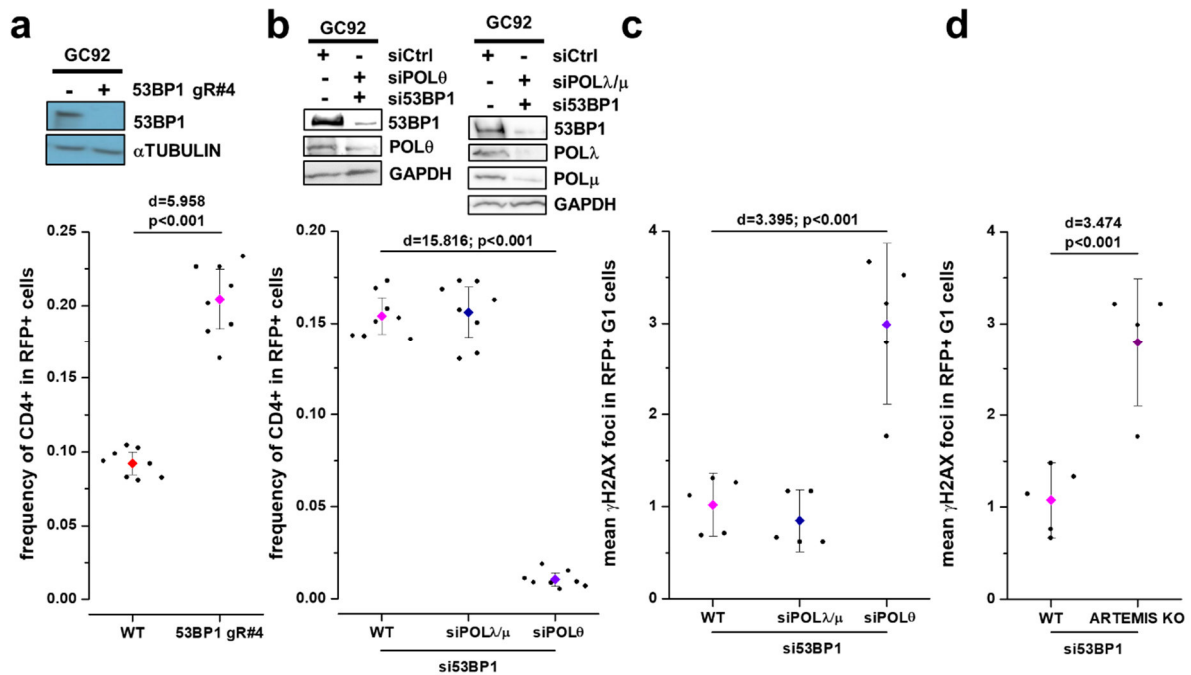


Figure S8.10 Supplement to Figures 3.12, 3.13 and 3.14

(a, b, c, d) Impact of 53BP1 CRISPR/Cas9 viral transduction (a) or co-depletion of polymerases with 53BP1 (b, c) on the misrepair (a, b) or overall repair (c, d) in GC92 cells. (a) GC92 cells were virally transduced with CRISPR/Cas9 and 53BP1 gRNA #4 plasmids and selected by selection medium. Downregulation by CRISPR/Cas9 was confirmed by immunoblotting. (b, c, d) GC92 WT or ARTEMIS KO cells were treated with siRNAs against POL θ , POL λ/μ , and/or 53BP1. (a, b) Cells were harvested 72 h post-co-transfection with I-SceI and RFP plasmids and stained with anti-CD4, anti-RFP AB, and DAPI. Samples were scanned using Metafer software and only plasmid-transfected cells were analyzed. Data represent the mean of 8 independent experiments performed in duplicate ($n = 8$). (c, d) Cells were co-transfected with RFP and I-SceI plasmids and treated with EdU and nocodazole 30 min prior to harvest. Harvest took place 72 h post-plasmid transfection. Cells were stained with anti- γ H2AX, anti-RFP AB, and DAPI. Samples were scanned using Metafer software and only plasmid-transfected G₁ cells were analyzed. Data represent the mean of

5 independent experiments ($n = 5$). (a, b, c, d) RFP was used as a marker for cells with damage induction (see chapter 3.1.1). Error bars show the 95% CI. Effect size was calculated by Cohen's d and p -value was obtained by one-way ANOVA with Bonferroni correction (for b, c) or by two-sample Student's t -test (for a, d).

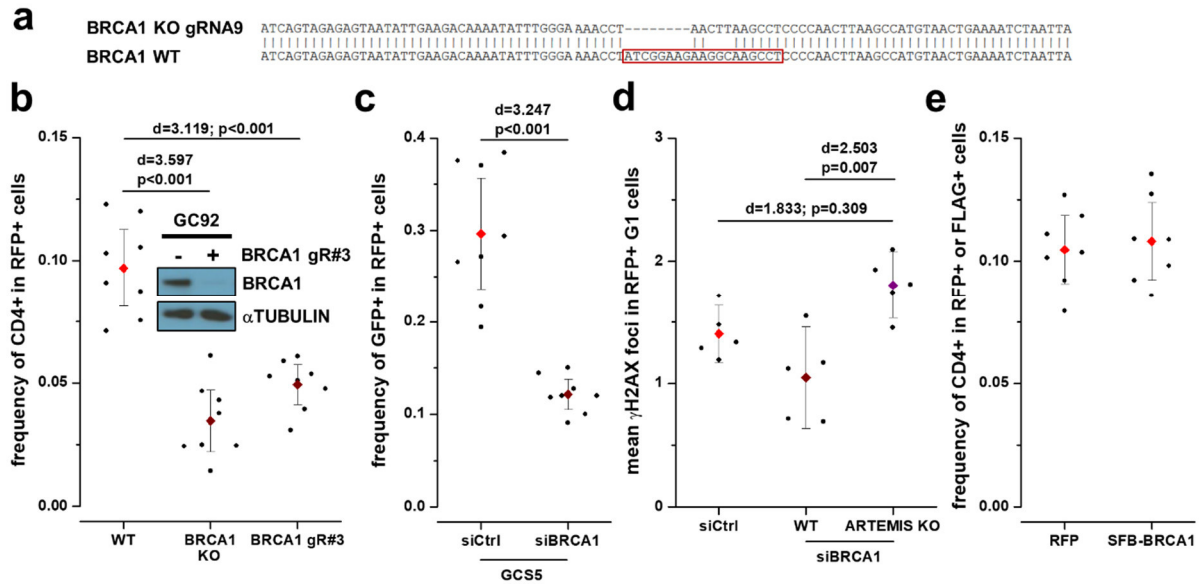


Figure S8.11 Supplement to Figure 3.15 and 3.16

(a) Generation of GC92 BRCA1 KO cells by CRISPR/Cas9 technology with gRNA #9 (red box). KO was confirmed by sequencing. The GC92 BRCA1 KO cell line entails an 8 nt deletion resulting in premature termination of the amino acid sequence. Of note, due to the position of the gRNA, the RING domain is still fully present but the BRCT domain is completely depleted. (b, c, d, e) Impact of BRCA1 impairment (b, c, d) or overexpression (e) on misrepair (b, c, e) or overall repair (d) in GC92 (b, d, e) or GCS5 (c) cells. GCS5, GC92 WT, or ARTEMIS KO cells were treated with siRNAs against BRCA1. As a control, cells were treated with control siRNA. (b) GC92 cells were virally transduced with CRISPR/Cas9 and BRCA1 gRNA #3 plasmids and selected by selection medium. Downregulation by CRISPR/Cas9 was confirmed by immunoblotting. (b, c) Cells were harvested 72 h post-co-transfection with I-SceI and RFP plasmids. Cells were stained with anti-CD4 or anti-GFP plus anti-RFP AB and DAPI. (d) Cells were co-transfected with RFP and I-SceI plasmids and treated with EdU and nocodazole 30 min prior to harvest. Harvest took place 72 h post-plasmid transfection. Cells were stained with anti- γ H2AX, anti-RFP AB, and DAPI. Samples were scanned using Metafer software and only plasmid-transfected G₁ cells were analyzed. Data represent the mean of 5 independent experiments ($n = 5$). (e) GC92 cells were transfected with the RFP or SFB-BRCA1 plasmid. 36 h after plasmid transfection, cells were transfected with I-SceI and harvest took place after an additional 72 h. Cells were stained with anti-RFP or anti-FLAG plus anti-CD4 AB and DAPI. (b, c, e) Samples were scanned using Metafer software and only plasmid-transfected cells were analyzed. Data represent the mean of 8 independent experiments performed in duplicate ($n = 8$). Overexpression was confirmed by microscopy in a facility without a microscope camera. (b, c, d, e) RFP and FLAG were used as markers for cells with damage induction and exogenous protein (see chapter 3.1.1). Error bars show the 95% CI. Effect size was calculated by Cohen's d and p -value was obtained by one-way ANOVA with Bonferroni correction (for b, d) or by two-sample Student's t -test (for c).

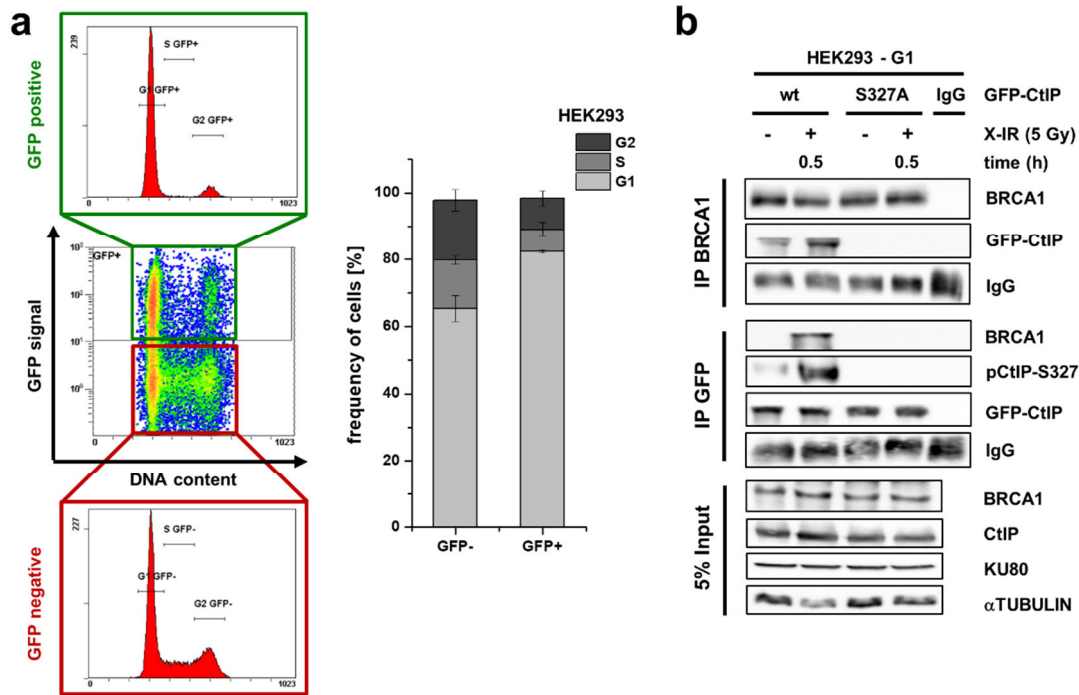


Figure S8.12 BRCA1-CtIP interacts in G₁ phase after damage induction and is dependent on CtIP phosphorylation at S327

(a) Cell cycle distribution of G₁-synchronized HEK293 cells. HEK293 cells were transfected with the GFP-CtIP-WT plasmid which resulted in G₁ synchronization in GFP-positive cells 24 h post-transfection. Cells were harvested and stained with anti-GFP AB and PI. Samples were analyzed by flow cytometry. Data represent the mean of 3 independent experiments ($n = 3$). Error bars show the SD. (b) BRCA1-CtIP co-immunoprecipitation from G₁-synchronized HEK293 cells. Exogenous GFP-CtIP-WT, GFP-CtIP-S327A, or endogenous BRCA1 was immunoprecipitated from HEK293 cells 30 min post-5 Gy X-IR or from unirradiated controls with anti-GFP or anti-BRCA1 ABs. Protein levels were analyzed after immunoblotting of the samples.

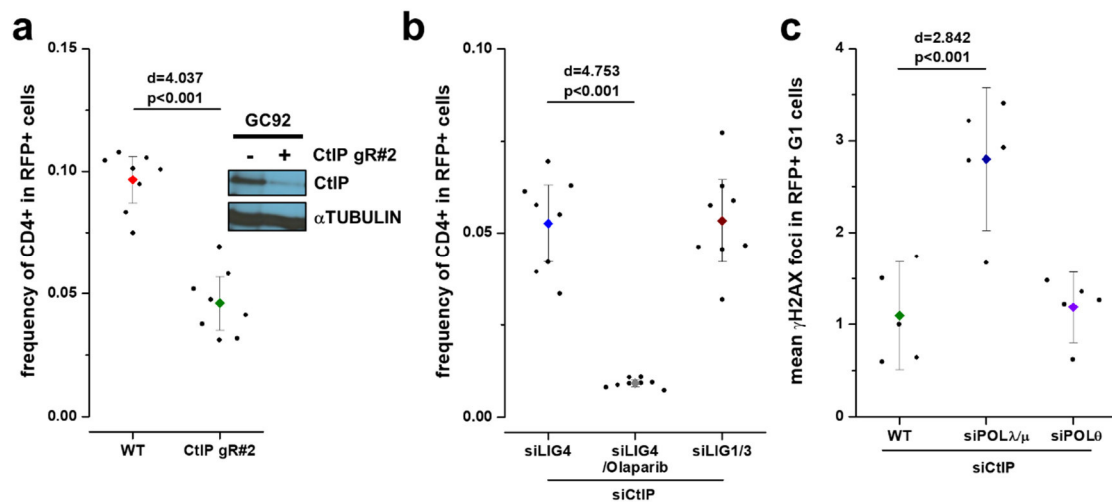


Figure S8.13 Supplement to Figure 3.17 and 3.19

(a, b, c) Impact of CtIP CRISPR/Cas9 viral transduction (a) or co-depletion of ligases (b) or polymerases (c) with CtIP on the misrepair (a, b) or overall repair (c) in GC92 cells. (a) GC92 cells were virally transduced with CRISPR/Cas9 and CtIP gRNA #2 plasmids and selected using selection medium. Downregulation by CRISPR/Cas9 was confirmed by immunoblotting. (b, c) GC92 cells were treated with siRNA against PARP (Olaparib), LIG4, LIG1/3, POL θ , POL λ/μ , and/or CtIP. (a, b) Cells were harvested 72 h post-co-transfection with the I-SceI and RFP plasmids. Cells were stained with anti-CD4, anti-RFP AB, and DAPI. Samples were scanned using Metafer software and only plasmid-transfected cells were analyzed. Data represent the mean of 8 independent experiments performed in duplicate ($n = 8$). (c) Cells were co-transfected with RFP and I-SceI plasmids and treated with EdU and nocodazole

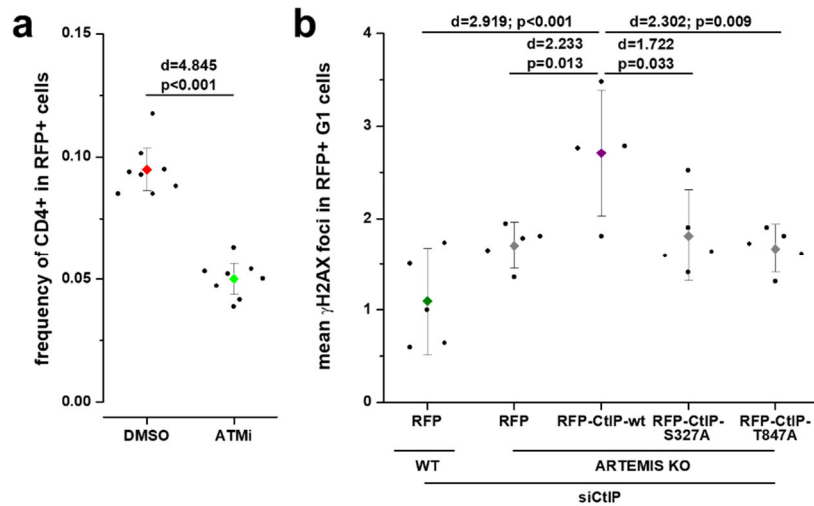


Figure S8.14 Supplement to Figure 3.22 and 3.23

(a) Impact of ATM inhibition on misrepair in GC92 cells. GC92 cells were treated with an inhibitor against ATM (Ku60019). As a control, cells were treated with DMSO. Cells were harvested 72 h post-co-transfection with I-SceI and RFP plasmids. Cells were stained with anti-CD4, anti-RFP AB, and DAPI. Samples were scanned using Metafer software and only plasmid-transfected cells were analyzed. Data represent the mean of 8 independent experiments performed in duplicate ($n = 8$). (b) Impact of CtIP complementation with phospho-mutants S327A and T847A on overall repair in CtIP-depleted GC92 WT and ARTEMIS KO cells. Cells were treated with siRNA against CtIP and transfected with the RFP or siRNA-resistant RFP-CtIP-WT, RFP-CtIP-S327A, or RFP-CtIP-T847A plasmid. 36 h after plasmid transfection, cells were transfected with I-SceI and treated with EdU and nocodazole 30 min prior to harvest. Harvest took place 72 h post-I-SceI plasmid transfection. Cells were stained with anti- γ H2AX, anti-RFP AB, and DAPI. Samples were scanned using Metafer software and only plasmid-transfected G₁ cells were analyzed. Data represent the mean of 5 independent experiments ($n = 5$). (a, b) RFP was used as a marker for cells with damage induction and exogenous protein (see chapter 3.1.1). Error bars show the 95% CI. Effect size was calculated by Cohen's d and p -value was obtained by one-way ANOVA with Bonferroni correction (b) or by two-sample Student's t -test (a).

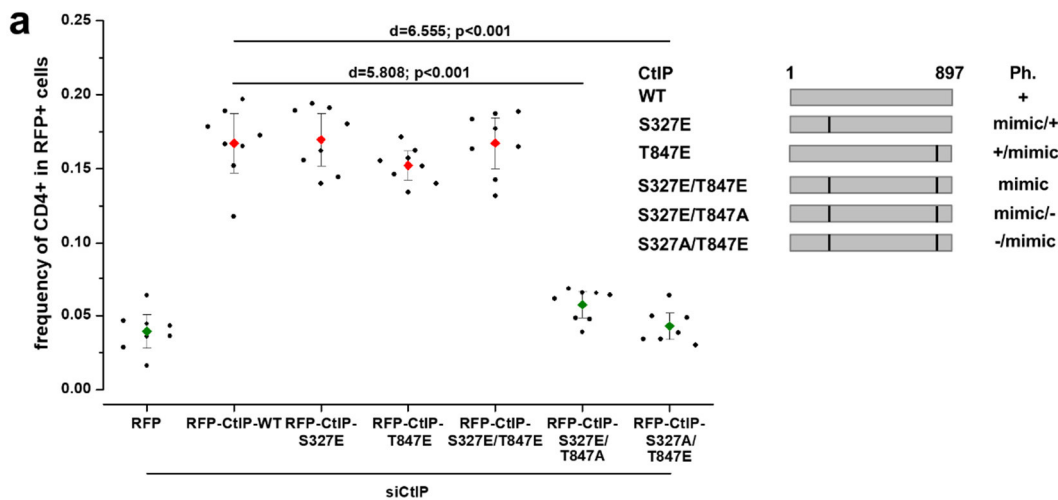


Figure S8.15 Both CtIP S327 and T847 phosphorylation sites need to be phosphorylated for misrepair in GC92 cells

(a) Impact of CtIP complementation with phospho-mimic- and phospho-mutants on misrepair in CtIP-depleted GC92 cells. GC92 cells were treated with siRNA against CtIP. Cells were transfected with the RFP or siRNA-resistant RFP-CtIP-WT, RFP-CtIP-S327E, RFP-CtIP-T847E, RFP-CtIP-S327E/T847E, RFP-CtIP-S327E/T847A, or RFP-CtIP-S327A/T847E plasmid. 36 h after plasmid transfection, cells were transfected with I-SceI and harvest took place after an additional 72 h. Diagrams of the exogenous CtIP WT, the S327E and/or T847E phospho-mimic-mutants and the mixed phospho-mimic-/phospho-mutants are not drawn to scale. Cells were stained with anti-CD4, anti-RFP AB, and DAPI. Samples were scanned using Metafer software and only plasmid-transfected cells were analyzed. Data represent the mean of 8 independent experiments performed in duplicate ($n = 8$). RFP was used as a marker for cells

with damage induction and exogenous protein (see chapter 3.1.1). Error bars show the 95% CI. Effect size was calculated by Cohen's d and p -value was obtained by one-way ANOVA with Bonferroni correction.

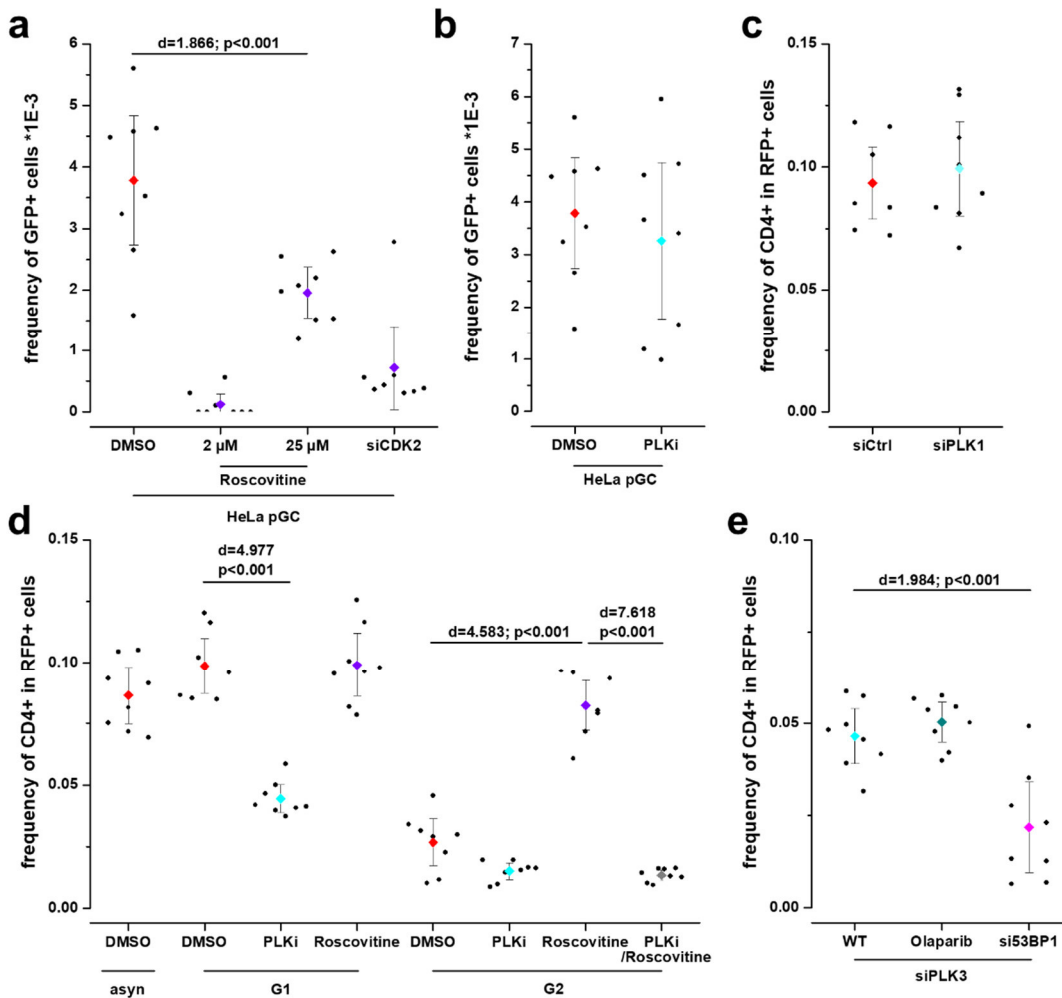


Figure S8.16 Supplement to Figure 3.24 and 3.25

(a, b, c, d, e) Impact of CDK impairment (a, d), PLK3 inhibition or depletion (b, d, e), PLK1 depletion (c), or PLK3 depletion in combination with PARP or 53BP1 impairment (e) on gene conversion (a, b) or misrepair (c, d, e) in HeLa pGC (a, b), GC92 (c, e), or synchronized GC92 (d) cells. GC92 or HeLa pGC cells were treated with inhibitors and/or siRNAs against CDK1/2 (roscovitine), CDK2, PLK1/3 (GW843682X), PLK1, PARP (Olaparib), 53BP1, and/or PLK3. As a control, cells were treated with DMSO or control siRNA. (a, b, c, e) Harvest took place 72 h post-transfection with the RFP and/or I-SceI plasmids. Cells were stained with anti-GFP and DAPI or anti-CD4, anti-RFP AB, and DAPI. Samples were scanned using Metafer software and only plasmid-transfected GC92 cells or all HeLa pGC cells were analyzed. (d) GC92 cells were synchronized with double thymidine block and subsequently maintained in G₁/G₀ by serum starvation or in G₂ by CDK inhibitor treatment (RO-3306). EdU was added and cells were harvested 72 h post-co-transfection with the I-SceI and RFP plasmids. Cells were stained with anti-CD4, anti-RFP AB, and DAPI. Samples were scanned using Metafer software and only plasmid-transfected EdU-negative cells were analyzed. The treatment was very harmful to the cells and therefore only between 500 and 1,000 cells could be analyzed per experiment. (a, b, c, d, e) Data represent the mean of 8 independent experiments performed in duplicate ($n = 8$). RFP was used as a marker for cells with damage induction (see chapter 3.1.1). Error bars show the 95% CI. Effect size was calculated by Cohen's d and p -value was obtained by one-way ANOVA with Bonferroni correction. (a, b) Several data points were part of the analysis in Barton et al. (2014).

Table 8.7 PLK3-dependent CtIP phosphorylation sites

(a, b) CtIP sites *in vitro* phosphorylated by recombinant PLK3 (a) or phosphorylated by PLK3 in a damage-inducible manner (b). SFB-CtIP-WT was precipitated and purified from stably-transfected HEK293 cells with streptavidin beads. (a) SFB-CtIP-WT was incubated with recombinant PLK3 *in vitro* where indicated ($n = 2$). (b) Precipitation took place 30 min or 2 h after X-IR with or without PLK inhibitor (GW843682X) treatment 1 h prior to irradiation ($n = 1$). (a, b) The numbers represent the Ascore. An Ascore < 19 is an unlikely phosphorylation, while values ≥ 19 indicate a likely phosphorylation. Sites that did not provide any data under a specific condition were given the value 0.1. An Ascore of 1,000 represents a certain phosphorylation signal in this experiment. For each detected phosphorylation site, the highest observed Ascore was used. The experimental procedure was conducted by J. Wang. MS and Ascore calculations were performed at the Taplin Mass Spectrometry Facility, Harvard Medical School. Several phosphorylation sites have not been described previously to Barton et al. (2014). Of note, lack of observation of a phosphorylation in this analysis does not mean that this phosphorylation does not exist in general. (a) This CtIP phosphorylation site analysis (without the ratios) was included in Barton et al. (2014).

a				b						
HEK293 Site	CtIP-wt	PLK3-wt CtIP-wt	Ratio	HEK293 Site	DMSO 30 min	PLKi 30 min	DMSO 2 h	PLKi 2 h	Ratio 30 min	Ratio 2 h
S163	46	30	0.65217	S163	14	8	0.1	0.1	0.57143	1
S171	43	19	0.44186							
T190	0.1	2	20							
S197	0.1	1000	10000							
S231	44	34	0.77273	S231	6	9	0.1	0.1	1.5	1
S233	51	38	0.74510	S233	51	31	20	24	0.60784	1.2
T245	22	0.1	0.00455	T245	0.1	20	13	19	200	1.46154
S298	0.1	16	160							
T302	0.1	22	220	T302	6	0.1	3	0.1	0.01667	0.03333
S305	19	34	1.78947	S305	10	0.1	2	3	0.01	1.5
S309	15	13	0.86667	S309	24	10	4	18	0.41667	4.5
S311	19	19	1	S311	19	12	17	9	0.63158	0.52941
T312	16	7	0.43750	T312	9	13	0.1	5	1.44444	50
S313	15	0.1	0.00667	S313	13	9	16	13	0.69231	0.8125
T315	40	53	1.325	T315	46	38	51	49	0.82609	0.96078
T323	22	27	1.22727	T323	9	3	7	0.1	0.33333	0.01429
S326	17	32	1.88235	S326	82	14	16	16	0.17073	1
S327	16	50	3.125	S327	72	22	16	21	0.30556	1.3125
T333	0.1	32	320	T333	0.1	0.1	0.1	5	1	50
T344	26	23	0.88462	T344	19	0.1	16	0.1	0.00526	0.00625
S345	38	38	1	S345	21	0.1	23	15	0.00476	0.65217
S347	31	31	1	S347	37	13	31	46	0.35135	1.48387
S349	0.1	56	560							
T361	0.1	85	850							
T367	0.1	8	80							
S377	40	4	0.1	S377	23	16	20	26	0.69565	1.3
S379	25	16	0.64	S379	19	15	23	32	0.78947	1.39130
S382	5	27	5.4	S382	7	13	5	6	1.85714	1.2
T386	6	3	0.5	T386	0.1	11	0.1	8	110	80
S389	0.1	22	220	S389	0.1	12	0.1	8	120	80
S413	0.1	52	520							
S415	0.1	49	490							
S439	1000	31	0.031	S439	1000	1000	1000	39	1	0.039
T450	19	0.1	0.00526							
S454	0.1	11	110							
T520	0.1	71	710							
T527	7	7	1							
S539	43	38	0.88372	S539	60	22	20	51	0.36667	2.55
T544	8	56	7							
S549	30	8	0.26667							
S555	29	37	1.27586	S555	12	0.1	0.1	0.1	0.00833	1
S568	58	53	0.91379	S568	35	32	48	53	0.91429	1.10417
S593	97	79	0.81443	S593	1000	87	89	68	0.087	0.76404
T596	11	23	2.09091	T596	11	0.1	0.1	0.1	0.00909	1
				S608	24	0.1	0.1	0.1	0.00417	1
S627	0.1	71	710							
S649	35	16	0.45714	S641	30	18	18	12	0.6	0.66667
T671	0.1	77	770	S649	35	31	17	16	0.88571	0.94118
S679	11	0.1	0.00909	S679	19	8	18	15	0.42105	0.83333
T687	0.1	47	470							
T693	0.1	50	500	T693	6	0.1	0.1	0.1	0.01667	1
S713	0.1	26	260							
S714	0.1	23	230							
S723	1000	1000	1	S723	1000	1000	1000	1000	1	1
T731	5	0.1	0.02							
S743	24	0.1	0.00417	S743	6	0.1	0.1	0.1	0.01667	1
S745	21	0.1	0.00476							
Y780	0.1	26	260							
T788	0.1	13	130							
S789	0.1	15	150							
T847	0.1	24	240							
T859	0.1	4	40							
Y867	0.1	1000	10000							
S889	127	110	0.86614	S889	110	81	74	92	0.73636	1.24324

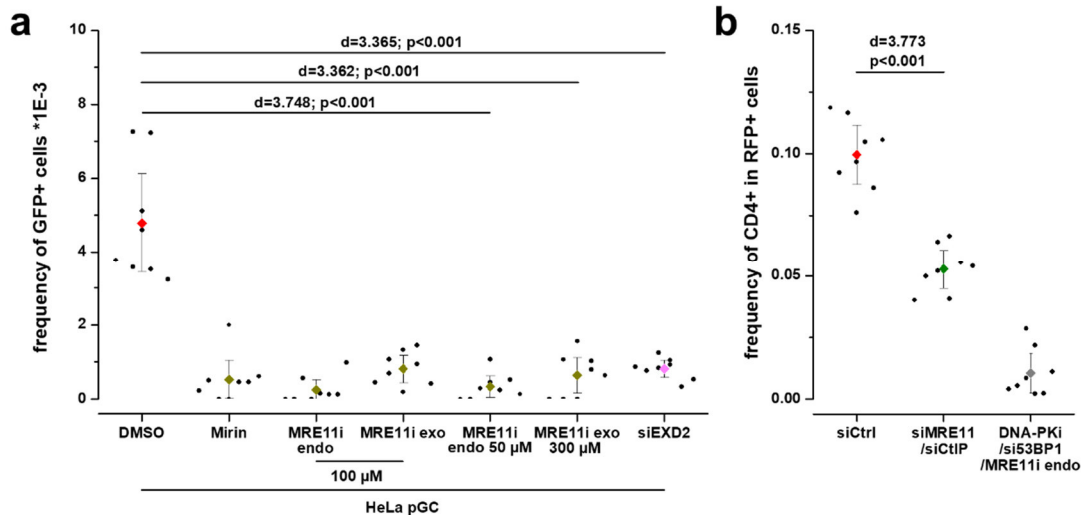


Figure S8.17 Supplement to Figure 3.28

(a, b) Impact of MRE11 inhibition, EXD2 (a), MRE11, and/or CtIP (b) depletion on misrepair in GC92 cells (b) or gene conversion in HeLa pGC cells (a). GC92 or HeLa pGC cells were treated with inhibitors and/or siRNAs against MRE11 endonuclease activity (PFM01), MRE11 exonuclease activity (PFM39, Mirin), MRE11, CtIP, 53BP1, DNA-PK (Nu7441), or EXD2. As a control, cells were treated with DMSO or control siRNA. Harvest took place 72 h post-transfection with RFP and/or I-SceI plasmids. Cells were stained with anti-CD4, anti-RFP AB, and DAPI (for GC92 cells) or with anti-GFP and DAPI (for HeLa pGC cells). Samples were scanned using Metafer software and only plasmid-transfected GC92 cells or all HeLa pGC cells were analyzed. Data represent the mean of 8 independent experiments performed in duplicate ($n = 8$). RFP was used as a marker for cells with damage induction (see chapter 3.1.1). Error bars show the 95% CI. Effect size was calculated by Cohen's d and p -value was obtained by one-way ANOVA with Bonferroni correction. (a) Several data points were part of the analysis in Biéhs et al. (2017).

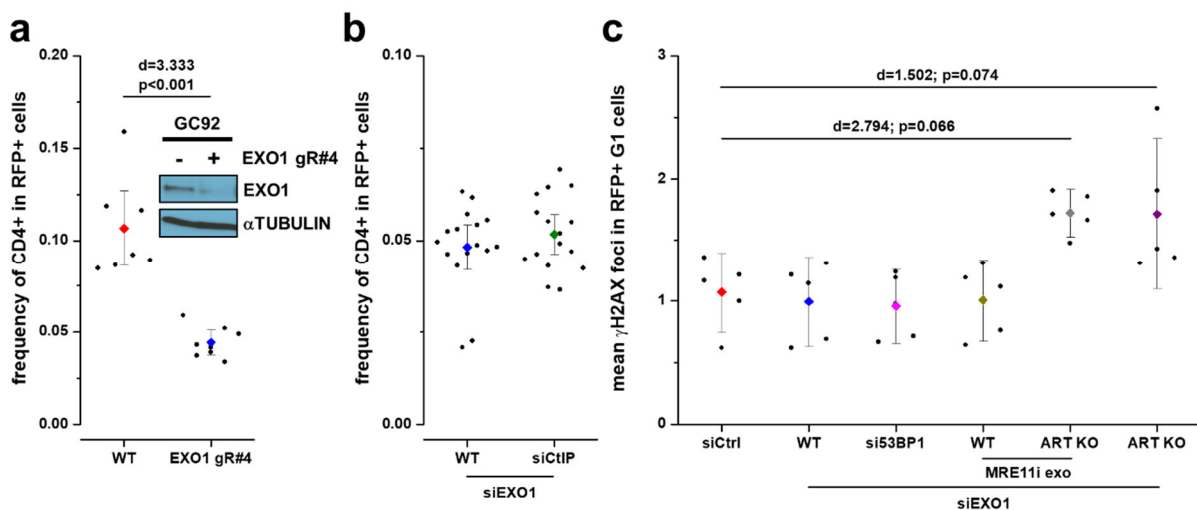


Figure S8.18 Supplement to Figure 3.30

(a, b) Impact of EXO1 CRISPR/Cas9 viral transduction (a) or EXO1-CtIP co-depletion (b) on misrepair in GC92 cells. (c) Impact of EXO1 complementation in combination with other factors on overall repair in GC92 WT or ARTEMIS KO cells. (a) GC92 cells were virally transduced with CRISPR/Cas9 and EXO1 gRNA #4 plasmids and selected using selection medium. Downregulation by CRISPR/Cas9 was confirmed by immunoblotting. (b, c) GC92 WT or ARTEMIS KO cells were treated with inhibitors and/or siRNAs against MRE11 exonuclease activity (PFM39), 53BP1, CtIP, and/or EXO1. As a control, cells were treated with control siRNA. (a, b) Cells were harvested 72 h post-co-transfection with the I-SceI and RFP plasmids. Cells were stained with anti-CD4, anti-RFP AB, and DAPI. Samples were scanned using Metafer software and only plasmid-transfected cells were analyzed. Data represent the mean of 8 or 16 independent experiments performed in duplicate ($n = 8$ for a; $n = 16$ for b). (c) Cells were co-transfected with RFP and I-SceI plasmids and treated with EdU and nocodazole 30 min prior to harvest. Harvest took place 72 h post-plasmid transfection. Cells were stained with anti- γ H2AX, anti-RFP AB, and DAPI. Samples were scanned using Metafer software and only plasmid-transfected G₁ cells were analyzed. Data represent the mean of 5 independent

experiments ($n = 5$). (a, b, c) RFP was used as a marker for cells with damage induction (see chapter 3.1.1). Error bars show the 95% CI. Effect size was calculated by Cohen's d and p -value was obtained by one-way ANOVA with Bonferroni correction (c) or by two-sample Student's t -test (a).

Table 8.8 EXO1-associated factors

SFB-EXO1-WT was precipitated and purified from stably-transfected HEK293 cells with streptavidin beads. Precipitation took place in unirradiated controls and 30 min post-5 Gy X-IR (all conditions $n = 1$). MS was performed by the Taplin Mass Spectrometry Facility, Harvard Medical School. Conditions where no interaction was observed were given a value of 0.1 for further analysis. The minimum amount of interacting peptides of a potential interaction partner was used to calculate the ratio of the irradiated sample compared to the unirradiated condition. Therefore, values greater than 1 show an interaction increase while values less than 1 show an interaction decrease following X-IR. Interesting possible novel interacting proteins and some established interacting proteins are included in this table.

EXO1 TAP-MS Protein	min # pep.		Ratio 30 min
	0 Gy	5Gy 30 min	
BLM	3	1	0.33333
BRCA1	0.1	11	110
CDK4	0.1	4	40
CHEK1	1	6	6
EXD2	1	2	2
EXO1	62	68	1.09677
MRE11A	3	4	1.33333
MSH3	59	85	1.44068
PRKDC	3	13	4.33333
RAD50	0.1	10	100
XRCC5	9	15	1.66667
XRCC6	7	16	2.28571

8.2. Curriculum Vitae

Name Ronja Anugwom, née Biehs
Date of birth 02/23/1989
Place of birth Idar-Oberstein, Germany

Education

2013-2017 **Graduate student** in the research group of Prof. Dr. M. Löbrich (Radiation Biology & DNA repair, TU Darmstadt, Germany) with the topic “Resection-dependent canonical non-homologous end-joining induces genomic rearrangements”
2011-2013 **Master of Science Biomolecular Engineering** TU Darmstadt, Profile: Biosystems Engineering; Thesis: “Analysis of NHEJ-induced genomic rearrangements” research group of Prof. Dr. M. Löbrich, TU Darmstadt, Germany
Majors: Radiation Biology, Genetics, Biophysics, and Neurobiology
2008-2011 **Bachelor of Science Biomolecular Engineering** TU Darmstadt
1999-2008 Higher education entrance qualification (*Abitur*) Humboldt-Gymnasium, Wiesbaden, Germany

Further Education

2015-2016 **Laboratory Exchange at the University of Texas MD Anderson Cancer Center**, Houston, Texas, USA; Department of Experimental Radiation Oncology; Supervisor J. Chen, PhD; Laboratory Supervisor Z. Gong, MD, PhD
2015-2016 **Certificate** for higher education teaching
2014-2016 **Lectures, workshops, and further training:** clinical radiation biology; safety in genetic engineering (German certificate); statistic courses; scientific writing in English; presentation training; guiding and promoting teamwork; supervising undergraduate theses
01/2007 Internship at Max-Planck-Institute for Biophysics, Frankfurt am Main, Germany; Supervisor Dr. J. Rettinger

Affiliation

2015-present **EACR** (The European Association for Cancer Research)
2015-present **GBS** (*Gesellschaft für Biologische Strahlenforschung e.V.*)
2014-present **ERRS** (European Radiation Research Society)
2014-2016 **Member and student representative** of the DFG-funded (*Deutsche Forschungsgemeinschaft*) Graduate College (GrK) 1657: Molecular and cellular responses to ionizing radiation

8.3. Publications, awards, and conference contributions

Publications

Biehs R, Steinlage M, Barton O, Juhász S, Künzel J, Spies J, Shibata A, Jeggo P, Löbrich M. **2017**. DNA double-strand break resection occurs during non-homologous end-joining in G₁ but is distinct to resection during homologous recombination in G₂. *Mol. Cell* 65:1–14. doi:10.1016/j.molcel.2016.12.016.

Barton O, Naumann SC, Diemer-Biehs R, Künzel J, Steinlage M, Conrad S, Makharashvili N, Wang J, Feng L, Lopez BS, et al. **2014**. Polo-like kinase 3 regulates CtIP during DNA double-strand break repair in G₁. *J. Cell Biol.* 206:877–94. doi:10.1083/jcb.201401146.

Awards and honors

04/2017	GlaxoSmithKline Travel Grant
2015-2016	Keystone Symposia – Genomic Instability and DNA Repair, Santa Fe Training grant for Exchange at MD Anderson Cancer Center, Houston DFG-funded training grant as a member of the GrK 1657
2015-2016	PhD Scholarship DFG-funded full scholarship as a member of the GrK 1657
06/2015	Supervisor for the DAAD (<i>Deutsche Akademische Austauschdienst e. V.</i>) RISE (Research Internships in Science and Engineering) program
05/2015	ERRS Young Investigator Award 15 th International Congress of Radiation Research, Kyoto
02/2015	EACR Poster Prize EACR Conference on Radiation Biology and Cancer, Essen
07/2014	EACR Poster Prize Annual Meeting of the Association of Radiation Research 2014, Brighton
2013-2015	PhD Scholarship DFG-funded full scholarship

Conference contributions

- Biehs R, Steinlage M, Barton O, Juhász S, Künzel J, Spies J, Shibata A, Jeggo P, Löbrich M.
Poster: Characterization of a resection-dependent c-NHEJ repair pathway in G₁
Keystone Symposia 2017 – Genomic Instability and DNA Repair in Santa Fe, New Mexico, USA (04/2017)
- Diemer-Biehs R, Barton O, Steinlage M, Shibata A, Jeggo P, Löbrich M.
Poster: BRCA1 regulates a resection-dependent NHEJ pathway in G₁
Abcam - Maintenance of Genomic Stability 2016 in Panama City, Panama (03/2016)
- Diemer-Biehs R, Lopez B, Barton O, Steinlage M, Löbrich M.
Poster and short talk: A canonical end-joining pathway in G₁-phase involves a CtIP- and Artemis-dependent resection
15th International Congress of Radiation Research in Kyoto, Japan (05/2015)
- Diemer-Biehs R, Lopez B, Barton O, Löbrich M.
Poster: A canonical end-joining pathway in G₁-phase involves a CtIP- and Artemis-dependent resection
EACR Conference on Radiation Biology and Cancer – From Molecular Responses to the Clinic in Essen, Germany (02/2015)
- Diemer-Biehs R, Steinlage M, Lopez B, Barton O, Löbrich M.
Poster and proffered paper talk: A CtIP-dependent double-strand break repair process in G₁ generates genomic rearrangements in a NHEJ-reporter-assay
Annual Meeting of the GBS 2014 in Tübingen, Germany (09/2014)
- Biehs R, Steinlage M, Lopez B, Barton O, Löbrich M.
Poster: A CtIP-dependent double-strand break repair process in G₁ generates genomic rearrangements in a NHEJ-reporter-assay
Annual Meeting of the Association of Radiation Research 2014 in Brighton, UK (06/2014)
- Biehs R, Künzel J, Lopez B, Barton O, Löbrich M.
Poster: The influence of CtIP and Artemis in the slow repair process in G₁
Annual Meeting of the GBS 2013 in Darmstadt, Germany (09/2013)

8.4. Acknowledgements

I thank M. Löbrich for giving me the opportunity to write my thesis on this very interesting topic in his working group. Furthermore, I want to thank him for all the extensive scientific discussions and for all the successful work together over the years. Second, I want to thank K. Hamacher for taking on the role of second referee as well as A. Löwer and H. Kolmar for agreeing to be part of my thesis committee.

A special thank you to J. Chen and Z. Gong for the great collaboration and their supervision and council during my time at MD Anderson Cancer Center. Additionally, many thanks to P. Jeggo and A. Shibata for the close collaboration. Thank you also to B. Lopez and J. Guirouilh-Barbat for providing the fibroblast reporter assay cell lines without which this thesis would not have been possible. In addition, many thanks to M. Wolf for the valuable experimental input on KU foci.

Thank you to the DFG for funding my research, the exchange at MD Anderson Cancer Center, and further education through the GrK 1657. Many thanks also to the EACR, ERRS, GlaxoSmithKline foundation, and the gender equality team of the biology department of the TU Darmstadt, which all gave me the opportunity to contribute to national and international conferences.

Next, I want to thank all the members and former members of the working group of M. Löbrich for their advice, support, teamwork, and all the interesting lunch conversations during these past years. Here, I want to specifically mention: M. Steinlage for our close work together for two publications, her input during our time in the laboratory, her input to this thesis, and her ongoing support; O. Barton for her counsel and supervision in the first year; the technical assistants for the invaluable laboratory support, especially during the revision process of our publication; and R. Weimar, C. Reul, M. Ensminger, and especially J. Mirsch for their teamwork and input during the time in the laboratory and/or for their input to this thesis.

Furthermore, thank you to the undergraduate students C. Ruder and C. Alvarado whom I had the pleasure to supervise and who contributed actively to this work. Many thanks also to the members of the working group of J. Chen and the members of our graduate college GrK 1657 for all the discussions we had during retreats and other meetings.

Many thanks to J. Diemer for all the support in the years we spent together. Thank you to my brother Jascha for all the times driving me around to just spend time or to help me visiting the places and people I wanted to.

My deepest thanks for the active help, support, and love of my husband Bruce, especially during the final stages of writing this thesis when there were so many other things to take care of and organize to start our life together.

Finally, the biggest thank you goes to my parents, Suni and Berthold. You will have my lifelong gratitude for providing me with this exceptional education, for giving me the opportunity to do what I want in life, and essentially for always supporting me unconditionally. Also, a special thank you for your unparalleled support and help during the final stages of writing my thesis.

Ehrenwörtliche Erklärung

Ich erkläre hiermit ehrenwörtlich, dass ich die vorliegende Arbeit entsprechend den Regeln guter wissenschaftlicher Praxis selbstständig und ohne unzulässige Hilfe Dritter angefertigt habe.

Sämtliche aus fremden Quellen direkt oder indirekt übernommenen Gedanken sowie sämtliche von Anderen direkt oder indirekt übernommenen Daten, Techniken und Materialien sind als solche kenntlich gemacht. Die Arbeit wurde bisher bei keiner anderen Hochschule zu Prüfungszwecken eingereicht.

Darmstadt, den 01.11.2017

.....

Ronja Anugwom